

AMHYCO

Research and Innovation Action (RIA)

This project has received funding from the Euratom research and innovation programme 2014-2018 under Grant Agreement No 945057

Start date: 2020-10-01 Duration: 48 Months



Synthesis and outcomes of performed experiments results related to PARs behaviour

Authors : Dr. Ernie REINECKE (FZJ), Araceli Domínguez-Bugarín (UPM), Gabriela Nobrega (IRSN)

AMHYCO - Contract Number: 945057

Project officer: PASSALACQUA Roberto

Document title	Synthesis and outcomes of performed experiments results related to PARs behaviour
Author(s)	Dr. Ernie REINECKE, Araceli Domínguez-Bugarín (UPM), Gabriela Nobrega (IRSN)
Number of pages	134
Document type	Deliverable
Work Package	WP3
Document number	D3.2
Issued by	FZJ
Date of completion	2023-12-04 08:48:29
Dissemination level	Public

Summary

The molten corium-concrete interaction in the ex-vessel phase of a severe accident in a water-cooled nuclear reactor is the source of significant amounts of hydrogen and carbon monoxide among other gaseous products. The European project AMHYCO addresses open issues related to the understanding of the impact of hydrogen and carbon monoxide on phenomena occurring in the late accident phase. One of these phenomena is the operational behaviour of passive autocatalytic recombiners (PARs), which are installed inside the containment of many nuclear power plants to mitigate the hydrogen combustion risk. The main objective of AMHYCO Task 3.2 is to ensure that the impact of carbon monoxide on the PAR performance is properly addressed in numerical PAR models, which will be used in full containment accident simulations in the work program of WP4. An experimental program alongside model development activities has been performed in order to improve the predictive capabilities of numerical models assessing the efficiency of PARs as hydrogen mitigation measure: Framatome correlation (correlation-based model for the specific Framatome-PAR type) - REKO-DIREKT (mechanistic PAR model involving diffusion-controlled reaction kinetics) - PARUPM (mechanistic PAR model involving surface chemistry) SPARK (mechanistic PAR model involving full surface and gas-phase chemistry) Supported by an experimental program, which has been addressing related knowledge gaps, the predictive capabilities of numerical PAR models to evaluate the efficiency of PARs as hydrogen mitigation measure have been advanced. The experimental program has investigated PAR operation in the presence of hydrogen and carbon monoxide, which can be divided into three different regimes: - Regime I: Undisturbed parallel reaction of hydrogen and carbon monoxide with oxygen (oxygen-rich atmosphere) - Regime II: Constrained parallel reaction of hydrogen and carbon monoxide with oxygen (oxygen-lean atmosphere) - Regime III: Interruption of reaction due to catalyst deactivation (poisoning) For the first time, the experimental program has investigated the effect of carbon monoxide on both platinum- and palladium-based catalysts, in order to obtain information on the differences in behaviour. The analyses of the results of the accident scenario simulations obtained from WP2 led to the following conclusions with regard to the experimental program: - Almost through the entire ex-vessel phase, the atmosphere is oxygen-lean wit...

Approval	
Date	Ву
2023-12-04 19:28:39	Mrs. Nabiha CHAUMEIX (CNRS)
2023-12-05 09:09:38	Dr. Gonzalo JIMENEZ (UPM)



Enhancing H₂ & CO Combustion Risk Management

Research and Innovation Action

NFRP-2019-2020

D3.2 - Synthesis and outcomes of performed experiments and numerical results related to PAR behaviour

WP3 - Task 3.2

April 2023

Authors: Ernie Reinecke (FZJ), Araceli Domínguez-Bugarín (UPM), Gabriela Nobrega (IRSN)

Contributors: Matthias Braun (FRG)





Disclaimer

The content of this deliverable reflects only the author's view. The European Commission is not responsible for any use that may be made of the information it contains.

Table of Contents

1.	Introd	uction	17
2.	State o	of knowledge at the start of the task	18
2	2.1. Exp	pected boundary conditions	19
	2.1.1.	Oxygen starvation	20
	2.1.2.	PAR ignition	28
	2.1.3.	Conclusions from scenario analyses	32
2	2.2. Nu	ımerical PAR models	32
	2.2.1.	Framatome correlation	35
	2.2.2.	PARUPM	35
	2.2.3.	SPARK	37
	2.2.4.	REKO-DIREKT	39
3.	Experi	mental program	41
3	8.1. Sco	oping tests	41
	3.1.1.	Description of the REKO-1 test facility	41
	3.1.2.	Catalyst samples	45
	3.1.3.	Test matrix and test procedure	46
	3.1.4.	Results	47
	3.1.5.	Conclusions of scoping tests	59
3	3.2. Ca	talyst section tests	60
	3.2.1.	Description of the REKO-3 test facility	60
	3.2.2.	Catalyst samples	66
	3.2.3.	Data post-processing and evaluation	67
	3.2.4.	Test matrix and test procedure	70
	3.2.5.	Results	71
	3.2.6.	Conclusions	82
3	8.3. Na	tural convection tests	82
	3.3.1.	Description of the REKO-4 test facility	82
	3.3.2.	Catalyst samples	90

	3.3.3.	Data post-processing and evaluation	90
	3.3.4.	Test matrix and test procedure	92
	3.3.5.	Results	92
	3.3.6.	Conclusions	96
4.	Model	development	97
4	.1. Exp	perimental databases	97
	4.1.1.	REKO-3 database	97
	4.1.2.	THAI database	98
4	.2. Mc	del improvements	
	4.2.1.	Framatome correlation	102
	4.2.2.	PARUPM	106
	4.2.3.	SPARK	111
	4.2.4.	REKO-DIREKT	130
5.	Biblion	uranhy	132

List of Figures

Figure 1. Oxygen starvation: Effect of oxygen fraction on catalyst temperature (REKO-1)	22
Figure 2. Oxygen starvation: Effect of oxygen fraction on catalyst temperature (THAI HR-11).	23
Figure 3. PWR-KWU SBLOCA: Period of oxygen starvation	24
Figure 4. PWR-W SBO: Period of oxygen starvation	25
Figure 5. PWR-W SBLOCA: Period of oxygen starvation	26
Figure 6. PWR-W LBLOCA: Period of oxygen starvation	27
Figure 7. PAR ignition: Concentration threshold for hydrogen/carbon monoxide mixtures	29
Figure 8. PWR-KWU SBLOCA: Period of potential PAR ignition	30
Figure 9. PWR-W SBO: Period of potential PAR ignition	31
Figure 10. PWR-W SBLOCA: Period of potential PAR ignition	32
Figure 11. PWR-W LBLOCA: Period of potential PAR ignition	33
Figure 12. SPARK: Recombiner configuration and numerical domain	38
Figure 13. REKO-DIREKT: Model approach	39
Figure 14. REKO-1: Cylindrical flow reactor (left); catalyst temperature measurement (right)	42
Figure 15. REKO-1: Flow diagram	42
Figure 16. REKO-1: Measurement uncertainty of type K thermocouples	44
Figure 17. REKO-1: Pyrometer calibration for the platinum-based catalyst	45
Figure 18. REKO-1: Catalyst samples	46
Figure 19. REKO-1: Catalyst surface temperature along the catalyst length	48
Figure 20. REKO-1: Effect of hydrogen concentration on the catalyst temperature	48
Figure 21. REKO-1: Effect of inlet gas temperature on the catalyst temperature	49
Figure 22. REKO-1: Effect of inlet flow velocity on the catalyst temperature	49
Figure 23. REKO-1: Effect of steam on the catalyst temperature	50
Figure 24. REKO-1: Effect of oxygen starvation on the catalyst temperature	51
Figure 25. REKO-1: Effect of carbon monoxide fraction on the catalyst temperature	51
Figure 26. REKO-1: Effect of carbon monoxide fraction on the catalyst temperature	52
Figure 27. REKO-1: Effect of inlet gas temperature on the catalyst temperature	52
Figure 28. REKO-1: Effect of inlet flow velocity on the catalyst temperature	53
Figure 29. REKO-1: Oxygen starvation threshold at 1 vol.% carbon monoxide	53
Figure 30. REKO-1: Oxygen starvation threshold at 2 vol.% carbon monoxide	54
Figure 31. REKO-1: History of the catalyst temperature during a typical poisoning experiment	55
Figure 32. REKO-1: Catalyst poisoning temperatures obtained with different test procedures	56
Figure 33. REKO-1: Catalyst poisoning temperatures for different gas compositions	57
Figure 34. REKO-1: Catalyst poisoning temperatures for different inlet gas temperatures	57
Figure 35. REKO-1: Catalyst poisoning temperatures for different flow velocities	58
Figure 36. REKO-1: Catalyst poisoning temperatures for dry and wet conditions	58
Figure 37. REKO-1: Comparison of poisoning temperatures for Pt- and Pd-based catalysts	59
Figure 38, REKO-3: Rectangular flow reactor set-up	61

Figure 39. REKO-3: Flow diagram	61
Figure 40. REKO-3: Optical measurement of the catalyst temperature	62
Figure 41. REKO-3: Different offsets in the hydrogen signal during the calibration procedur	
Figure 42. REKO-3: Offset correction for oxygen	65
Figure 43. REKO-3: Offset correction for carbon monoxide	65
Figure 44. REKO-3: Offset correction for carbon dioxide	66
Figure 45. REKO-3: Catalyst sheets; palladium (left), platinum (right)	67
Figure 46. REKO-3: Molar balance of the gas analyzer	69
Figure 47. REKO-3: Flow velocity obtained from THAI HR-1 and HR-2	72
Figure 48. REKO-3: Comparison of the catalyst temperature with THAI HR-1 and HR-2	
Figure 49. REKO-3: Comparison of hydrogen outlet concentrations with THAI HR-1 and HR	273
Figure 50. REKO-3: Effect of oxygen starvation on the catalyst temperature (20 °C)	74
Figure 51. REKO-3: Effect of oxygen starvation on the catalyst temperature (80 °C)	74
Figure 52. REKO-3: Effect of oxygen reduction on catalyst operation, Pd-based catalyst, 15	0 °C,
3 vol.% H ₂ , 0 vol.% CO (R3-CO-B-06)	75
Figure 53. REKO-3: Effect of oxygen starvation on catalyst operation, Pd-based catalyst, 15	
3 vol.% H ₂ , 1 vol.% CO (R3-CO-B-06)	76
Figure 54. REKO-3: Effect of oxygen starvation on catalyst operation, Pd-based catalyst, 15	
3 vol.% H ₂ , 3 vol.% CO (R3-CO-B-06)	
Figure 55. REKO-3: Effect of oxygen starvation on catalyst operation, Pd-based catalyst, 80	
vol.% H ₂ , 3 vol.% CO (R3-CO-B-04)	
Figure 56. REKO-3: Ranges of partial and full poisoning for the platinum-based catalyst	
Figure 57. REKO-3: Ranges of partial and full poisoning for the palladium-based catalyst	
Figure 58. REKO-4: Basic design data of the pressure vessel	
Figure 59. REKO-4: Basic sketch of the instrumentation inside the pressure vessel	
Figure 60. REKO-4: Relevant measurement points inside the vessel	
Figure 61. REKO-4: Measurement uncertainty of the humidity sensor depending on the relative sensor depending s	
humidity	
Figure 62. REKO-4: Blank sensor on socket (left), sensor with sintered metal filter cap (center)	
sensor shrinking hose ready for mounting (right)	
Figure 63. REKO-4: Humidity correction of the hydrogen sensors	
Figure 64. REKO-4: Calibration function of the oxygen sensors	
Figure 65. REKO-4: Measurement uncertainties of the pressure sensors	
Figure 66. REKO-4: PAR catalyst section with ten sheets (palladium)	
Figure 67. REKO-4: Mounting of the PAR inside the pressure vessel	
Figure 68. REKO-4: Typical test sequence	
Figure 69. REKO-4: Test results for platinum-based catalyst (squares: 1 bar, diamonds: 2 ba	-
Figure 70. REKO-4: Test results for palladium-based catalyst (squares: 1 bar, diamonds: 2 k	
Figure 71. THAI-DB: Entire list of experiments (left) and selected experiments (right)	
Figure 72. THAI-DB: Experimental phases and selected measurement points	99

Figure 73. THAI-DB: Experimental phases and selected measurement points	100
Figure 74. THAI-DB: Experimental phases and selected measurement points	100
Figure 75. THAI-DB: Recombination rates with uncertainty bars bars	102
Figure 76. Comparison of the Framatome correlation rates with the THAI database	103
Figure 77. Illustration of the oxygen starvation part of the Framatome correlation	103
Figure 78. Original and improved Framatome correlation versus THAI HR-12 data	104
Figure 79. Comparison of the improved Framatome correlation rates with the THAI data	abase.105
Figure 80. PARUPM diffusion and reaction-based recombination rates against experime	ental
recombination rates (REKO-3)	107
Figure 81. PARUPM H2 (blue dots) and CO (open purple dots) recombination rates aga	inst
experimental recombination rates (REKO-3)	109
Figure 82. PARUPM: Recombination rate with PARUPM (grey line) and experimental	
recombination rates (purple dots) during the transient (HR-1)	110
Figure 83. PARUPM: Recombination rate with PARUPM (grey line) and experimental	
recombination rates (purple dots) during the transient (HR-13)	111
Figure 84. SPARK: Evolution of catalyst temperatures measured at the bottom of the ca	talyst
versus the hydrogen molar fraction at 0.5 m/s	114
Figure 85. SPARK: Comparison between SPARK simulations and REKO-1 data: Catalyst s	surface
temperature along catalyst length for 4 vol.% H_2 and O_2 content varying from 21 to 2 v	ol.%115
Figure 86. SPARK: Catalyst surface temperature along catalyst height for different H ₂ co	ntent:
Comparison between REKO-3 results and SPARK simulations	116
Figure 87. SPARK: Catalyst surface temperature along catalyst height for 3 vol.% H_2 and	l O ₂
content varying from 21 to 2 vol.%: Comparison between REKO-3 results and SPARK sin	mulations
	117
Figure 88. SPARK: Catalyst temperatures for a mixture of 2 vol.% H ₂ versus CO content	under dry
and steam conditions	117
Figure 89. Comparison of catalyst poisoning temperature versus CO concentration for I	REKO-1
and REKO-3 (4 vol.% H ₂)	
Figure 90. SPARK: Catalyst temperature for a mixture with 4 vol.% H_2 , 0.5 vol.% CO and	reduction
of oxygen	
Figure 91. SPARK: Catalyst temperature for a mixture with 4 vol.% H_2 , 2 vol.% CO, gas a	t 80°C
and reduction of oxygen	119
Figure 92. SPARK: Hydrogen distribution on the channel between catalysts, for 21 vol.%	O ₂ (left)
and 3 vol.% O ₂ (right)	120
Figure 93. SPARK: Carbon monoxide distribution in the REKO-3 channel between two c	atalyst
plates, for 21 vol.% O ₂ (left) and 3 vol.% O ₂ (right)	121
Figure 94. SPARK: Temperature fields for a mixture with 4 vol.% H_2 , 2 vol.% CO, gas at 8	30 °C and
21 vol.% O ₂ (left) and 3 vol.% O ₂ (right)	
Figure 95. SPARK: Hydrogen distribution in the REKO-3 channel between two catalyst p	lates for
2.6 vol.% O ₂ (left), 2.5 vol.% O ₂ (middle) and 2.3 vol.% O ₂ (right)	122

Figure 96. SPARK: Carbon monoxide distribution in the REKO-3 channel between two catalyst	Ĺ
plates for 2.6 vol.% O ₂ (left), 2.5 vol.% O ₂ (middle) and 2.3 vol.% O ₂ (right)	122
Figure 97. SPARK: Temperature fields for a mixture with 4 vol.% H ₂ , 2 vol.% CO, gas at 80°C	
during deactivation: 2.6 vol.% O ₂ (left), 2.5 vol.% O ₂ (middle) and 2.3 vol.% O ₂ (right)	123
Figure 98. SPARK: Carbon monoxide distribution along the catalyst plate for a mixture with 4	
vol.% H ₂ , 2 vol.% CO and oxygen varying from 21 to 2.3 vol.%	123
Figure 99. SPARK: Predicted poisoning temperature at different hydrogen fractions	124
Figure 100. SPARK: Predicted poisoning temperature for two flow velocities (2 vol.% H ₂)	125
Figure 101. SPARK: Predicted poisoning temperature for three initial gas temperatures (4 vol.	.%
H ₂)	125
Figure 102. SPARK: Predicted poisoning temperature for dry test and test with steam (4 vol.%	6
H ₂)	126
Figure 103. SPARK: Predicted oxygen content at poisoning versus the H_2+CO molar percent a	it
different initial gas temperatures	126
Figure 104. SPARK: Evolution of the poisoning temperature versus the CO molar percent at	
different H_2 content. Comparison between experiments (open symbols) and simulation (solid	
symbols)	127
Figure 105. SPARK: Evolution of the poisoning temperature versus the CO molar fraction at	
different flow velocities: 0.5 m/s and 1 m/s. Comparison between experimental results and	
SPARK simulation	
Figure 106. SPARK: Catalyst poisoning temperature at different carbon monoxide concentration	ons
for three initial gas temperatures: 20 °C, 80 °C and 150 °C. Comparison with REKO-1 and REKO	O-3
data	
Figure 107. REKO-DIREKT: Calculated outlet hydrogen concentration compared with data from	
the THAI database	
Figure 108. REKO-DIREKT: Calculated catalyst temperatures compared with data from the THA	ΑI
datalaga	121

List of Tables

Table 1. Relevant conditions during severe accident late phases scenarios	19
Table 2. Relevant conditions during severe accident late phase scenarios	20
Table 3. Deutschmann simplified combustion model for methane catalysed with Pt	
(Deutschmann et al., 1996)	36
Table 4. SPARK: Reaction mechanisms for the catalytic oxidation of H ₂ and CO over Pt (left);	
Reaction mechanism for the gaseous combustion of H ₂ and CO (right)	38
Table 5. REKO-3: Poisoning conditions for palladium-based catalyst (dry conditions)	79
Table 6. REKO-3: Poisoning conditions for palladium-based catalyst (wet conditions)	80
Table 7. REKO-3: Poisoning conditions for platinum-based catalyst (dry conditions)	80
Table 8. REKO-3: Poisoning conditions for platinum-based catalyst (wet conditions)	81
Table 9. REKO-4: Test matrix	92
Table 10. PARUPM: Comparison of calculated recombination rates with REKO-3 data for 5	
different oxygen concentrations and 2 inlet temperatures	108
Table 11. SPARK: Updated reaction mechanism; units: S_0 [–], A [cm, s, K], E_a [J/mol], coverage	h [–
]	112
Table 12. SPARK: Surface reaction mechanism on palladium; units: A [mol, cm, s], Ea [kJ/mol],	S^0
[-]); Pd(s) denotes bare surface sites; reaction rate: $k = A T_n \exp(-E_a/RT)$	113

Abbreviations and Acronyms

Acronym Description		
СО	Carbon monoxide	
CO ₂	Carbon dioxide	
H_2	Hydrogen molecule	
H ₂ O	Water	
LB-LOCA	Large Break Loss of Coolant Accident	
LOCA	Loss of Coolant Accident	
MCCI	Molten Core-Concrete Interaction	
O ₂	Oxygen	
PAR	Passive Autocatalytic Recombiner	
PWR	Pressurized Water Reactor	
SAMG	Severe Accident Management Guidelines	
SB-LOCA	Small Break Loss of Coolant Accident	
SBO	Station Blackout	
WP	Work Package	

Executive Summary

The molten corium-concrete interaction in the ex-vessel phase of a severe accident in a water-cooled nuclear reactor is the source of significant amounts of hydrogen and carbon monoxide among other gaseous products. The European project AMHYCO addresses open issues related to the understanding of the impact of hydrogen and carbon monoxide on phenomena occurring in the late accident phase. One of these phenomena is the operational behaviour of passive autocatalytic recombiners (PARs), which are installed inside the containment of many nuclear power plants to mitigate the hydrogen combustion risk. The main objective of AMHYCO Task 3.2 is to ensure that the impact of carbon monoxide on the PAR performance is properly addressed in numerical PAR models, which will be used in full containment accident simulations in the work program of WP4.

An experimental program alongside model development activities has been performed in order to improve the predictive capabilities of numerical models assessing the efficiency of PARs as hydrogen mitigation measure:

- Framatome correlation (correlation-based model for the specific Framatome-PAR type)
- REKO-DIREKT (mechanistic PAR model involving diffusion-controlled reaction kinetics)
- PARUPM (mechanistic PAR model involving surface chemistry)
- SPARK (mechanistic PAR model involving full surface and gas-phase chemistry)

Supported by an experimental program, which has been addressing related knowledge gaps, the predictive capabilities of numerical PAR models to evaluate the efficiency of PARs as hydrogen mitigation measure have been advanced.

The experimental program has investigated PAR operation in the presence of hydrogen and carbon monoxide, which can be divided into three different regimes:

- Regime I: Undisturbed parallel reaction of hydrogen and carbon monoxide with oxygen (oxygen-rich atmosphere)
- Regime II: Constrained parallel reaction of hydrogen and carbon monoxide with oxygen (oxygen-lean atmosphere)
- Regime III: Interruption of reaction due to catalyst deactivation (poisoning)

For the first time, the experimental program has investigated the effect of carbon monoxide on both platinum- and palladium-based catalysts, in order to obtain information on the differences in behaviour.

The analyses of the results of the accident scenario simulations obtained from WP2 led to the following conclusions with regard to the experimental program:

- Almost through the entire ex-vessel phase, the atmosphere is oxygen-lean with regard to PAR operation. Consequently, the experimental program and model development needs to focus on such conditions.
- PAR models should be validated for atmospheres with temperatures between 40 °C and 140 °C, pressure up to 3.7 bar and steam at saturation.
- Hydrogen fractions are typically higher than or equal to carbon monoxide fractions.
- Potential for PAR ignition should be considered in the models with corresponding criteria, if no catalyst temperature is calculated.

At the same time, based on the simulations performed in WP2, the following phenomena can be considered unlikely to occur in an accident, and thus could be discarded from the experimental study:

- No sudden increase of the oxygen fraction was observed in the late accident phases of the simulations. Consequently, it seems not necessary to study whether a potentially poisoned catalyst could be re-activated if a transition from oxygen-lean to oxygen-rich would occur.
- None of the scenarios gives indication that a second hydrogen and/or carbon monoxide generation phase might occur after the PARs have stopped operation. Consequently, no experiments are required to study PAR start-up, e.g. in the presence of carbon monoxide.

Another aspect shaping the experimental program were the results of scoping tests performed in the REKO-1 facility. The results indicate that platinum-based catalysts seem to be significantly more impacted by carbon monoxide than palladium-based catalysts. Furthermore, the effect on the palladium-based catalyst showed a stronger temperature-dependency.

The experimental program in the REKO-3 facility studied the impact of carbon monoxide on both platinum-based and palladium-based catalysts. Catalyst sections consisting of four parallel sheets were exposed to steady-state flows of gaseous mixtures including hydrogen, oxygen, nitrogen, steam and carbon monoxide inside a vertical flow reactor. Specific focus was on mixtures with low amounts of oxygen. Measurements of the catalyst temperature and the outlet

gas concentrations enabled to assess the catalyst activity (i.e. the occurrence of any surface reaction) and efficiency (i.e. the level of conversion).

Based on the experimental results, a database was generated including steady-state recombination rates for both hydrogen and carbon monoxide and catalyst temperature profiles for different inlet gas mixtures and conditions. Furthermore, the conditions for catalyst deactivation in the presence of carbon monoxide were identified.

The experimental program in the REKO-4 facility studied the effect of pressure on the poisoning conditions. A PAR consisting of a catalyst section of ten parallel catalyst sheets was exposed to a continuous injection of hydrogen and carbon monoxide in oxygen-lean atmosphere. The characteristic drop of the catalyst temperature allowed to determine the conditions when catalyst poisoning occurred. The results didn't indicate any significant effect of the pressure on the poisoning conditions.

The processes in Regime I are well understood and mechanistic approaches for the different PAR models exist. For the transition from Regime I to Regime II, the approach of diffusion-controlled reaction kinetics has been successfully applied to provide a criterion which is applicable for both correlation model as well as detailed codes. This approach is independent of the type of catalyst (Pt or Pd).

The experimental data obtained for Regime III from the catalyst poisoning tests suggest that gas temperature and oxygen concentration are the most relevant parameters to describe PAR poisoning for both catalyst types. The results allow to derive empirical criteria for catalyst poisoning with sufficient (if necessary conservative) precision, which are based on easy to obtain parameters (gas temperature and oxygen concentration) even for those PAR models that don't involve surface chemistry.

In addition to the REKO-3 database, which is especially suited for model development and validation for the PAR geometry independent mechanistic models, a second database of quasi-steady state measurement points was derived from the transient experiments performed in the framework of the OECD/NEA-THAI projects. This new database allows validation of the PAR model performance for the boundary conditions of the entire experimental program rather than only comparing single transient experiments with model calculations. It is suited for both correlation model and mechanistic PAR models.

The new generated THAI database has been applied to confirm existing deficiencies of the Framatome correlation in modelling PAR operation under oxygen-lean conditions, which had been identified for a single case in the framework of the SAMHYCO-NET project, the precursor to the AMHYCO project. Improvements of the correlation based on the laws of diffusion-controlled reaction kinetics have been implemented, which allow for a more consistent

transition from oxygen-rich to oxygen-lean PAR operation. The calculation of the entire THAI database demonstrates the successful improvement of the correlation as well as the suitability of the THAI database for model validation.

The Framatome correlation is used by most of the AMHYCO partners participating in WP4. The improved model has been transferred for testing and implementation in the corresponding thermo-hydraulic codes within the WP4 framework.

Within the AMHYCO project, the PARUPM code has been proposed as an appropriate tool for assessing the performance of PARs in full containment simulations. In the framework of Task 3.2, the PARUPM code has been further developed and validated. Most relevant enhancements include the implementation of a chimney model as well as a diffusion-based reaction model. The results obtained demonstrate that the physico-chemical strategy used in the PARUPM model can simulate the behaviour of the recombiner under a variety of conditions, from typical concentrations and settings to more extreme ones such as oxygen starvation, catalyst poisoning, or elevated inlet temperatures. Furthermore, the code can reproduce the behaviour of a PAR in transient conditions, where pressure, temperature, and gas concentrations are constantly changing at the recombiner inlet. The PARUPM code is planned to be implemented in 3D thermo-hydraulic analysis codes, such as GOTHIC, as it was implemented in the past in lumped parameters codes like MELCOR.

The further development of the SPARK code includes an update of the surface reaction mechanisms for platinum-based catalysts as well as an approach to implement a surface mechanism for palladium-based catalysts. The new Pt mechanism allows PAR simulation during deactivation conditions in the presence of carbon monoxide. The enhanced SPARK code has been used for post-calculations of both REKO-1 and REKO-3 data to verify that the SPARK code is able to reproduce the experimental results. The numerical results are consistent with the experimental results for all the cases, confirming that the SPARK code can predict the catalyst temperature for rich-oxygen conditions, oxygen starvation conditions and when in presence of steam.

Advancements of the REKO-DIREKT code concern the implementation of different poisoning criteria for both catalyst types (Pt and Pd) based on the findings from REKO-3 poisoning experiments. The status of the PAR model has been validated against the new THAI database developed in Task 3.2. General good agreement was obtained, specifically regarding the catalyst temperature, which is one of the specific features of the code.

Keywords

Hydrogen mitigation, Carbon monoxide, Passive autocatalytic recombiners, Experiments, Model development

1. Introduction

In the context of protecting nuclear power plants from the consequences of accident-related massive hydrogen and carbon monoxide releases, the European AMHYCO project focuses its attention particularly on the late phase of a severe accident. Here, the molten corium-concrete interaction (MCCI) is the source of significant amounts of carbon monoxide among other gaseous products (Petit et al., 2001). Consequently, the project addresses open issues related to the understanding of the impact of carbon monoxide on both hydrogen combustion phenomena and hydrogen mitigation under the conditions of the late accident phase.

The effect of carbon monoxide on the performance of passive auto-catalytic recombiners (PARs) has been studied in AMHYCO in the framework of Task 3.2. Supported by an experimental program, which has been addressing related knowledge gaps, the predictive capabilities of numerical PAR models to evaluate the efficiency of PARs as hydrogen mitigation measure have been advanced.

The present report encompasses two major parts. The first part deals with the experimental program while the second part is devoted to the model improvements.

Chapter 2 briefly summarizes the state of knowledge at the project start, describes the boundary conditions for PAR operation as derived from AMHYCO report D2.2 (Herranz & Fontanet, 2022) and gives an overview of the numerical PAR models of the project partners.

The experimental program described in chapter 3 involves three parts: Scoping tests (section 3.1), catalyst section tests (section 3.2) and natural convection tests (section 3.3). In each of these sections, the test facilities including instrumentation and catalyst samples, as well as data post-processing and the evaluation methodology are described in detail. Finally, test procedures and experimental results are explained.

Chapter 4 gives an overview of the achieved PAR model improvements. First, the obtained databases from both REKO and THAI experiments is described. Then, one sub-chapter is devoted to each of the PAR models describing the progress made in Task 3.2.

2. State of knowledge at the start of the task

Passive auto-catalytic recombiners (PARs) have been retrofitted in water-cooled reactors, both LWRs and CANDUs, worldwide (with only few exceptions) as a consequence of hydrogen explosions in the course of nuclear reactor accidents in North America (Three Mile Island, 1979) and Japan (Fukushima Daiichi, 2011) (Liang et al., 2014). Since the 1990s, numerous national and international scientific projects have investigated the operational behaviour of PARs to advance the evaluation of the effectiveness of the implementation. Examples for early projects are the experimental series performed in the French H2PAR and KALI facilities in the 1990s (Bachellerie et al., 2003), while the present OECD/NEA-THEMIS project (OECD-NEA, 2023) is an evidence of the continued unwavering interest in this topic.

Although some of the aforementioned projects have been addressing the effect of ex-vessel phenomena, such as the presence of carbon monoxide and nuclear aerosols in the containment atmosphere, there are still open knowledge gaps with regard to understanding the effect of carbon monoxide on the efficiency of PAR operation.

Previous research on the effect of carbon monoxide on PAR operation has revealed the complex nature of this interaction (Reinecke et al., 2018; Liang et al., 2020; Klauck et al., 2021). Basically, three regimes have been identified. Firstly, unaffected competing hydrogen and carbon monoxide reaction with oxygen to form water and carbon dioxide has been observed in oxygen-rich atmosphere when the catalyst temperature is sufficiently high. When the oxygen concentration falls below the value required for optimum conversion of hydrogen and carbon monoxide (i.e. oxygen-lean conditions), competitive hydrogen and carbon monoxide reactions occur, which yields smaller reaction rates than in oxygen-rich conditions. Finally, catalyst deactivation due to catalyst poisoning by carbon monoxide could be observed when the catalyst temperature falls below a certain threshold value.

Klauck et al. (2014) have studied the effect of carbon monoxide on the operation of PARs under oxygen-rich conditions and found that the hydrogen recombination takes place without interference, while carbon monoxide is simultaneously converted to carbon dioxide. This AMHYCO Task 3.2 focuses on the effect of carbon monoxide on the operation of PARs under oxygen-lean conditions. These conditions are characterized by the fact that there is not enough oxygen available to the recombiner, which would allow optimal conversion of hydrogen and carbon monoxide. As a consequence, these conditions can lead to a so-called poisoning of the catalyst, which is caused by persistent adsorption of carbon monoxide on the catalyst surface, thus, preventing adsorption of oxygen in a sufficient amount. Specifically, the exact conditions to distinguish between the above-mentioned regimes, which are expected to depend on gas composition, temperature and pressure, need to be further clarified in detail.

To support the subsequent AMHYCO Work Package 4, related to the assessment of late-phase scenarios, the numerical models describing PAR operation need to be enhanced and validated. A first step into this direction had been taken within the PAR model development exercise in the framework of the SAMHYCO-NET project (Reinecke et al., 2022). In the present work, the further development of the numerical models is based on a broader experimental database with a specific focus on severe accident sequences with high combustion risk.

2.1. Expected boundary conditions

At the start of Task 3.2, an initial test matrix for the experimental program has been defined based on the range of boundary conditions of severe accident scenarios presented by A. Bentaib (2020), see Table 1.

Table 1. Relevant	conditions durin	ng severe	accident late	phases scenarios

	Lower value	Upper value
Hydrogen fraction	0.26 vol.%	8 vol.%
Oxygen fraction	1.2 vol.%	6 vol.%
Carbon monoxide fraction	3.5 vol.%	6 vol.%
Temperature	350 K	420 K
Abs. pressure	1.2 bar	6.6 bar

In the further course of the AMHYCO project, the accident sequence simulations of three PWR designs performed in WP2 served as a base to further refine and consolidate the test matrix (Herranz & Fontanet, 2022). Four accident scenarios have been considered in WP2, which involve specifically high combustion risks. From the simulation results based on a PWR of Westinghouse design ("PWR-W"), the identified scenarios were SBO, SBLOCA and LBLOCA, while an SBLOCA scenario was considered for PWR of KWU design ("PWR-KWU"). A review of the results was performed in Task 3.2 focusing on the range of relevant parameters in the ex-vessel phase (Table 2).

It is important to mention that the simulations did not consider the operation of PARs during both in-vessel and ex-vessel phase. Hence, the concentrations of oxygen, hydrogen and carbon monoxide yield unrealistic high values to shape an experimental program for PAR operation. Furthermore, the temperatures, ranging overall between 40 °C and 140 °C, could be considered to be higher in case of exothermal PAR operation.

Table 2. Relevant conditions during severe accident late phase scenarios

	PWR-KWU SBLOCA	PWR-W SBO	PWR-W SBLOCA	PWR-W LBLOCA
Pressure	1.7-2.3 bar	3.0-3.7 bar	1.8-2.7 bar	1.2-3.2 bar
Temperature	70-90 °C	120-140 °C	70-100 °C	40-100 °C
H ₂	5-17 vol.%	6-10 vol.%	4-11 vol.%	6-13 vol.%
CO (max.)	7 vol.%	9 vol.%	11 vol.%	13 vol.%
H ₂ /CO ratio	> 3	> 1	> 1	1
0,	13-9 vol.%	8-5 vol.%	12-8 vol.%	17-7 vol.%
H _O _{2 vap}	15-30 vol.%	60-35 vol.%	15-60 vol.%	5-30 vol.%

Especially the hydrogen/carbon monoxide ratio is interesting as it excludes scenarios with carbon monoxide fractions higher than hydrogen fractions.

Two specific aspects relevant for PAR operation have been further analysed: oxygen starvation and PAR ignition.

2.1.1.Oxygen starvation

In the context of PAR operation, oxygen-lean conditions (or "low-oxygen conditions") are defined as gas mixtures where the oxygen fraction is below the value that is required for optimum conversion of hydrogen and/or carbon monoxide.

If reaction kinetics is diffusion-controlled, which is the case in almost the entire range of PAR operation, the recombination rate \dot{r} of species i is equal to the species diffusion rate $\dot{n}_{D,i}$ through the boundary layer from the gas bulk to the catalytic surface. The recombination rate can be expressed with a mass transfer approach as

$$\dot{r}_i = \dot{n}_{D,i} = Sh \cdot \frac{D_{i,m}}{d} \cdot C_i, \tag{2.1}$$

where Sh is the dimensionless Sherwood number, $D_{i,m}$ is the diffusion coefficient of species i in the gas mixture in m^2/s , d is the characteristic geometric value in m, and C_i is the bulk concentration of species i in mol/m³ (Reinecke et al., 2004). Hence, the individual species molar

flows to the catalytic surface can be expressed by the diffusion coefficients and the volumetric/molar fraction y_i :

$$\dot{n}_{D,i} \sim D_{i,m}^{2/3} \cdot y_i.$$
(2.2)

The exponent of $\frac{2}{3}$ is a result of the fact that the diffusion coefficient also appears in the denominator of the dimensionless Schmidt number Sc, which is part of typical correlations to calculate Sh (with an exponent of $\frac{1}{3}$).

According to the reaction equation of hydrogen recombination

$$H_2 + \frac{1}{2}O_2 \to H_2O$$
 (2.3)

the minimum oxygen diffusion rate enabling optimum hydrogen recombination can be written as

$$\dot{n}_{O_2} \ge \frac{1}{2} \dot{n}_{H_2}. \tag{2.4}$$

Using eq. 2.2 in eq. 2.4, we obtain

$$y_{O_2} \ge \frac{1}{2} \left[\left(\frac{D_{H_2}}{D_{O_2}} \right)^{2/3} \cdot y_{H_2} \right].$$
 (2.5)

In case of presence of carbon monoxide, oxygen is also required in the competing reaction

$$CO + \frac{1}{2}O_2 \to CO_2$$
. (2.6)

Consequently, the minimum oxygen diffusion rate can now be expressed as

$$\dot{n}_{O_2} \ge \frac{1}{2}\dot{n}_{H_2} + \frac{1}{2}\dot{n}_{CO} \tag{2.7}$$

and we obtain

$$y_{O_2} \ge \frac{1}{2} \left[\left(\frac{D_{H_2}}{D_{O_2}} \right)^{2/3} \cdot y_{H_2} + \left(\frac{D_{CO}}{D_{O_2}} \right)^{2/3} \cdot y_{CO} \right].$$
 (2.8)

If we insert values for the diffusion coefficients according to Fuller, Schettler and Giddings (1966), we obtain the correlations

$$y_{O_2} \ge 1.19 \cdot y_{H_2} \tag{2.9}$$

and

$$y_{O_2} \ge 1.19 \cdot y_{H_2} + 0.49 \cdot y_{CO}$$
, (2.10)

respectively.

While in oxygen-rich conditions the PAR recombination rate depends linearly on the concentration of combustible gases, under oxygen-lean conditions, the recombination rate depends linearly from the oxygen fraction. The transition of hydrogen-limited to oxygen-limited recombination can be seen in Figure 1 (Nobrega, 2022), where, instead of recombination rate, the catalyst temperature is plotted, which, however, are closely linked.

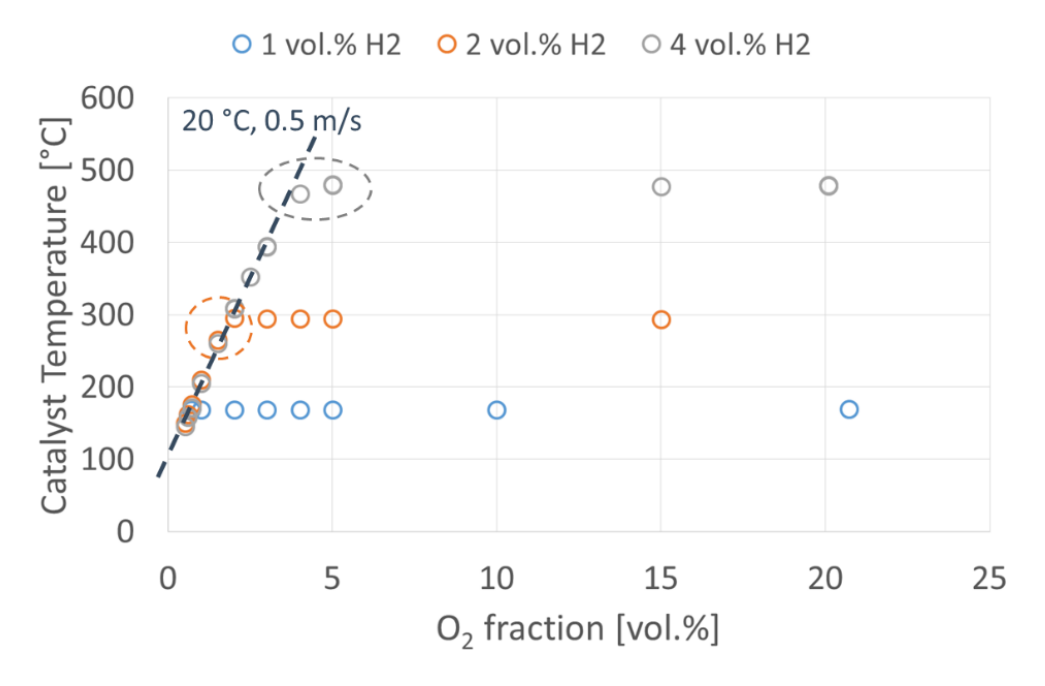


Figure 1. Oxygen starvation: Effect of oxygen fraction on catalyst temperature (REKO-1)

The transition from oxygen-rich to oxygen-lean can as well be observed in the THAI HR-11 experiment (Figure 2). The first injection/depletion phases take place in oxygen-rich atmosphere. The second injection phase starts in oxygen-rich atmosphere as well (two red points at 2 and 3 vol.% hydrogen). When the hydrogen concentration is 3 vol.%, the oxygen concentration needs to be at least 3.6 vol.% according to eq. 2.9. The measurement yields 4.3 vol.%, hence above the threshold value. For the next hydrogen concentration (4 vol.%), eq. 2.9 yields a threshold value of 4.8 vol.% oxygen. However, the oxygen concentration was measured to be 4.1 vol.%, and the significant drop of the catalyst temperature confirms the transition to oxygen-lean conditions.

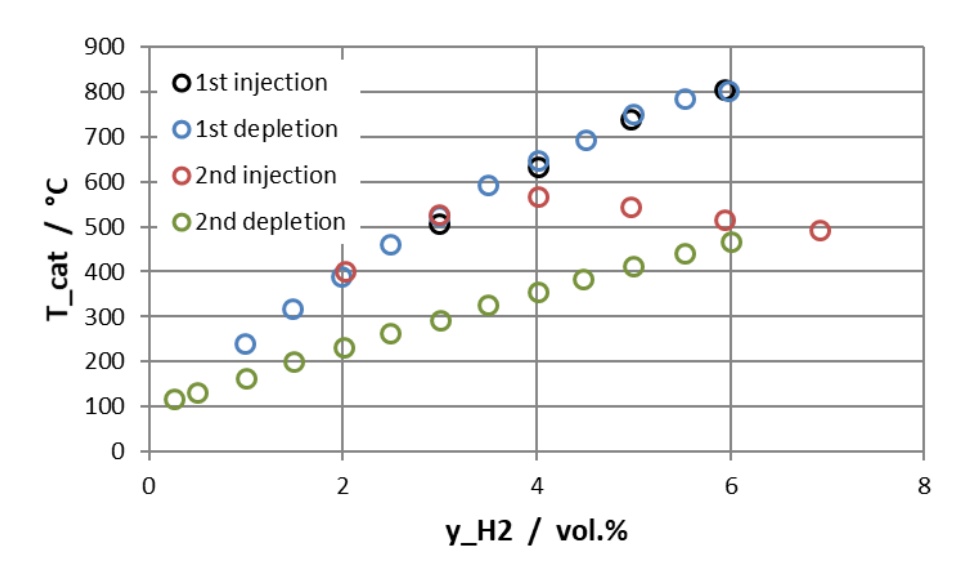


Figure 2. Oxygen starvation: Effect of oxygen fraction on catalyst temperature (THAI HR-11)

Using eqs. 2.9 and 2.10, the simulated accident sequences have been analysed in order to identify periods of oxygen starvation. Figs. 3-6 show the relevant simulation results with ranges of oxygen-lean atmospheres marked. It becomes obvious that in all considered scenarios oxygen-lean conditions are reached shortly after MCCI starts.

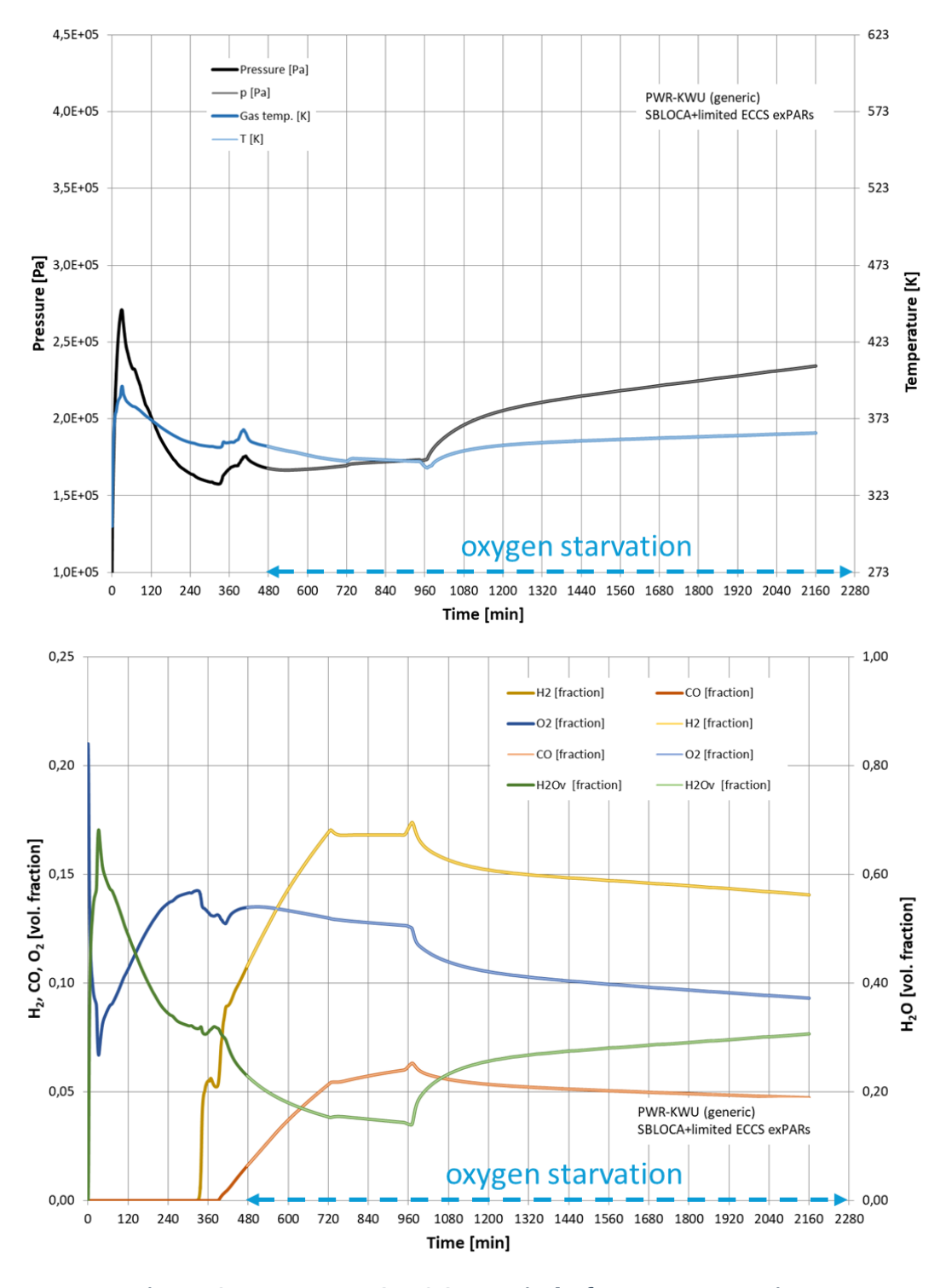
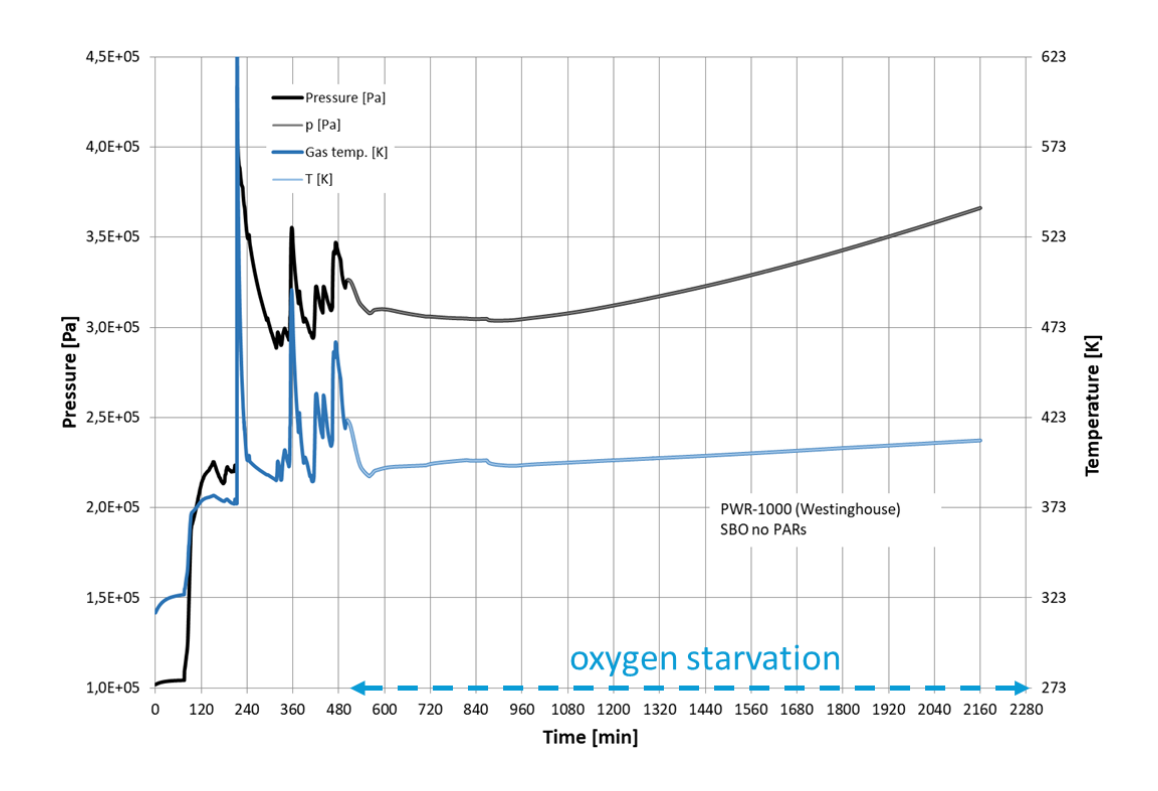


Figure 3. PWR-KWU SBLOCA: Period of oxygen starvation



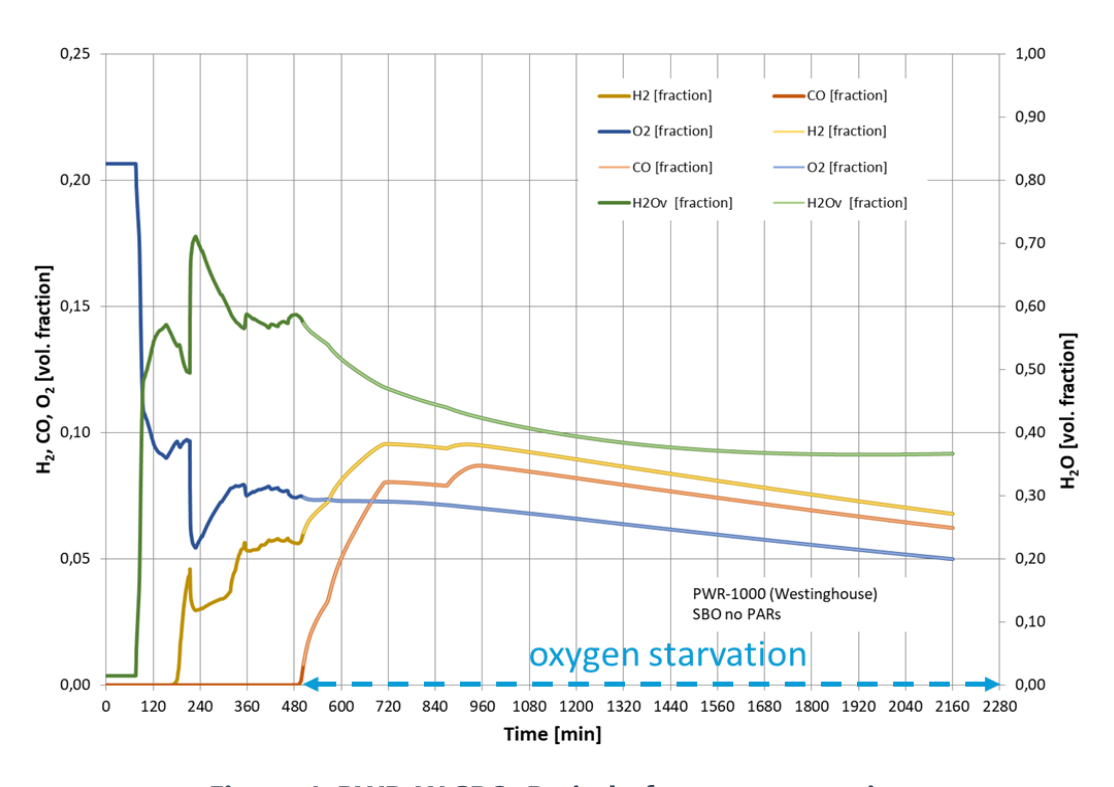
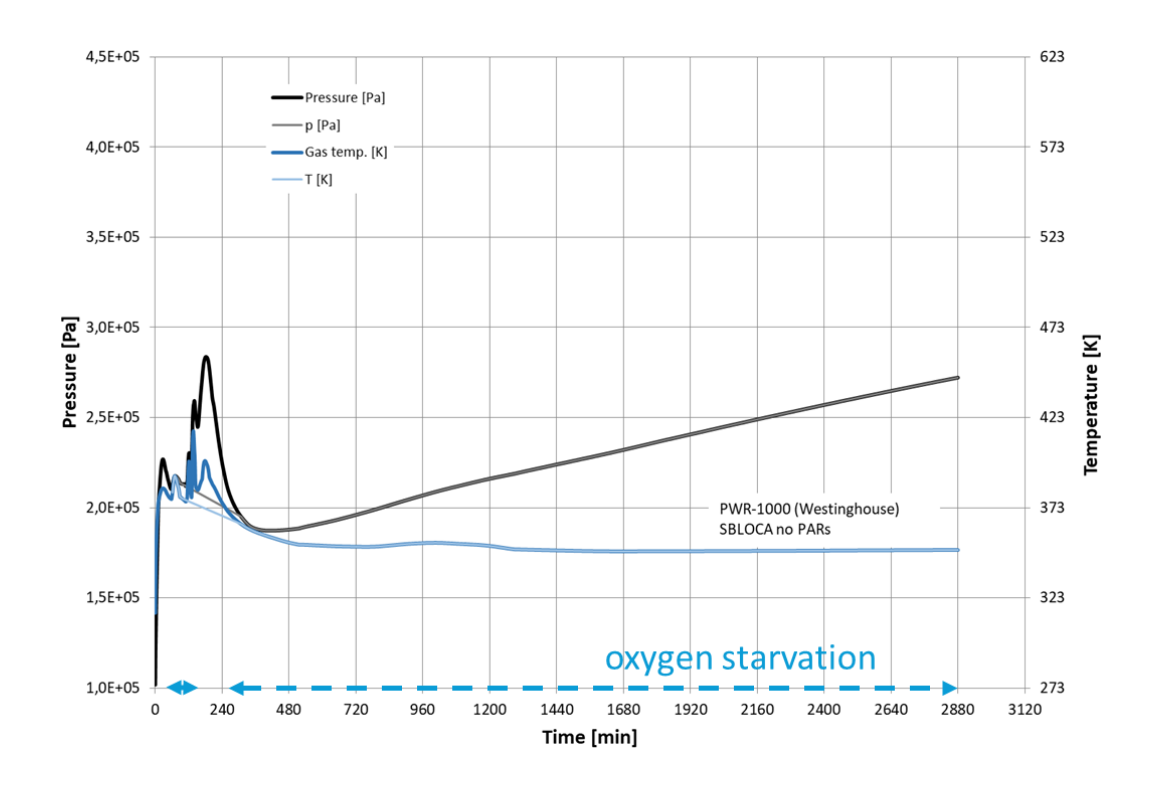


Figure 4. PWR-W SBO: Period of oxygen starvation



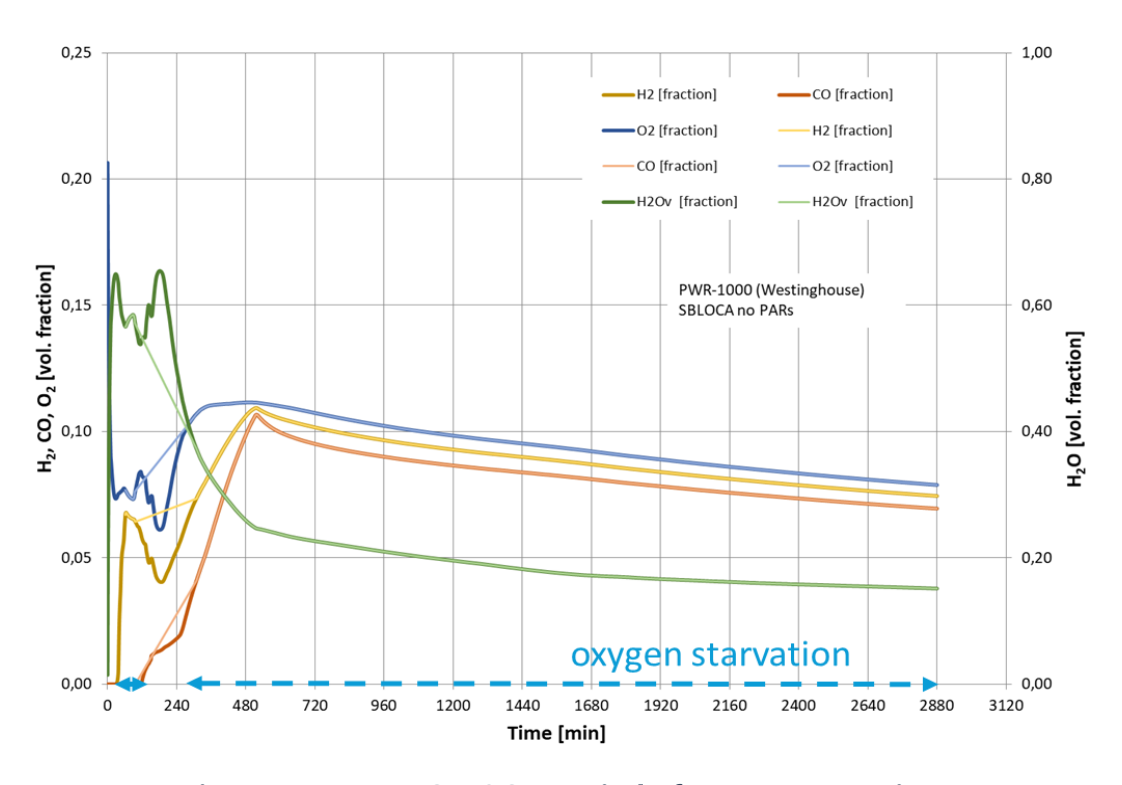
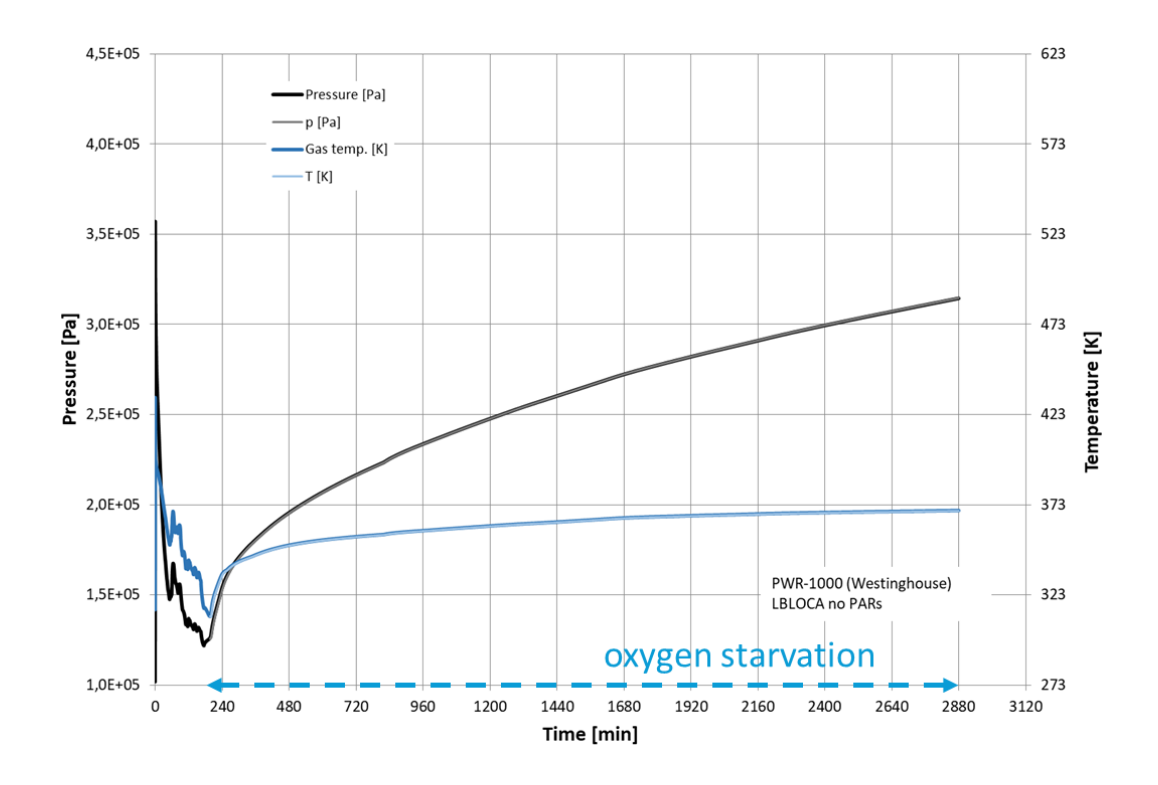


Figure 5. PWR-W SBLOCA: Period of oxygen starvation



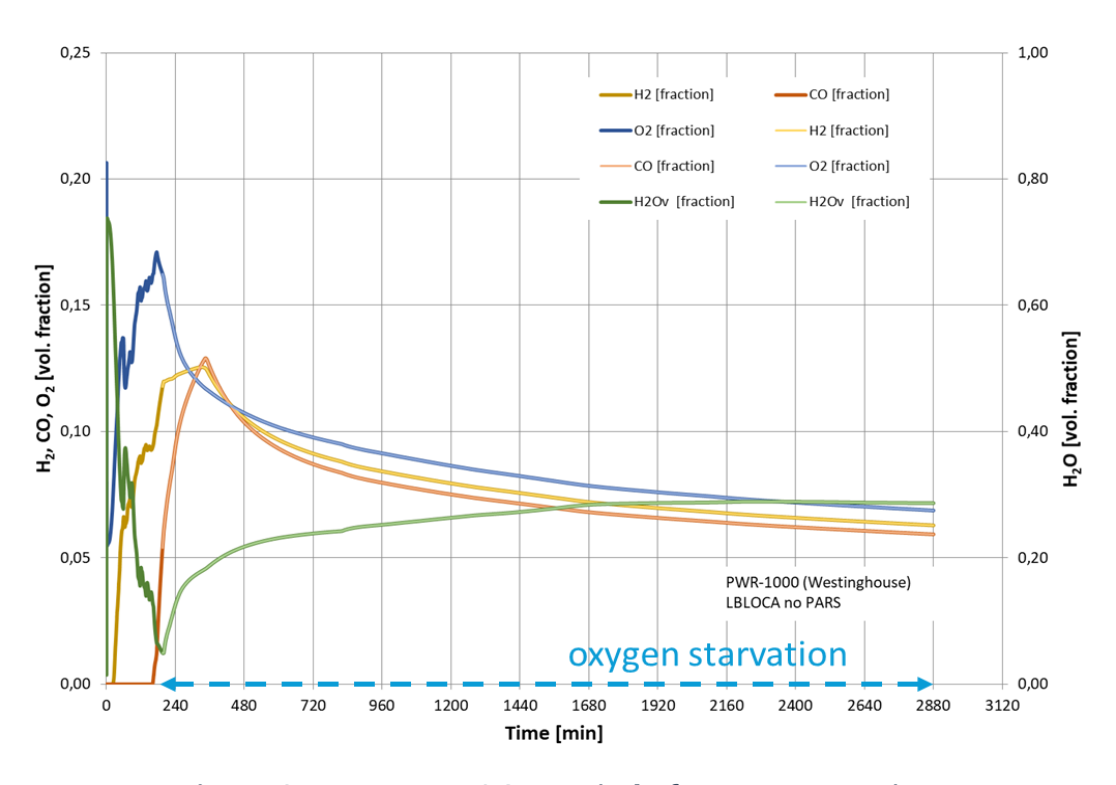


Figure 6. PWR-W LBLOCA: Period of oxygen starvation

2.1.2.PAR ignition

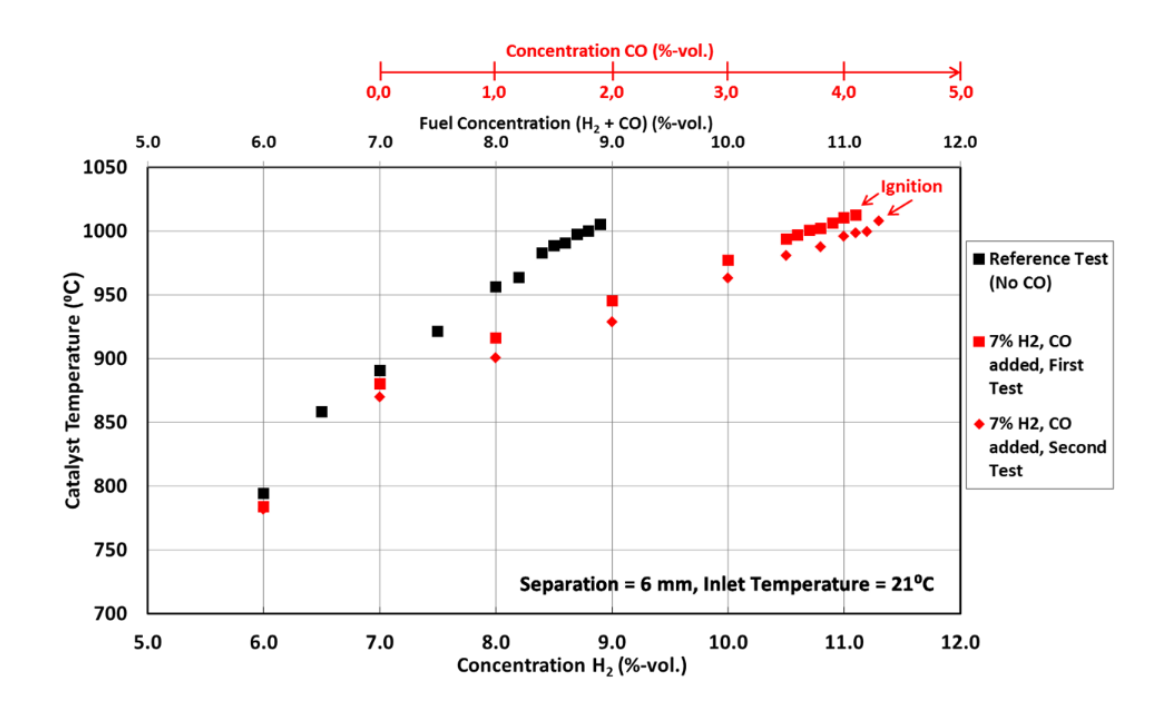
In the context of PAR operation, PAR ignition is defined as initiation of a homogeneous combustion process by hot catalysts and/or PAR structures. Depending on the specific PAR design, the threshold hydrogen concentration for PAR ignition increases with the steam concentration.

To determine the potential of PAR ignition in the presence of carbon monoxide, 0.5 vol.% can be added to the actual hydrogen fraction for each vol.% of carbon monoxide, as has been shown in an experimental study (Chakraborty et al., 2017; Chakraborty, 2020). Figure 7 shows ignition induced by catalytic sheets for 9 vol.% hydrogen, a mixture of 8 vol.% hydrogen and 2.2 vol.% carbon monoxide, and a mixture of 7 vol.% hydrogen and 4.1 vol.% carbon monoxide, respectively.

It should be noted that above mentioned threshold values are only valid if the PAR is operating in oxygen-rich conditions (see section 2.1.1). Further conditions have to be fulfilled for flame propagation to occur inside the containment.

The simulated accident sequences have been analysed accordingly in order to identify periods of possible PAR ignition (Figs. 8 - 11). In a conservative approach, the threshold value has been set to 6.5 vol.%, which is a typical value for PAR ignition under dry conditions for a Framatome PAR.

In contrast to the oxygen starvation analysis, the picture here is very divers. While PAR ignition is possible right at the beginning of MCCI for the SBLOCA scenario in PWR-KWU, it would for the PWR-W only occur approx. 2 h after MCCI start. For the PWR-W LBLOCA scenario, PAR ignition is already possible well before the MCCI, while no PAR ignition could occur in the PWR-W SBO scenario due to the low oxygen fraction in the whole transient.



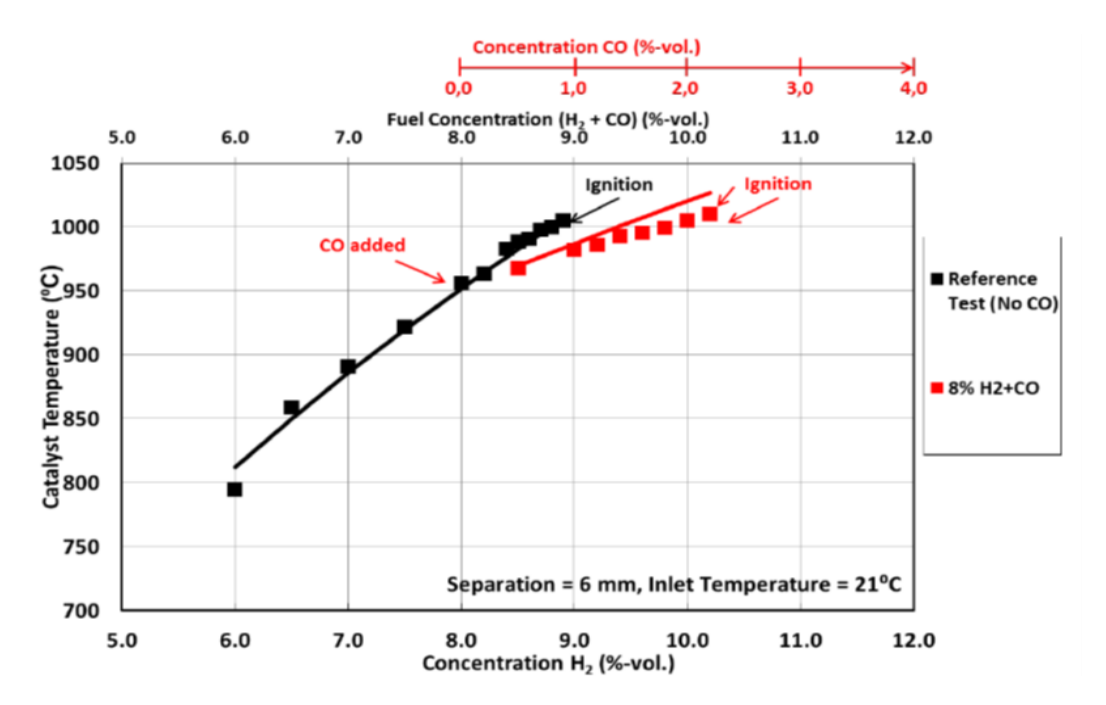
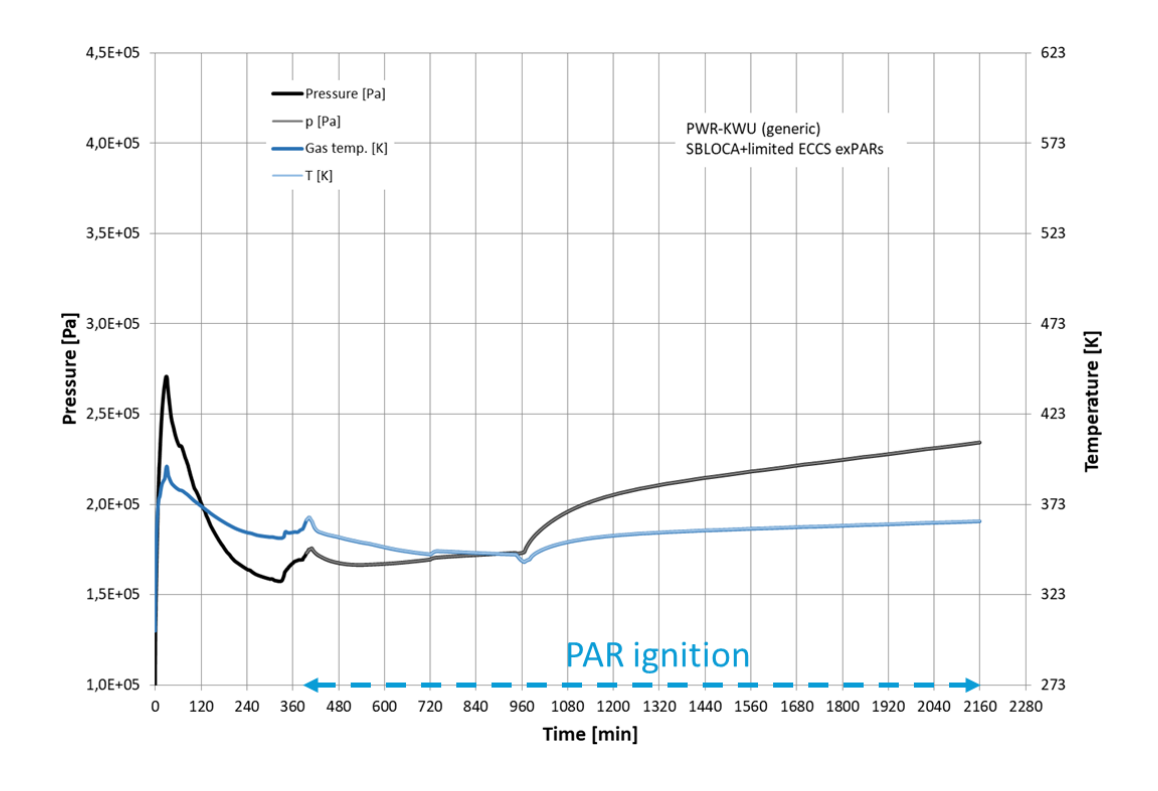


Figure 7. PAR ignition: Concentration threshold for hydrogen/carbon monoxide mixtures



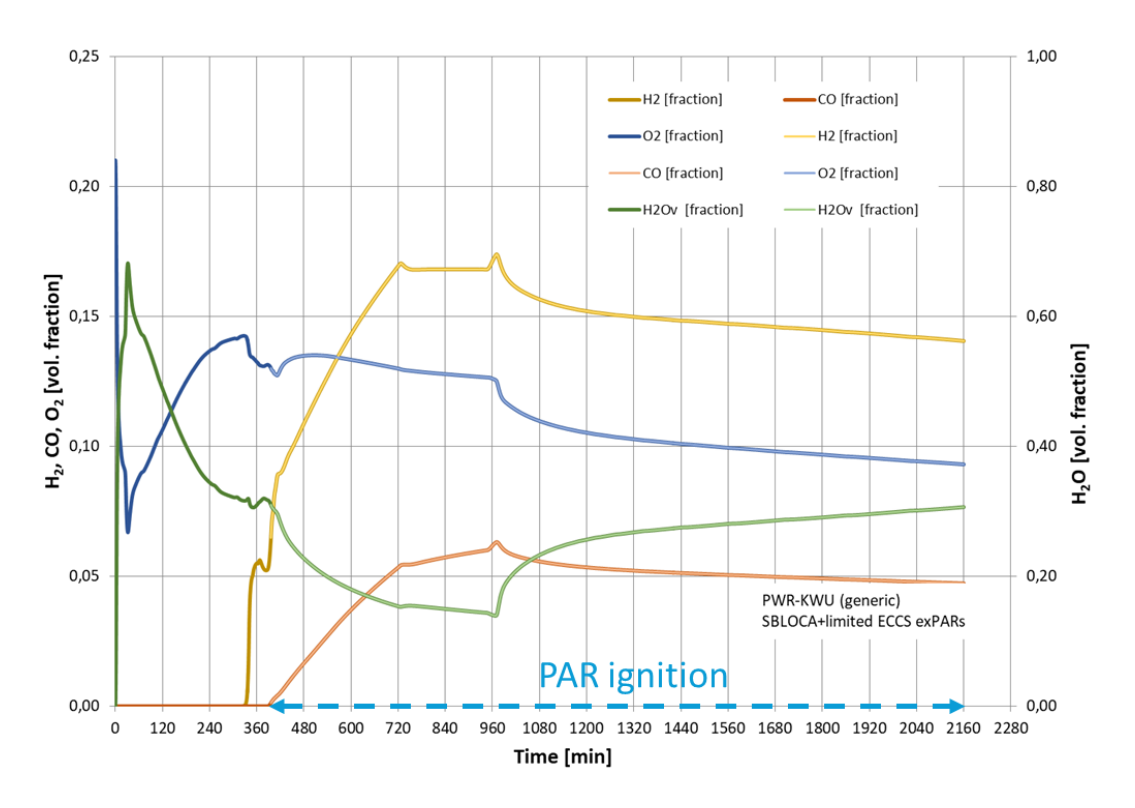
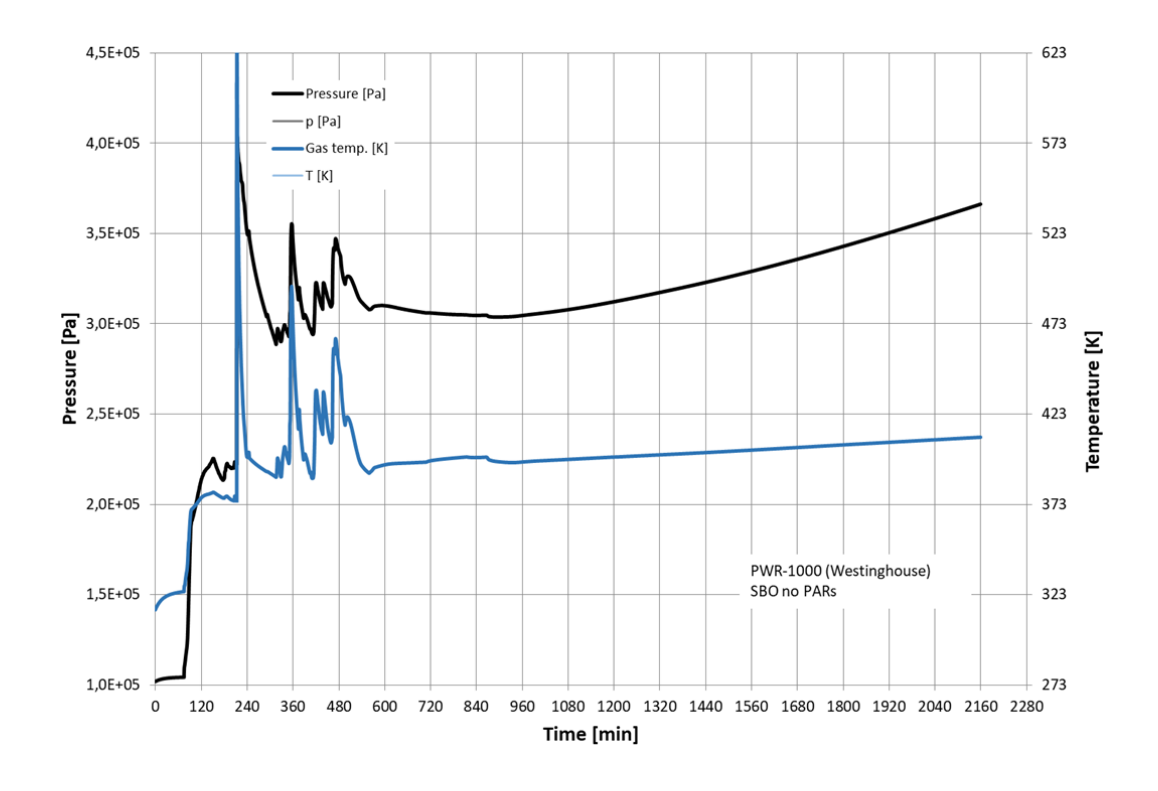


Figure 8. PWR-KWU SBLOCA: Period of potential PAR ignition



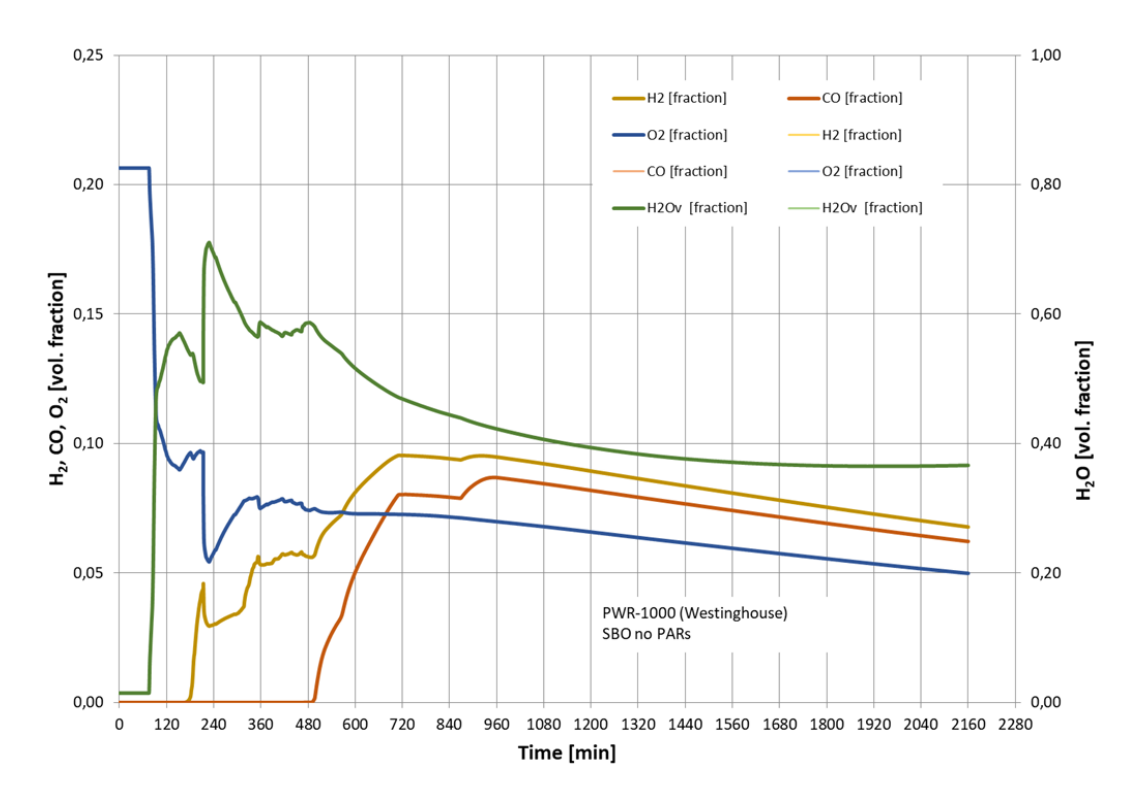
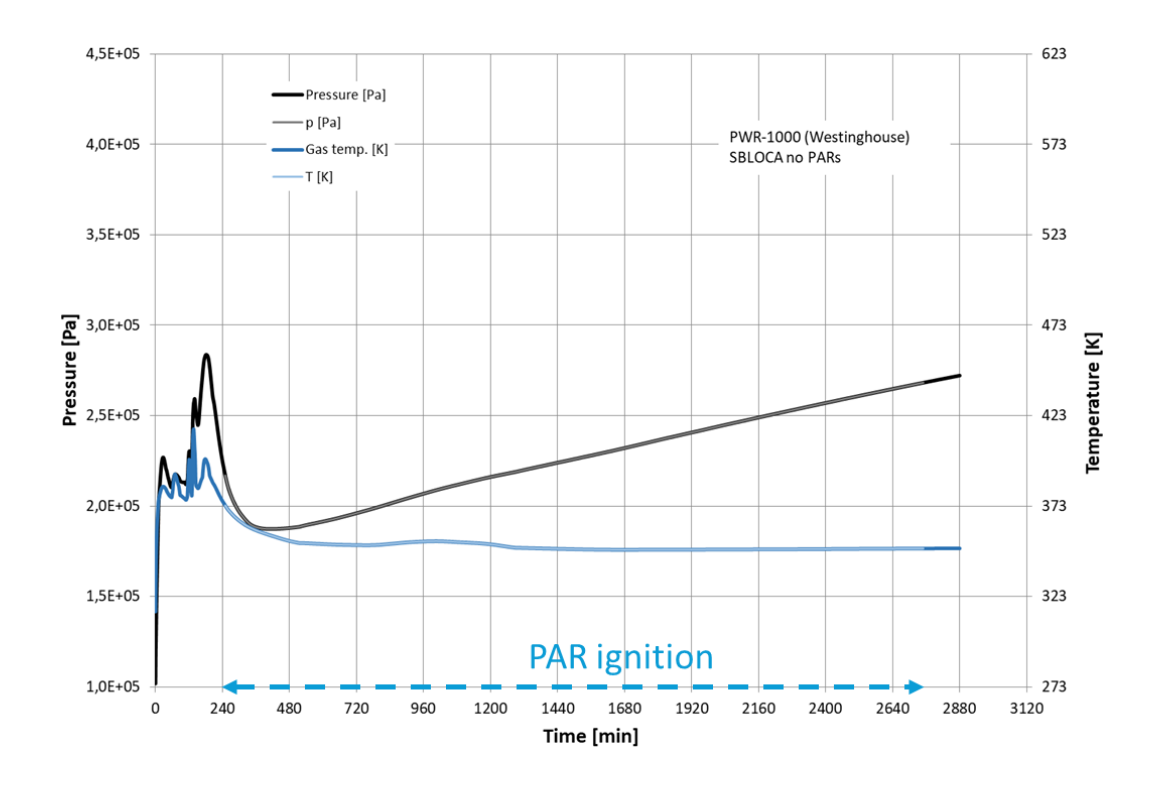


Figure 9. PWR-W SBO: Period of potential PAR ignition



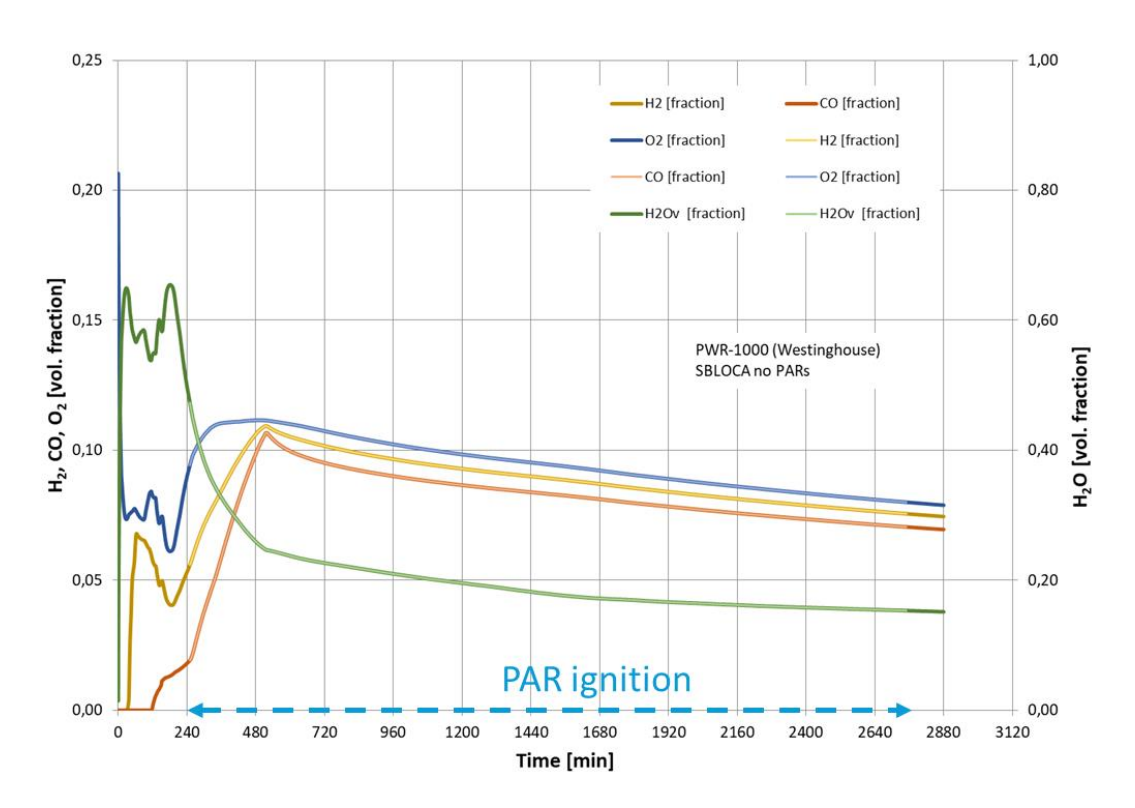
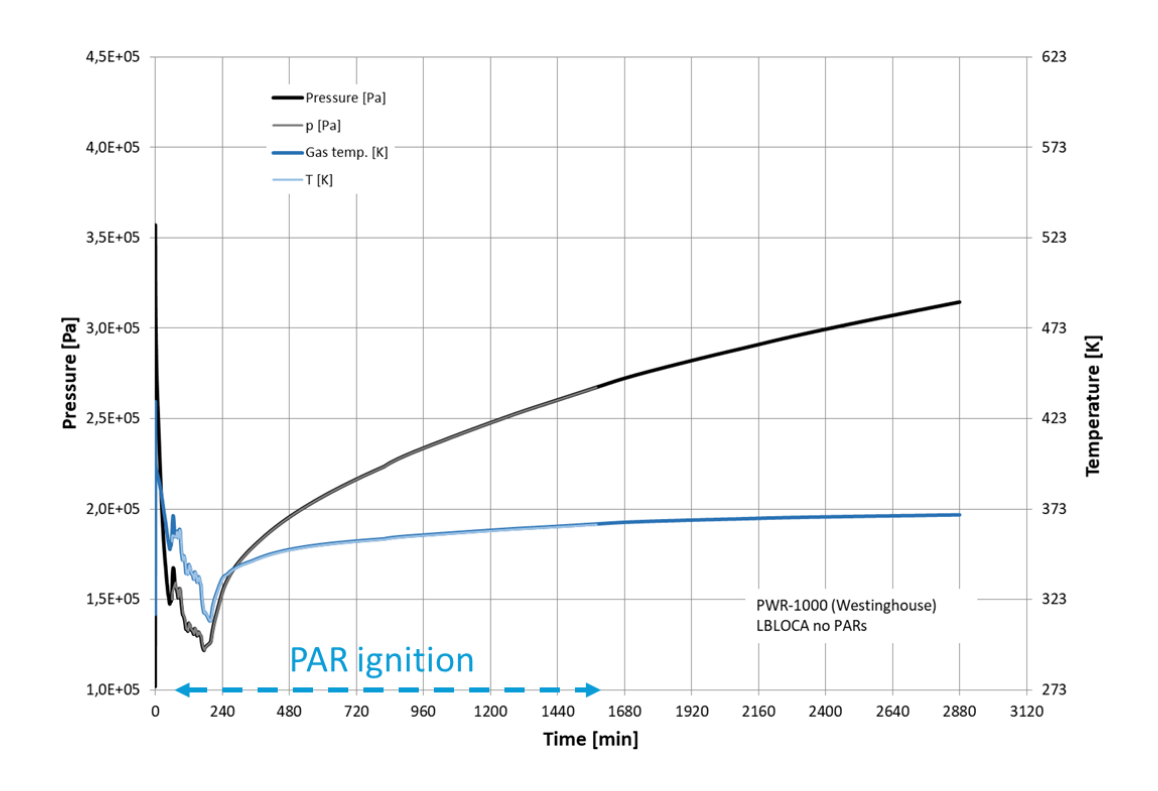


Figure 10. PWR-W SBLOCA: Period of potential PAR ignition



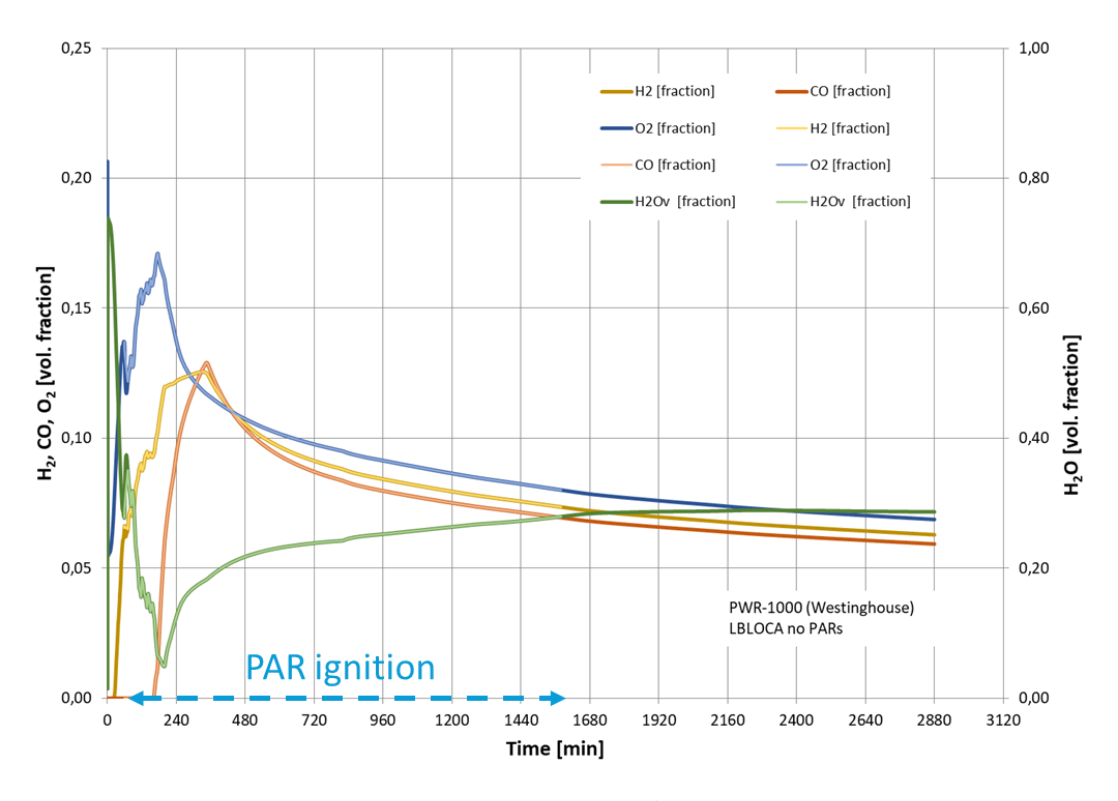


Figure 11. PWR-W LBLOCA: Period of potential PAR ignition

2.1.3. Conclusions from scenario analyses

The analyses of the results of the accident scenario simulations obtained from WP2 led to the following conclusions with regard to the design of the experimental program:

- Almost through the entire ex-vessel phase, the atmosphere is oxygen-lean with regard to PAR operation. Consequently, the experimental program and model development needs to focus on such conditions.
- PAR models should be validated for atmospheres with temperatures between 40 °C and 140 °C, pressure up to 3.7 bar and steam at saturation.
- Hydrogen fractions are typically higher than or equal to carbon monoxide fractions.
- Potential for PAR ignition should be considered in the models with corresponding criteria, if no catalyst temperature is calculated.

At the same time, the following phenomena could be discarded from the experimental study:

- No sudden increase of the oxygen fraction was observed in the late accident phases.
 Consequently, it is not necessary to study if a potentially poisoned catalyst could be reactivated if a transition from oxygen-lean to oxygen-rich would occur.
- None of the scenarios gives indication that a second hydrogen and/or carbon monoxide generation phase might occur after the PARs have stopped operation. Consequently, no experiments are required to study PAR start-up, e.g. in the presence of carbon monoxide.

2.2. Numerical PAR models

The Framatome PAR (Framatome, 2019) is the dominant PAR type installed in European nuclear power plants with a large experimental database available from the OECD/NEA THAI projects (Gupta et al., 2016). Framatome has developed a numerical correlation model describing both hydrogen and carbon monoxide recombination rates. This correlation model is one of the PAR models implemented in the ASTEC code developed by IRSN for severe accident simulation (Chatelard et al., 2014) as well as in other accident codes used in the framework of AMHYCO. Furthermore, the PAR codes PARUPM (developed by UPM), REKO-DIREKT (developed by FZJ), and SPARK (developed by IRSN) were used. These codes are suitable to simulate the operation of PARs with plate-type catalyst elements, as used in Framatome PARs.

Referring to "Framatome PAR" or "Framatome PAR correlation" always refers to the technology of PARs originally developed by Siemens KWU, later AREVA and today Framatome.

2.2.1.Framatome correlation

To describe the PAR recombination rates of Framatome PAR in terms of hydrogen mass converted over time (in g/s) an empirical equation was deduced (Mimouni et al., 2011):

$$\frac{dm_{H2}}{dt} = -\frac{\eta}{1000} \cdot X \cdot (A \cdot p + B) \cdot tanh[100 \cdot (X - X_{min})]$$
 (2.11)

The correlation considers a linear dependence on the absolute pressure p (in bar) on the recombination rate. Different PAR sizes are considered by variation of the parameters A and B. The relevant gas concentration X (in units of vol%) depends either on the gas concentration of oxygen (X_{O2}) , on hydrogen (X_{H2}) , or an upper cut-off of 8 vol% is set:

$$X = min(X_{H2}, 2 \cdot X_{O2}, 0.08). \tag{2.12}$$

The dimensionless efficiency factor η considers oxygen-rich (X_{H2} < X_{O2} ; η = 1) and oxygen-lean mixtures (X_{H2} > X_{O2} ; η = 0.6). Further, a lower cut-off hydrogen concentration of $X_{min} \sim 0.5$ vol% is defined, at which the low gas concentration does no longer allow for PAR operation.

This empirical correlation predicts the hydrogen recombination rate of PARs with sufficient accuracy to be used in integral containment analyses, to be used in nuclear safety cases. Note that that empirical correlation is only valid for PAR of the Framatome design.

This model has been enhanced by Framatome with a corresponding correlation for the conversion of carbon monoxide to carbon dioxide. Partners of the SAMHYCO-NET project (Reinecke et al., 2022) have obtained a detailed model description. Due to the contractual agreement between the project partners within the framework of SAMHYCO-NET, the CO part of the correlation and the related interactions with the hydrogen correlation cannot be published in the present report.

Research activities in the SAMHYCO-NET work package "Mitigation" were related to the performance of passive auto-catalytic recombiners in the presence of hydrogen/carbon monoxide mixtures. In the course of three validation steps, both hydrogen and carbon monoxide recombination rates have been well reproduced by the correlation model for oxygen-rich conditions. However, under oxygen-lean conditions the model shows significant deviations from the experimental data, mostly over-predicting the recombination rates.

2.2.2.PARUPM

PARUPM (Jiménez, 2007) is a non-proprietary code developed at the Universidad Politécnica de Madrid (UPM) that uses a physicochemical model, based on surface-chemistry involving platinum-based catalytic surfaces and gaseous mixtures of hydrogen, carbon monoxide, air, steam and carbon dioxide, to numerically simulate the behaviour of a PAR device.

The PAR itself is considered a series of vertical parallel plates which form vertical flow channels (Jiménez et al., 2007). PARUPM considers relevant phenomena involved in PAR operation: convective/diffusive heat and mass transfer between the gaseous mixture and the catalytic surface in a vertical flow driven by the chimney model, the adsorption/desorption of species on the plate surface, chemical surface reactions with subsequent heat release, and radiative heat exchange with the surrounding structures.

Table 3. Deutschmann simplified combustion model for methane catalysed with Pt (Deutschmann et al., 1996)

	Elemental Reaction	S _{ia}	A _i	E ^{act} _i (J/mol)
1a	$H_2 + 2 Pt(s) \rightarrow 2H(s)$	0.046	-	-
1d	$2H(s) \rightarrow H_2 + 2Pt(s)$	-	3.7×10 ¹⁷	R(8110-7220 _H)
2a	O_2 + 2 Pt(s) \rightarrow 2O(s)	0.07× (300/T)	-	-
2d	$2O(s) \rightarrow O_2 + 2Pt(s)$	-	3.7×10 ¹⁷	R(25631-7220θ _O)
3a	$H_2O + Pt(s) \rightarrow H_2O(s)$	0.75	-	-
3d	$H_2O(s) \rightarrow H_2O + Pt(s)$	-	10 ¹³	40300
IV	$OH + Pt(s) \rightarrow OH(s)$	1.00	-	-
4	$H(s) + O(s) \rightarrow OH(s) + Pt(s)$	-	3.7×10 ¹⁷	11500
5	$H(s) + OH(s) \rightarrow H_2O + Pt(s)$	-	3.7×10 ¹⁷	17400
6	$OH(s) + OH(s) \to H_2O + O(s)$	-	3.7×10 ¹⁷	48200
7a	$CO + Pt(s) \rightarrow CO(s)$	0.84	-	-
7d	$CO(s) \rightarrow CO + Pt(s)$	-	10 ¹³	125500
8d	$CO_2(s) \rightarrow CO_2 + Pt(s)$	-	10 ¹³	20500
9	$CO(s) + O(s) \rightarrow CO_2(s) + Pt(s)$	-	3.7×10 ¹⁷	105000
10	$CH_4 + 2 Pt(s) \rightarrow CH_3(s) + H(s)$	-	4.63×10 ¹⁶	-
11	$CH_3(s) + Pt(s) \rightarrow CH_2(s) + H(s)$	-	3.7×10 ¹⁷	20000
12	$CH_2(s) + Pt(s) \rightarrow CH(s) + H(s)$	-	3.7×10 ¹⁷	20000
13	$CH(s) + Pt(s) \rightarrow C(s) + H(s)$	-	3.7×10 ¹⁷	20000
14+	$C(s) + O(s) \rightarrow CO(s) + Pt(s)$	-	3.7×10 ¹⁷	62800
14-	$CO(s) + Pt(s) \rightarrow C(s) + O(s)$	-	10 ¹⁴	184000

These phenomena occur simultaneously and are resolved in a coupled manner. The coupling is carried out through expressions of the mass and energy balance at the interface between the catalytic plate and the gaseous current that runs constantly over it (Jiménez et al., 2007). PARUPM is specially tailored and developed for the surface chemistry on platinum-coated

catalyst surfaces and gaseous mixtures of H₂, CO, air, steam, and CO₂. The model is based on a simplified scheme from surface methane combustion reaction (Deutschmann et al., 1996) and heat transfer between parallel plates induced by natural convection (Elenbaas, 1942). The series of 20 reactions of the chemical model that, reduced to the species present in this application for PARs, simplifies to a total number of 10 as shown in Table 3.

2.2.3.SPARK

The SPARK (Simulation for Passive Autocatalytic Recombiners' risK) code is a CFD code dedicated to the numerical simulations of catalytic recombiners (Payot et al., 2012). The calculation tool, developed at IRSN, solves the two-dimensional steady-state Navier–Stokes equations in the vorticity-velocity formulation by including complex gas phase and surface chemistry, multicomponent transport and heat radiation (Meynet et al., 2014).

The code allows the description of the thermochemistry and transport mechanisms governing the catalytic conversion of hydrogen and carbon monoxide and to numerically predict the transition of the heterogeneous catalytic combustion regime (flameless) to the homogeneous combustion in the gas phase (with flame).

The detailed modelling allows to investigate and to predict the behaviour of recombiners during severe accidents and to evaluate the associated risks. The SPARK code had been used to study the ignition of hydrogen by recombiners for different gas mixtures, to investigate the interaction of recombiners with carbon monoxide, to predict the performance of recombiners for various thermo-hydraulic conditions, and other applications that allow the evaluation of the recombiners behaviour (Meynet, 2015).

The numerical domain is a consequence of the box-type PAR geometry with a row of vertical catalytic sheets as show in Figure 12. Infinitely thin catalytic sheets are assumed in order to neglect possible horizontal solid heat conduction. Since external heat losses are not considered, the flow can be assumed to be symmetrical so the numerical domain is reduced to half channel between two catalytic sheets in the median plane of the recombiner.

The surface mechanism used for the catalytic oxidation of hydrogen and carbon monoxide over platinum was developed by Deutschmann et al. (1996). It contains 8 surface species and 8 gaseous species and consists of 20 reactions (Table 4, left). The kinetic-chemical mechanism used for the homogeneous combustion of hydrogen and carbon monoxide in air was proposed by Warnatz et al. (1996) and consists of 12 gaseous species and 31 reactions as proposed Table 4, right).

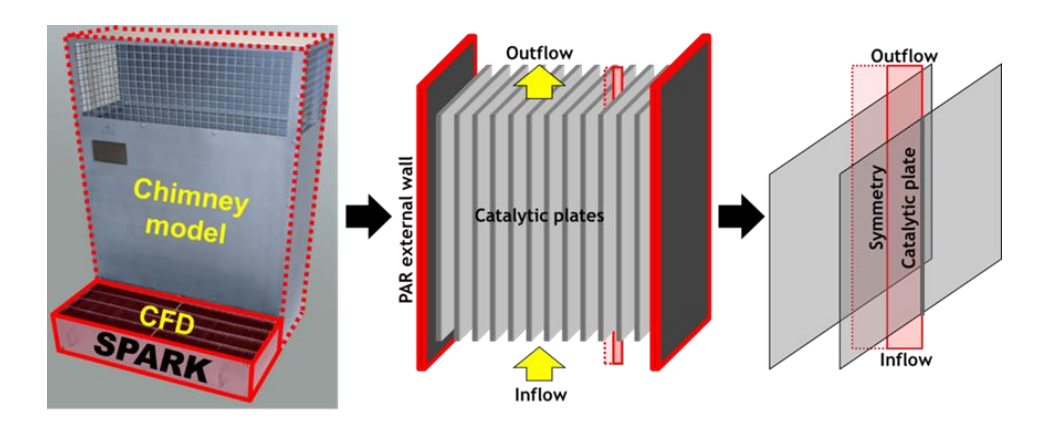


Figure 12. SPARK: Recombiner configuration and numerical domain

Table 4. SPARK: Reaction mechanisms for the catalytic oxidation of H₂ and CO over Pt (left); Reaction mechanism for the gaseous combustion of H2 and CO (right)

Ads	orption reactions ^a	S	
1°.	$H_2 + 2Pt^{(s)} \rightarrow 2H^{(s)}$	0.046	
2.	$H+Pt^{(s)}\!\to H^{(s)}$	1.000	
3.	$O_2 + 2Pt^{(s)} \rightarrow 2O^{(s)}$	0.023	
4 ^d .	$O_2 + 2Pt^{(s)} \rightarrow 2O^{(s)}$	0.070	
5.	$O + Pt^{(s)} \rightarrow O(s)$	1.000	
6.	$H_2O + Pt^{(s)} \rightarrow H_2O^{(s)}$	0.750	
7.	$OH + Pt^{(s)} \rightarrow OH^{(s)}$	1.000	
8e.	$CO + Pt^{(s)} \rightarrow CO^{(s)}$	0.840	
Surface reactions ^b		A	Е
9.	$H^{(s)} + O^{(s)} \Leftrightarrow OH^{(s)} + Pt^{(s)}$	3.7 10 ²¹	2749
10.	$H^{(s)} + OH^{(s)} \Leftrightarrow H_2O^{(s)} + Pt^{(s)}$	$3.7 \ 10^{21}$	4159
11.	$OH^{(s)} + OH^{(s)} \Leftrightarrow H_2O^{(s)} + O^{(s)}$	$3.7 \ 10^{21}$	11520
12.	$CO^{(s)}+O^{(s)} \rightarrow CO_2^{(s)}+Pt^{(s)}$	$3.7 \ 10^{21}$	25096
13.	$C^{(s)} + O^{(s)} \rightarrow CO^{(s)} + Pt^{(s)}$	$3.7 \ 10^{21}$	15010
14.	$CO^{(\mathfrak{s})} + Pt^{(\mathfrak{s})} \to C^{(\mathfrak{s})} + O^{(\mathfrak{s})}$	$1.0\ 10^{18}$	43977
Desorption reactions ^b		A	E
15.	$H^{(s)} + H^{(s)} \rightarrow H_2 + 2Pt^{(s)}$	3.7 10 ²¹	16109 – 1434 σ _H
16.	$O^{(s)} + O^{(s)} \rightarrow O_2 + 2Pt^{(s)}$	$3.7 \ 10^{21}$	$50908 - 14340 \sigma_{O}$
17.	$H_2O^{(s)} \rightarrow H_2O^+ Pt^{(s)}$	$1.0\ 10^{13}$	9632
18.	$OH^{(s)} \rightarrow OH + Pt^{(s)}$	$1.0\ 10^{13}$	46128
19.	$CO^{(s)} \rightarrow CO + Pt^{(s)}$	$1.0\ 10^{13}$	30115
20.	$CO_2^{(s)} \rightarrow CO_2 + Pt^{(s)}$	$1.0\ 10^{13}$	4900
2-1	1-1		

H_2/O	2 reactions ^a	A	n	Ea
1.	$H + O_2 \Leftrightarrow O + OH$	3.55 1015	-0.40	16600
2.	$O + H_2 \Leftrightarrow H + OH$	5.0810^{04}	2.70	6290
3.	$H_2 + OH \Leftrightarrow H_2O + H$	2.1610^{08}	1.50	3430
4.	$O + H_2O \Leftrightarrow OH + OH$	$2.97\ 10^{06}$	2.00	134000
5 ^b .	$H_2 + M \Leftrightarrow H + H + M$	$4.58\ 10^{19}$	-1.40	104000
6 ^b .	$O + O + M \Leftrightarrow O_2 + M$	6.1610^{15}	-0.50	0
7 ^b .	$O + H + M \Leftrightarrow OH + M$	$4.71\ 10^{18}$	-1.00	0
8 ^b .	$H + OH + M \Leftrightarrow H_2O + M$	$3.80\ 10^{22}$	-2.00	0
9c,e.	$H + O_2 (+M) \Leftrightarrow HO_2 (+M)$	$1.48\ 10^{12}$	0.60	0
		$6.37\ 10^{20}$	-1.72	525
10.	$HO_2 + H \Leftrightarrow H_2 + O_2$	$1.66\ 10^{13}$	0.00	823
11.	$HO_2 + H \Leftrightarrow OH + OH$	$7.08 \ 10^{13}$	0.00	295
12.	$HO_2 + O \Leftrightarrow O_2 + OH$	$3.25 \ 10^{13}$	0.00	0
13.	$HO_2 + OH \Leftrightarrow H_2O + O_2$	$2.89 \ 10^{13}$	0.00	-497
14.	$HO_2 + HO_2 \Leftrightarrow H_2O_2 + O_2$	$4.20\ 10^{14}$	0.00	12000
	$HO_2 + HO_2 \Leftrightarrow H_2O_2 + O_2$	$1.30\ 10^{11}$	0.00	-1630
15 ^{b,f} .	H_2O_2 (+M) \Leftrightarrow OH + OH (+M)	$2.95\ 10^{14}$	0.00	48400
		$1.20\ 10^{17}$	0.00	45500
16.	$H_2O_2 + H \Leftrightarrow H_2O + OH$	$2.41\ 10^{13}$	0.00	3970
17.	$H_2O_2 + H \Leftrightarrow HO_2 + H_2$	4.82 1013	0.00	7950
18.	$H_2O_2 + O \Leftrightarrow OH + HO_2$	9.5510^{06}	2.00	3970
19 ^b .	$H_2O_2 + OH \Leftrightarrow HO_2 + H_2O$	$1.00\ 10^{12}$	0.00	0
	$H_2O_2 + OH \Leftrightarrow HO_2 + H_2O$	$5.80\ 10^{14}$	0.00	9560
CO r	eactions ^a	A	n	Ea
20 ^b .	$CO + O (+M) \Leftrightarrow CO_2 (+M)$	1.80 1010	0.00	2380
		$1.55 \ 10^{24}$	-2.79	4190
21.	$CO + O_2 \Leftrightarrow CO_2 + O$	$2.53\ 10^{12}$	0.00	47700
22.	$CO + HO_2 \Leftrightarrow CO_2 + OH$	3.0110^{13}	0.00	23000
23.	$\mathrm{CO} + \mathrm{OH} \Leftrightarrow \mathrm{CO_2} + \mathrm{H}$	$2.23\ 10^{05}$	1.90	-1160
HCO reactions ^a		A	n	Ea
24 ^d .	$HCO + M \Leftrightarrow H + CO + M$	$4.75\ 10^{11}$	0.70	14900
25.	$HCO + O_2 \Leftrightarrow CO + HO_2$	$7.58 \ 10^{12}$	0.00	410
26.	$HCO + H \Leftrightarrow CO + H_2$	$7.23\ 10^{13}$	0.00	0
27.	$HCO + O \Leftrightarrow CO + OH$	$3.02\ 10^{13}$	0.00	0
28.	$\text{HCO} + \text{OH} \Leftrightarrow \text{CO} + \text{H}_2\text{O}$	$3.02\ 10^{13}$	0.00	0
29.	$HCO + O \Leftrightarrow CO_2 + H$	$3.00\ 10^{13}$	0.00	0
29.		2 00 1012	0.00	0
30.	$HCO + HO_2 \Leftrightarrow CO_2 + OH + H$	3.00 1013	0.00	U

A Sticking coefficients: s. b Reaction rate coefficients: k = A exp(-E/RT) with A [mole-cm- Kelvin-sec] and E [cal/mole]. The hydrogen adsorption is first order with respect to platinum. The hydrogen attended to the total coefficient is temperature dependent: s_{02} = 0.07(T_0 /T) with T_0 =300 K. e. The carbon monoxide adsorption is second order with respect to platinum.

b Third body efficiencies: $\alpha_{\rm H2}=2.5$, $\alpha_{\rm H2O}=12.0$, $\alpha_{\rm CO}=1.9$, $\alpha_{\rm CO2}=3.8$. c Third body efficiencies: $\alpha_{\rm H2}=2.0$, $\alpha_{\rm H2O}=11.0$, $\alpha_{\rm CO}=1.9$, $\alpha_{\rm CO2}=3.8$, $\alpha_{\rm O2}=0.78$. d Third body efficiencies: $\alpha_{\rm H2}=2.5$, $\alpha_{\rm H2O}=6.0$, $\alpha_{\rm CO2}=3.9$, $\alpha_{\rm CO2}=3.8$. c Reaction 9 is a Troe reaction with $F_c=0.8$ (first entries are for high pressures). f Reaction 15 is a Troe reaction with $F_c=0.5$ (first entries are for high pressures).

2.2.4.REKO-DIREKT

REKO-DIREKT developed at FZJ is a 2D mechanistic PAR model based on Fortran 90 (Böhm, 2007). The fundamental approach of REKO-DIREKT consists of modelling the heat and mass transfer phenomena inside the catalyst section combined with a generic chimney model (Figure 13). Local reaction rates inside a single channel formed by two catalyst sheets are calculated by means of a mechanistic diffusive transport approach. This single channel is expanded to a full recombiner catalyst section to calculate, in the final step, the buoyancy-driven flow through the PAR box as well as the radiative and convective heat fluxes from the PAR to its environment. Besides the recombination rate, REKO-DIREKT provides the local gas composition as well as the catalyst temperature profile inside the PAR.

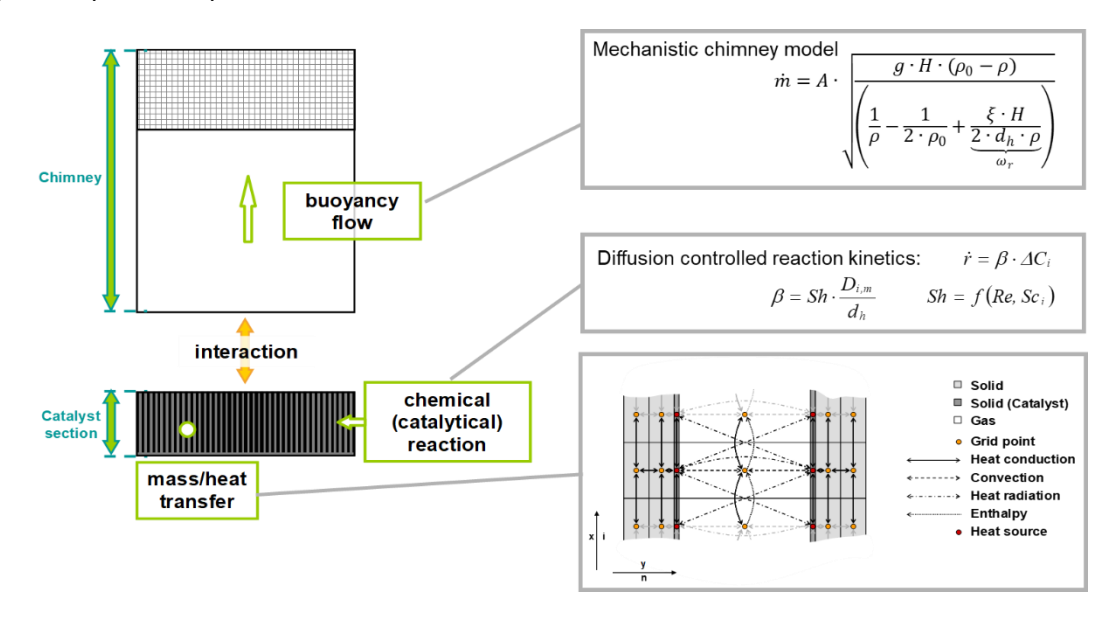


Figure 13. REKO-DIREKT: Model approach

The model in Cartesian coordinates considers the state equations in flow direction (x-direction) as well as between both adjacent plates (y-direction). Changes of the state variables along the plate across the flow direction are considered as negligible and hence not calculated. In the flow channel only one mesh in y-direction is applied in order to permit the use of empirical heat and mass transfer laws.

Heat sources resulting from the exothermal reaction are calculated in each flow mesh on the left and right boundary provided catalytic activity has been defined for the respective surface. Under the given conditions, the catalytic recombination is diffusion controlled. Consequently, the modelling of the reaction kinetics is based on a mass transfer approach instead of the Arrhenius-type approach for chemical surface reactions.

The resulting steady-state equation system is transformed into a band matrix and then solved by means of a direct closed algorithm. As this approach doesn't require spatial iterations the numerical solutions are very stable and exact.

The capabilities as well as the improvement potentials of REKO-DIREKT were demonstrated on the basis of an extensive post-calculation of the entire OECD/NEA-THAI HR test series (Reinecke et al., 2016). The model has been coupled to thermal-hydraulic codes such as COCOSYS and the CFD tools ANSYS-CFX and containmentFOAM.

3. Experimental program

The experimental program in Task 3.2 encompasses experiments in three facilities located in the Hydrogen Laboratory at Forschungszentrum Juelich (FZJ). The REKO-1 facility serves for performing scoping tests with single catalyst samples in order to obtain a basic understanding of relevant parameters. A section of catalyst sheets in representative scale is investigated in the REKO-3 facility. Finally, the REKO-4 facility allows to study phenomena influenced by chimney flow and effects of pressure.

3.1. Scoping tests

Scoping tests have been performed in the REKO-1 facility to understand the impact of parameters such as gas and catalyst temperatures, gas composition, and flow velocity on the catalyst deactivation process for both platinum- and palladium-based catalysts. Due to the small size of the catalyst samples these experiments can be carried out very efficiently in a comparatively short time. At the same time, the results are rather qualitative in nature, since e.g. geometry effects and heat radiation losses are not representatively mapped.

3.1.1. Description of the REKO-1 test facility

The REKO-1 facility is a modular flow reactor which is composed of different tube elements according to the test specifications and requirements. The facility allows the investigation of the recombination behaviour of small catalyst specimen (here: $5 \times 5 \text{ cm}^2$) under well-defined forced flow boundary conditions.

3.1.1.1. Cylindrical flow reactor

The vertical flow channel is an assembly of several cylindrical stainless-steel tube modules (German: 1.4301, AISI/SAE: 304, DIN: X5CrNi 1810) with a wall thickness of 2 mm. In the present set-up, the cylindrical channel has a total height of approx. 100 cm with an inner diameter of 70 mm (Figure 14).

Figure 15 shows the flow diagram of the set-up which consists of the instrumented cylindrical flow tube (A) embedded in a gas supply infrastructure (B). The gas flow passes through the flow reactor before entering a venting line on top. Before entering the venting line, a gas probe is continuously sampled to the gas analyser system (C) in order to determine the outlet gas composition.



Figure 14. REKO-1: Cylindrical flow reactor (left); catalyst temperature measurement (right)

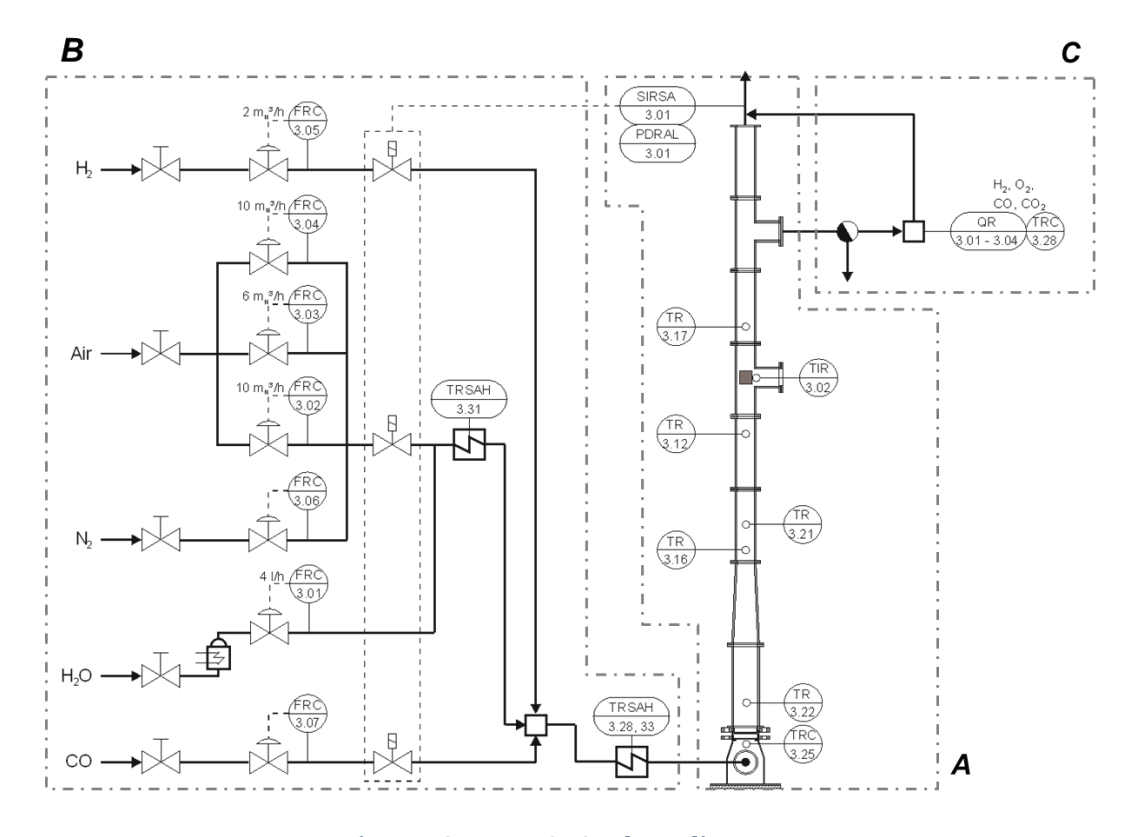


Figure 15. REKO-1: Flow diagram

3.1.1.2. **Gas supply**

The role of the gas supply is to provide a steady-state volumetric gas flow with constant gas composition and temperature. The gas supply allows the preconditioning of a mixture of different gas species, typically including air, hydrogen, nitrogen, water vapour and carbon monoxide. The gas components are fed into the system by means of mass flow controllers. A steam generator provides up to 10 L/h of water vapour. Several gas pre-heaters allow controlling the gas mixture temperature at the channel inlet.

For experiments in oxygen-lean conditions, air and nitrogen flows are mixed in order to obtain the desired oxygen concentration.

In the present set-up, the following mass flow controllers (FRC) are used to produce the gas mixture:

- Air: FRC 3.02 10 n-m³/h; FRC 3.03 6 n-m³/h; FRC 3.04 10 n-m³/h
- Nitrogen: FRC 3.06 25 n-m³/h
- Hydrogen: FRC $3.05 0.5 \text{ n-m}^3/\text{h}$ or $2.0 \text{ n-m}^3/\text{h}$
- Carbon monoxide: FRC 3.07 0.5 n-m³/h or 2.0 n-m³/h

As specified by the manufacturer, the measurement uncertainty for all mass flow controllers amounts to $\leq +/-1$ % of the measurement range.

Steam is provided by an ATHMOS-RS5 direct steam generator (company ADROP Feuchtemesstechnik GmbH) with a maximum capacity of 10 L/h (liquid water). The water flow is controlled by a Coriolis flow meter with a typical measurement uncertainty of +/- 0.15 % of the measurement range.

The REKO-1 facility operates at ambient pressure.

3.1.1.3. Instrumentation

The instrumentation includes thermocouples, a multi-component gas analyser, and a pyrometer. The most relevant measurement points are:

- Gas temperature at the channel inlet (TR 3.22)
- Gas temperature below and above the catalyst sample (TR 3.25 and TR 3.17, resp.)
- Catalyst temperature (TIR 3.02)
- Gas composition above the catalyst sample (QIR 3.01 QIR 3.04)

Gas temperature measurement

Gas temperatures are measured by means of thermocouples of type K (cromel-alumel) with a diameter of 1 mm. Thermocouples of class 2 and corresponding measurement transducers have a measurement range of up to 1372 °C. The measurement uncertainty according to the manufacturer is given in Figure 16. However, due to the heat radiation effect from the hot catalyst samples, unavoidable higher measurement errors have to be considered depending on the thermocouple position, especially below the catalyst specimen.

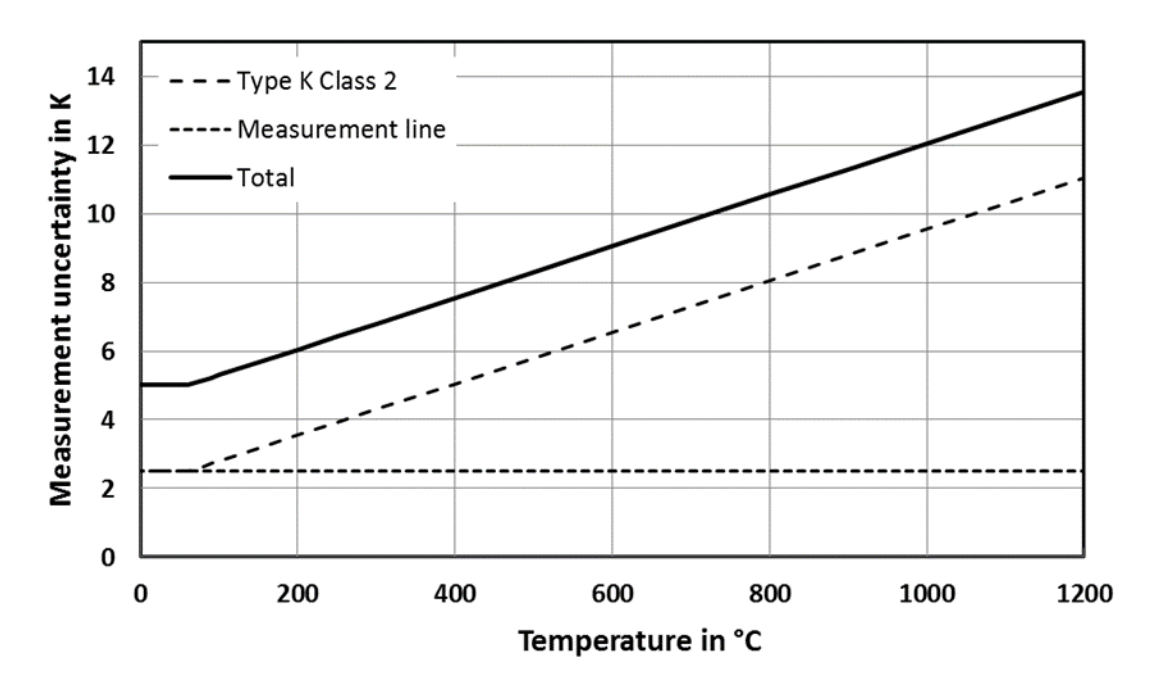


Figure 16. REKO-1: Measurement uncertainty of type K thermocouples

Catalyst temperature measurement

Catalyst temperatures are measured by means of a pyrometer with a measurement range of 70 °C to 550 °C. The pyrometer has been calibrated before the experiments in order to achieve accurate measurements. For this purpose, a thermocouple has been coupled to a catalyst sample at the same spot where the pyrometer measurement was obtained. Hydrogen/air mixtures were injected in the flow tube to cover a relevant range of catalyst temperatures by means of different hydrogen concentrations. The emissivity of the pyrometer was adjusted to obtain the same temperature measurement as indicated by the thermocouple. This procedure was performed for both platinum- and palladium-based catalyst samples and with and without steam. For dry conditions, the emissivity obtained was 60 % for the platinum catalyst and 54 % for the palladium catalyst. Figure 17 shows the agreement of temperatures for each emissivity value obtained for the Pt catalyst.

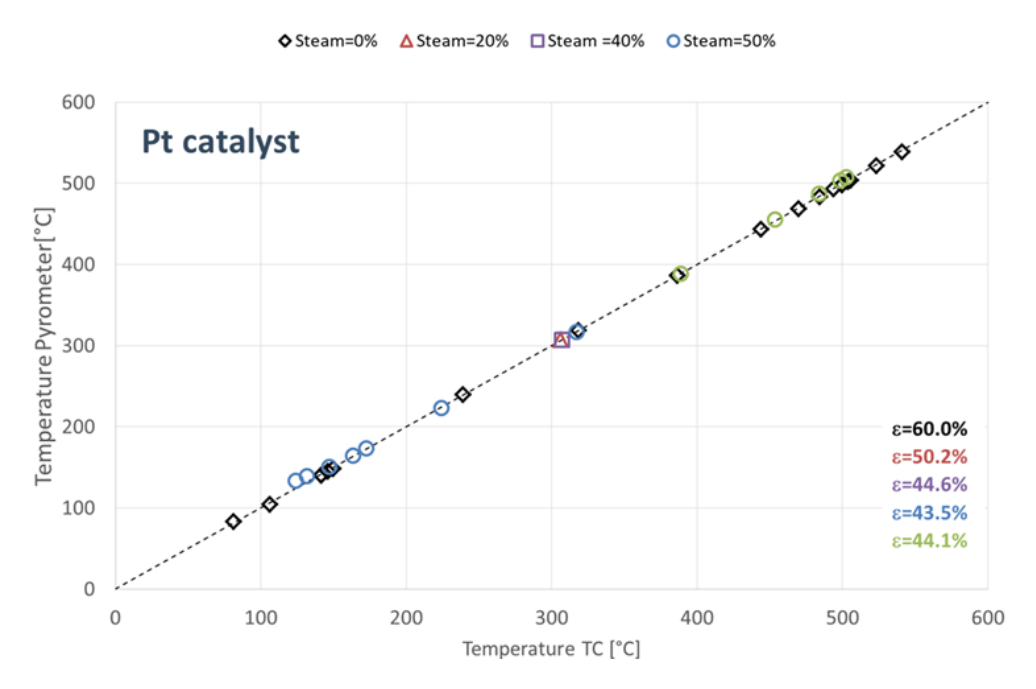


Figure 17. REKO-1: Pyrometer calibration for the platinum-based catalyst

As the pyrometer has been calibrated by means of temperature measurements with a thermocouple, the same measurement uncertainty as for the thermocouple can be assumed (see Figure 16).

Gas composition measurement

The gas concentration measurement is of secondary relevance in the scoping tests, as the small catalyst sample mounted inside the cylindrical flow tube has a very limited recombination efficiency and cannot be considered as representative for a catalyst arrangement inside a PAR. Hence, the description of the multi-component gas analyser used is given in section 3.2.1.3, in the description of the RECO-3 tests.

3.1.2. Catalyst samples

The scoping tests have been performed with single catalyst samples with a size of 5 x 5 cm², as shown in Figure 18. The generic catalysts have been manufactured by company Chemical Consulting Dornseiffer in Aachen/Germany. The supporting material is a thin sheet of stainless steel with a thickness of 50 μ m. The ceramic washcoat consists of 4 mg/cm² γ -Al₂O₃. The amount of catalytic active material (either platinum or palladium) is 1 mg/cm².

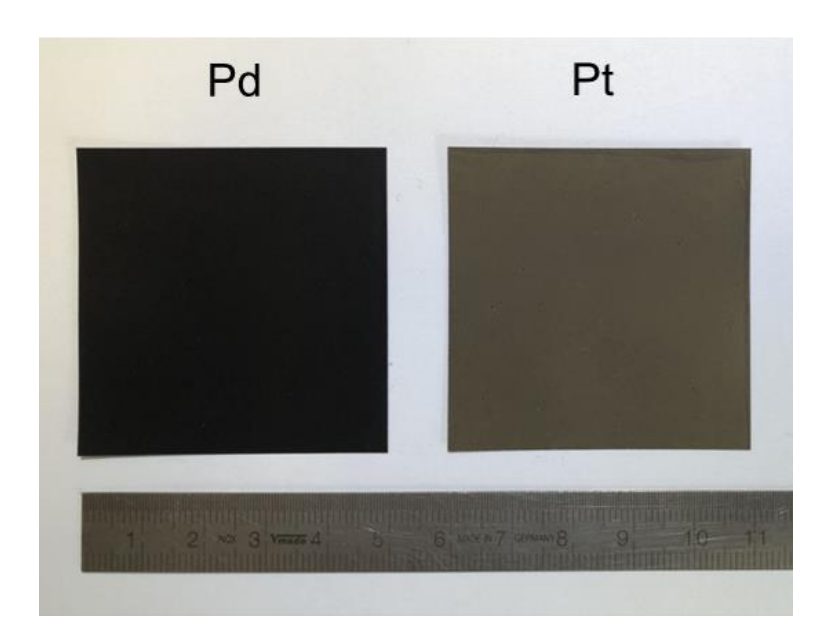


Figure 18. REKO-1: Catalyst samples

3.1.3. Test matrix and test procedure

A generic test sequence consists of the following steps:

- Calibration of the gas analysers
- **Continuous injection** of air at the nominal flow rate
- **Gas pre-heating** to obtain the nominal inlet temperature
- Continuous injection of steam to obtain the nominal steam concentration
- **Continuous injection of nitrogen** to obtain the nominal oxygen concentration (in case of oxygen starvation tests)
- Continuous injection of hydrogen to obtain the nominal hydrogen concentration
- Continuous injection of carbon monoxide to obtain the nominal gas concentration
- When a steady-state reaction process has established:
 Measurement of the catalyst temperature (average over several minutes)
- A series of several steady-state measurement points is obtained by step-wise changing the gas composition at the flow tube inlet
- Stop of carbon monoxide injection

- Stop of hydrogen injection
- Switch from mixed air/nitrogen injection to pure air injection
- Stop of steam injection
- Stop of gas pre-heating
- After cooling, stop of air injection

The entire test sequence is driven by the operation of the mass flow controllers. When a gas species is added to or removed from the gas mixture, the other gas flows are adapted accordingly in order to maintain a constant total flow rate at the channel inlet.

3.1.4.Results

In order to prepare for the catalyst poisoning tests, reference experiments have been performed without carbon monoxide to understand the effect of different parameters on the catalyst sample performance.

3.1.4.1. Reference tests

Figure 19 shows the catalyst temperature profile measured with the pyrometer in different positions of the catalyst. The dotted square indicates the catalyst surface area that is available for optical temperature measurements. The blue symbols represent a mixture auf 2 vol.% hydrogen in dry air. When 2 vol.% carbon monoxide is added to the mixture, the surface temperatures increases (red symbols). According to the laws of diffusion-controlled reaction kinetics, the catalyst temperature, which corresponds with the recombination rate, is higher at the lower edge of the catalyst (higher gas concentration in the gas phase and not yet fully developed boundary layer).

Figure 20 shows the catalyst temperature at the lower edge of the sheet for different hydrogen fractions in the gas mixture at ambient temperature and pressure and a flow velocity of 0.5 m/s. At 5 vol.% hydrogen, the upper limit of the pyrometer's measurement range is reached.

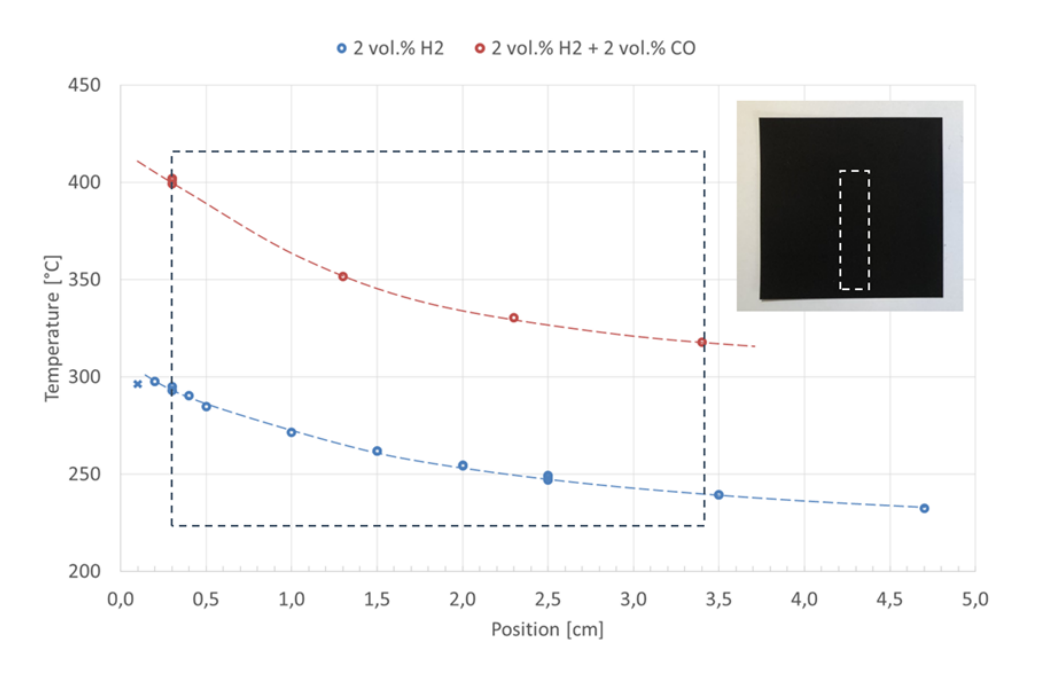


Figure 19. REKO-1: Catalyst surface temperature along the catalyst length

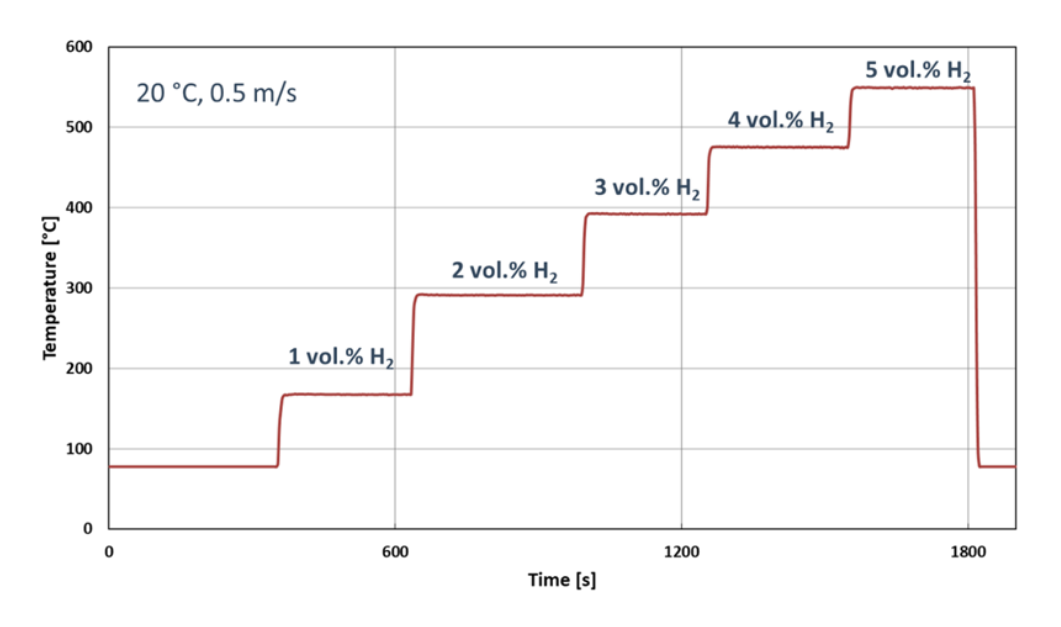


Figure 20. REKO-1: Effect of hydrogen concentration on the catalyst temperature

Figure 21 shows the effect of the initial gas temperature on the catalyst temperature. The tests have been performed for gas mixtures at 20 °C, 80 °C and 150 °C, with 0.5 m/s flow velocity. Although the catalyst temperature level increases with the inlet temperature, the absolute temperature increase is smaller than the raise in the gas temperature. The effect becomes smaller for high recombination rates at elevated hydrogen fractions.

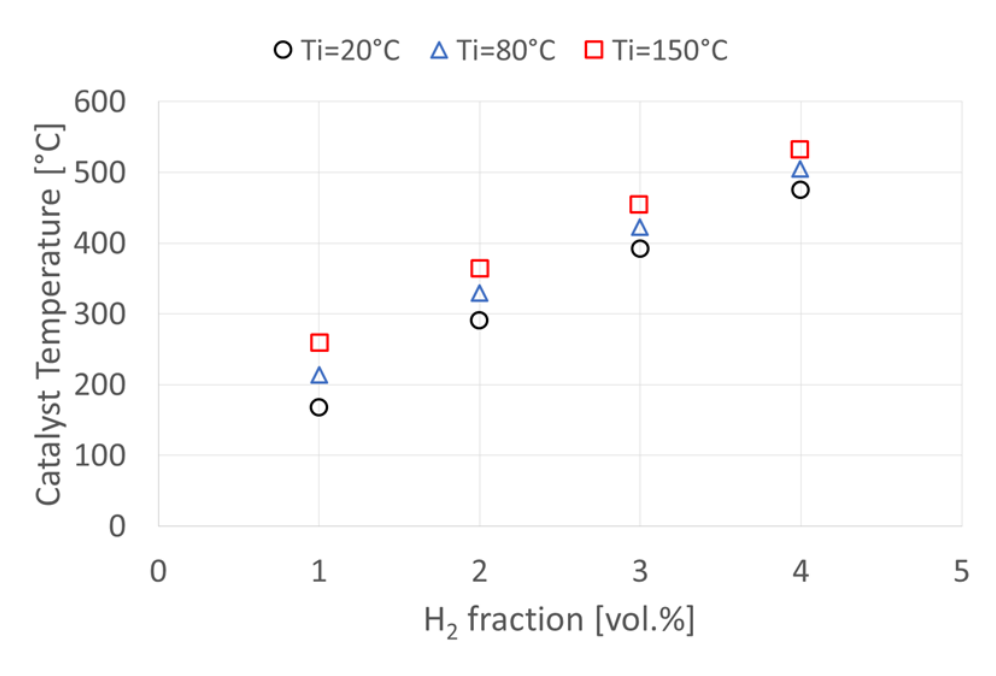


Figure 21. REKO-1: Effect of inlet gas temperature on the catalyst temperature

The effect of the flow velocity on the catalyst temperature is shown in Figure 22. The experimental data obtained at ambient temperature reveals only a small increase in the catalyst temperature although the flow velocity has been increased from 0.5 m/s to 1.0 m/s. Obviously, the increase in mass transfer and consequently heat production is balanced by the increase in convective cooling.

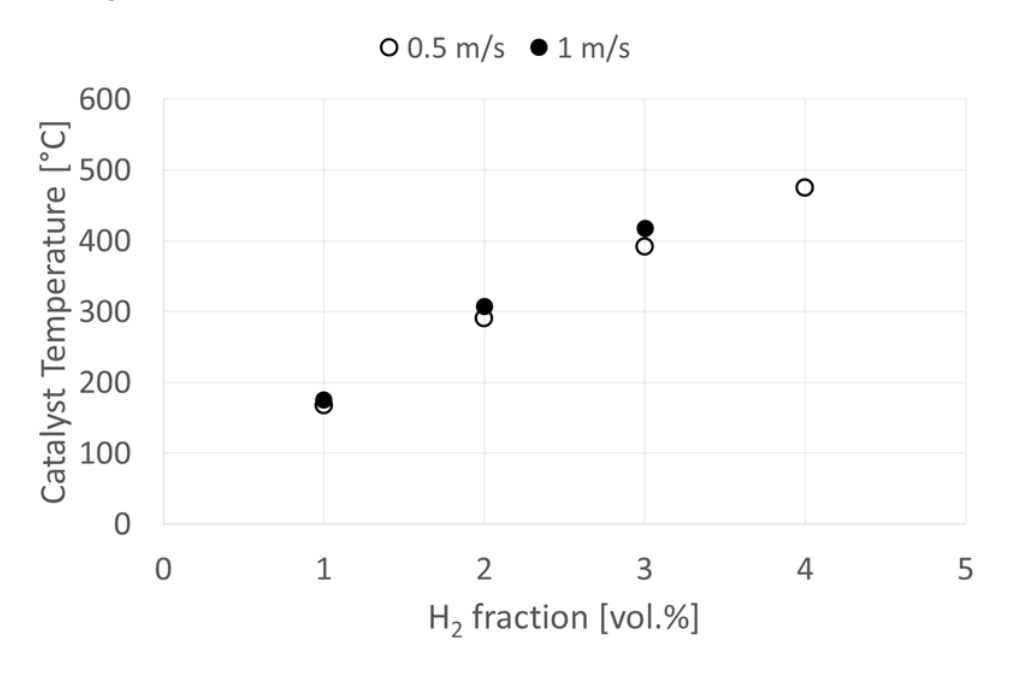


Figure 22. REKO-1: Effect of inlet flow velocity on the catalyst temperature

Figure 23 compares the catalyst temperatures obtained for hydrogen recombination under dry and wet conditions (100 % relative humidity) at an inlet temperature of 80 °C. No significant difference between both cases is observed.

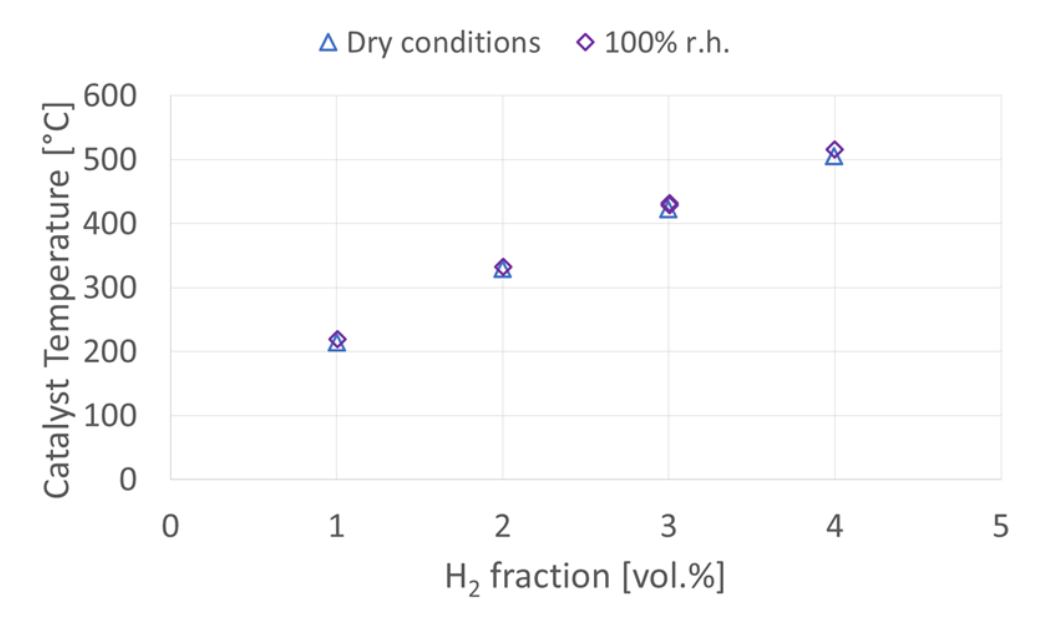


Figure 23. REKO-1: Effect of steam on the catalyst temperature

The effect of oxygen starvation was studied for several hydrogen fractions. For this purpose, the initial oxygen fraction (approx. 20 vol.%) was step-wise decreased. Figure 24 shows that the oxygen fraction has no effect on the catalyst temperature until the oxygen fraction falls below a threshold value (see section 2.1.1). The experimental threshold values obtained for the three different hydrogen fractions match well with the calculation values given in eq. 2.9. In the oxygen starvation regime, the recombination rate starts to depend linearly on the oxygen fraction, independent from the hydrogen fraction.

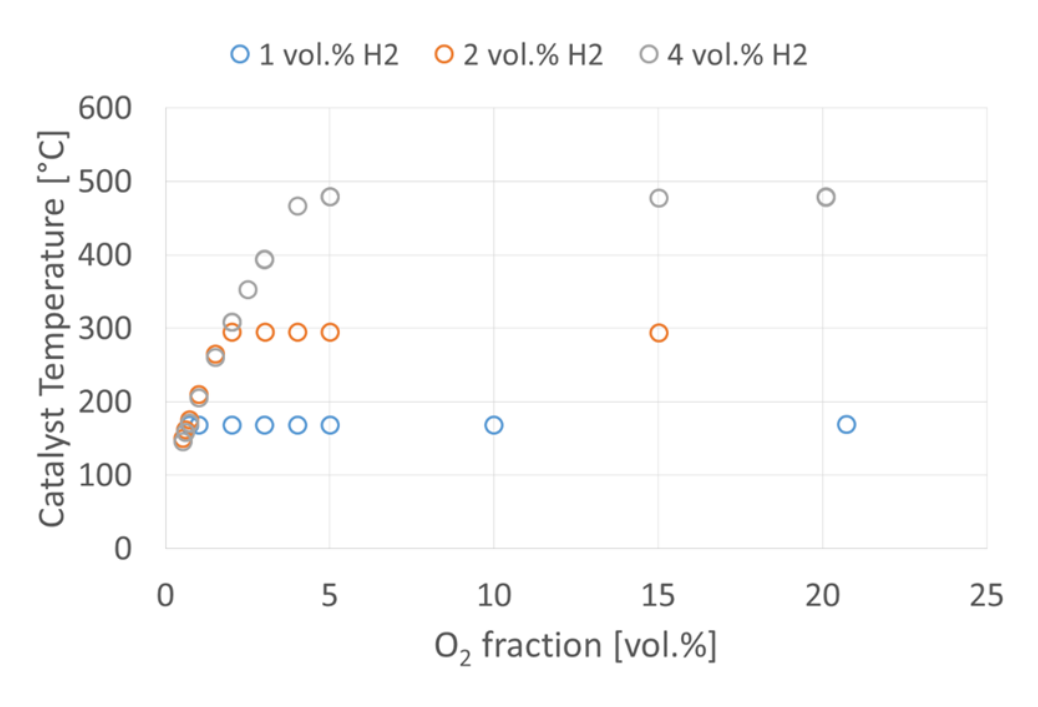


Figure 24. REKO-1: Effect of oxygen starvation on the catalyst temperature

Figure 25 shows the catalyst temperature for a gas mixture of ambient air with 2 vol.% hydrogen with step-wise addition of carbon monoxide. As the PAR is already in operation at high catalyst temperature, carbon monoxide is converted to carbon dioxide, contributing to further increase of the catalyst temperature.

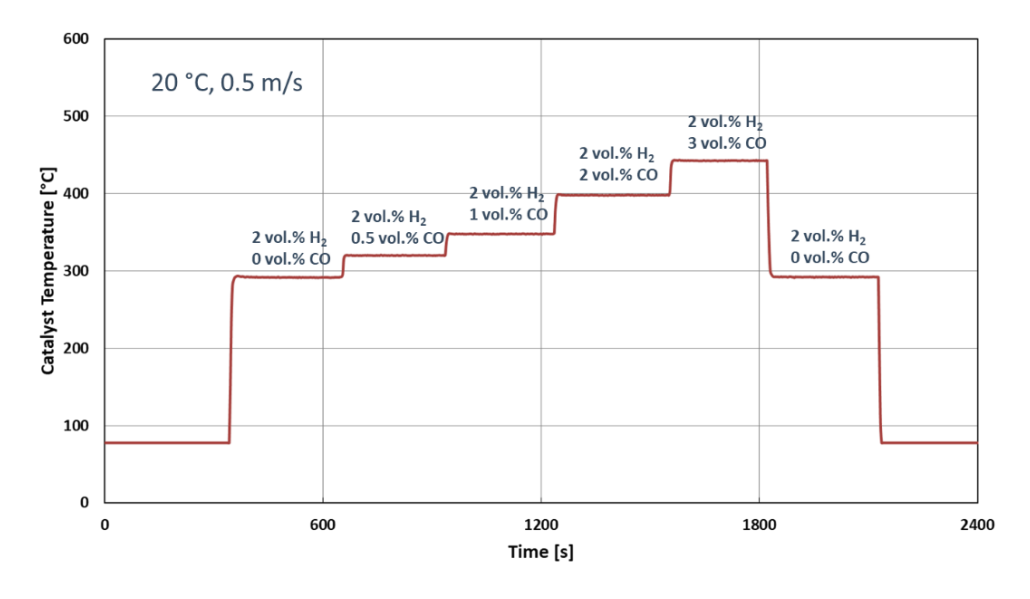


Figure 25. REKO-1: Effect of carbon monoxide fraction on the catalyst temperature

The same effect is demonstrated in Figure 26, where steady state catalyst temperatures for different hydrogen/carbon monoxide mixtures in air have been plotted.

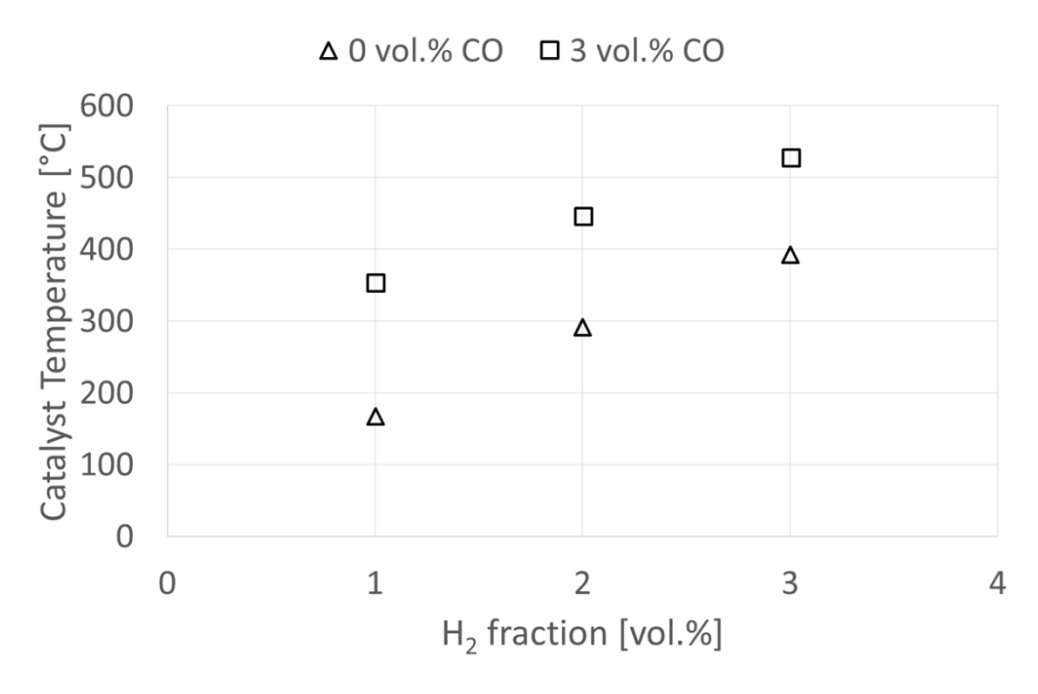


Figure 26. REKO-1: Effect of carbon monoxide fraction on the catalyst temperature

Under parallel reaction of hydrogen and carbon monoxide, gas temperature and flow velocity have the same limited effect on the catalyst temperature as seen before for hydrogen recombination only, compare Figure 27 with Figure 21 and Figure 28 with Figure 22, respectively.

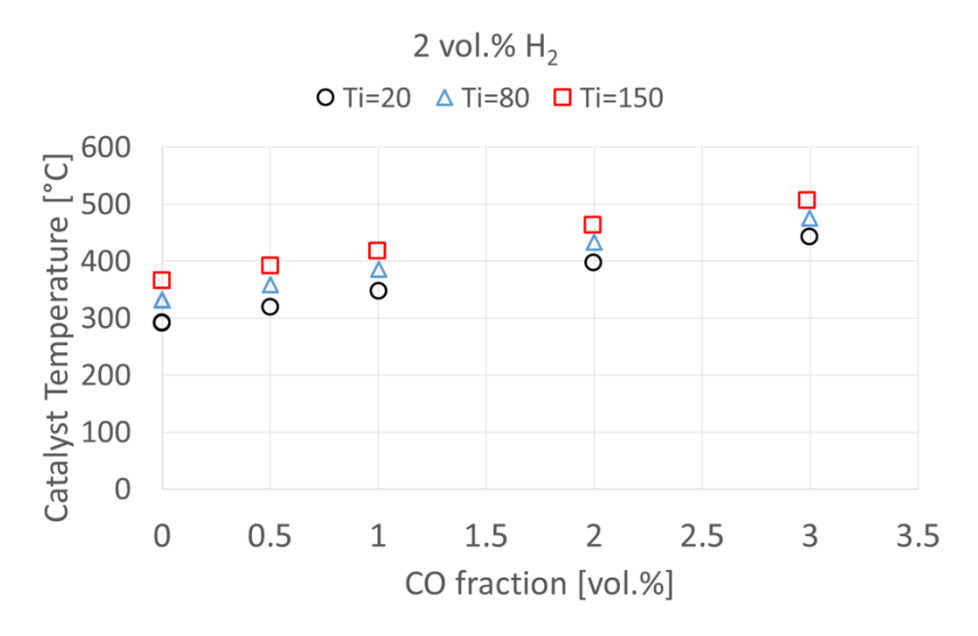


Figure 27. REKO-1: Effect of inlet gas temperature on the catalyst temperature

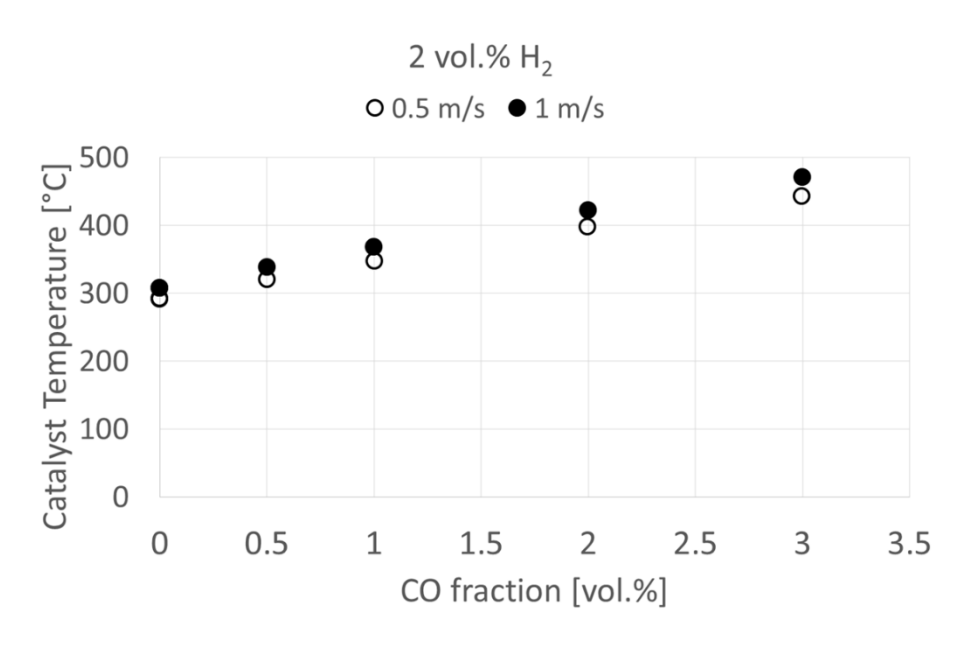


Figure 28. REKO-1: Effect of inlet flow velocity on the catalyst temperature

Due to the competition for oxygen between hydrogen and carbon monoxide, oxygen starvation occurs earlier (i.e. at higher oxygen concentration) than for hydrogen alone. In Figure 29 and Figure 30, the oxygen fraction from different experiments with hydrogen/carbon monoxide mixtures is plotted before (black circles) and after the effect of oxygen starvation has been observed (red circles).

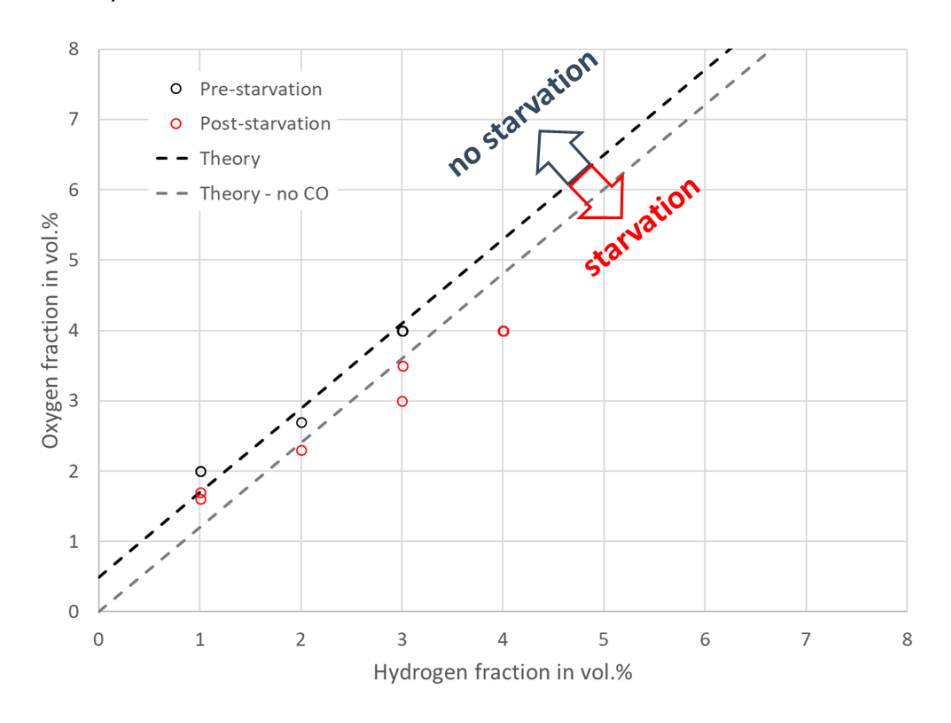


Figure 29. REKO-1: Oxygen starvation threshold at 1 vol.% carbon monoxide

The black dashed lines indicate the threshold line dividing oxygen-rich and oxygen-lean range according to eq. 2.10 (see section 2.1.1). In order to demonstrate the effect of carbon monoxide, the grey dashed line shows the threshold line for hydrogen recombination only.

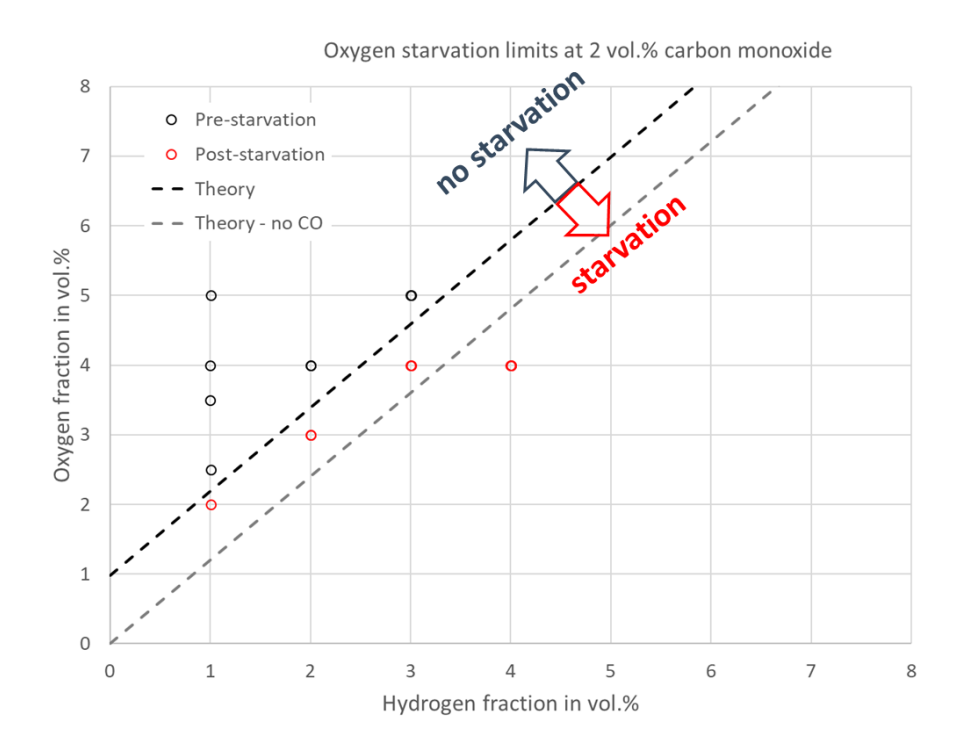


Figure 30. REKO-1: Oxygen starvation threshold at 2 vol.% carbon monoxide

3.1.4.2. Catalyst poisoning results

As has already been mentioned in section 2, previous experimental data indicate that PAR operation in the presence of hydrogen and carbon monoxide can be divided into three different regimes:

- Regime I: Undisturbed parallel reaction of hydrogen and carbon monoxide with oxygen (oxygen-rich atmosphere)
- Regime II: Constrained parallel reaction of hydrogen and carbon monoxide with oxygen (oxygen-lean atmosphere)
- Regime III: Interruption of reaction due to catalyst deactivation (poisoning)

While the transition between the first two regimes can be determined by calculating the threshold value of the oxygen fraction (see derivation of eqs. 2.9 and 2.10 in section 2.1.1 and examples in Figure 29 and Figure 30) independently of the catalyst (Pt or Pd), determining the conditions that cause catalyst deactivation is the goal of the present experimental program.

The results obtained in the scoping tests confirm these three regimes for both platinum- and palladium-based catalysts. Figure 31 shows the history of catalyst temperature measurement throughout an entire test sequence to illustrate the behaviour of a platinum-based catalyst sample in the presence of carbon monoxide.

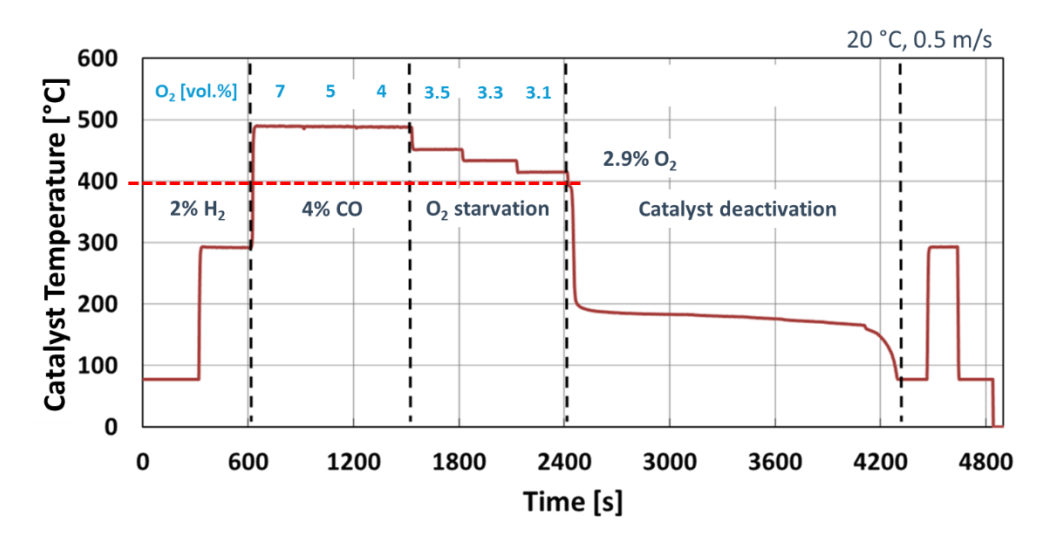


Figure 31. REKO-1: History of the catalyst temperature during a typical poisoning experiment

In this experiment, the composition of the gas mixture initially introduced in the flow channel is 2 vol.% hydrogen, 4 vol.% carbon monoxide and 7 vol.% oxygen (air diluted by nitrogen) at a flow velocity of 0.5 m/s and ambient temperature. At each of the consecutive step, the gas composition is changed, and then the system equilibrates for five minutes in order to achieve steady-state conditions.

Upon injection of hydrogen, the catalyst temperature increases to approx. 295 °C, which indicates the start of the catalytic reaction. Once carbon monoxide is added to the gas mixture, the catalyst temperature increases to approx. 490 °C due to the additional exothermal conversion into carbon dioxide. Next, the oxygen fraction is being stepwise reduced (see given values in Figure 31). Until 4 vol.% oxygen, there is no change in the catalyst temperature, which shows that the catalyst operation is still in oxygen-rich atmosphere.

As soon as the oxygen fraction is decreased to 3.5 vol.%, the temperature decreases to 452 °C, showing that the reaction is now taking place in oxygen starvation (regime II). The next two oxygen steps (3.3 vol.% and 3.1 vol.%) show that under oxygen-lean conditions the recombination rate (and catalyst temperature) depends on the oxygen fraction.

When the oxygen content is reduced to 2.9 vol.%, there is a significant drop in the catalyst temperature, indicating the start of the deactivation process. Initially, the catalyst continues to

operate, albeit with significantly reduced efficiency. Over a lengthy transient, the catalyst temperature slowly decreases until reaction stops completely (approx. 4350 s).

After stopping the injection of carbon monoxide, the catalyst temperature immediately increases to the same temperature as before, demonstrating the reversible effect of carbon monoxide on the catalyst. The information taken from this specific test sequence is, that for the given gas mixture catalyst poisoning occurs at a catalyst temperature of 400 °C ("poisoning temperature").

As being demonstrated, a typical test sequence is performed with a fixed hydrogen and carbon monoxide mixture while the oxygen fraction is step-wise decreased. In order to ensure that the test procedure has no effect on the results, a second test sequence was briefly tested where the hydrogen and oxygen composition has been fixed while the carbon monoxide fraction has been increased. In the end, both types of test sequence result in the same catalyst poisoning temperature, which can be seen in Figure 32.

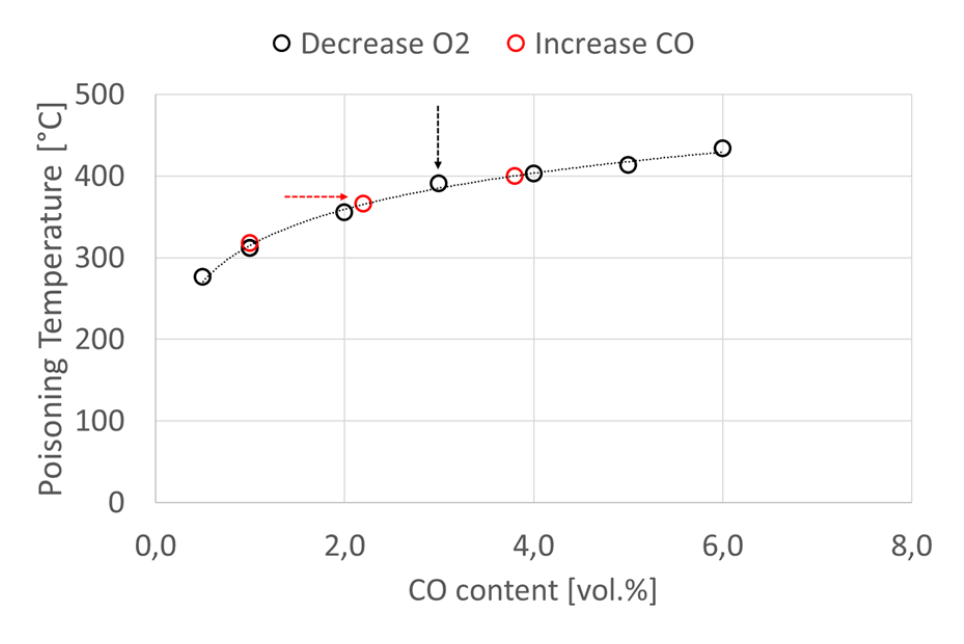


Figure 32. REKO-1: Catalyst poisoning temperatures obtained with different test procedures

Figure 33 shows the catalyst temperature at which catalyst poisoning occurs for different combinations of hydrogen and carbon monoxide fractions. Each symbol represents a different hydrogen fraction. Each measurement point in the diagram results from the initiation of catalyst deactivation observed in a different test (see Figure 31). All tests have been performed at 20 °C with 0.5 m/s flow velocity. The poisoning temperature seems to be a function of the carbon monoxide fraction, but independent from the hydrogen fraction. For the case of 1 vol.% hydrogen (blue symbols), the catalyst temperature was not high enough to sustain the reaction and the catalyst was deactivated before oxygen starvation could be observed.

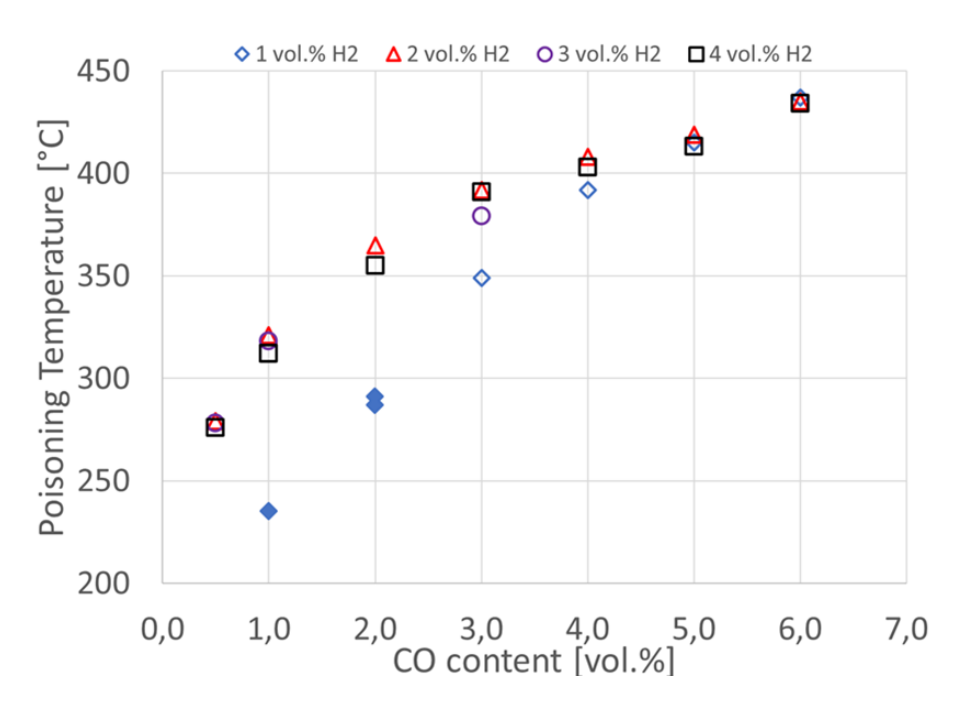


Figure 33. REKO-1: Catalyst poisoning temperatures for different gas compositions

In Figure 34, the effect of the initial gas temperature on the poisoning temperature is shown for the platinum-based catalyst. For this purpose, the catalyst temperature is plotted against the molar concentration of carbon monoxide (with 4 vol.% hydrogen). The poisoning temperature seems to be independent from the gas temperature and only depends on the carbon monoxide molar concentration.

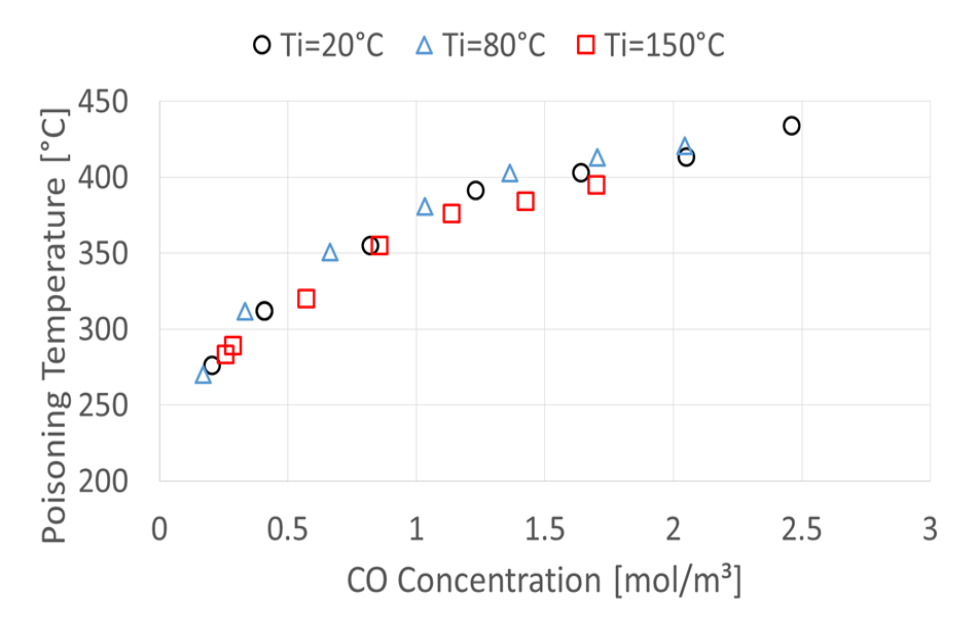


Figure 34. REKO-1: Catalyst poisoning temperatures for different inlet gas temperatures

The effect of the flow velocity on the catalyst deactivation by carbon monoxide for the platinum-based catalyst is shown in Figure 35. For two different flow velocities (0.5 m/s and 1.0 m/s),

catalyst poisoning occurs at the same catalyst temperature for each carbon monoxide fraction (2 vol.% hydrogen).

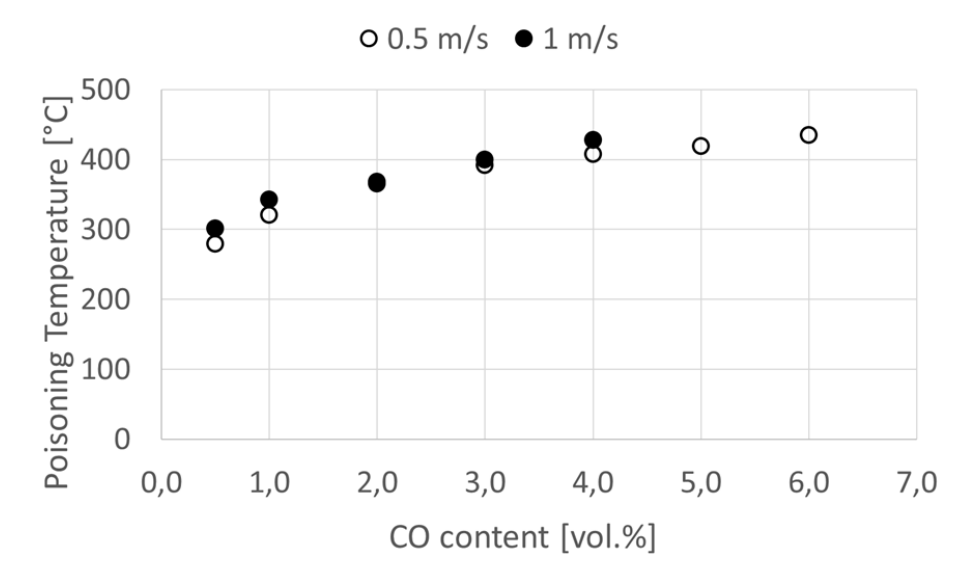


Figure 35. REKO-1: Catalyst poisoning temperatures for different flow velocities

The comparison of the catalyst deactivation for dry and humid conditions is shown in Figure 36. The tests have been performed at 80 °C and 100 % relative humidity with the platinum catalyst (4 vol.% hydrogen). Interestingly, the poisoning temperature is significantly higher in high humidity, probably due to limited H_2O desorption from the catalyst surface. The result stresses the relevance of wet conditions being considered in the full-scale test program.

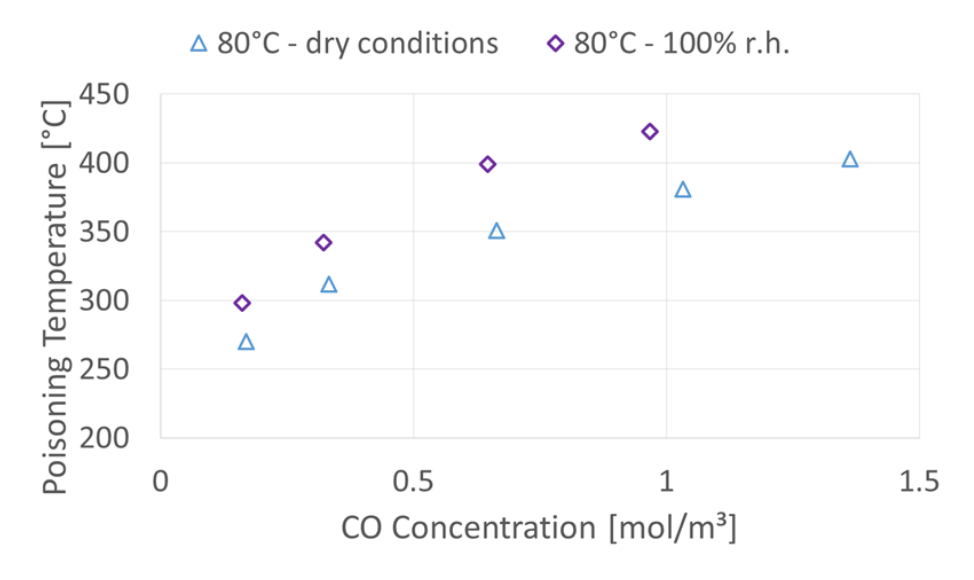


Figure 36. REKO-1: Catalyst poisoning temperatures for dry and wet conditions

Performing the test program with the palladium-based catalyst reveals a significant difference between both catalysts with regard to the effect of the gas temperature. Figure 37 shows the

catalyst poisoning temperatures obtained for three different gas temperatures (4 vol.% hydrogen). Obviously, the palladium-based catalyst (red symbols) remains longer active than the platinum-based catalyst (black symbols) and becomes deactivated at lower catalyst temperatures. Furthermore, the gas temperature has a significant influence on the deactivation of the palladium-based catalyst, while for the platinum-based catalyst the gas temperature played no role (see Figure 34).

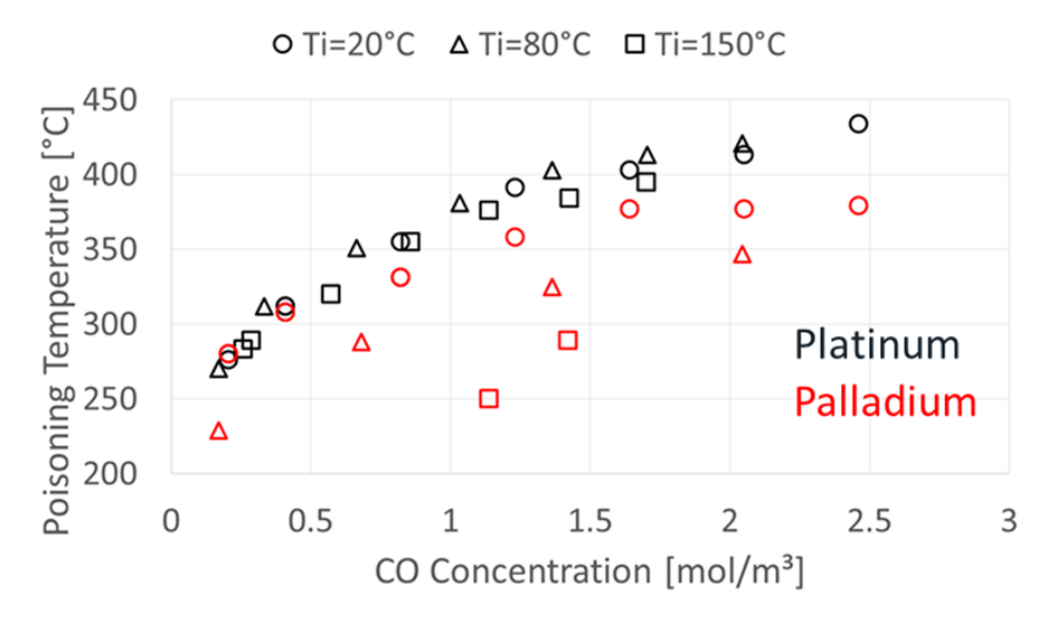


Figure 37. REKO-1: Comparison of poisoning temperatures for Pt- and Pd-based catalysts

3.1.5. Conclusions of scoping tests

The scoping tests have been performed to understand the impact of parameters such as gas and catalyst temperatures, gas composition, and flow velocity on the catalyst deactivation process for both platinum- and palladium-based catalysts. These are the conclusions taken for the experimental program of the catalyst section tests:

- Platinum- and palladium-based catalyst behave differently with regard to catalyst deactivation.
- The relevant gas species for catalyst poisoning are oxygen and carbon monoxide. The amount of hydrogen in the gas mixture seems to be of secondary importance.
- The effect of the gas temperature on the catalyst deactivation needs to be considered, especially for the palladium-based catalyst.
- Catalyst deactivation needs to be studied under humid conditions as different results may be obtained compared to dry conditions.
- The flow velocity of the gas mixture has only minor effect on catalyst deactivation.

3.2. Catalyst section tests

The experimental program on an entire catalyst section is performed in the REKO-3 facility. These tests provide steady-state data on full-scale catalyst sheets suitable for model development and validation. The resulting database has been used by the Task 3.2 partners to further advance their numerical PAR models.

3.2.1. Description of the REKO-3 test facility

Using the identical peripheral set-up as REKO-1, the REKO-3 facility is equipped with a vertical modular flow tube reactor with rectangular cross section, which is composed of different elements according to the test specifications and requirements. The setup allows investigation of the recombination behaviour of catalyst sheets under well-defined and steady-state forced flow boundary conditions. For the present study, four parallel catalyst sheets are exposed to stationary flows of gaseous mixtures including hydrogen, oxygen, nitrogen, steam and carbon monoxide inside a vertical flow reactor.

3.2.1.1. Rectangular flow reactor

The vertical flow channel is an assembly of rectangular stainless-steel tube modules with a wall thickness of 2 mm. In the present study, the rectangular channel has a total height of approx. 100 cm with an inner cross section of 146 mm x 46 mm (Fig. 38). The assembly includes:

- 1. Insulated inlet section (length 30 cm)
- 2. Section holding the catalyst sample with optical access (length 15 cm)
- 3. Outlet section connecting to the exhaust hood (length 60 cm)

Figure 39 shows the flow chart of the experimental set-up which consists of the instrumented rectangular flow channel (A) embedded in a gas supply infrastructure (B). The gas flow passes through the flow tube reactor before entering the venting line on top. Before entering the venting line, a gas probe is continuously sampled to the gas analyser system (C) in order to determine the outlet gas composition.



Figure 38. REKO-3: Rectangular flow reactor set-up

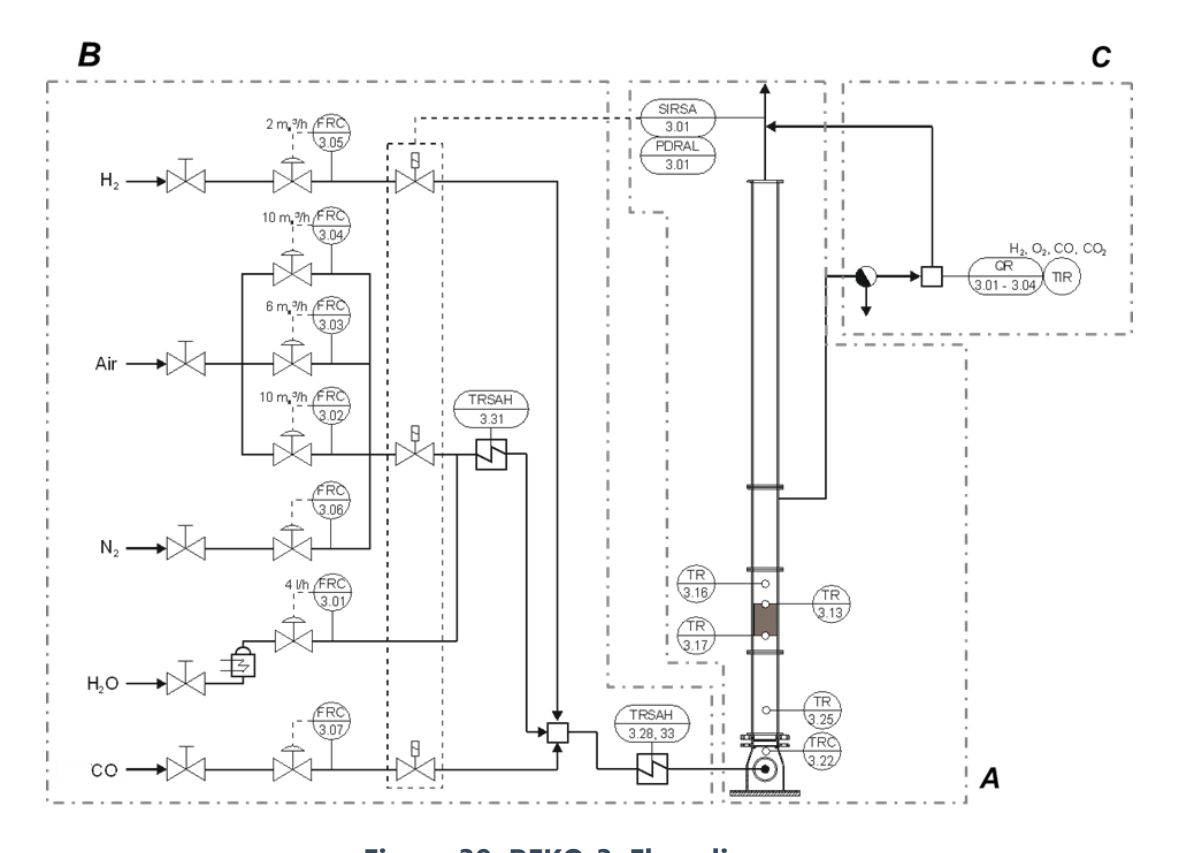


Figure 39. REKO-3: Flow diagram

3.2.1.2. **Gas supply**

For a detailed description of the gas supply, see section 3.1.1.2.

3.2.1.3. Instrumentation

The instrumentation includes thermocouples, a multi-component gas analyser, and a pyrometer. The most relevant measurement points are:

- Gas temperature at the channel inlet (TR 3.25)
- Gas temperature above the catalyst section (TR 3.16)
- Catalyst temperature (TIR 3.02)
- Gas composition above the catalyst sample (QIR 3.01 QIR 3.04)

Gas temperature measurement

For details on the gas temperature measurement and related measurement uncertainties, see section 3.1.1.3.

Catalyst temperature measurement

Catalyst temperatures are measured by means of a pyrometer with a measurement range of 70 °C to 550 °C. For this purpose, the flow channel is equipped with a glass window (Figure 40). In order to allow measurement of the catalyst temperature on one of the inner catalyst sheets, the outer catalyst sheet located next to the optical access has been equipped with four circular openings (diameter approx. 6 mm) at elevations 10 mm, 40 mm, 80 mm, and 130 mm distance from the bottom edge (Fig. 40). Through these holes in the outer catalytic sheet, the inner catalytic sheet becomes accessible for the pyrometric temperature measurement.



Figure 40. REKO-3: Optical measurement of the catalyst temperature

For more details on the pyrometer calibration and related measurement uncertainties, see section 3.1.1.3.

Gas composition measurement

The gas probe removes continuously a part of the off-gas at constant flow rate through a heated line in order to avoid condensation. Before entering the multi-component gas analyser, the gas is cooled down to 5 °C in order to remove condensing gases (water vapour). The remaining amount of water vapour behind the condenser is \leq 0.86 vol.%. The gas is then passing through a sequence of gas analysers determining the concentration of

- hydrogen,
- oxygen,
- carbon monoxide, and
- carbon dioxide.

The oxygen analyser is based on a para-magnetic sensor. The impact of the other gases is negligible (100 vol.% H_2 : +0.24 vol.% O_2 ; 100 vol.% CO_2 : -0.27 vol.% O_2). The oxygen sensor is calibrated with nitrogen (zero gas) and synthetic air (20.95 +/- 0.2 vol.% O_2 in N_2).

Carbon monoxide and carbon dioxide are measured with infrared sensors. These sensors are insensitive to the other gas components used in the tests. For calibration of both sensors, nitrogen (zero gas) and a mixture of 10.04 +/- 0.1 vol.% CO and 10.02 +/- 0.1 vol.% CO₂ in nitrogen is used.

The hydrogen analyser uses a heat conductivity sensor. The measurement uncertainty according to the manufacturer is ≤ 1 % of the measurement range. It should be noted that any change in the heat conductivity of the gas is interpreted by the analyser as a change in hydrogen concentration. As the sensor is calibrated with nitrogen as background gas (zero gas: nitrogen, span gas: 10.05 + - 0.1 vol.% hydrogen in nitrogen), the use of air, carbon monoxide and especially carbon dioxide, which has a significantly smaller heat conductivity than nitrogen, will influence the measurement signal. For this reason, an analytical post-processing of the measurement data is required in order to eliminate the cross-sensitivities.

The effect of the different gases on the hydrogen concentration measurement is illustrated on the basis of data from the calibration procedure (Figure 41). The presence of 20.2 vol.% of CO₂ during CO/CO₂ calibration causes an offset in the hydrogen concentration signal of approx. 2.9 vol.%. Pure air with an oxygen concentration of approx. 21 vol.% causes an offset in the hydrogen concentration signal of approx. 0.3 vol.%.

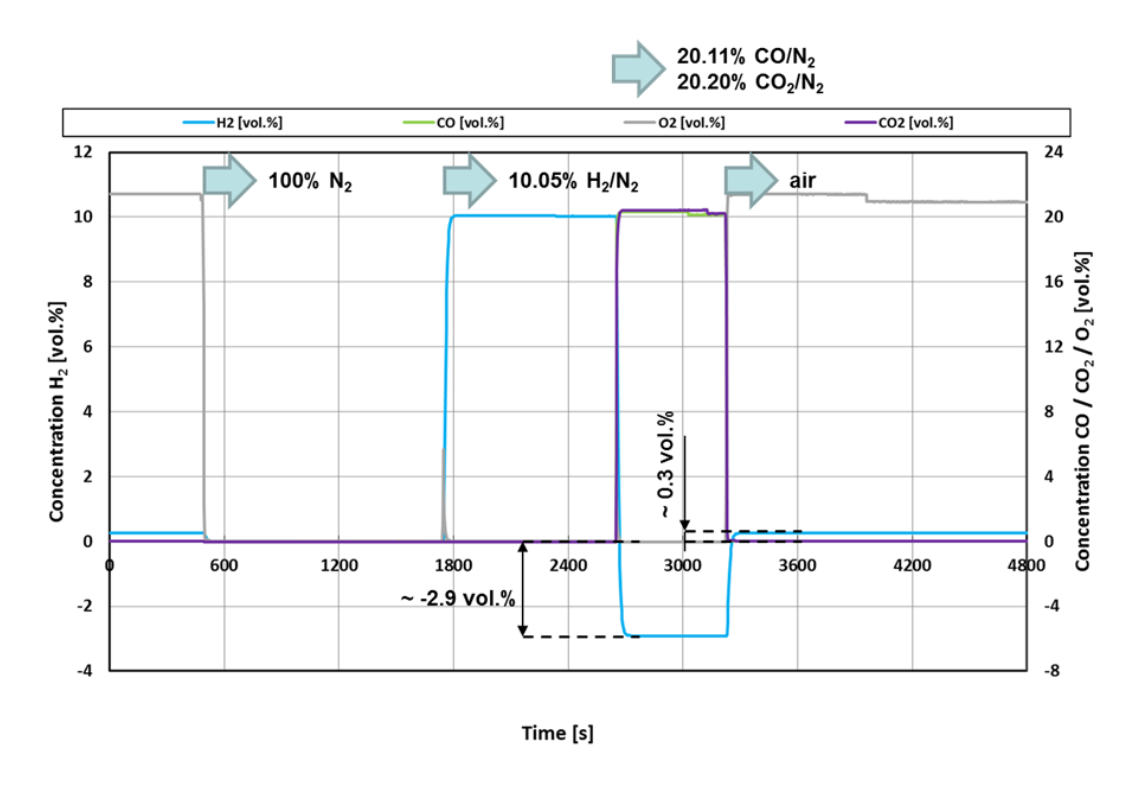


Figure 41. REKO-3: Different offsets in the hydrogen signal during the calibration procedure

Figure 42 to Figure 44 show measurement data used to derive correlations to correct the offset in the hydrogen signal. Based on these measurements, the following correlations were deduced to remove the sensor-cross-dependencies from the actual measured hydrogen concentration $y_{H_2}^m$ to obtain the cross-dependency-free hydrogen concentration $y_{H_2}^{corr}$:

$$y_{H_2}^{corr} = y_{H_2}^m + \Delta y^{O_2} + \Delta y^{CO} + \Delta y^{CO_2}$$
(3.0)

Impact of O₂:
$$\Delta y^{O_2} = -8.6 \cdot 10^{-5} \cdot (y_{O_2}^m)^2 + 1.56 \cdot 10^{-2} \cdot y_{O_2}^m$$
 (3.1)

Impact of CO:
$$\Delta y^{CO} = -1.345 \cdot 10^{-4} \cdot (y_{CO}^m)^2 - 1.3062 \cdot 10^{-2} \cdot y_{CO}^m$$
 (3.2)

Impact of CO₂:
$$\Delta y^{CO_2} = -4.39895 \cdot 10^{-3} \cdot (y_{CO_2}^m)^2 - 1.26411 \cdot 10^{-1} \cdot y_{CO_2}^m$$
 (3.3)

This correction depends on the measured molar fractions of the other gases $i=\{O_2, CO, CO_2\}$.

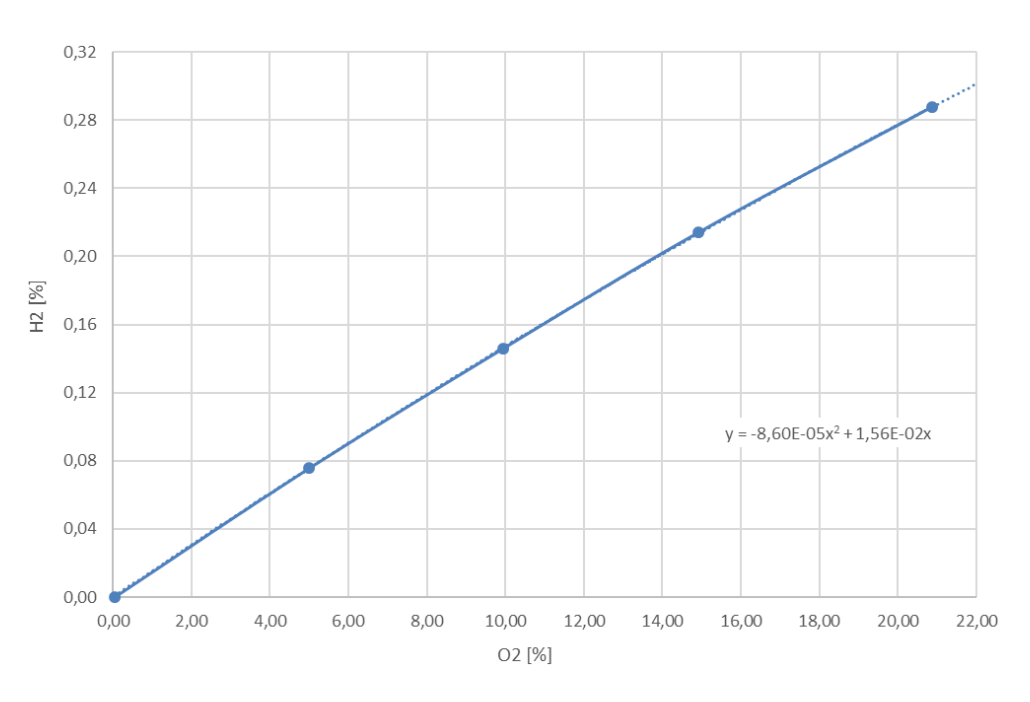


Figure 42. REKO-3: Offset correction for oxygen

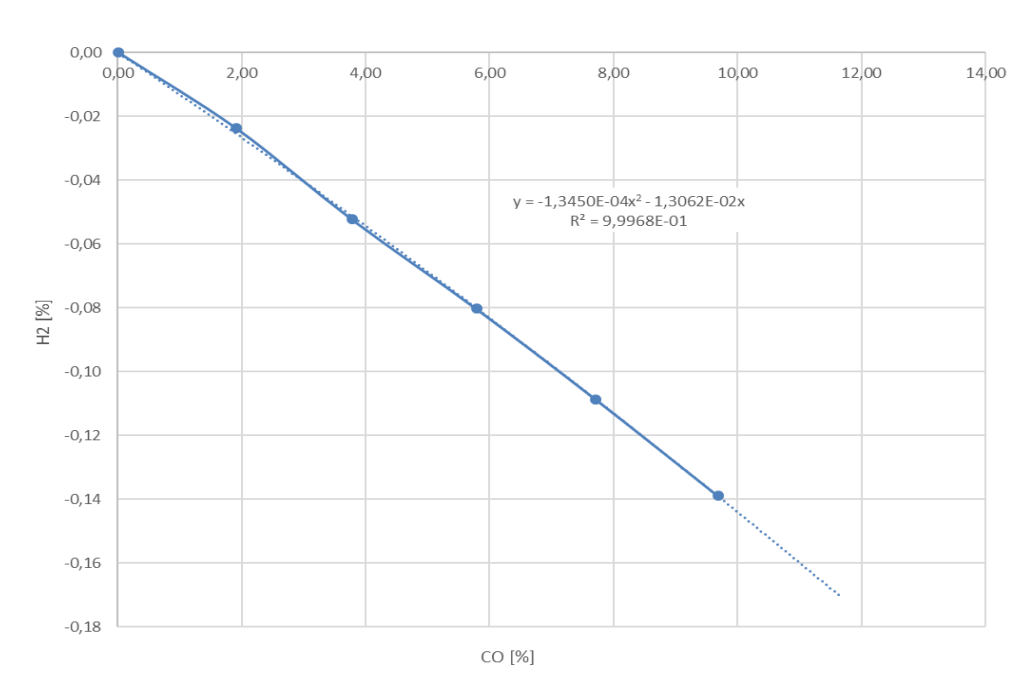


Figure 43. REKO-3: Offset correction for carbon monoxide

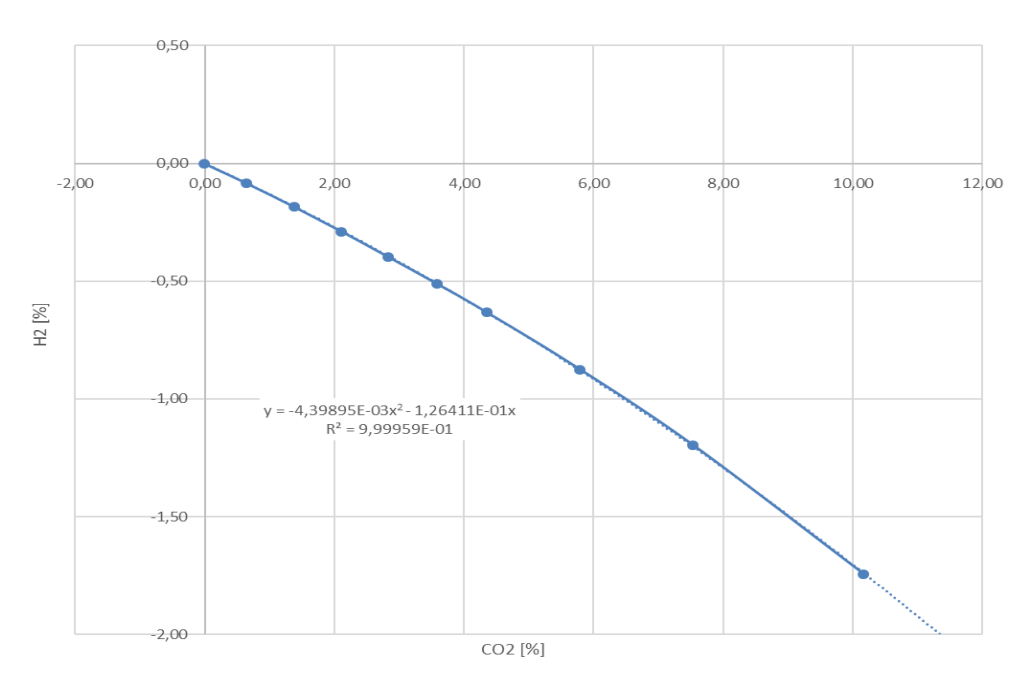


Figure 44. REKO-3: Offset correction for carbon dioxide

As mentioned above, water vapour which is either injected into the flow reactor or generated during the hydrogen recombination reaction is removed before the gas is entering the analytical section. As a consequence, the measured gas composition is not identical with the gas composition behind the catalyst. In order to determine the gas composition behind the catalyst, a balance of the molar flows considering the hydrogen recombination rate must be applied (see section 3.2.3.4).

3.2.2.Catalyst samples

The catalyst section tests have been performed with four identical catalyst sheets with a size of $14.3 \times 14.3 \text{ cm}^2$ each, either coated with Pt or Pd, see Figure 45. The generic catalysts have been manufactured by company Chemical Consulting Dornseiffer in Aachen/Germany. The supporting material is a thin sheet of stainless steel with a thickness of 50 μ m. The ceramic washcoat consists of 4 mg/cm² γ -Al₂O₃. The amount of catalytic active material (platinum or palladium) is 1 mg/cm².

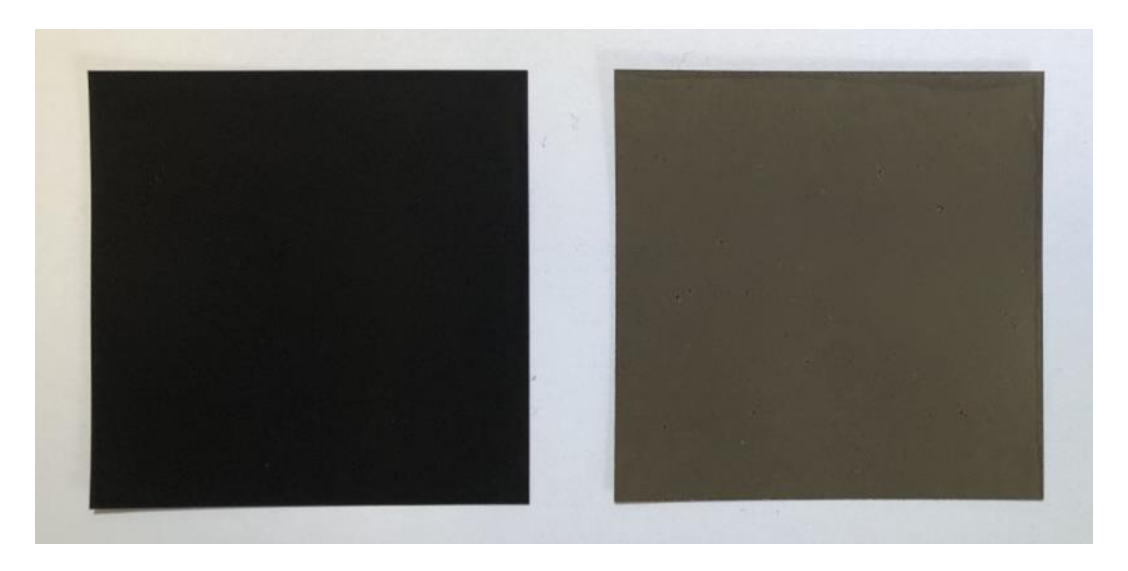


Figure 45. REKO-3: Catalyst sheets; palladium (left), platinum (right)

3.2.3. Data post-processing and evaluation

In addition to the aforementioned correction of the hydrogen concentration measurements (section 3.2.1.3), post-processing is required in order to calculate derived values (actual values of inlet concentrations, flow velocity, reaction rates and efficiencies, and the outlet concentrations).

3.2.3.1. Calculation of the actual inlet concentrations

The molar flow of gas component i is calculated from the volumetric flow given by the mass flow controllers according to the law for ideal gases:

$$\dot{n}_i^{in} = \frac{p_n}{R \cdot T_n} \cdot \dot{V}_i^{in} \tag{3.4}$$

with p_n = 1.013 (normal pressure), T_n = 273.15 K (normal temperature), R = 8.314 J/(mol K) (universal gas constant).

The inlet concentration y_i^{in} of the gas species i is calculated from the molar flows according to

$$y_i^{in} = \frac{n_i^{in}}{n_{tot}^{in}} \tag{3.5}$$

3.2.3.2. Calculation of actual flow velocity

The actual flow velocity is calculated with the actual value of the normal volumetric flow \dot{V}_{tot}^{in} according to

$$v = \frac{\dot{V}_{tot}^{in}}{A} \cdot \frac{T_{in}}{T_n}$$
 (3.6)

with the flow cross section of the flow channel A and $T_n = 273.15$ K (normal temperature).

3.2.3.3. Calculation of reaction rates and efficiencies

The reaction rate is defined as the difference between the inlet and outlet molar flow rate. For both reacting species hydrogen and carbon monoxide we obtain

$$\dot{r}_{H_2} = \dot{n}_{H_2}^{in} - \dot{n}_{H_2}^{out} \tag{3.7}$$

and

$$\dot{r}_{CO} = \dot{n}_{CO}^{in} - \dot{n}_{CO}^{out}. \tag{3.8}$$

In order to calculate the unknown outlet molar flow rates of hydrogen and carbon monoxide, the outlet concentration of both species and the total molar outlet flow rate must be determined. According to the chemical equations

$$H_2 + \frac{1}{2} O_2 \to H_2 O$$
 (3.9)

and

$$CO + \frac{1}{2} O_2 \to CO_2$$
, (3.10)

the total molar outlet flow rate depends on the reaction rates for the different gas species:

$$\dot{n}_{H_2}^{out} = \dot{n}_{H_2}^{in} - \dot{r}_{H_2} \,, \tag{3.11}$$

$$\dot{n}_{CO}^{out} = \dot{n}_{CO}^{in} - \dot{r}_{CO} \,, \tag{3.12}$$

$$\dot{n}_{O_2}^{out} = \dot{n}_{O_2}^{in} - 0.5 \cdot \dot{r}_{H_2} - 0.5 \cdot \dot{r}_{CO} , \qquad (3.13)$$

$$\dot{n}_{H_2O}^{out} = \dot{n}_{H_2O}^{in} + \dot{r}_{H_2}, \qquad (3.14)$$

$$\dot{n}_{CO_2}^{out} = \dot{n}_{CO_2}^{in} + \dot{r}_{CO} , \qquad (3.15)$$

and

$$\dot{n}_{N_2}^{out} = \dot{n}_{N_2}^{in} \,. \tag{3.16}$$

The total molar outlet flow is then

$$\dot{n}_{\rm tot}^{out} = \dot{n}_{\rm tot}^{in} - 0.5 \cdot \dot{r}_{H_2} - 0.5 \cdot \dot{r}_{CO} \,.$$
 (3.17)

For the outlet concentrations the condensate removal from the measurement gas before entering the gas analysers needs to be considered with a molar balance (Figure 46). The different sensors determine the species' concentrations of the dry gas:

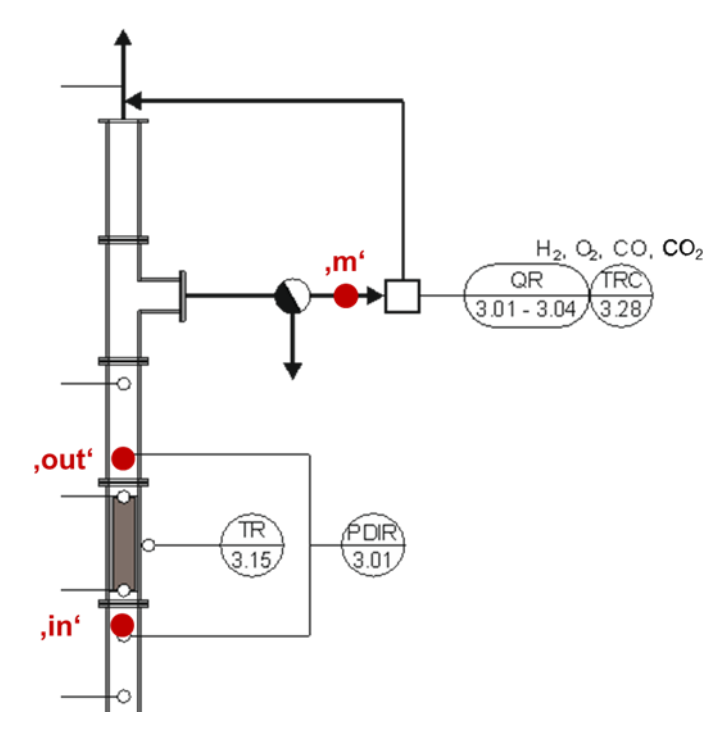


Figure 46. REKO-3: Molar balance of the gas analyzer

$$y_{H_2}^m = \frac{\dot{n}_{H_2}^{out}}{\dot{n}_{tot}^{out} - \dot{n}_{H_2O}^{out}},\tag{3.18}$$

$$y_{CO}^{m} = \frac{\dot{n}_{CO}^{out}}{\dot{n}_{tot}^{out} - \dot{n}_{H_{2O}}^{out}},$$
(3.19)

$$y_{CO_2}^m = \frac{\dot{n}_{CO_2}^{out}}{\dot{n}_{tot}^{out} - \dot{n}_{H_2O}^{out}}.$$
 (3.20)

Replacing the unknown outlet flow rates with equations (3.11) to (3.17) we obtain

$$y_{H_2}^m = \frac{\dot{n}_{H_2}^{in} - \dot{r}_{H_2}}{\dot{n}_{tot}^{in} - 0.5 \cdot \dot{r}_{H_2} - 0.5 \cdot \dot{r}_{CO} - \dot{n}_{H_2O}^{in} - \dot{r}_{H_2}} = \frac{\dot{n}_{H_2}^{in} - \dot{r}_{H_2}}{\dot{n}_{tot}^{in} - \dot{n}_{H_2O}^{in} - 1.5 \cdot \dot{r}_{H_2} - 0.5 \cdot \dot{r}_{CO}},$$
 (3.21)

$$y_{CO}^{m} = \frac{\dot{n}_{CO}^{in} - \dot{r}_{CO}}{\dot{n}_{tot}^{in} - \dot{n}_{H_{2}O}^{in} - 1.5 \cdot \dot{r}_{H_{2}} - 0.5 \cdot \dot{r}_{CO}},$$
(3.22)

$$y_{CO_2}^m = \frac{\dot{n}_{CO_2}^{in} + \dot{r}_{CO}}{\dot{n}_{tot}^{in} - \dot{n}_{H_2O}^{in} - 1.5 \cdot \dot{r}_{H_2} - 0.5 \cdot \dot{r}_{CO}}.$$
(3.23)

Combining equations (3.22) and (3.23) yields

$$y_{CO}^{m} \cdot (\dot{n}_{CO_{2}}^{in} + \dot{r}_{CO}) = y_{CO_{2}}^{m} \cdot (\dot{n}_{CO}^{in} - \dot{r}_{CO}). \tag{3.24}$$

Solving this equation for the carbon monoxide reaction rate yields

$$\dot{r}_{CO} = \frac{y_{CO_2}^m \cdot \dot{n}_{CO}^{in} - y_{CO}^m \cdot \dot{n}_{CO_2}^m}{y_{CO_2}^m + y_{CO}^m}$$
(3.25)

where all variables are known from the measurement data.

Solving equation (3.21) for the hydrogen reaction rate yields

$$\dot{r}_{H_2} = \frac{\dot{n}_{H_2}^{in} - y_{H_2}^{m} \cdot \left(\dot{n}_{tot}^{in} - \dot{n}_{H_2O}^{in} - 0.5 \cdot \dot{r}_{CO} \right)}{1 - 1.5 \cdot y_{H_2}^{m}}.$$
(3.26)

where again all variables are known from the measurement data and from eq. (3.25).

For experiments without carbon monoxide, eq. (3.26) simplifies to

$$\dot{r}_{H_2} = \frac{n_{H_2}^{in} - y_{H_2}^{m} \cdot \left(n_{tot}^{in} - n_{H_2O}^{in}\right)}{1 - 1.5 \cdot y_{H_2}^{m}}.$$
(3.27)

The reaction efficiency is defined as the ratio of the reaction rate and the inlet molar flow rate:

$$\eta_{H_2} = \frac{\dot{r}_{H_2}}{\dot{n}_{H_2}^{in}}.\tag{3.28}$$

and

$$\eta_{CO} = \frac{\dot{r}_{CO}}{\dot{n}_{CO}^{in}}.\tag{3.29}$$

3.2.3.4. Calculation of actual outlet concentrations

The molar flow rate of gas component i is calculated from eqs. (11) to (17) using the reaction rates calculated with eqs. (25) and (26). The actual outlet concentration y_i^{out} of the gas species i is then calculated from the outlet molar flow rates according to

$$y_i^{out} = \frac{n_i^{out}}{n_{tot}^{out}}. (3.30)$$

3.2.4. Test matrix and test procedure

A generic test sequence consists of the following steps:

- Calibration of the gas analysers
- Continuous injection of air at the nominal flow rate
- Gas pre-heating to obtain the nominal inlet temperature
- Continuous injection of steam to obtain the nominal steam concentration
- **Continuous injection of nitrogen** to obtain the nominal oxygen concentration (in case of oxygen starvation tests)

- Continuous injection of hydrogen to obtain the nominal hydrogen concentration
- Continuous injection of carbon monoxide to obtain the nominal carbon monoxide concentration
- When a steady-state reaction process has established: Measurement of the catalyst temperature (single measurement or measurements in all four vertical positions) and outlet gas concentrations (average over several minutes)
- A series of several steady-state measurement points is obtained by step-wise changing the gas composition at the flow tube inlet
- Stop of carbon monoxide injection
- Stop of hydrogen injection
- Switch from mixed air/nitrogen injection to pure air injection
- Stop of steam injection
- Stop of gas pre-heating
- After cooling, stop of air injection

The whole test sequence is driven by the operation of the mass flow controllers. When a gas species is added to or removed from the gas mixture, the other gas flows are adapted accordingly in order to maintain a constant total flow rate.

3.2.5. Results

The REKO-3 experimental program includes the generation of a database with steady-state data to support the advancement of the numerical PAR models as well as tests to identify the conditions for catalyst deactivation in the presence of carbon monoxide.

3.2.5.1. Reference tests

In order to deduce relevant operating parameters of a real PAR to be established in the REKO-3 facility, measurements from the OECD/NEA-THAI HR-1 and HR-2 experiments were reviewed, which were performed at a vessel pressure of 1 bar.

The flow velocity to be applied in the REKO-3 facility was determined from the THAI tests, see Figure 47. Exposing the catalyst in the REKO-3 facility to corresponding gas mixtures, the resulting catalyst temperatures at the leading edge (Figure 48) and hydrogen outlet concentrations (Figure 49) obtained in the run R3-A-020 are both in very good agreement with the THAI data.

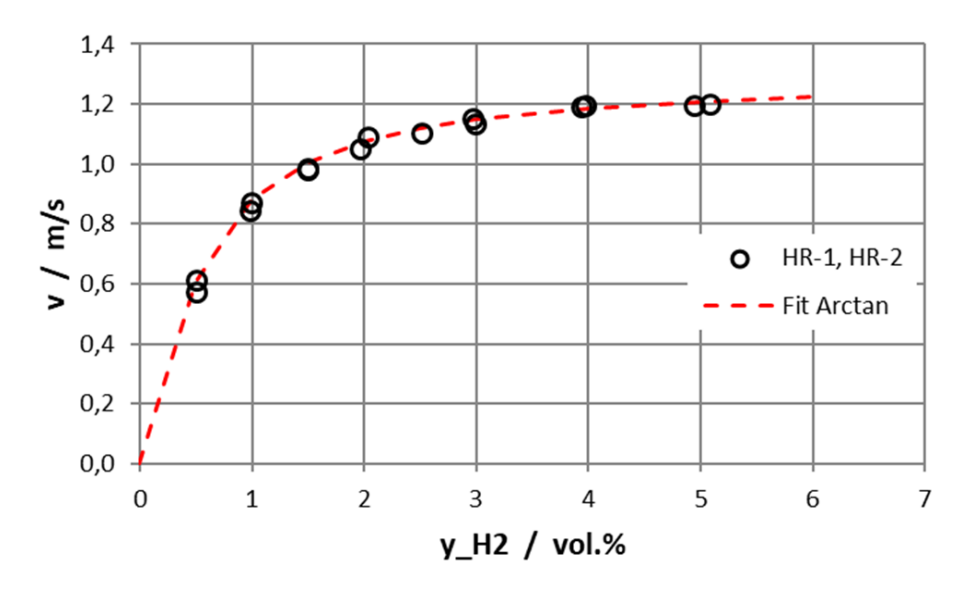


Figure 47. REKO-3: Flow velocity obtained from THAI HR-1 and HR-2

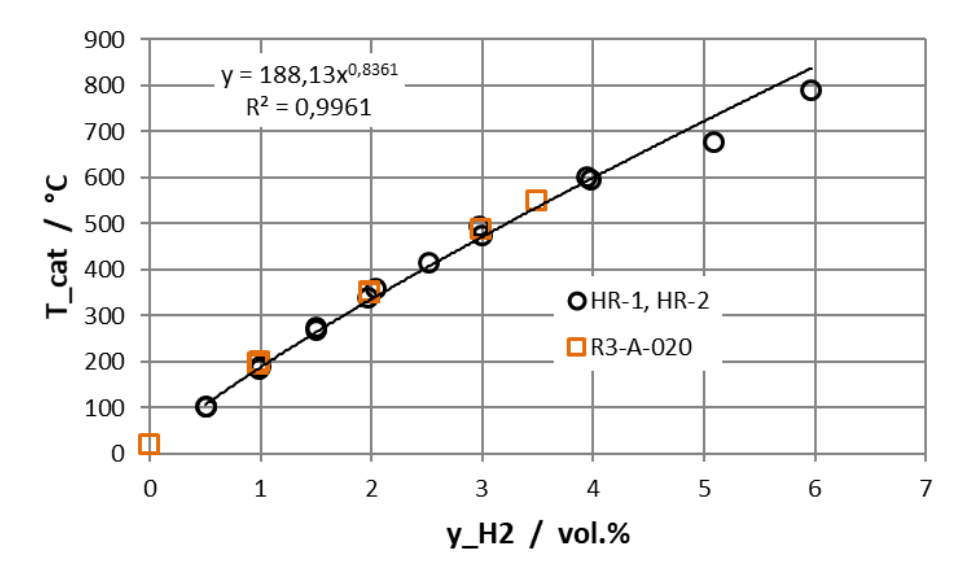


Figure 48. REKO-3: Comparison of the catalyst temperature with THAI HR-1 and HR-2

For the database, the catalyst temperature was measured in different positions of the catalyst sheet to obtain the temperature profiles for the different gas compositions. According to the laws of diffusion-controlled reaction kinetics, the catalyst temperature, which corresponds with the recombination rate, is higher at the leading edge of the catalyst.

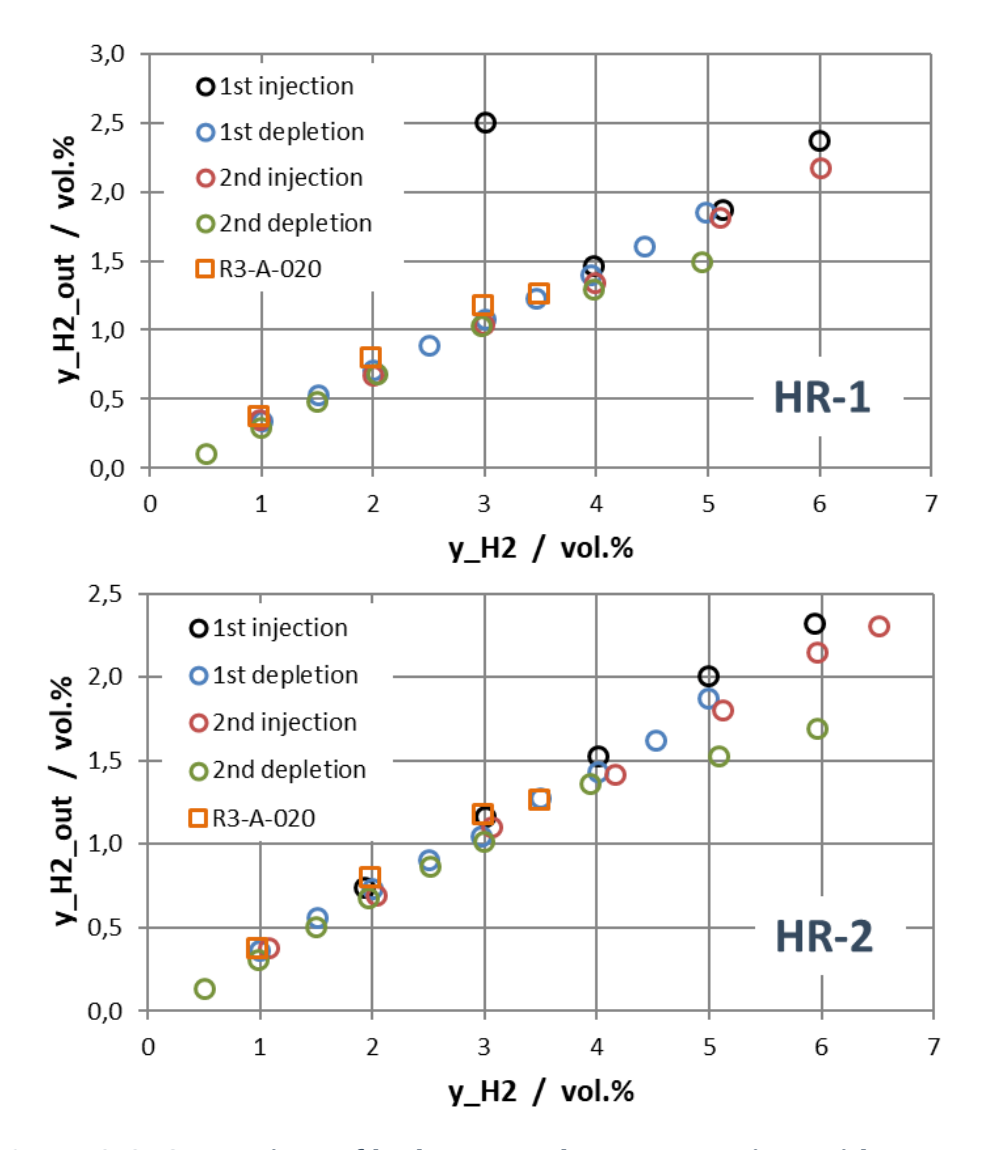
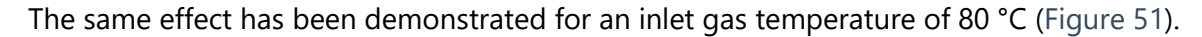


Figure 49. REKO-3: Comparison of hydrogen outlet concentrations with THAI HR-1 and HR-2

The effect of oxygen starvation on the temperature profile is shown in Figure 50. For this purpose, the initial oxygen fraction (approx. 20 vol.% of hydrogen mixture with air) was stepwise decreased as indicated in the diagram. The measurements were performed for a gas mixture with 3 vol.% hydrogen at 20 °C.

The temperature profile for approx. 20 vol.% oxygen is represented by the black circles. Once the oxygen fraction is decreased to 3 vol.% (green circles), oxygen starvation is first observed in the lower region of the catalyst. When the oxygen fraction is further decreased to 2 vol.% (purple circles), the oxygen starvation effect becomes more pronounced and the entire temperature profile level decreases.



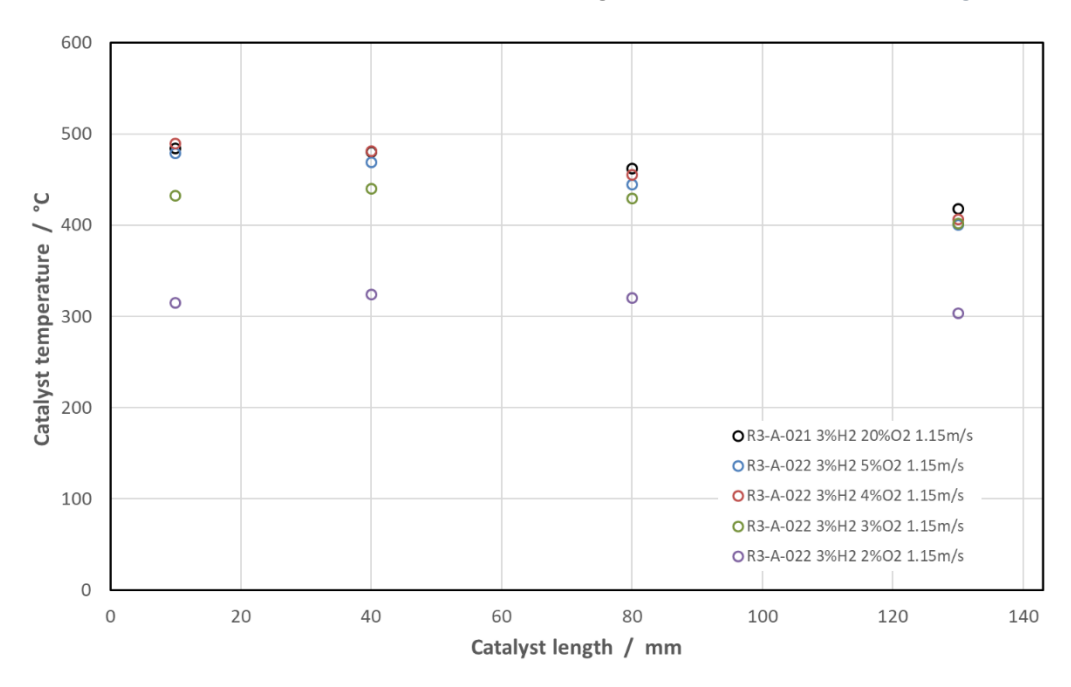


Figure 50. REKO-3: Effect of oxygen starvation on the catalyst temperature (20 °C)

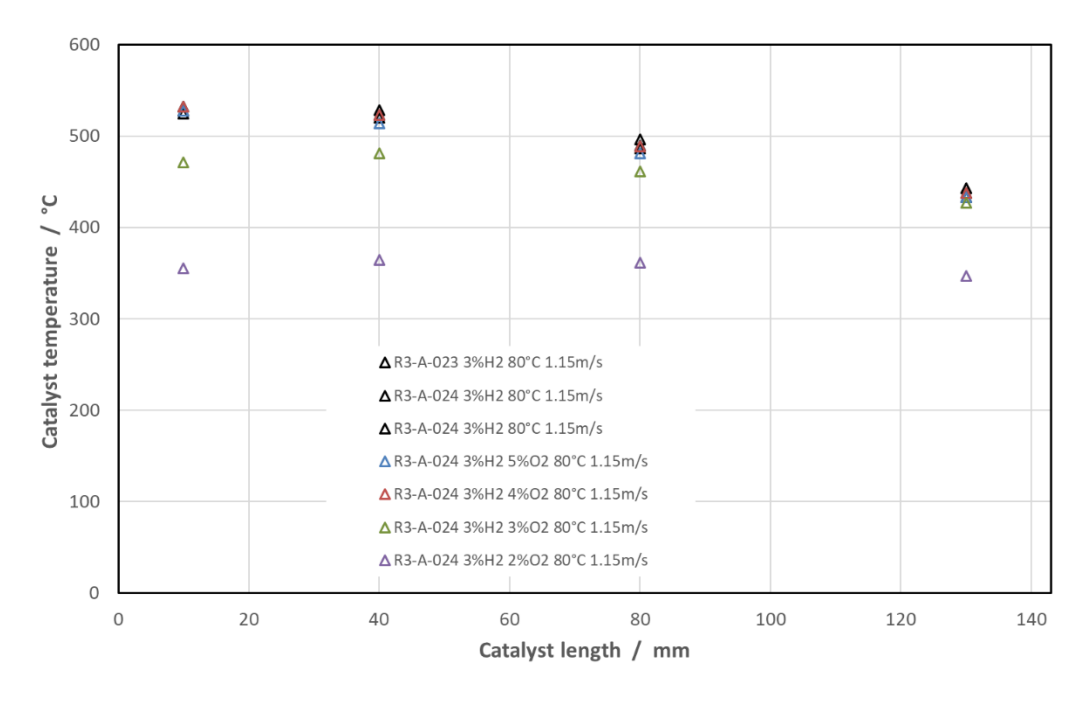


Figure 51. REKO-3: Effect of oxygen starvation on the catalyst temperature (80 °C)

Figure 52 illustrates the observations of stepwise reduction of the oxygen concentration without the presence of carbon monoxide (run R3-CO-B-06). The gas mixture has an initial oxygen concentration of 3 vol.% ("inlet O2") at a constant temperature of nominal 150 °C ("TR 3.22").

When the hydrogen injection starts with 3 vol.% hydrogen at approx. 570 s, the Pd-catalyst temperature (in the lowest measurement position) increases to 515 °C as a consequence of the exothermic reaction, which can also be seen from the outlet hydrogen and oxygen concentrations ("outlet H2" and "outlet O2", respectively). It should be noted that the catalyst is already operating in oxygen-lean conditions.

When, in the following, the oxygen concentration is reduced to values of 2.0 vol.%, 1.5 vol.%, 1.0 vol.%, and 0.5 vol.%. A corresponding decrease in the recombination rate can be observed, reflecting in an increasing outlet concentration of hydrogen and a decreasing catalyst temperature.

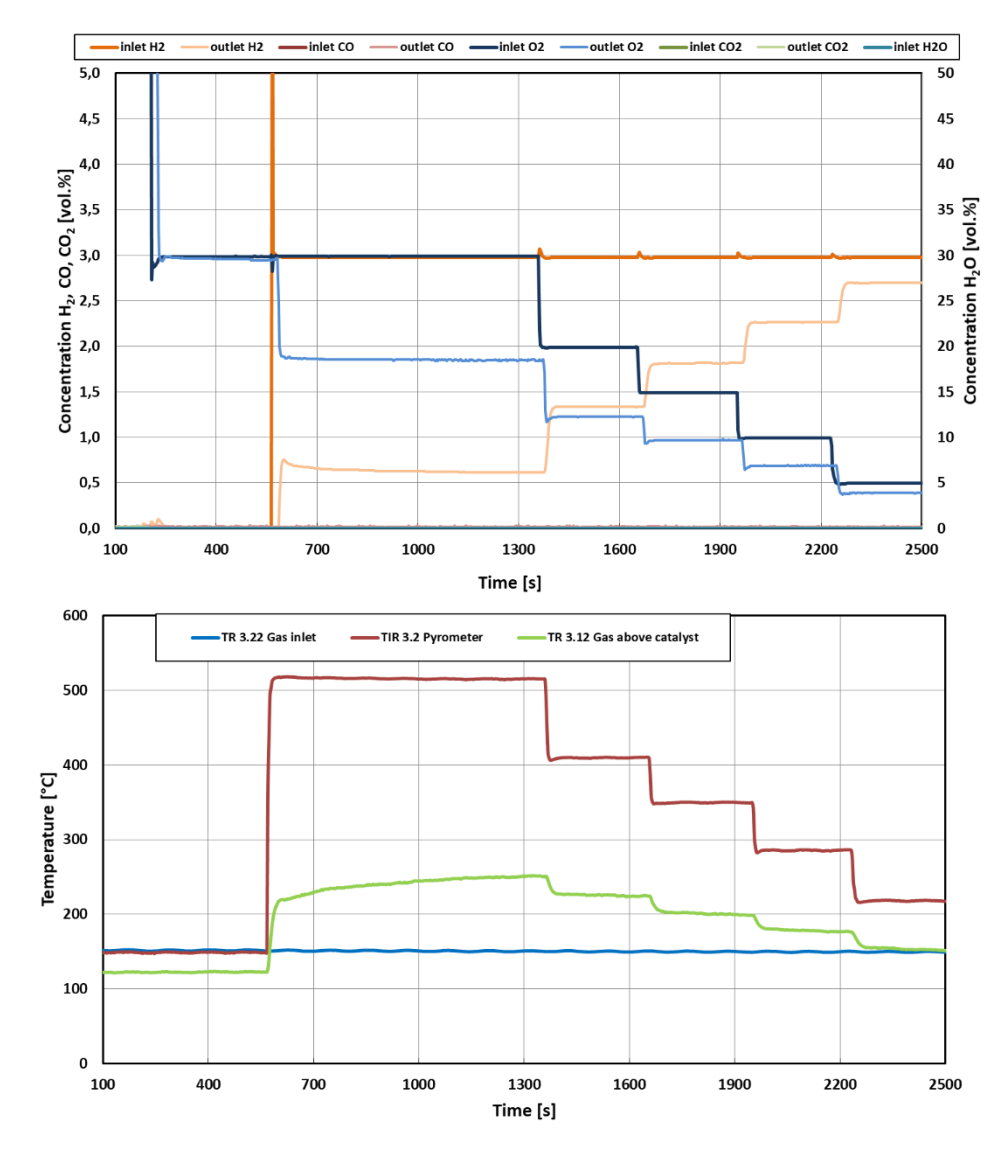


Figure 52. REKO-3: Effect of oxygen reduction on catalyst operation, Pd-based catalyst, 150 °C, 3 vol.% H₂, 0 vol.% CO (R3-CO-B-06)

It should be noted that the catalyst stays active even for the extreme low oxygen concentration of 0.5 vol.%.

In Figure 53 the experimental sequence was repeated with the same boundary conditions. This time, the gas mixture includes 1 vol.% carbon monoxide ("inlet CO"). When the oxygen concentration is stepwise reduced, we observe the same trends as before: The hydrogen concentration increases and the catalyst temperature decreases. In addition, we now observe an increase in the carbon monoxide outlet concentration ("outlet CO") and a decrease in the carbon dioxide outlet concentration ("outlet CO2"). However, it should be noted that the catalyst is no longer active at 0.5 vol.% oxygen (i.e. poisoned). This process already starts slightly at 1 vol.% oxygen, which can be seen in the more pronounced temperature drop (i.e. partially poisoned).

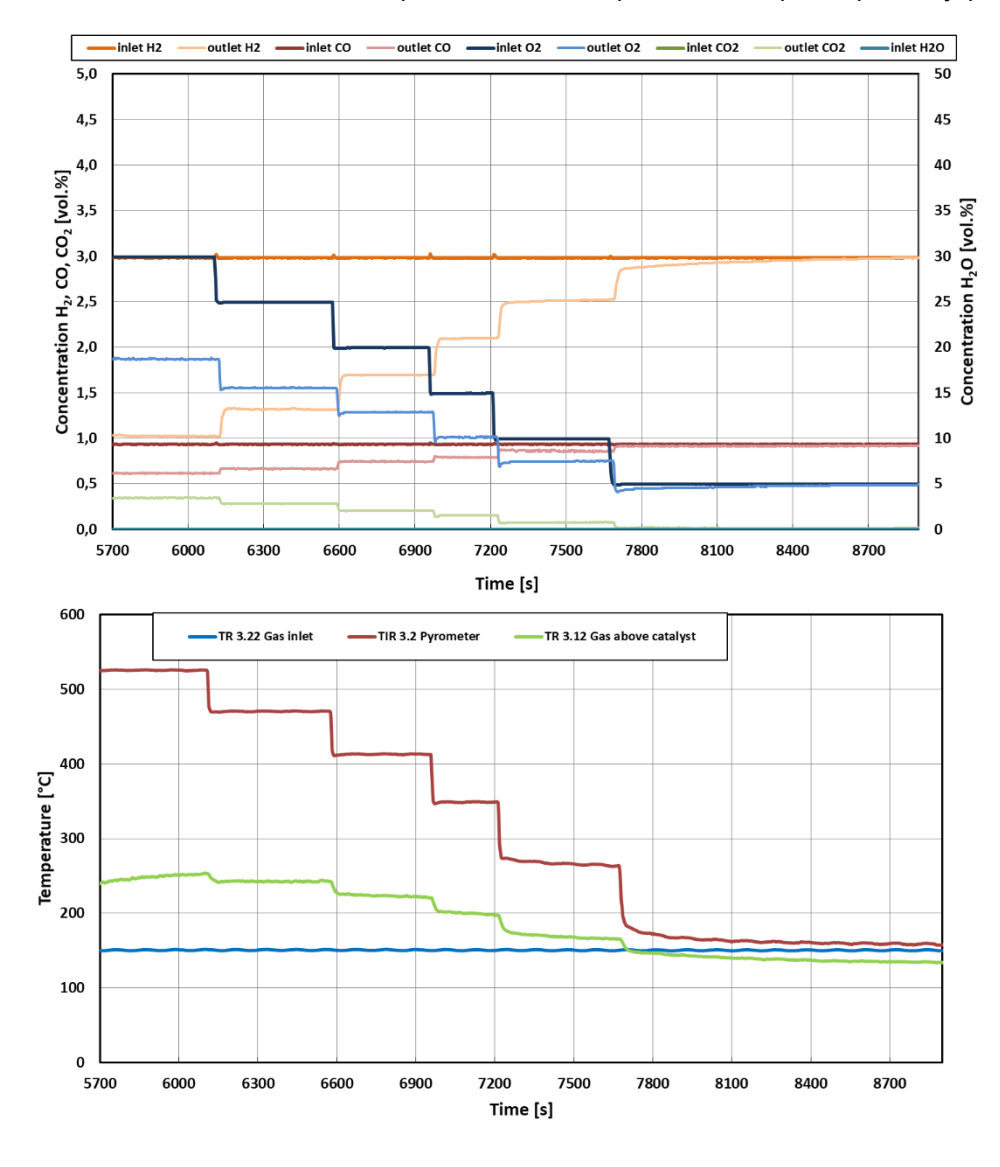


Figure 53. REKO-3: Effect of oxygen starvation on catalyst operation, Pd-based catalyst, 150 °C, 3 vol.% H₂, 1 vol.% CO (R3-CO-B-06)

Figure 54 shows the same test sequence as before, now with 3 vol.% carbon monoxide in the gas mixture. The first sign of partial catalyst deactivation occurs again at 1 vol.% oxygen. Due to the larger amount of carbon monoxide, the effect is more pronounced than before. However, after ~900 s the system seems to reach a still stable operational point with reduced PAR recombination. Only after the oxygen concentration reaches 0.5 vol.%, the catalyst becomes fully poisoned.

Although the effect of partial poisoning is more pronounced for the test with 3 vol.% carbon monoxide compared to the one with 1 vol.% carbon monoxide, both events occur at the same oxygen concentration, within the accuracy of 0.5 vol.% steps chosen for the oxygen starvation process.

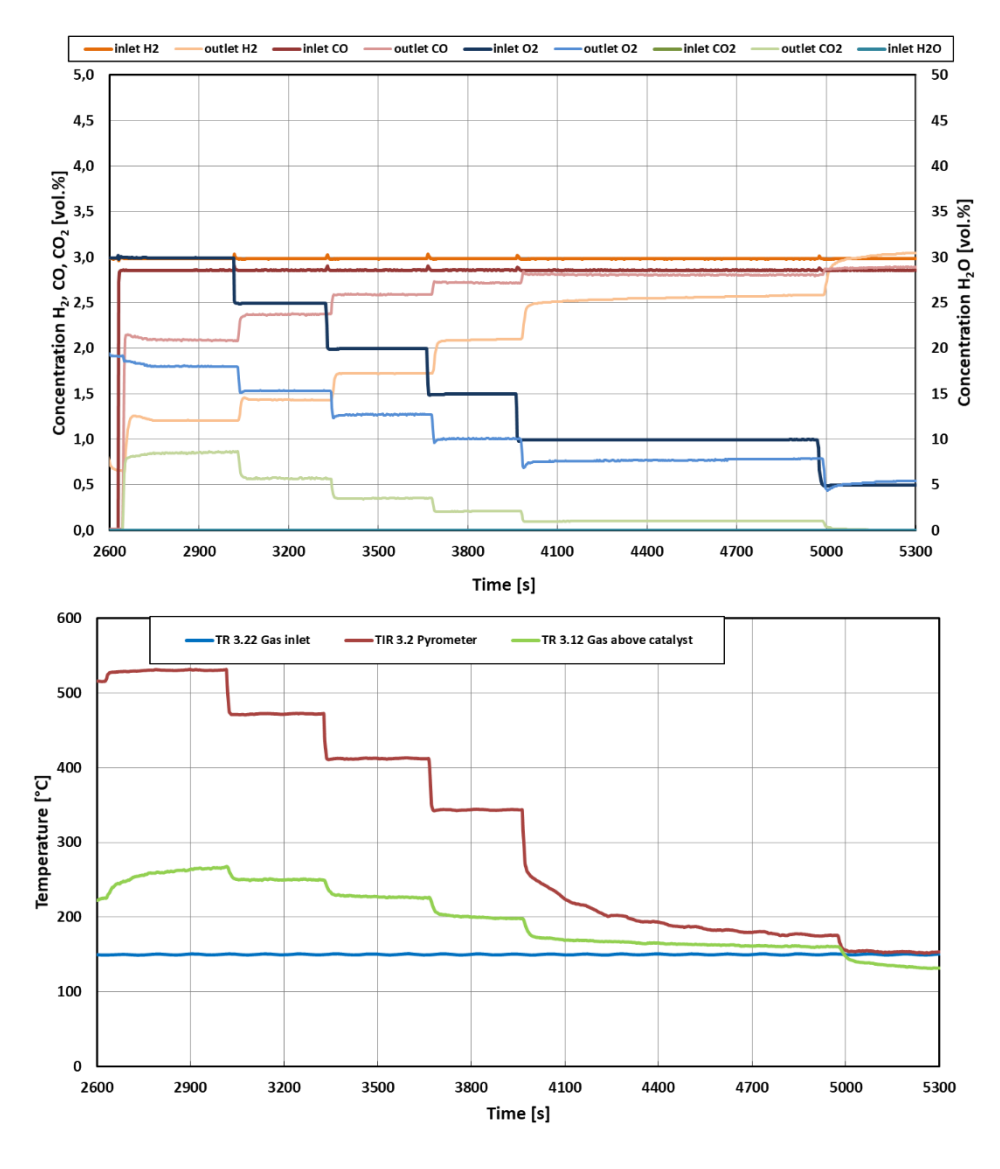


Figure 54. REKO-3: Effect of oxygen starvation on catalyst operation, Pd-based catalyst, 150 °C, 3 vol.% H₂, 3 vol.% CO (R3-CO-B-06)

The gas temperature influences the oxygen concentration where catalyst poisoning starts. Figure 55 shows the transient observed for the same gas mixture at a gas inlet temperature of 80 °C. The numbers in the bottom graph indicate the position of the catalyst temperature measurement as explained in Figure 40. Here, first deactivation effects are observed at 2 vol.% of oxygen indicated by the initial temperature fluctuation in position 1 ($6200 - 6500 \, s$). The catalyst is fully poisoned at 1.5 vol.% oxygen.

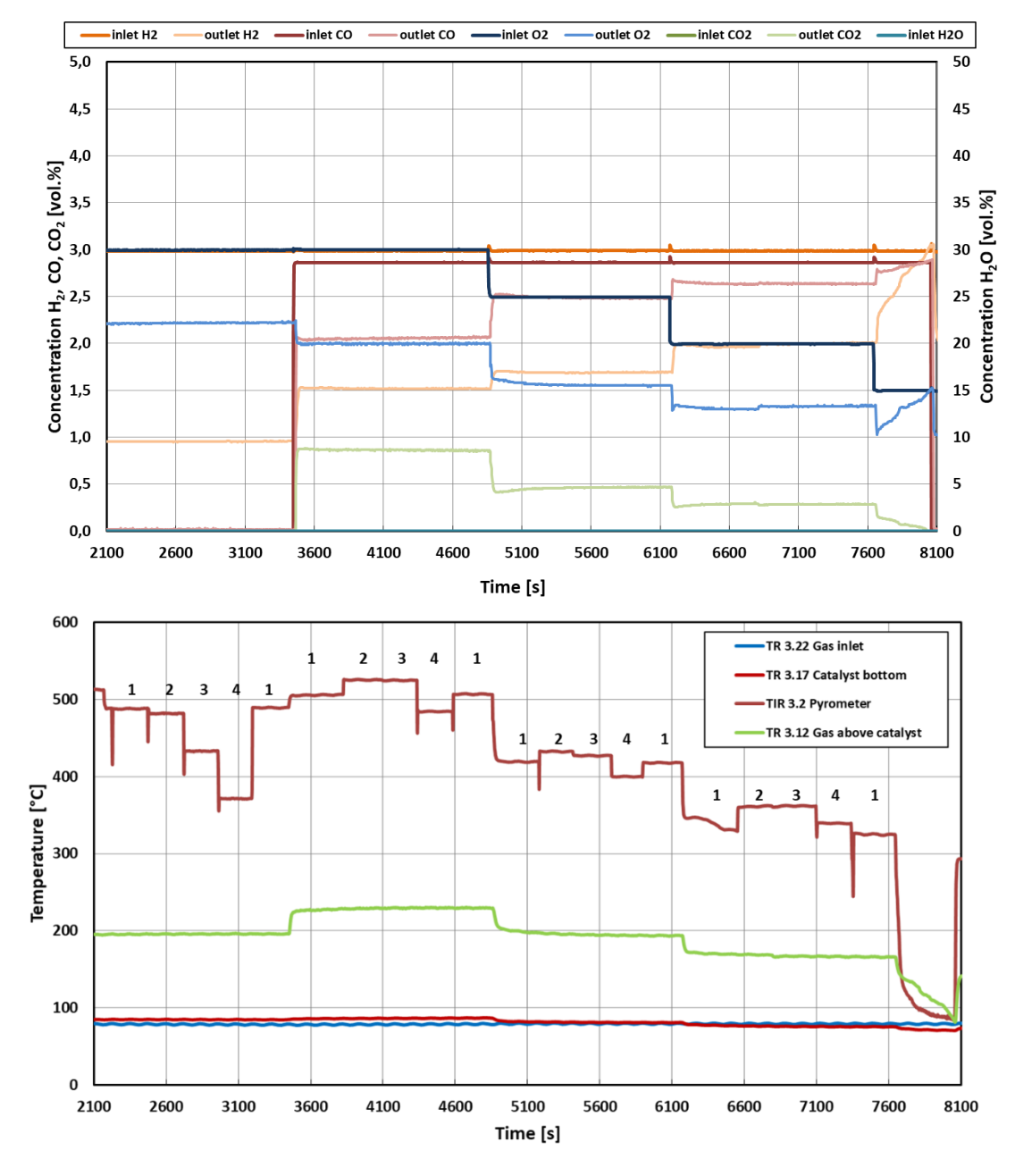


Figure 55. REKO-3: Effect of oxygen starvation on catalyst operation, Pd-based catalyst, 80 °C, 3 vol.% H₂, 3 vol.% CO (R3-CO-B-04)

Table 5 summarizes the findings for the palladium-based catalyst under dry conditions. In general, no poisoning was observed for oxygen concentrations 2.5 vol.% and higher (green). Below 2.5 vol.% oxygen, poisoning depends on the gas temperature. First signs of deactivation are observed for the lowest temperature investigated (80 °C) at 2 vol.% oxygen for hydrogen/carbon monoxide ratio equal to 1 (yellow). At 1.5 vol.% oxygen, the catalyst is fully poisoned (red). For 115 °C, the oxygen threshold moves to 1.0 vol.%, while for 150 °C full poisoning occurs at 0.5 vol.% oxygen.

Table 5. REKO-3: Poisoning conditions for palladium-based catalyst (dry conditions)

Poisoning [Pd]											
Name	Steam	H ₂	СО	Т	O ₂						
	vol.%	vol.%	vol.%	°C			vo	l.%			
3%H2 0%CO	0,0	3,0	0,0	20 - 150	3,0	2,5	2,0	1,5	1,0	0,5	
5%H2 5%CO	0,0	5,0	5,0	80	3,0	2,5	2,0	1,5			
4%H2 4%CO	0,0	4,0	4,0	80	3,0	2,5	2,0	1,5			
3%H2 3%CO	0,0	3,0	3,0	80	3,0	2,5	2,0	1,5			
3%H2 3%CO	0,0	3,0	3,0	80	3,0	2,5	2,0	1,5			
3%H2 2%CO	0,0	3,0	2,0	80	3,0	2,5	2,0	1,5			
3%H2 1%CO	0,0	3,0	1,0	80	3,0	2,5	2,0	1,5			
3%H2 1%CO	0,0	3,0	1,0	80	3,0	2,5	2,0	1,5			
5%H2 1%CO	0,0	5,0	1,0	80	3,0	2,5	2,0	1,5			
5%H2 5%CO	0,0	5,0	5,0	115	3,0	2,5	2,0	1,5			
4%H2 4%CO	0,0	4,0	4,0	115	3,0	2,5	2,0	1,5	1,0		
3%H2 3%CO	0,0	3,0	3,0	115	3,0	2,5	2,0	1,5	1,0		
3%H2 1%CO	0,0	3,0	1,0	115	3,0	2,5	2,0	1,5	1,0		
5%H2 1%CO	0,0	5,0	1,0	115	3,0	2,5	2,0	1,5	1,0		
5%H2 5%CO	0,0	5,0	5,0	150	3,0	2,5	2,0	1,5	1,0		
4%H2 4%CO	0,0	4,0	4,0	150	3,0	2,5	2,0	1,5	1,0		
3%H2 3%CO	0,0	3,0	3,0	150	3,0	2,5	2,0	1,5	1,0	0,5	
3%H2 3%CO	0,0	3,0	3,0	150	3,0	2,5	2,0	1,5	1,0	0,5	
3%H2 2%CO	0,0	3,0	2,0	150	3,0	2,5	2,0	1,5	1,0	0,5	
3%H2 1%CO	0,0	3,0	1,0	150	3,0	2,5	2,0	1,5	1,0	0,5	
3%H2 1%CO	0,0	3,0	1,0	150	3,0	2,5	2,0	1,5	1,0	0,5	
5%H2 1%CO	0,0	5,0	1,0	150	3,0	2,5	2,0	1,5	1,0	0,5	

For wet conditions, the oxygen threshold for poisoning is slightly moving to lower values (Table 6). For all temperatures, first signs of partial deactivation occur at the same oxygen concentration. However, full poisoning doesn't occur for temperatures above 115 °C (with one exception).

Table 6. REKO-3: Poisoning conditions for palladium-based catalyst (wet conditions)

Poisoning [Pd]										
Name	Steam	H ₂	СО	Т	O ₂					
	vol.%	vol.%	vol.%	°C			vo	l.%		
3%H2 0%CO	46,8	3,0	0,0	20 - 150	3,0	2,5	2,0	1,5	1,0	0,5
5%H2 5%CO	46,8	5,0	5,0	80	3,0	2,5	2,0	1,5		
3%H2 3%CO	46,8	3,0	3,0	80	3,0	2,5	2,0	1,5		
5%H2 1%CO	46,8	5,0	1,0	80	3,0	2,5	2,0	1,5		
7%H2 1%CO	46,8	7,0	1,0	80	3,0	2,5	2,0	1,5	1,0	
5%H2 5%CO	46,8	5,0	5,0	115	3,0	2,5	2,0	1,5	1,0	0,5
3%H2 3%CO	46,8	3,0	3,0	115	3,0	2,5	2,0	1,5	1,0	
5%H2 1%CO	46,8	5,0	1,0	115	3,0	2,5	2,0	1,5	1,0	0,5
7%H2 1%CO	46,8	7,0	1,0	115	3,0	2,5	2,0	1,5	1,0	0,5
5%H2 5%CO	46,8	5,0	5,0	150	3,0	2,5	2,0	1,5	1,0	0,5
3%H2 3%CO	46,8	3,0	3,0	150	3,0	2,5	2,0	1,5	1,0	0,5
5%H2 1%CO	46,8	5,0	1,0	150	3,0	2,5	2,0	1,5	1,0	0,5
7%H2 1%CO	46,8	7,0	1,0	150	3,0	2,5	2,0	1,5	1,0	0,5

For the platinum-based catalysts, no significant difference between dry and wet conditions can be observed (see Table 7 and Table 8).

Table 7. REKO-3: Poisoning conditions for platinum-based catalyst (dry conditions)

Poisoning [Pt]										
Name	Steam	H ₂	СО	Т	02					
	vol.%	vol.%	vol.%	°C			vol	l.%		
3%H2 0%CO	0,0	3,0	0,0	20 - 150	50 3,0 2,5 2,0 1,5 1,0 0				0,5	
3%H2 3%CO	0,0	3,0	3,0	80	3,0	2,5				
3%H2 2%CO	0,0	3,0	2,0	80	3,0	2,5	2,0			
3%H2 1%CO	0,0	3,0	1,0	80	3,0	2,5	2,0			
3%H2 3%CO	0,0	3,0	3,0	115	3,0	2,5	2,0			
3%H2 2%CO	0,0	3,0	2,0	115	3,0	2,5	2,0			
3%H2 1%CO	0,0	3,0	1,0	115	3,0	2,5	2,0	1,5		
3%H2 3%CO	0,0	3,0	3,0	150	3,0	2,5	2,0	1,5		
3%H2 2%CO	0,0	3,0	2,0	150	3,0	2,5	2,0	1,5		
3%H2 1%CO	0,0	3,0	1,0	150	3,0	2,5	2,0	1,5		

For the lowest temperature investigated (80 °C), the earliest poisoning occurs for oxygen concentrations below 3.0 vol.% for gas mixtures with a hydrogen/carbon monoxide ratio of 1. The oxygen threshold slightly decreases for higher temperatures. However, in the presence of carbon monoxide, no reaction can be observed in the entire temperature range for oxygen concentrations below 2.0 vol.%.

Table 8. REKO-3: Poisoning conditions for platinum-based catalyst (wet conditions)

Poisoning [Pt]											
Name	Steam	H ₂	СО	Т	O ₂						
	vol.%	vol.%	vol.%	°C			٧	ol.%			
3%H2 0%CO	46,8	3,0	0,0	20 - 150	3,0	2,5	2,0	1,5	1,0	0,5	0,0
5%H2 5%CO	46,8	5,0	5,0	80	3,0	2,5					
3%H2 3%CO	46,8	3,0	3,0	80	3,0	2,5					
3%H2 3%CO	46,8	3,0	3,0	80	3,0	2,5					
3%H2 2%CO	46,8	3,0	2,0	80	3,0	2,5	2,0				
3%H2 2%CO	46,8	3,0	2,0	80	3,0	2,5	2,0				
3%H2 1%CO	46,8	3,0	1,0	80	3,0	2,5	2,0				
3%H2 1%CO	46,8	3,0	1,0	80	3,0	2,5	2,0				
5%H2 1%CO	46,8	5,0	1,0	80	3,0	2,5	2,0				
5%H2 5%CO	46,8	5,0	5,0	115	3,0	2,5					
4%H2 4%CO	46,8	4,0	4,0	115	3,0	2,5	2,0				
3%H2 4%CO	46,8	3,0	4,0	115	3,0	2,5	2,0				
3%H2 3%CO	46,8	3,0	3,0	115	3,0	2,5	2,0				
3%H2 3%CO	46,8	3,0	3,0	115	3,0	2,5	2,0				
4%H2 3%CO	46,8	4,0	3,0	115	3,0	2,5	2,0				
3%H2 2%CO	46,8	3,0	2,0	115	3,0	2,5	2,0				
3%H2 2%CO	46,8	3,0	2,0	115	3,0	2,5	2,0				
4%H2 2%CO	46,8	4,0	2,0	115	3,0	2,5	2,0				
5%H2 1%CO	46,8	5,0	1,0	115	3,0	2,5	2,0	1,5			
5%H2 5%CO	46,8	5,0	5,0	150	3,0	2,5	2,0				
3%H2 3%CO	46,8	3,0	3,0	150	3,0	2,5	2,0				
3%H2 3%CO	46,8	3,0	3,0	150	3,0	2,5	2,0				
3%H2 2%CO	46,8	3,0	2,0	150	3,0	2,5	2,0	1,5			
3%H2 2%CO	46,8	3,0	2,0	150	3,0	2,5	2,0	1,5			
3%H2 1%CO	46,8	3,0	1,0	150	3,0	2,5	2,0	1,5			
3%H2 1%CO	46,8	3,0	1,0	150	3,0	2,5	2,0	1,5			
5%H2 1%CO	46,8	5,0	1,0	150	3,0	2,5	2,0	1,5			

3.2.6.Conclusions

Despite the complex surface processes, the experimental data allow to derive empirical criteria for catalyst poisoning with sufficient (if necessary conservative) precision, which are based on two easy to obtain parameters, i.e. the gas temperature and the oxygen concentration.

Figure 56 and Figure 57 propose ranges of partial (yellow) and full catalyst poisoning (red) for platinum-based and palladium-based catalyst, respectively, for gas temperatures between 80 °C and 150 °C. Depending on the requested level of conservatism, partial deactivation can already be treated as a fully poisoned catalyst.

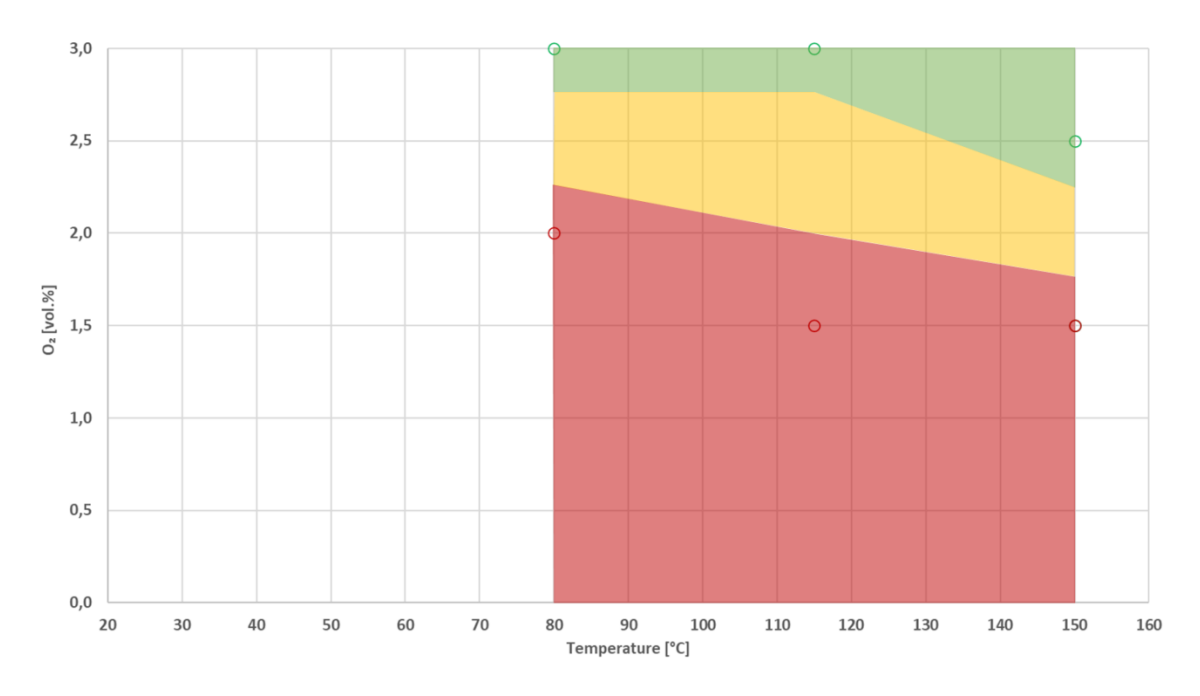


Figure 56. REKO-3: Ranges of partial and full poisoning for the platinum-based catalyst

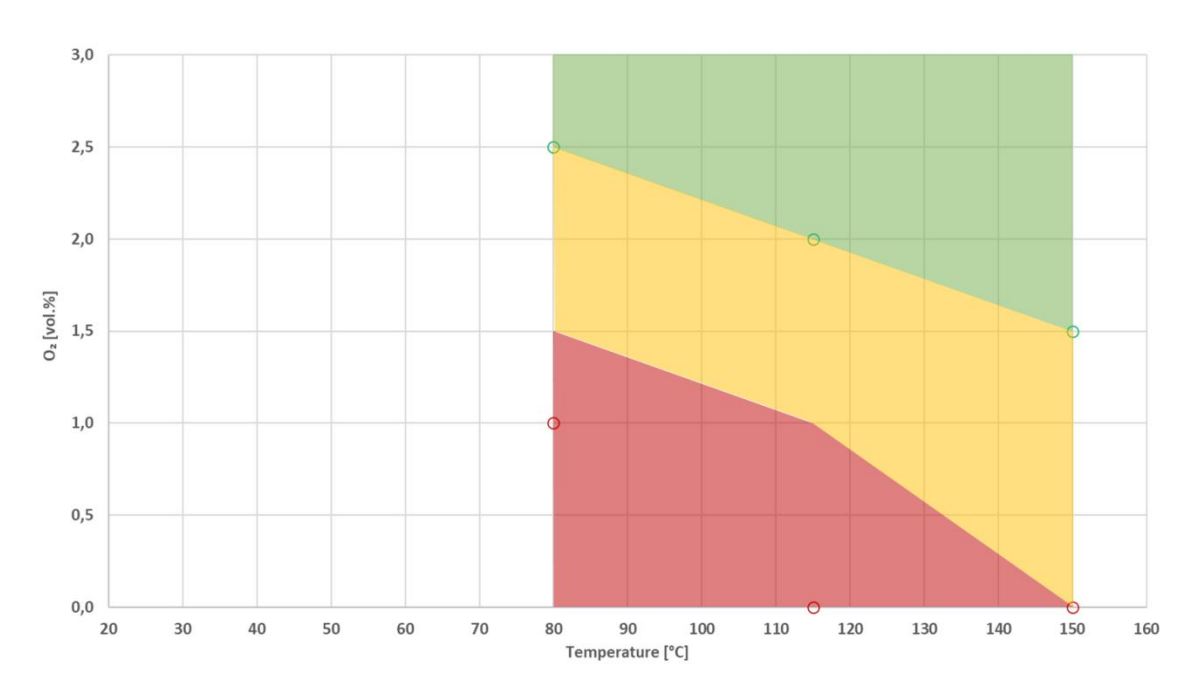


Figure 57. REKO-3: Ranges of partial and full poisoning for the palladium-based catalyst

3.3. Natural convection tests

The experiments under natural flow conditions have been performed in the REKO-4 facility. The REKO-4 test facility was designed to investigate the operational behaviour of passive auto-catalytic recombiners under natural flow conditions inside a cylindrical steel pressure vessel.

3.3.1. Description of the REKO-4 test facility

3.3.1.1. Pressure vessel

The cylindrical steel pressure vessel has a free volume of 5.3 m³ (1.4 m diameter, 3.7 m height), including wall heating and outer insulation (Figure 58). The vessel is designed to perform experiments with flammable hydrogen/air mixtures up to 2 bar operational pressure (absolute) at 280 °C. The vessel is equipped with 32 flanges and a manhole with a diameter of approx. 60 cm.

Internal diameter flanges	105 mm
Internal diameter manhole	594 mm
Design pressure	25 bar (a)
Blow-off pressure rupture disks	23 bar (a)
Permissible operating pressure	0 - 2 bar (a)
Blow-off pressure of safety relief valve	2.3 bar (a)
Design temperature of vessel	280 °C
Insulation thickness	200 mm



Figure 58. REKO-4: Basic design data of the pressure vessel

Gases are injected in radial direction into the vessel by means of mass flow controllers (Figure 59). Water vapour is provided by a mobile steam generator. The vessel is equipped with thermocouples for wall and gas temperature measurements at different elevations as indicated in Figure 59. To determine the pressure inside the vessel, relative and absolute pressure sensors are applied. Furthermore, hydrogen, oxygen, and humidity sensors are installed to measure on-

line the gas distribution in the course of an experiment. A vertical fan enables the homogenization of the vessel atmosphere.

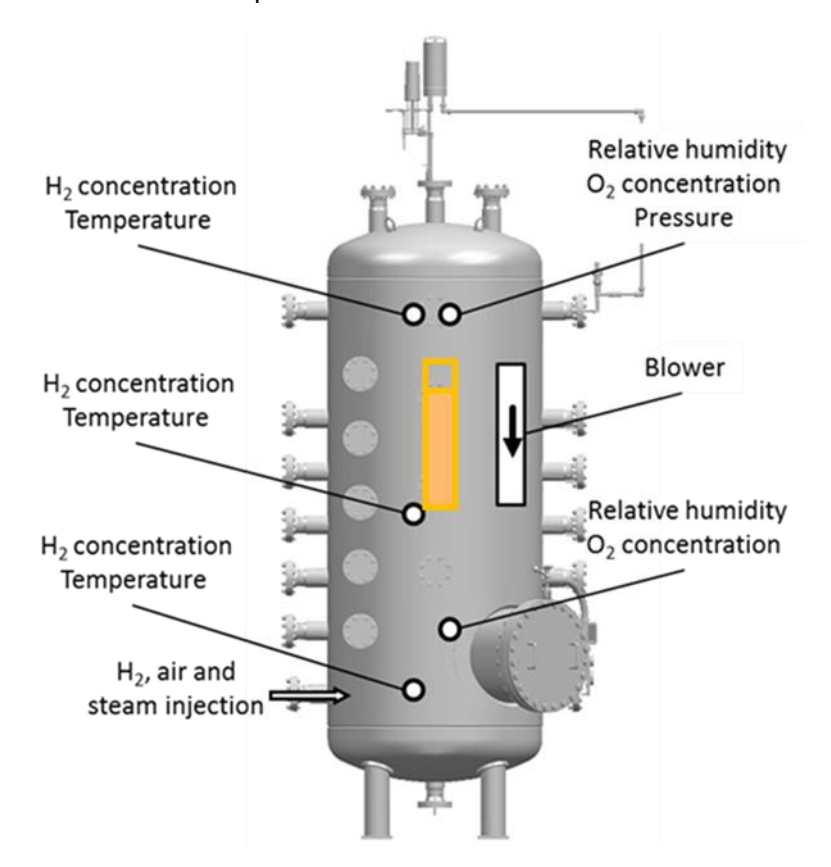


Figure 59. REKO-4: Basic sketch of the instrumentation inside the pressure vessel

3.3.1.2. **Gas supply**

Gases (hydrogen, air, nitrogen, carbon monoxide) are injected in radial direction into the vessel at an elevation of approx. 20 cm above the bottom grid by means of mass flow controllers. Water vapour is provided by a mobile steam generator.

Gases are injected via mass flow controllers. In the present set-up, a mass flow controller with a maximum flow rate of 2 n-m³/h is used for hydrogen injection (FRC 4.01). Air is injected either directly with a manually operated valve or controlled by a mass flow controller (FRC 4.02) with a maximum flow rate of 6 n-m³/h. Carbon monoxide injection is realized with a mass flow controller (FRC 4.03) at a maximum rate of 0.5 n-m³/h.

As specified by the manufacturer, the measurement uncertainty for the mass flow controllers amounts to $\leq +/-1$ % of the measurement range.

Steam is provided by an aTHMOS-RS5 direct steam generator (company ADROP Feuchtemesstechnik GmbH) with a maximum capacity of 10 L/h (liquid water). The water flow is

controlled by a Coriolis flow meter with a typical measurement uncertainty of +/- 0.15 % of the measurement range.

3.3.1.3. Instrumentation

The instrumentation includes thermocouples (TR), gas sensors for hydrogen (KR) and oxygen (O2R), pressure gauges (PR), and humidity sensors (HR). Figure 60 gives an overview of the relevant measurement points.

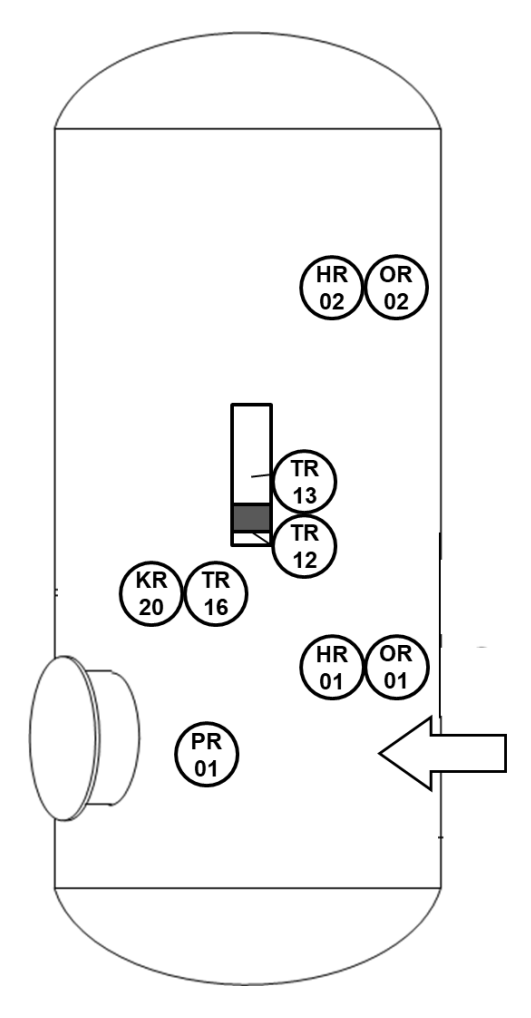


Figure 60. REKO-4: Relevant measurement points inside the vessel

Gas temperature measurement

Gas temperatures are measured by means of thermocouples of type K (cromel-alumel) with a diameter of 1 mm. Thermocouples of class 2 and corresponding measurement transducers have a measurement range of up to 1372 °C. The measurement uncertainty according to the manufacturer is given in Figure 16. However, due to the heat radiation effect from the hot catalyst samples, unavoidable higher measurement errors have to be considered depending on the thermocouple position, especially below the catalyst specimen.

Catalyst temperature measurement

Catalyst temperature is measured by means of a thermocouple of type K (cromel-alumel) with a diameter of 1 mm. Measurement range and measurement uncertainty according to the manufacturer is given above. Depending on the attachment to the catalyst surface higher measurement errors may occur.

Gas concentration measurement

The capacity humidity sensors provide measurement values for the relative humidity, absolute humidity and the sensor temperature. The measurement uncertainty for the relative humidity according to the manufacturer is given in Figure 61 for an electronic temperature of 20°C (acclimatized lab room) and 90°C process temperature. Before the test series, the sensor has been calibrated according to the procedure proposed by the manufacturer.

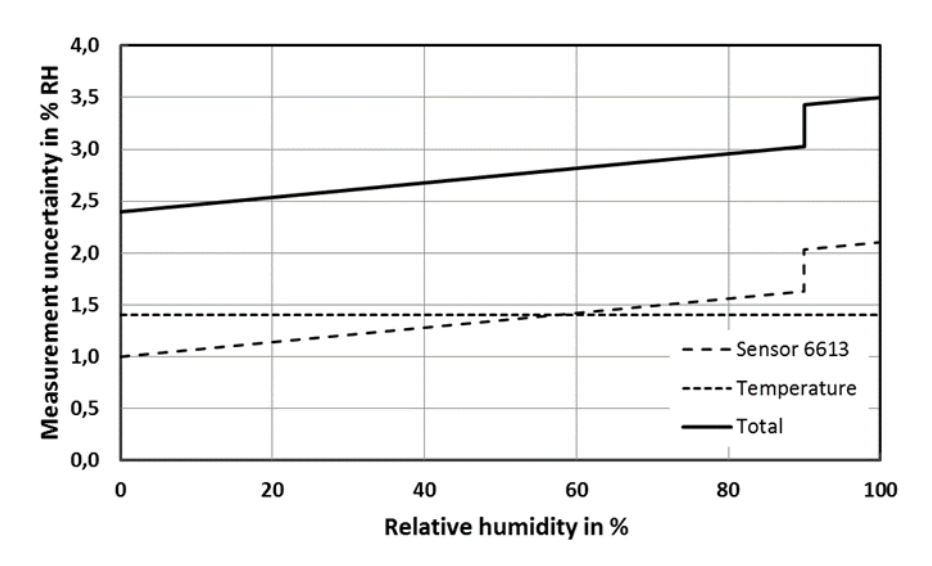


Figure 61. REKO-4: Measurement uncertainty of the humidity sensor depending on the relative humidity

For in-situ measurement of the hydrogen concentration, heat conductivity sensors (Company: Xensor Integration, Type: XEN-TCG3880 + Pt100) are installed (Figure 62). The relevant sensor is positioned close to the PAR inlet. The sensor is positioned in due distance of the catalyst surface in order to avoid the effect of heat radiation. At the PAR outlet, the effect of hot gases passing the sensor affects the sensor signals significantly. For this reason, no sensor has been placed in this position.



Figure 62. REKO-4: Blank sensor on socket (left), sensor with sintered metal filter cap (center), sensor shrinking hose ready for mounting (right)

The measurement accuracy of the hydrogen sensors depends strongly on the surrounding conditions. In particular, the pressure, temperature and the humidity have an impact on the sensor behaviour. In previous work, the long-term stability of the sensors with a maximum absolute deviation of 0.1 vol.% could be demonstrated.

The impact of humidity on the hydrogen readings (humid air has a higher heat conductivity than dry air) is corrected using the function shown in Figure 63, which results from mapping the deviation from the hydrogen readings over the absolute humidity.

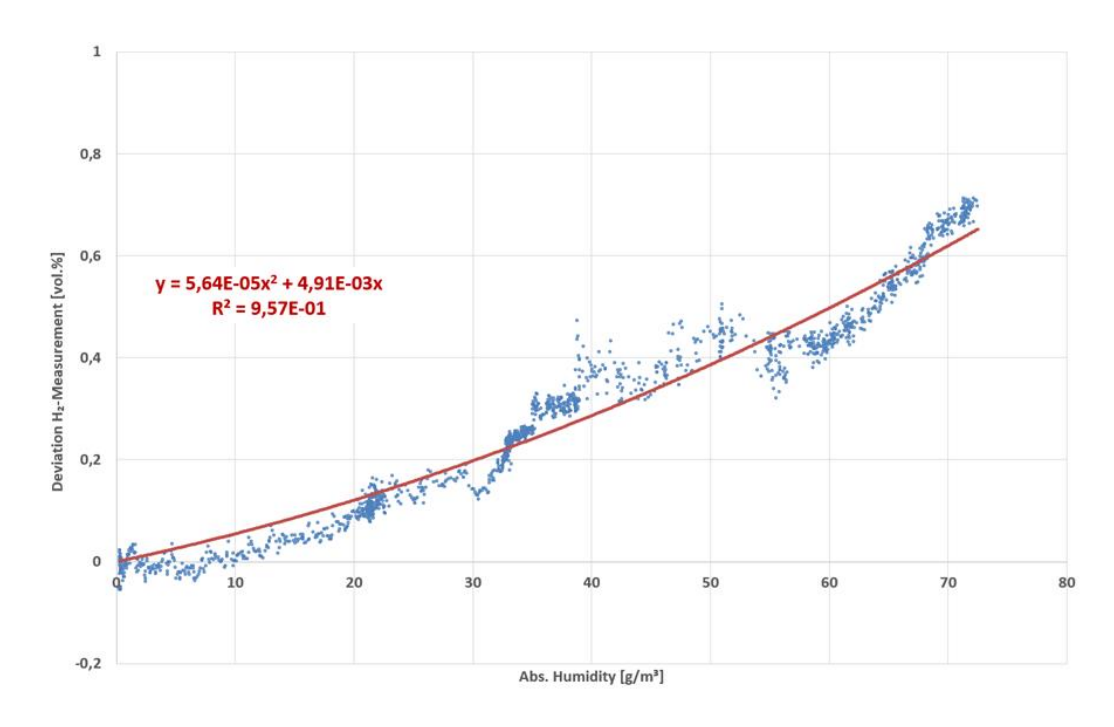


Figure 63. REKO-4: Humidity correction of the hydrogen sensors

Two optical oxygen sensors (VisiFerm DO Arc 425 by Hamilton, principle of luminescence quenching) are installed in the upper and the lower vessel region (see Figure 60). The operating pressure range is between 0-12 bar (a), the temperature range between -10 and 85 °C, and the measuring range of oxygen between 0.1 and 600 mbar partial pressure. Furthermore, the sensor is IP68-rated and withstands high humidity during tests.

The oxygen sensors measure the oxygen partial pressure of the vessel atmosphere, which is converted with the absolute pressure into an oxygen concentration. Consequently, the error of the absolute pressure sensor has to be included into the considerations of the measurement uncertainty. For an oxygen concentration of 21 vol.%, the manufacturer gives a maximum absolute measurement error of < +/- 0.2 vol.%.

The oxygen sensors are calibrated against the oxygen analyser described in chapter 3.2.1.3. Figure 64 shows the calibration curve used in the present test program.

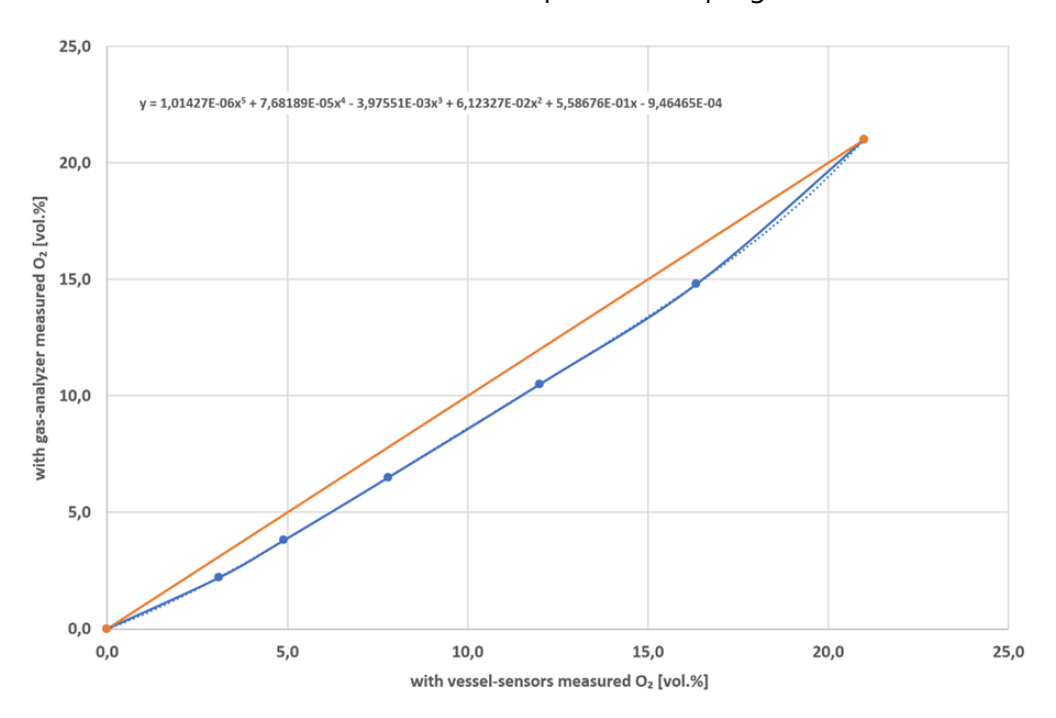


Figure 64. REKO-4: Calibration function of the oxygen sensors

Pressure measurement

Two digital manometers including a measuring cell with a piezoelectric sensor are installed to measure the absolute and relative vessel pressure. The gauge pressure sensor is a Kobold MAN-LD3S 0 to 2.5 bar (g) and allows fluid temperatures between -30 to 85 °C. The maximum ambient temperature is limited to 60 °C. The absolute pressure sensor is a WIKA S-10 with a

pressure range from 0 to 1.6 bar (a). This sensor is suitable for fluid temperatures from -30 $^{\circ}$ C to 100 $^{\circ}$ C and ambient maximum temperatures up to 80 $^{\circ}$ C

The accuracies of the absolute pressure sensor and the gauge pressure sensor are given in Figure 65. The temperature error can be neglected, because the sensors are mounted on the outside of the vessel and the lab room's temperature control keeps the ambient temperature in a range of 20-25 °C. Both measurement devices have the same accuracy class and the maximum deviation is only depending on the span of the sensor.

Quantity	Gauge pressure sensor	Absolute pressure sensor
Measurement range	1 - 2.5 bar (a)	0 - 1.6 bar (a)
Accuracy	\pm 0.5 % of span	\pm 0.5% of span
Temperature error		
- zero point	$\leq \pm 0.2\%$ of span/10 K	$\leq \pm 0.2\%$ of span/10 K
- span	$\leq \pm 0.1\%$ of span/10 K	$\leq \pm 0.2\%$ of span/10 K
Max. deviation	0.0125 bar (a)	0.008 bar (a)

Figure 65. REKO-4: Measurement uncertainties of the pressure sensors

3.3.2. Catalyst samples

The PAR used in the experiments is equipped with ten identical catalyst sheets (Figure 66) with a size of $14.3 \times 14.3 \text{ cm}^2$ each, either coated with Pt or Pd, see Figure 45. The generic catalysts have been manufactured by company Chemical Consulting Dornseiffer in Aachen/Germany. The supporting material is a thin sheet of stainless steel with a thickness of 50 µm. The ceramic washcoat consists of 4 mg/cm² γ -Al₂O₃. The amount of catalytic active material (platinum or palladium) is 1 mg/cm².

The catalyst section is enhanced with a chimney on top in order to enhance the natural flow rate and the corresponding recombination rates. The entire PAR is mounted inside the pressure vessel in center position (Figure 67).

3.3.3.Data post-processing and evaluation

The goal of the experiments is to determine the oxygen concentration when catalyst poisoning starts. The oxygen concentration is measured in-situ by sensors. In order to obtain the concentration of the other gas species, the vessel is connected with the external gas analyser (chapter 3.2.1.3) after the recombiner has entirely stopped operation.

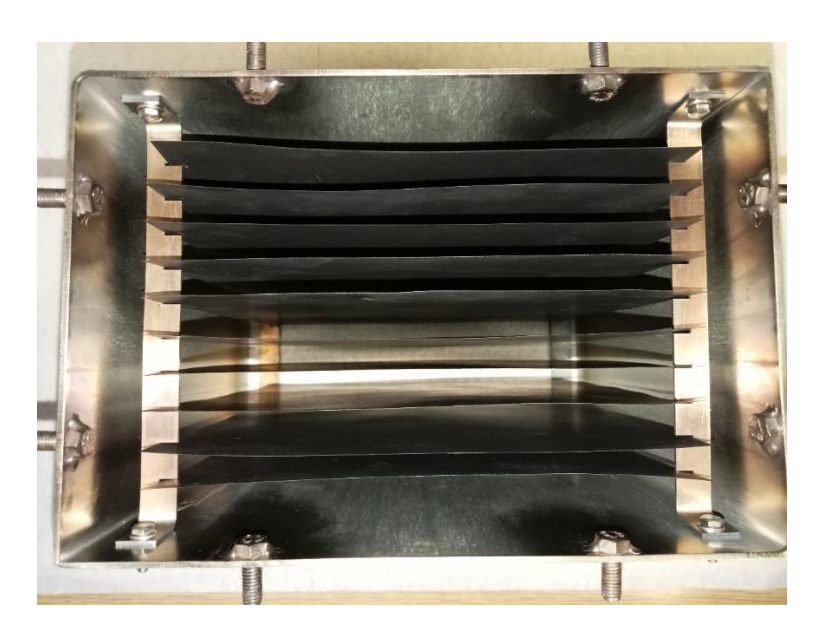


Figure 66. REKO-4: PAR catalyst section with ten sheets (palladium)

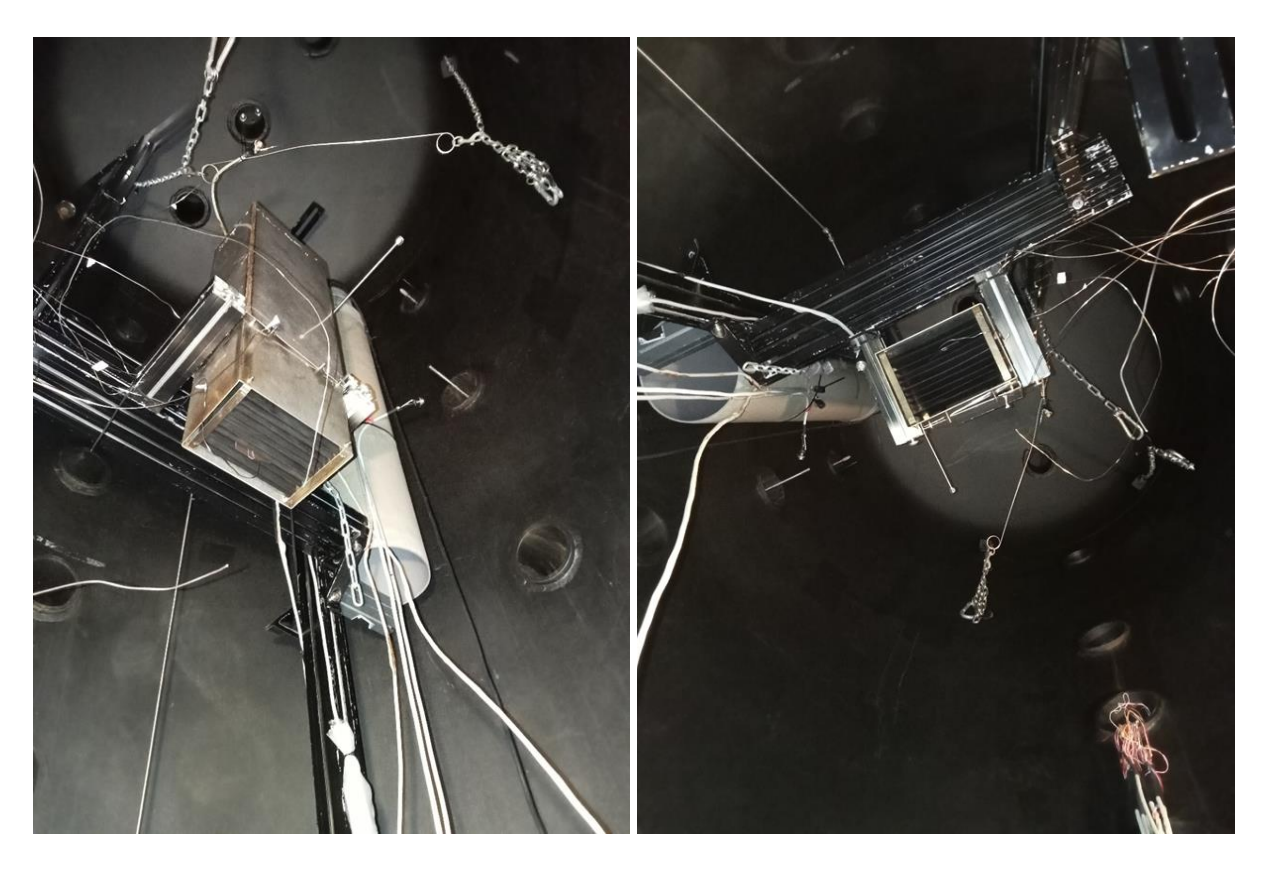


Figure 67. REKO-4: Mounting of the PAR inside the pressure vessel

3.3.4. Test matrix and test procedure

Table 9 gives an overview of the experiments performed in the REKO-4 facility. Catalyst poisoning has been studied for two different pressures at nominal gas temperatures ranging from 20 $^{\circ}$ C to 80 $^{\circ}$ C.

Table 9. REKO-4: Test matrix

	Abs. pressure	H ₂ fraction vol.%	CO fraction vol.%	Gas temperature °C					
	Platinum catalyst								
		/	0.0	20					
R4_A_01	1	2.2	0.8	26					
R4_A_03		3.6	1.4	73					
		/	0.0	20					
R4_A_02	2	3.0	1.2	29					
R4_A_04		4.4	1.1	72					
R4_A_05		3.6	1.4	73					
	F	Palladium catalyst							
R4_B_01		3.0	0.0	20					
R4_B_10	1	2.6	1.6	26					
R4_B_04	l l	2.6	3.0	48					
R4_B_03		3.0	2.3	89					
R4_B_02		3.0	0.0	20					
R4_B_08	2	2.9	1.6	57					
R4_B_05	2	3.0	1.8	56					
R4_B_06		3.1	1.9	78					

A generic test sequence consists of the following steps:

- **Calibration** of the gas analysers
- Vessel pre-heating to obtain the nominal gas temperature
- Reduction of the oxygen fraction to 5-6 vol.% by repeated injection of 1 bar nitrogen followed by release of 1 bar of the vessel atmosphere; in tests with a nominal absolute pressure of 2 bar the last release is omitted
- **Continuous injection of hydrogen** with manually controlled injection rate to obtain the nominal hydrogen fraction of 3 vol.%
- After start of the catalytic hydrogen recombination: **Continuous injection of carbon monoxide** with manually controlled injection rate to obtain the nominal carbon monoxide fraction of 3 vol.%
- When catalyst poisoning is observed: Stop of hydrogen and carbon monoxide injection
- Release of the vessel overpressure and measurement of the gas composition with the external gas analyser
- Vessel purging with dry air

A typical test sequence is shown in Figure 68. Test R4-B04 starts with a pre-reduced oxygen concentration of 6.2 vol.% (black: O2R 4.01) at a gas temperature of approx. 40 °C (green: TR 4.16). Immediately after the hydrogen injection starts (blue: hydrogen fraction KR-4-20), the recombination starts on the catalyst surface as indicated by the increase of the catalyst temperature (red: TR 4-12) and the temperature inside the PAR chimney (orange: TR 4-13). At the same time, the carbon monoxide injection starts (not represented in the graph). As a consequence, the oxygen concentration as well as the catalyst temperature is continuously decreasing (oxygen-lean conditions). At approx. 3150 s, the negative temperature gradient of the catalyst temperature changes rapidly indicating an abrupt stop of the catalytic reaction. The oxygen fraction measured at the point of change of the temperature gradient (blue circle) is considered to be the poisoning concentration.

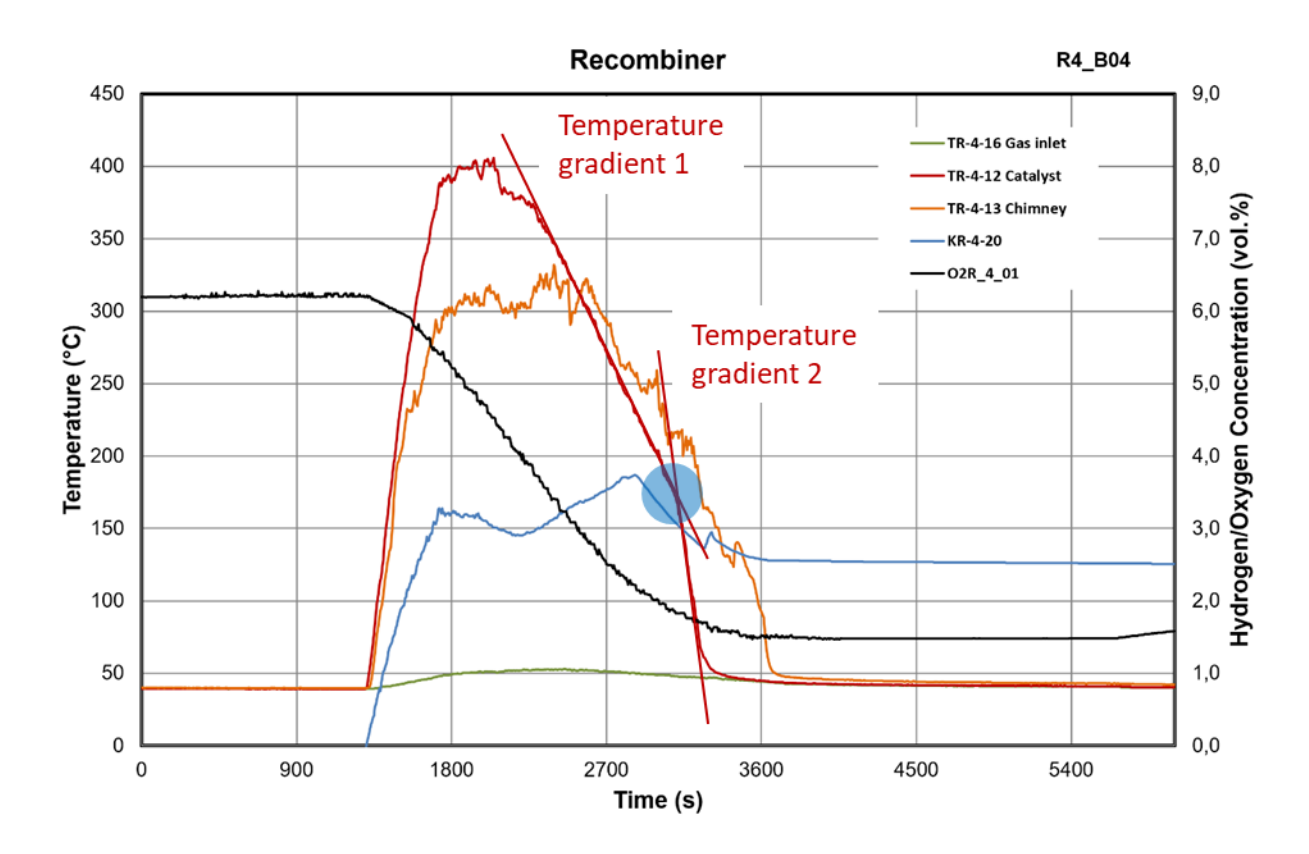


Figure 68. REKO-4: Typical test sequence

3.3.5. Results

The oxygen concentrations and the corresponding gas temperature where poisoning has been observed in the REKO-4 tests have been added to the ranges of partial and full poisoning obtained from the REKO-3 experiments (Figure 69 for the platinum-based catalyst and Figure 70 for the palladium-based catalyst).

For both catalysts, the results show no significant difference between experiments performed at 1 bar absolute pressure (squares) and 2 bar absolute pressure (diamonds). For the platinum-based catalyst, no temperature effect can be observed between 20 °C and 80 °C, which corresponds with the previous findings of only minor impact of the gas temperature on the poisoning process. The obtained data for the palladium-based catalyst confirm quite accurately the significant temperature effect observed before.

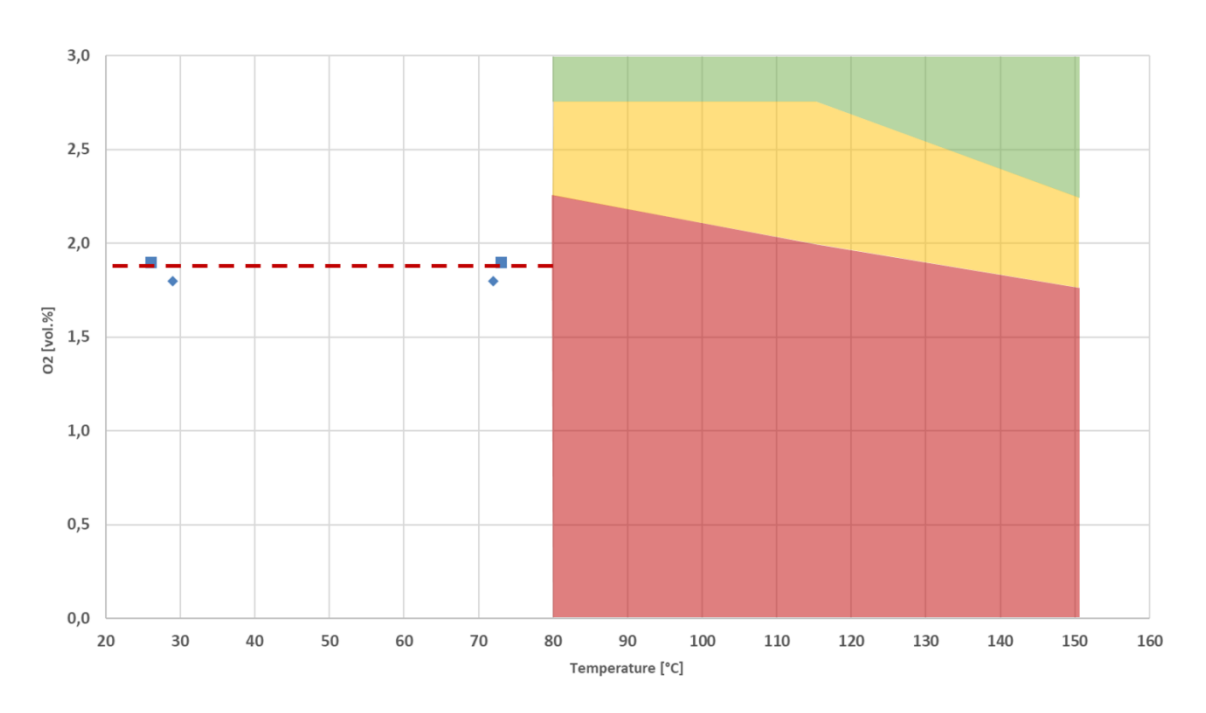


Figure 69. REKO-4: Test results for platinum-based catalyst (squares: 1 bar, diamonds: 2 bar)

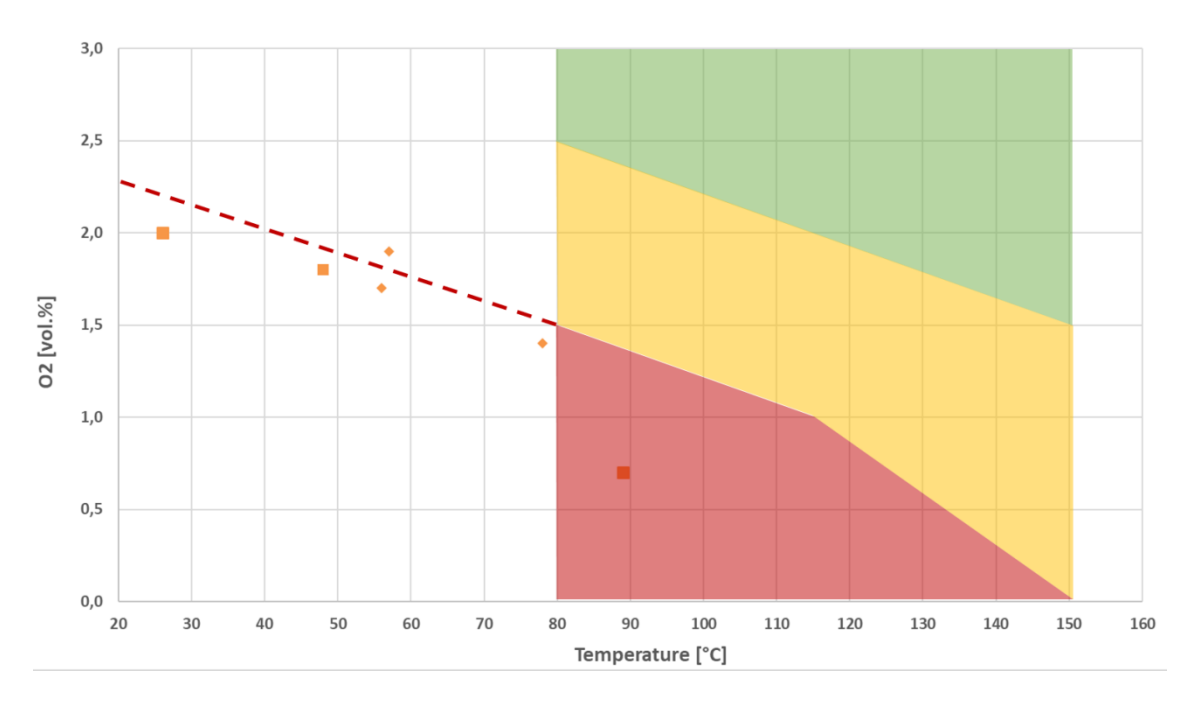


Figure 70. REKO-4: Test results for palladium-based catalyst (squares: 1 bar, diamonds: 2 bar)

3.3.6.Conclusions

With due consideration of the required accuracy of full containment analysis with system codes, and considering as well the measurement uncertainties, the following empirical correlations are proposed to describe the effect of catalyst deactivation (poisoning) by carbon monoxide in the temperature range of 20 °C to 150 °C:

- For platinum-based catalysts, poisoning occurs if the oxygen fraction decreases below a value of 2.0 vol.% (conservative value: 2.5 vol.%). Poisoning occurs quite instantaneously. Partial poisoning has been observed only for a few cases.
- For palladium-based catalysts, poisoning occurs if the oxygen fraction decreases below a
 value which depends significantly on the gas temperature. Different approaches to
 derive an empirical function according to the data presented in Figure 70 can be
 considered, for example

$$y_{02}^{pois} = 2.82 - 0,016 \cdot T$$
 for T = 20 °C to 115 °C $y_{02}^{pois} = 4.35 - 0,029 \cdot T$ for T = 115 °C to 150 °C

Above 150 °C, no poisoning effects have been observed for the palladium-based catalyst.

The poisoning effects observed were independent of the pressure and didn't depend significantly on the hydrogen/carbon monoxide mixture. However, more sophisticated empirical models might consider even these small effects.

4. Model development

The present chapter summarizes the advances made in Task 3.2 in the field of PAR model development in order to improve the predictive capabilities in the assessment of PAR efficiency in severe accident scenarios. First, an overview of the available databases is given. Then, the model advances obtained for the Framatome correlation, PARUPM, REKO-DIREKT and SPARK are described.

4.1. Experimental databases

In the framework of Task 3.2, two databases have been developed. The REKO-3 database is based on the experimental program performed (see section 3.2). The THAI database was generated on the basis of available data from the OECD/NEA-THAI projects (Gupta et al., 2015).

4.1.1.REKO-3 database

The REKO-3 database contains steady-state data obtained from the experimental program. The experiments include both dry and wet tests and were performed with platinum- and palladium-based catalysts.

As the flow velocity is pre-defined and not a consequence of chimney flow operation, the database is not suited for correlation models. On the other hand, it allows validation of the mode detailed PAR models which can be run in forced-flow mode.

The following data values are available:

- Input data (atmospheric conditions at the PAR inlet)
 - The pressure is 1 bar in the entire database
 - Gas temperature in °C
 - Gas composition (H₂, O₂, CO, H₂O) in vol.%
 calculated according to eq. 3.5 (see section 3.2.3.1)
 - Flow velocity in m/s calculated according to eq. 3.6 (see section 3.2.3.2)
- Output data (values to be calculated by the PAR models)

- Recombination rates (H₂ and CO) in g/s
 calculated according to eqs. 3.25 and 3.26 (see section 3.2.3.3)
- Gas composition (H₂, O₂, CO, CO₂) in vol.%
 calculated according to eq. 3.30 (see section 3.2.3.4)
- Catalyst temperatures in °C at four vertical positions

Furthermore, the transient data obtained from the catalyst poisoning experiments can serve for validation of the surface reaction models included in the PAR models SPARK and PARUPM.

4.1.2.THAI database

The generation of a database of quasi-steady state measurement points derived from the transient THAI experiments aims at providing a validation database, which allows an overview of the PAR model performance for the entire experimental program rather than only comparing single transient experiments with model calculations. It is suited for both correlation model and detailed PAR models.

Figure 71 gives an overview of the entire THAI HR program (left) for Framatome-Type PAR and shows the tests which were selected to be included in the database (right) due to their suitability to obtain quasi-steady state data.

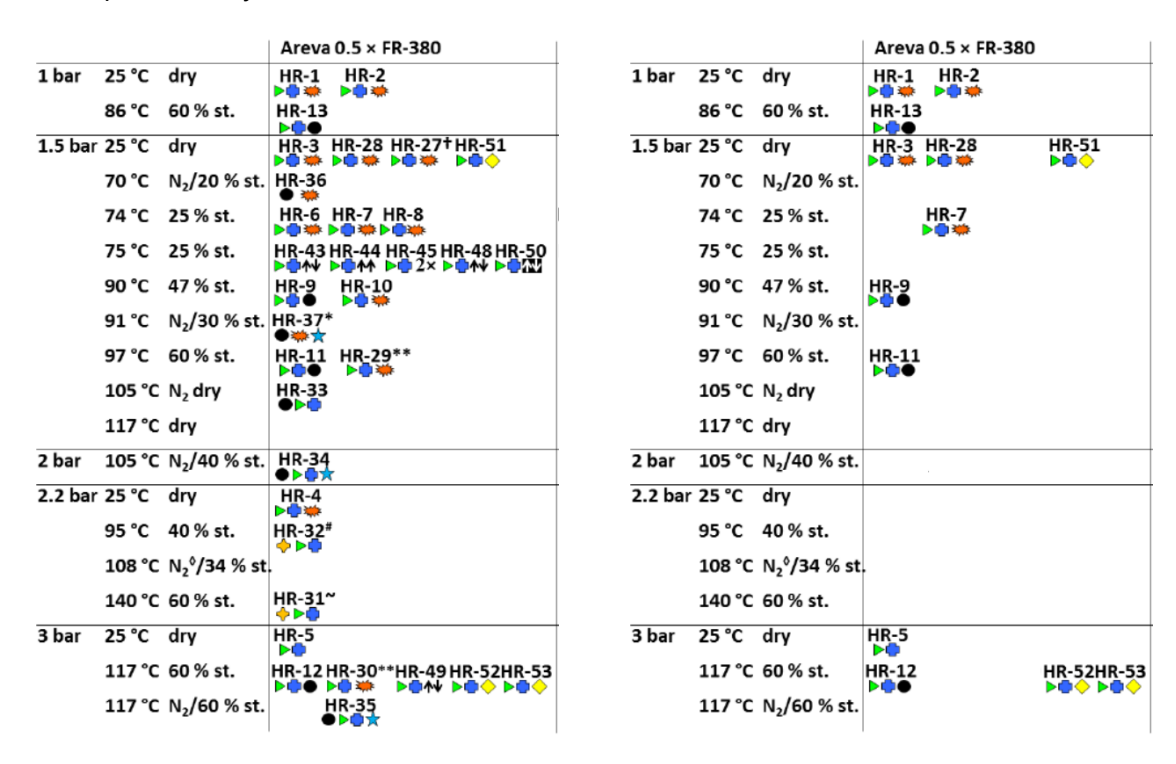


Figure 71. THAI-DB: Entire list of experiments (left) and selected experiments (right)

Figure 72 shows the progression of the hydrogen concentration at the PAR inlet over time of a typical test sequence (here: HR-3). The test involves a first hydrogen injection phase which is stopped when reaching approx. 6 vol.%. Over a period of approx. 1 h, the PAR recombines most of the hydrogen in the first depletion phase. The same procedure is followed afterwards, with the difference that now the first injection phase is stopped only after PAR induced ignition has occurred. The test sequence finishes with the second depletion phase.

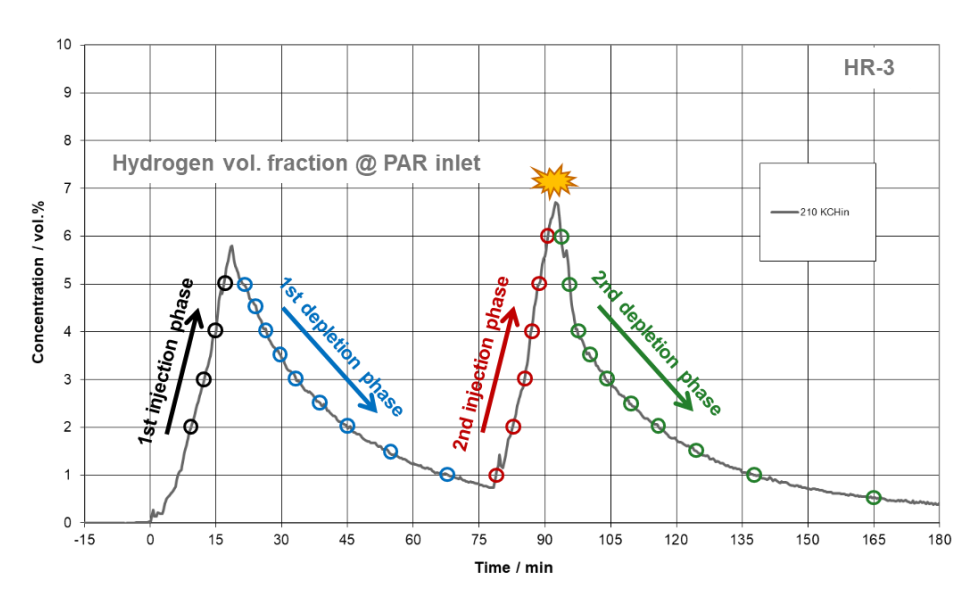


Figure 72. THAI-DB: Experimental phases and selected measurement points

Quasi-steady state measurement points have been identified as indicated with the coloured circles. For this purpose, the average values of each value before and after the selected hydrogen concentration has been calculated.

Figure 73 and Figure 74 show the measured flow velocity and the hydrogen outlet concentration over the inlet hydrogen concentration for all four phases. Both values are part of the formula calculating the recombination rate. It is obvious, that a formula calculating the recombination rate as a function of the hydrogen concentration would come to different results for the different phases.

Obviously, it takes until the second depletion phase until the PAR is in quasi-steady state operation. Based on this observation, the database considers only data from the second depletion phase.

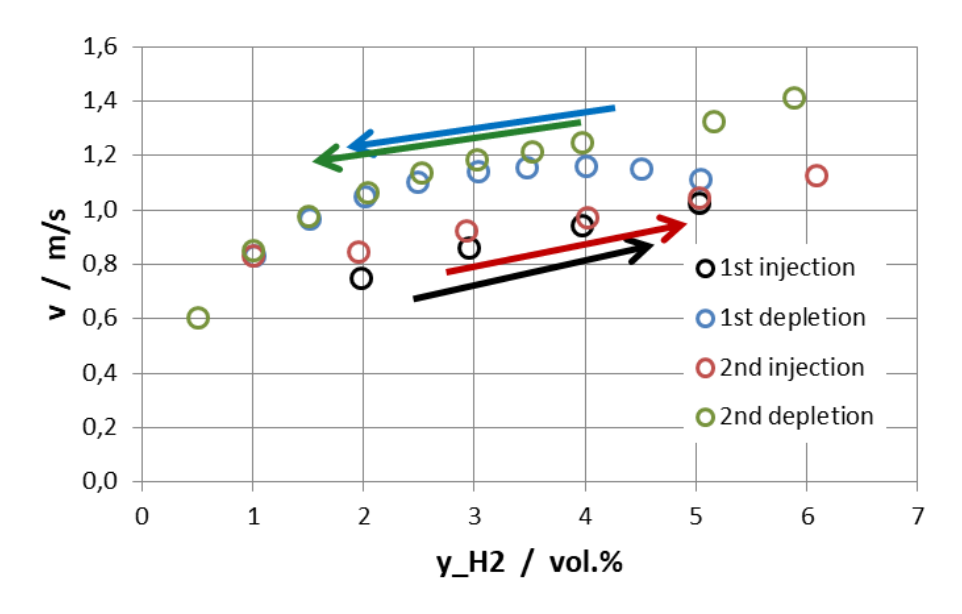


Figure 73. THAI-DB: Experimental phases and selected measurement points

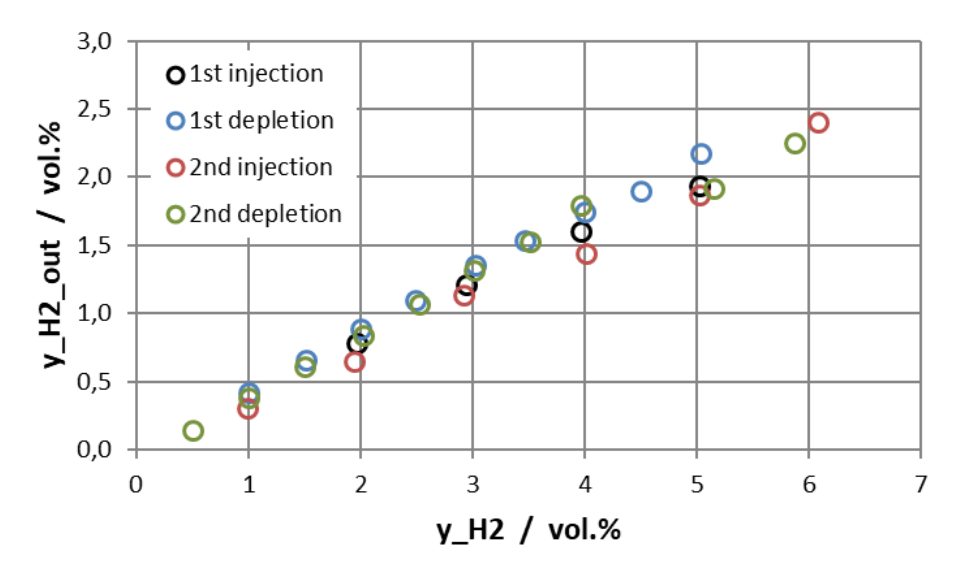


Figure 74. THAI-DB: Experimental phases and selected measurement points

From all second depletion phases, the following data values have been obtained:

- Input data (atmospheric conditions at the PAR inlet)
 - Pressure in bar
 - Of Gas temperature in °C

 As the temperature measurement at the PAR inlet is significantly influenced by the heat radiation from the hot catalyst sheets (Reinecke et al., 2014), the value from a different thermocouple at similar elevation has been selected (HR-1 HR-28: 067 BTF21H12; HR-51ff: 118 BTF13B07).

- o Gas composition (H₂, O₂, CO, CO₂, H₂O) in vol.%
- Output data (values to be calculated by the PAR models)
 - Gas temperature in °C
 An average value from the three temperature measurements at the PAR outlet has been calculated.
 - O Gas composition (H₂, O₂, CO, CO₂) in vol.% Due to the unclear measurement of one of the three measurement positions (Reinecke et al., 2014), two or three values have been optionally used for calculation of an average value.
 - Flow velocity in m/s
 - Recombination rates (H₂ and CO) in g/s Two different equations have been used to calculate the recombination rates. The official equation $\dot{r}_{H_2} = \frac{(y_{H2,in} y_{H2,out}) \cdot p \cdot v \cdot A_{inlet}}{R_{H_2} \cdot T_{in}}$ omits the reduction of the outlet molar flow, so an alternative value is calculated according to eqs. 3.26 or 3.27, respectively. Due to the uncertainties with regard to inlet temperature and outlet gas composition (see above), each of both correlations has been applied with different values: (i) official inlet temperature and average outlet concentrations of three values; (ii) alternate inlet temperature and average outlet concentrations of two values. These six different values are used to obtain uncertainty bars for the recombination rates (see example in Figure 75).
 - Catalyst temperatures at three vertical positions
 Average values have been calculated for measurements at identical positions on different catalyst sheets (low = 1 cm, mid = 7 cm, up = 13 cm).

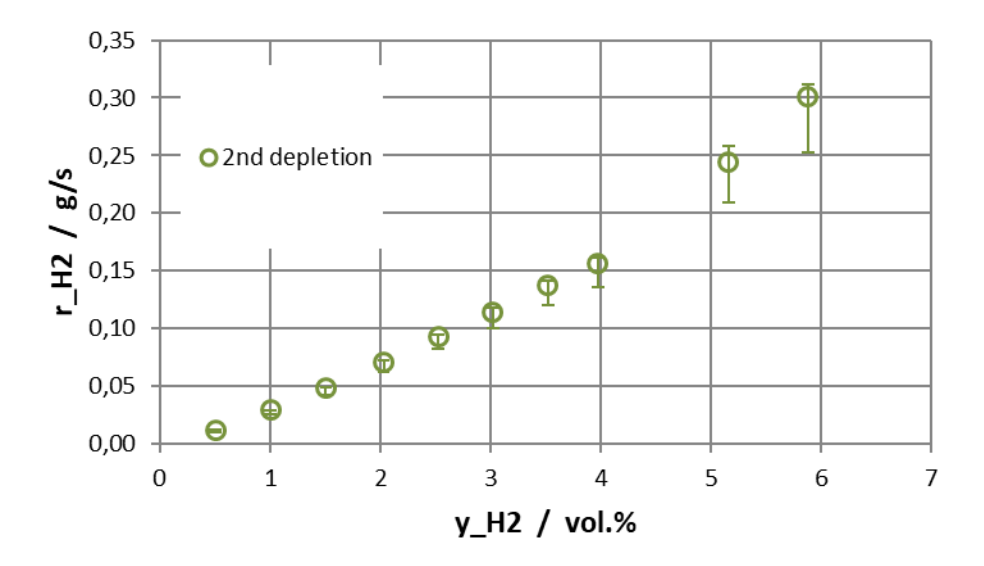


Figure 75. THAI-DB: Recombination rates with uncertainty bars

4.2. Model improvements

In the framework of Task 3.2, the four PAR models have been advanced according to the databases developed in the experimental program. The models will be further used in WP4 for accident simulations.

4.2.1. Framatome correlation

As an outcome of SAMHYCO-NET, deficiencies in modelling the oxygen-lean conditions have been pointed out (Reinecke et al., 2022). These deficiencies have been confirmed using the THAI database (see section 4.1.2).

Figure 76 shows a plot of the hydrogen recombination rates obtained with the Framatome correlation against the recombination rates obtained from the experimental data. The largest deviations from the ideal line are caused by experiments under oxygen-lean conditions. For most of the cases, the recombination rate is significantly over-estimated. As has been shown in the scenario analyses (see section 2.1.1), oxygen-lean conditions are expected to cover almost the entire ex-vessel phase of the accident scenarios. Hence, there is a substantial interest in improving the correlation model.

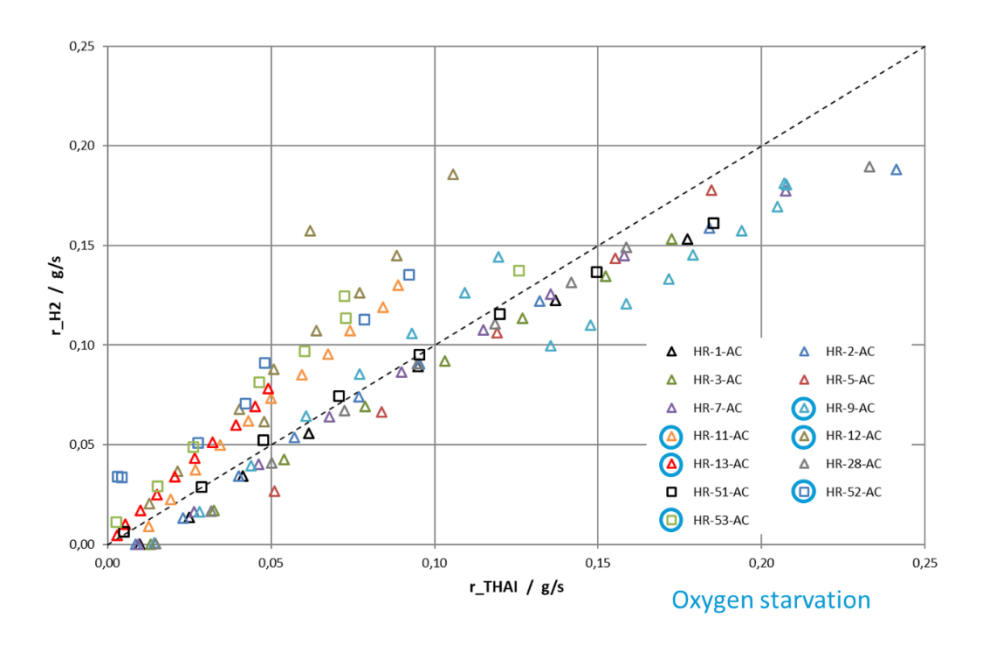


Figure 76. Comparison of the Framatome correlation rates with the THAI database

A detailed analysis of the oxygen starvation part of the model is shown in Figure 77. During oxygen-rich conditions, the correlation uses the hydrogen concentration v_{H2} and the efficiency factor $c_1 = 1.0$ to calculate the recombination rate (dark read curve). For oxygen-lean conditions, the model switches to the oxygen concentration 2 v_{O2} and to the phenomenological efficiency factor $c_1 = 0.6$. As can be shown in the present example, this transition is happening in an inconsistent way. The light red section shows the part of the model where the efficiency factor is already 0.6, but still the hydrogen concentration is used.

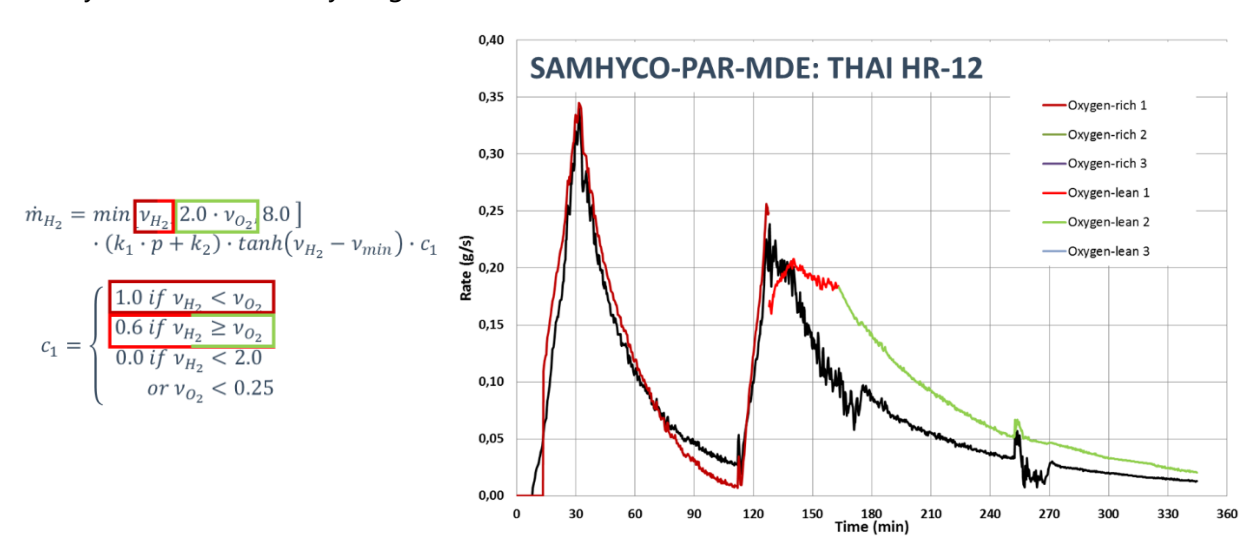


Figure 77. Illustration of the oxygen starvation part of the Framatome correlation

Apart from the inconsistent switch to oxygen-lean conditions, the recombination rate in oxygen-lean conditions is also significantly over-estimated (green curve).

In order to overcome these deficiencies, the following modifications have been proposed (Reinecke, 2022):

$$\dot{m}_{H_2} = (k_1 \cdot p + k_2) \cdot tanh(\nu_{H_2} - \nu_{min}) \cdot c_1 \tag{3.31}$$

where

$$c_{1} = \begin{cases} 1.00 \, \nu_{H_{2}} & \text{if } \nu_{H_{2}} < 0.84 \, \nu_{O_{2}} \\ 0.84 \, \nu_{O_{2}} & \text{if } \nu_{H_{2}} \ge 0.84 \, \nu_{O_{2}} \\ 0.0 & \text{if } \nu_{H_{2}} < 2.0 \\ & \text{or } \nu_{O_{2}} < 0.25 \end{cases}$$

$$(3.32)$$

The factor 0.84 represents a consequent implementation of the laws of diffusion-controlled reaction kinetics. It represents the expression $\left(\frac{D_{O_2}}{D_{H_2}}\right)^{2/3}$, which is the reciprocal of 1.19 (see eqs. 2.5 and 2.9 in section 2.1.1.

When implementing the model, it is important to first check the start conditions v_{H2} < 2.0 vol.% and v_{O2} < 0.25 vol.%. This condition conservatively describes a PAR start delay. The experimental data confirm that the PAR is able to recombine hydrogen down to at least 0.5 vol.%. A corresponding adoption needs to be implemented in the model.

Figure 78shows the performance of the improved correlation in the THAI HR-12 experiment. The switch between oxygen-rich and oxygen-lean conditions as well as the recombination rate during oxygen starvation meets the experimental data much better than before.

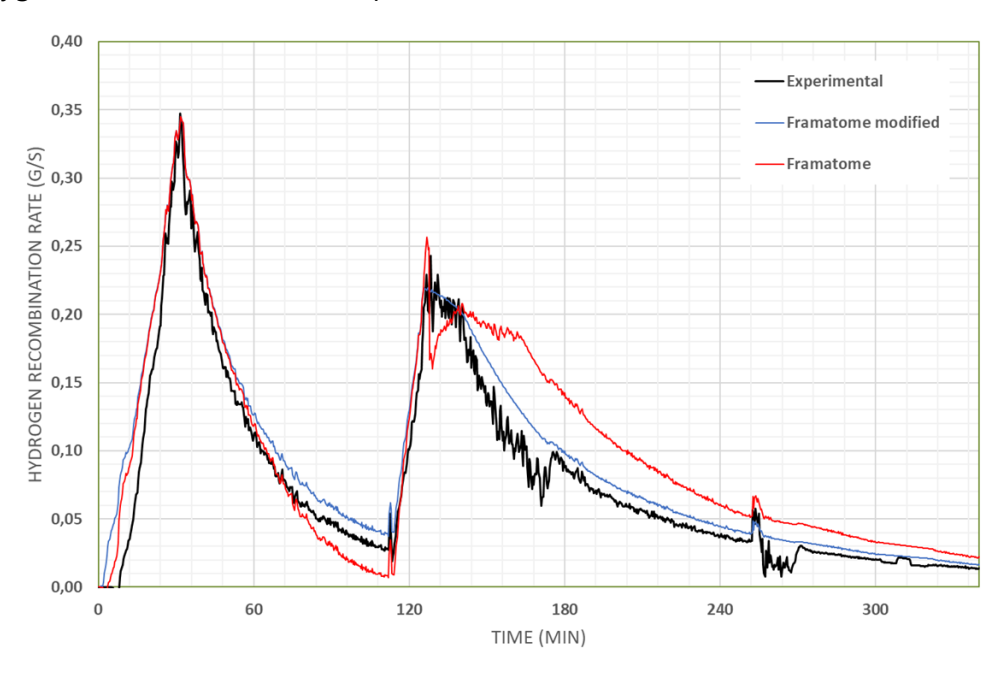


Figure 78. Original and improved Framatome correlation versus THAI HR-12 data

The calculation of the entire THAI database Figure 79 demonstrates the successful improvement of the correlation as well as the suitability of the THAI database for model validation.

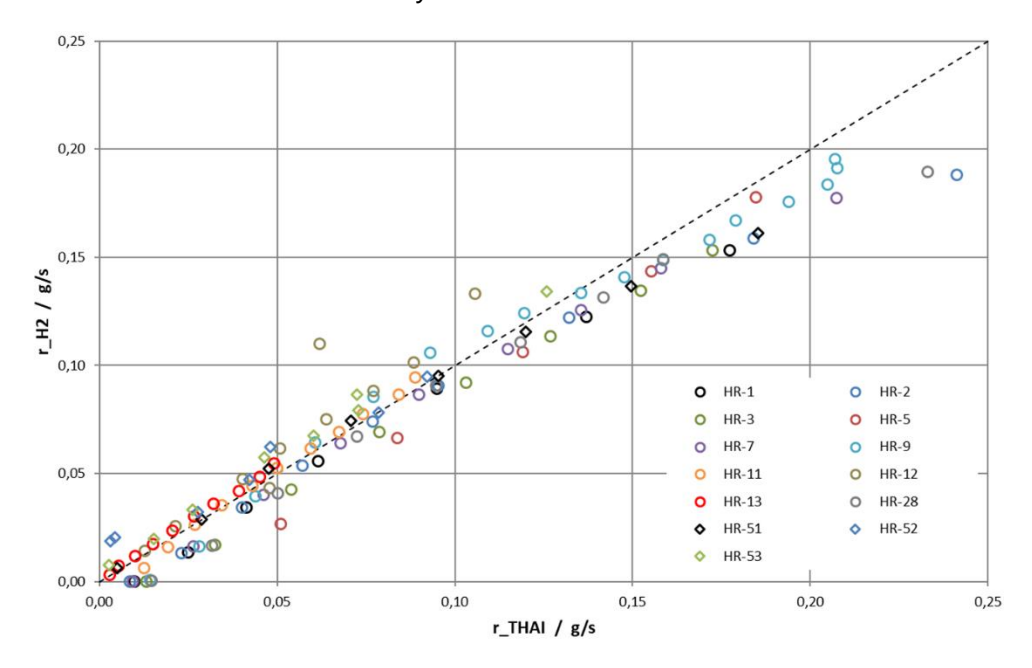


Figure 79. Comparison of the improved Framatome correlation rates with the THAI database

Considering both hydrogen and carbon monoxide recombination leads to the following proposal:

$$\dot{m}_{H_2} = (k_1 \cdot p + k_2) \cdot \tanh(\nu_{H_2} + \nu_{CO} - \nu_{min}) \cdot c_1 \tag{3.33}$$

where

$$c_{1} = \begin{cases} 1.00 \cdot v_{H_{2}} & \text{if } v_{O_{2}} > (1.19 v_{H_{2}} + 0.49 v_{CO}) \\ 0.84 \cdot v_{O_{2}} - min(0.414 v_{CO}, 0.84 v_{O_{2}}) & \text{if } v_{O_{2}} \leq (1.19 v_{H_{2}} + 0.49 v_{CO}) \\ 0.0 & \text{if } v_{H_{2}} + v_{CO} < 2.0 \\ & \text{or } v_{O_{2}} < 0.25 \end{cases}$$
(3.34)

and

$$\dot{m}_{CO} = (k_1 \cdot p + k_2) \cdot \tanh(\nu_{H_2} + \nu_{CO} - \nu_{min}) \cdot c_1 \cdot c_2 \tag{3.35}$$

where

$$c_{1} = \begin{cases} 0.414 \, \nu_{CO} & \text{if } \nu_{O_{2}} > (1.19 \, \nu_{H_{2}} + 0.49 \, \nu_{CO}) \\ \min \left(0.414 \, \nu_{CO}, 0.84 \, \nu_{O_{2}} \right) & \text{if } \nu_{O_{2}} \leq (1.19 \, \nu_{H_{2}} + 0.49 \, \nu_{CO}) \\ 0.0 & \text{if } \nu_{H_{2}} + \nu_{CO} < 2.0 \\ & \text{or } \nu_{O_{2}} < 0.25 \end{cases}$$

$$(3.36)$$

and

$$c_2 = 14$$
.

In case of oxygen starvation ($v_{O2} \le (1.19 \ v_{H2} + 0.49 \ v_{CO})$, hydrogen and carbon monoxide compete for the available oxygen. This model considers an extreme approach: CO is served first. This approach was quite successful in the OECD/NEA-THEMIS HR-57 blind benchmark, however will be refined after further evaluation of the REKO-3 experiments.

The corresponding validation data for CO recombination rates, which involve new experiment from the OECD/NEA THEMIS project, cannot be shown in the present document due to contractual reasons.

4.2.2.PARUPM

The improvements and validation work performed in the framework of AMHYCO has been published in (Domínguez-Bugarín, 2022) and (Domínguez-Bugarín, 2023).

4.2.2.1. Code advancement: diffusion model

Through the implementation of the linear system of differential equations that includes the simplified Deutschmann mechanism, PARUPM is capable of simulating the relevant phenomena associated with the recombination of hydrogen and carbon monoxide in PARs with plane-parallel catalyst sheets. The transient model can approximate both the PAR heating phase and its quenching, as well as the transient changes in the boundary conditions. Heterogeneous catalytic reactions involve both surface and transport phenomena. Initially, the recombination rate inside PARUPM was determined by the surface reactions of the species on the catalytic surface, described by

$$Rate_i = \omega_i \Gamma(2 L h) M_i \tag{3.28}$$

where ω_i is the reaction rates of the recombined species i, Γ is surface site density of platinum, L and h are the height and width of the plate, and M_i is the molar mass of the species.

To enhance the code for simulating the behaviour of recombiners, a mass transfer model has been added to the code to consider the diffusion through the boundary layer. In this case it is assumed that the diffusion process is sufficiently slow so all the moles of the species that get to the catalytic sheet by diffusion are recombined. This approach is described by

$$Rate_{i,dif} = \frac{Sh_i D_{dif,i}}{D_h} \left(\frac{p_i}{RT}\right) L \cdot h$$
 (3.28)

where Sh_i is the Sherwood number of the species i, $D_{dif,i}$ is the diffusivity of the species through the boundary layer, D_h is the hydraulic perimeter, p_i is the partial pressure of the species, R is the

ideal gas constant, T is the temperature of the gas in the inlet, and L and h are the length and width of the catalytic plate.

Recent works have proven that recombination process is primary driven by the diffusion phenomenon. Thus, although the code calculates the recombination rate by both diffusion and chemical reaction processes, the final value chosen for the recombination rates is the one obtained with the diffusion model. This decision is supported by the results shown in Figure 80. This graph shows the values for the recombination rates obtained with PARUPM against the experimental values for several experiments performed in REKO-3 experimental facility. Both the diffusion based (blue dots) and the reaction-bases rates (grey dots) are represented. The deviation of the recombination rates reduces from an average ~40 % in the case of the reaction-bases rates to just a ~5 % deviation with the diffusion-based rates.

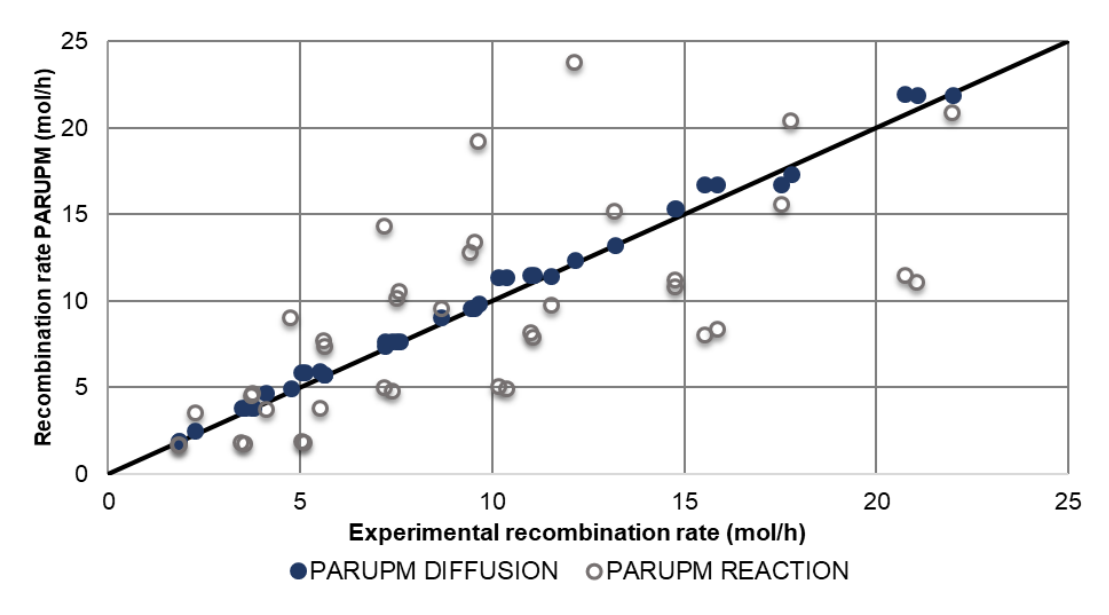


Figure 80. PARUPM diffusion and reaction-based recombination rates against experimental recombination rates (REKO-3)

4.2.2.1. Code advancement: oxygen starvation

To study the effect of oxygen starvation (i.e., low oxygen/nitrogen ratio), experiments where the oxygen molar fraction was progressively reduced were analysed. In these experiments (Reinecke et al., 2007) the hydrogen molar fraction was kept constant at 3 % while the oxygen molar fraction was gradually reduced from 20 % to 2 % of the total flow volume. The flow speed was kept constant at 1.15 m/s and the hydrogen recombination rates were obtained for inlet temperatures of 20.5 °C and 80.1 °C. In Table 10 the recombination rates obtained with PARUPM and from REKO-3 are shown.

Table 10. PARUPM: Comparison of calculated recombination rates with REKO-3 data for 5 different oxygen concentrations and 2 inlet temperatures

X _{H2} (-)	X ₀₂ (-)	T (°C)	v (m/s)	H _{rate} PARUPM (mol/h)	H _{rate} REKO-3 (mol/h)	ε _{rate} (-)
0.03	0.20	20.50	1.15	18.40	17.82	0.03
0.03	0.05	20.50	1.15	18.36	21.52	0.15
0.03	0.04	20.50	1.15	18.35	19.60	0.06
0.03	0.03	20.50	1.15	18.34	18.68	0.02
0.03	0.02	20.50	1.15	10.65	12.46	0.15
0.03	0.20	80.10	1.15	18.43	17.82	0.03
0.03	0.05	80.10	1.15	18.41	17.45	0.06
0.03	0.04	80.10	1.15	18.40	17.61	0.04
0.03	0.03	80.10	1.15	18.40	16.91	0.09
0.03	0.02	80.10	1.15	10.62	10.27	0.03

The relative deviation ε_{rate} between the recombination rates obtained with PARUPM and the experimental results show that the code is capable of accurately predicting the recombination rates once the oxygen starvation stage is reached, especially for higher inlet temperatures.

4.2.2.2. Code validation: CO recombination in REKO-3 tests

To study the effect of carbon monoxide on the hydrogen recombination rate and the carbon monoxide recombination capability of the code, several REKO-3 experiments were analysed from the series R3-A-03_CO, R3-A-04_CO, and R3-A-06_CO (Klauck et al., 2014). For three different hydrogen concentrations, other 3 different carbon monoxide concentrations where studied. The inlet flow temperature was kept at 21 °C for all the experiments and the flow velocity was 1.15 m/s for each run.

- Case 1: 2% H₂ for 0%, 0.5%, 1%, and 2% CO
- Case 2: 4% H₂ for 1%, 2%, and 4% CO
- Case 3: 5% H₂ for 1%, 2%, 3%, 3.5%, and 4% CO

The experimentally observed recombination rates and the rates predicted by PARUPM are compared in Figure 81.

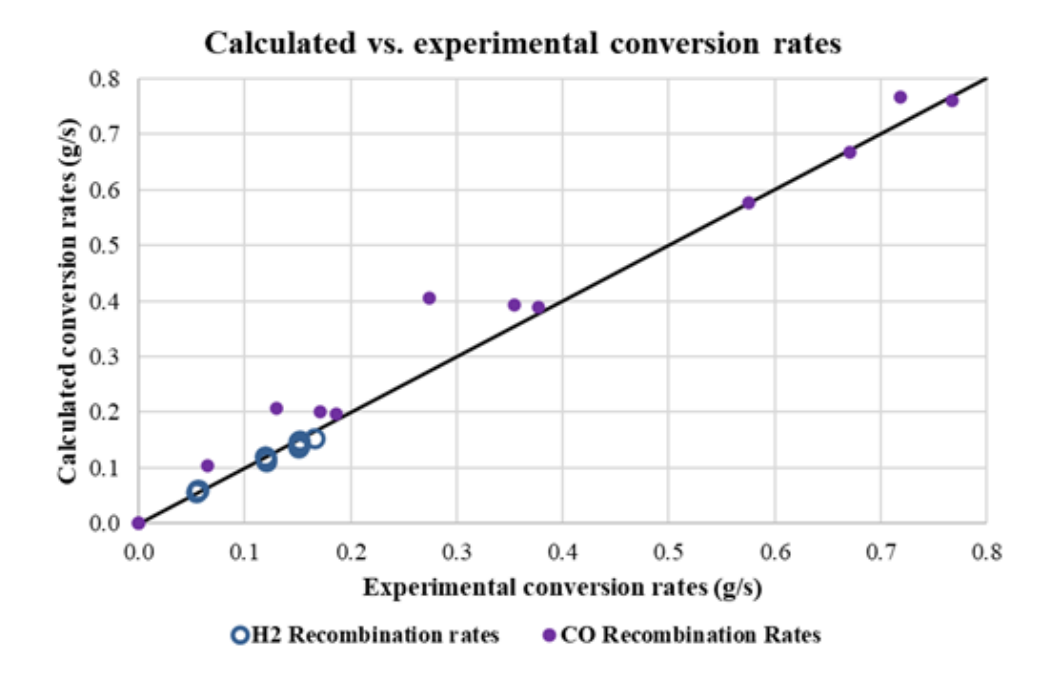


Figure 81. PARUPM H2 (blue dots) and CO (open purple dots) recombination rates against experimental recombination rates (REKO-3)

The average code-test deviation for the hydrogen recombination rates is \sim 3.2 % while the average deviation for the carbon monoxide recombination rates is \sim 19.1 % for case 1 although, for cases 2 and 3, the average deviation is \sim 5.5 % and \sim 4.3 %, respectively. Within these limits, the model is capable of calculating the recombination rates of both species in the presence of carbon monoxide.

4.2.2.3. Transient validation: THAI tests

Test HR-1 starts with a vessel atmosphere of dry air at an ambient temperature of 25 °C. During the first phase, hydrogen is injected in the vessel. After 25 minutes, the injection stops and a first depletion (recombination only) phase starts, which lasts for 60 minutes. Then, the second hydrogen injection phase takes place with a duration of 20 minutes followed by the second depletion phase which runs until the recombination stops.

Figure 82 shows the recombination rate obtained during the experiment HR-1 as well as the recombination rates from PARUPM using the boundary conditions from the experiment. Apart from a moderate overprediction of the recombination rate in the first injection phase of the experiment, the only significant discrepancy between the model and the experimental recombination rates occurs at the end of the second injection phase, which is due to a PAR induced ignition causing high recombination rates during the combustion process. PARUPM

doesn't contain an ignition module, thus this behaviour is not analysed by the code. Overall, the comparison with experimental data confirms that the code can simulate the behaviour of a real passive autocatalytic recombiner under realistic conditions.

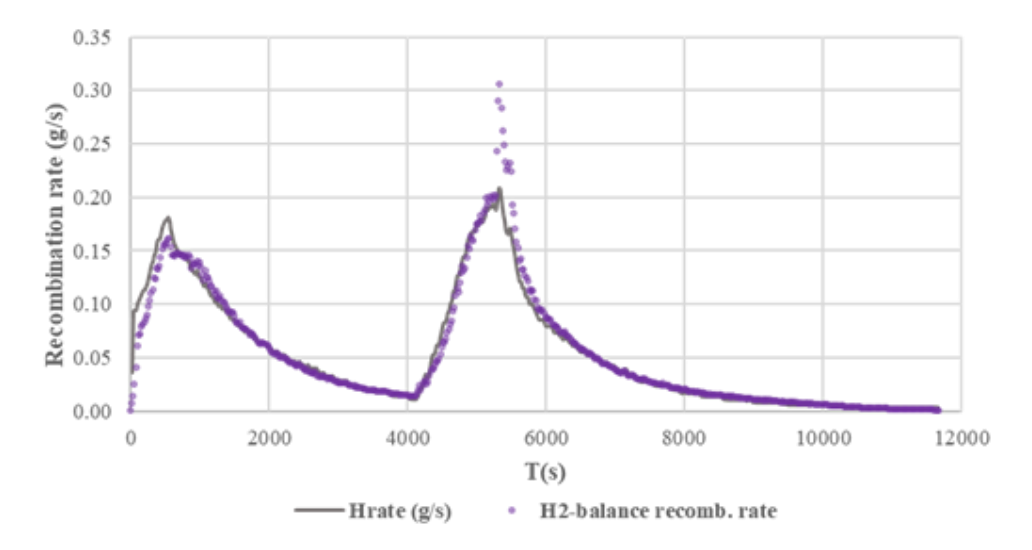


Figure 82. PARUPM: Recombination rate with PARUPM (grey line) and experimental recombination rates (purple dots) during the transient (HR-1)

The initial conditions of test HR-13 include a mixture of air with 60 vol.% steam at a temperature of 86 °C. The test follows the same pattern of injection and depletion as HR-1. However, during the second injection and subsequent depletion, the recombination runs under lean oxygen conditions.

Figure 83 shows the experimental recombination rate obtained from test HR-13 as well as the recombination rates calculated with PARUPM using the boundary conditions from the experiment. Despite another moderate overprediction of the recombination rate in the first injection phase, the results confirm that the code reproduces well the behaviour of a real passive autocatalytic recombiner inside a containment during the second injection and depletion (as well as the rest of the transient), when the recombiner is experiencing oxygen starvation.

The results obtained demonstrate that the physicochemical strategy used in the PARUPM model can simulate the behaviour of the recombiner under a variety of conditions, from typical concentrations and settings to more extreme ones such as oxygen starvation, presence of carbon monoxide, or elevated inlet temperatures. Furthermore, the code can reproduce the behaviour of a PAR in transient conditions, where pressures, temperatures, and gas concentrations are constantly changing at the recombiner inlet.

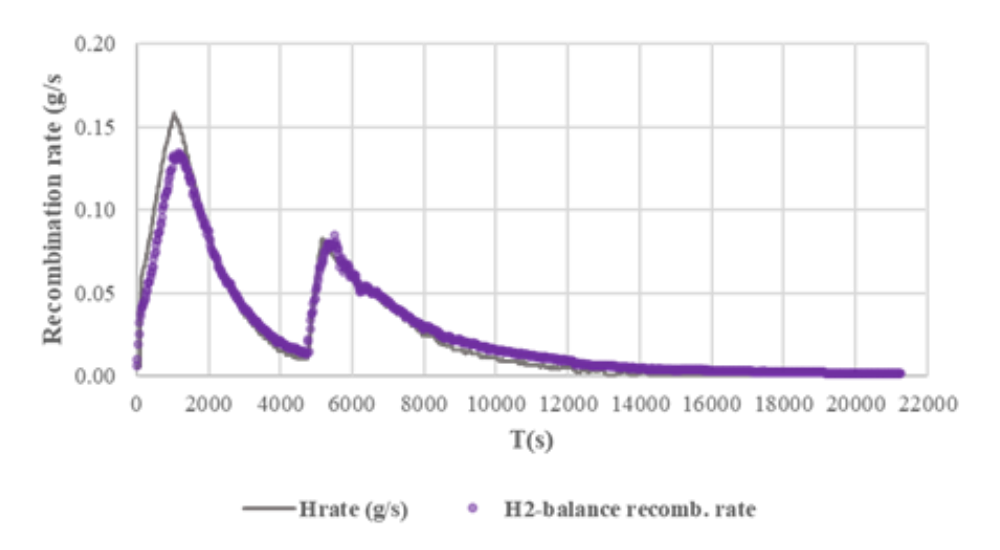


Figure 83. PARUPM: Recombination rate with PARUPM (grey line) and experimental recombination rates (purple dots) during the transient (HR-13)

4.2.2.4. Conclusions

Within the AMHYCO project, the PARUPM code has been proposed as an appropriate tool for assessing the performance of PARs in full containment simulations. The phenomenology observed in a severe accident can be examined in more detail once the PARUPM code is implemented in 3D thermo-hydraulic analysis codes, such as GOTHIC (EPRI, 2018), a general-purpose integrated thermo-hydraulic software package for the design, licensing, safety, and operational analysis of nuclear power plant containment and system components.

4.2.3.SPARK

The improvements and validation work performed in the framework of AMHYCO has been published in (Nobrega, 2022).

4.2.3.1. Code advancement

The surface mechanism initially used in SPARK for the catalytic oxidation of hydrogen and carbon monoxide over platinum was proposed by Deutschmann et al. (1996). It contains 8 surface species and 8 gaseous species and consists of 20 reactions. The reaction mechanisms were updated, as presented in Table 11 (adapted from Zheng, 2013), in order to allow simulation during deactivation conditions. R6–R11 are added HCOO reactions. R1 is given in terms of a sticking coefficient (S₀) and is second order with respect to Pt(s).

The previous versions of SPARK were designed for hydrogen and carbon monoxide combustion and recombination in recombiners. As of today, the code contains the reaction mechanisms for the catalytic oxidation of hydrogen and carbon monoxide over platinum. However, Pd and Pt

may react differently. Even though most recombiners use platinum as the catalyst, some recombiners use palladium or bimetallic Pt-Pd catalyst. It is necessary to enhance the SPARK code with the reaction mechanisms for hydrogen and carbon monoxide over palladium. This will allow a further comparison between the different catalysts and a better understanding of how the poisoning products act when in contact with palladium or platinum.

Table 11. SPARK: Updated reaction mechanism; units: S₀ [–], A [cm, s, K], E_a [J/mol], coverage h [–]

Reacti	ons	S ₀ (A)	n	Ea			
Adsorption and desorption reactions							
R1 ^a	$CO + Pt(s) \rightarrow CO(s)$	8.4E-2	0	0			
R2 ^a	$CO(s) \rightarrow CO + Pt(s)$	2.13E+13	0	136,190-33,000θCO(s)			
Surface reactions							
R3ª	$CO(s) + O(s) \rightarrow CO2(s) + Pt(s)$	3.70E+20	0	108,000-33,000θCO(s)			
R4ª	$H(s) + O(s) \rightarrow OH(s) + Pt(s)$	3.70E+20	0	70500			
R5ª	$OH(s) + Pt(s) \rightarrow H(s) + O(s)$	1.00E+20	0	130690			
R6	$OH(s) + CO(s) \rightarrow HCOO(s) + Pt(s)$	3.70E+21	0	94200			
R7	$HCOO(s) + Pt(s) \rightarrow OH(s) + CO(s)$	1.33E+21	0	870			
R8	$HCOO(s) + O(s) \rightarrow OH(s) + CO2(s)$	3.70E+21	0	0			
R9	$OH(s) + CO2(s) \rightarrow HCOO(s) + O(s)$	2.79E+21	0	151050			
R10	$HCOO(s) + Pt(s) \rightarrow CO2(s) + H(s)$	3.70E+21	0	0			
R11	$CO2(s) + H(s) \rightarrow HCOO(s) + Pt(s)$	2.79E+21	0	90050			

The literature presents the surface reaction scheme for hydrogen and oxygen over palladium based on thermochemical and kinetic data for the interaction of these elements (Deutschmann et al., 1996). The surface reaction mechanism for hydrogen over palladium is shown in Table 12. It is possible to observe that palladium leads to the same reaction mechanisms as platinum but with different rate coefficients.

The reaction mechanisms have been established based on data from the literature. The initial sticking coefficient for the dissociative hydrogen adsorption was chosen to be 0.7, which presents an average value of the existing data. For the associative hydrogen desorption, $A = 4.8 \times 10^{21}$ cm² (mol s⁻¹) and $E_a^{max} = 84$ kJ mol⁻¹ are used. An additional decrease of the activation energy with increasing hydrogen coverage due the adsorbate-adsorbate interactions is considered: $E_a = E_a^{max} - \Theta_{H(s)} \times 15$ kJ mol⁻¹. For the interaction of oxygen with palladium, the following values are adopted: $S^0 = 0.4$ and $E_a^{des} = 230$ kJ mol⁻¹. The pre-exponential factor was derived from the vibrational frequency of a Pd-O bond of 1.1×10^{13} s⁻¹. For the remaining

reactions, the kinetic data derived for a platinum surface were used. All those values have been established by Deutschmann et al. (1996) based on previous works.

Table 12. SPARK: Surface reaction mechanism on palladium; units: A [mol, cm, s], E_a [kJ/mol], S^0 [-]); Pd(s) denotes bare surface sites; reaction rate: $k = A T_n \exp(-E_a/RT)$

#	Reaction	A	Ea	S ⁰
1	$H_2+2Pd(s) => 2H(s)$			0.7
2	H+Pd(s) => H(s)			1.00
3			84 - 15	
	$2H(s) => H_2 + 2Pd(s)$	4.80×10^{21}	$\cdot HH(s)$	
4	$O_2+2Pd(s) => 2O(s)$			0.40
5	O+Pd(s) => O(s)			1.00
6	$2O(s) => O_2 + 2Pd(s)$	7.10×10^{21}	230	
7	$H_2O+Pd(s) => H_2O(s)$			0.75
9	$H_2O(s) \Longrightarrow H_2O + Pd(s)$	1.30×10^{13}	44.0	
10	OH+Pd(s) => OH(s)			1.00
11	$OH(s) \Rightarrow OH+Pd(s)$	1.30×10^{13}	213	
12	H(s)+O(s) <=>			
	OH(s)+Pd(s)	6.50×10^{21}	11.5	
13	H(s)+OH(s) <=>			
	$H_2O(s)+Pd(s)$	6.50×10^{21}	17.4	
14	OH(s)+OH(s) <=>			
	$H_2O(s)+O(s)$	6.5 x 10 ²¹	48.2	

4.2.3.2. Reference simulations

The catalyst temperature is the parameter used in the REKO experiments to identify catalyst deactivation by carbon monoxide. For this reason, first calculations have been performed for hydrogen-air mixtures in order to verify that the SPARK code is able to reproduce it, notably with low-oxygen content. The calculations using conditions from normal operation allow to compare with the results from the reference tests performed in REKO facilities.

SPARK simulations of REKO-1 experiments

Simulations with the REKO-1 geometry have been performed. Since the geometry of REKO-1 is a cylinder with a single catalyst sample, the 2D simulations performed at SPARK may not be the most adapted.

Figure 84 show the catalyst temperature measured at the lower edge of the catalyst for mixtures with different hydrogen fractions at 0.5 m/s and no carbon monoxide. During normal operation of the catalyst, SPARK gives coherent results for the catalyst temperature.

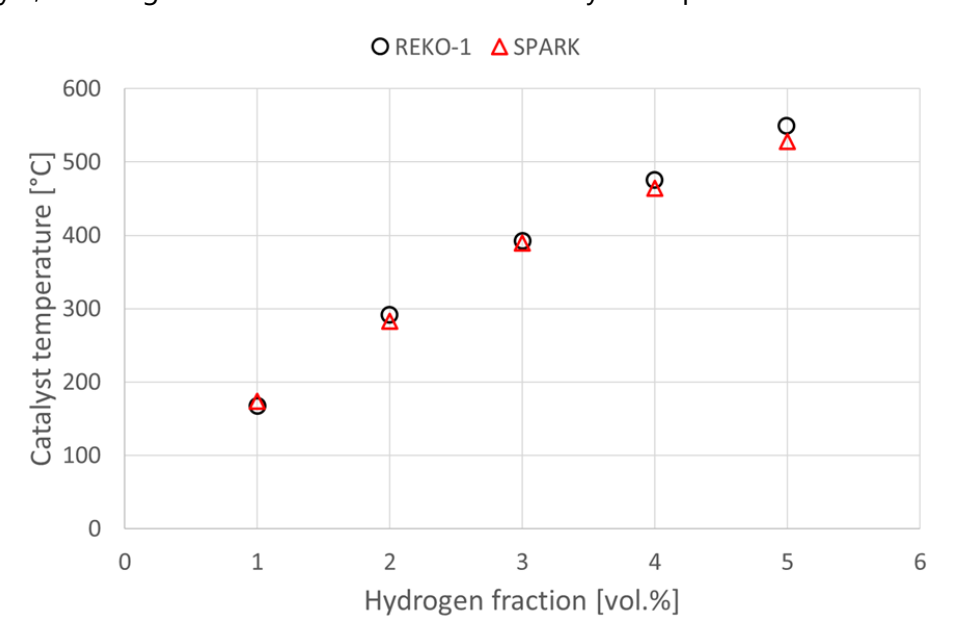


Figure 84. SPARK: Evolution of catalyst temperatures measured at the bottom of the catalyst versus the hydrogen molar fraction at 0.5 m/s

Figure 85 represents the temperature profile for a mixture of 4 vol.% hydrogen in air, without carbon monoxide and during oxygen starvation. The circles represent the values measured experimentally at REKO-1 and the lines the values calculated with SPARK. Until 4.5 vol.% of oxygen, SPARK predicts the temperature of the catalyst in a good agreement with the experimental results. However, the results show that SPARK predicts the on-set of oxygen starvation already for an oxygen fraction of 3.5 vol.%, which is slightly earlier than observed in the experiments.

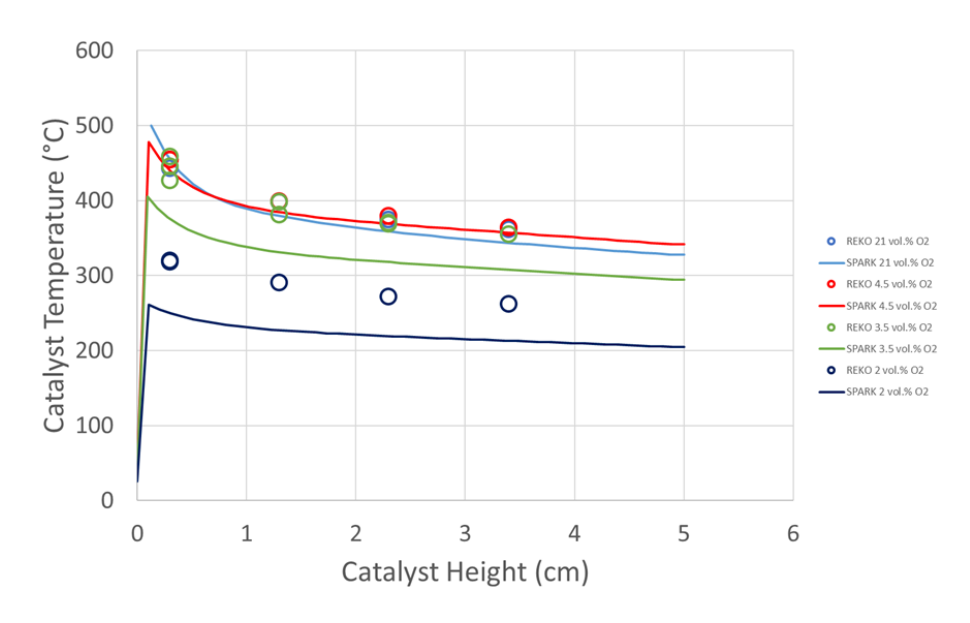


Figure 85. SPARK: Comparison between SPARK simulations and REKO-1 data: Catalyst surface temperature along catalyst length for 4 vol.% H₂ and O₂ content varying from 21 to 2 vol.%

SPARK simulations of REKO-3 experiments

The REKO-3 geometry was also used for SPARK simulations. Figure 86 shows the temperature profile along the catalyst height for different hydrogen fractions with 21 vol.% of oxygen and at ambient temperature. The circles represent the experimental results while the line represents the values calculated by the SPARK code. For 4 vol.% of hydrogen, there is no available data for the lower positions of the catalyst since the temperature was higher than the upper limit of the pyrometer. The experimental and numerical results are in very good agreement, confirming that the SPARK code can predict the catalyst temperature for oxygen-rich conditions.

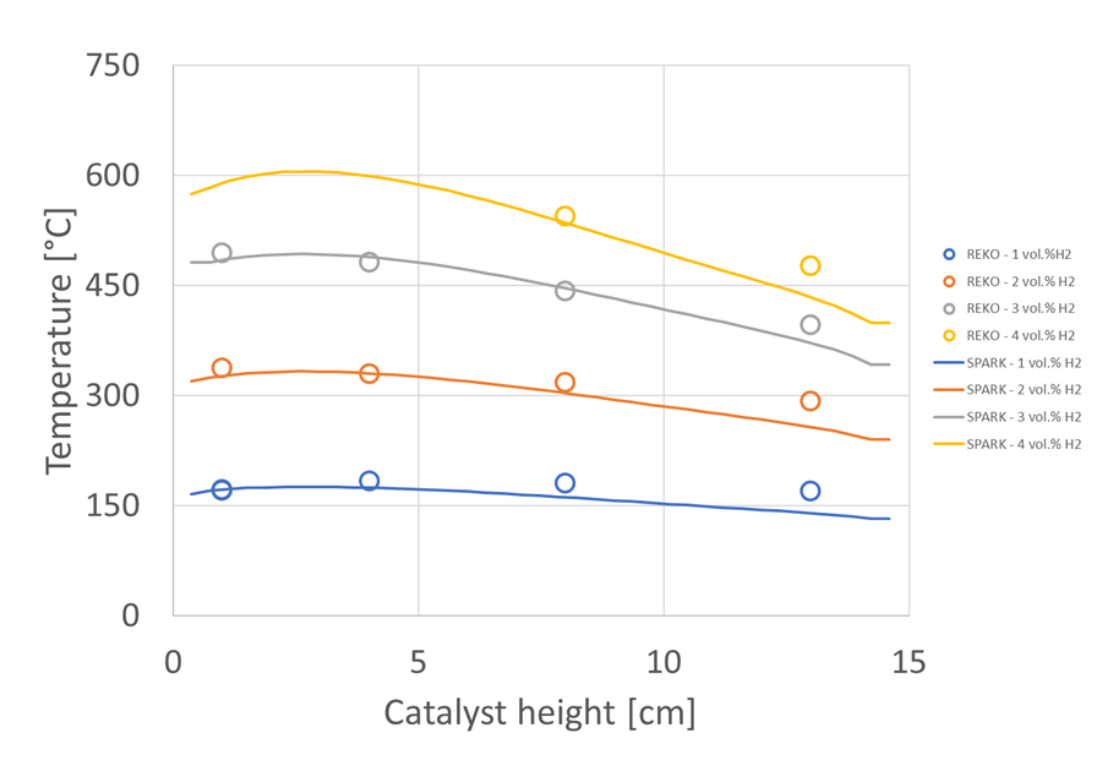


Figure 86. SPARK: Catalyst surface temperature along catalyst height for different H₂ content: Comparison between REKO-3 results and SPARK simulations

As mentioned earlier, once the oxygen content is below a certain value, the catalyst temperature decreases with the oxygen fraction, and gets eventually uniform along the catalyst height. A test series with 3 vol.% of hydrogen and the oxygen content varying from 21 to 2 % at 1.15 m/s have been calculated with SPARK (Figure 87). The numerical results are consistent with the experimental results: from 21 vol.% oxygen to 4 vol.%, there are no changes in the catalyst temperature, showing that the efficiency of the recombiner is maintained and once the oxygen content is 3 vol.%, the effect of oxygen starvation is observed.

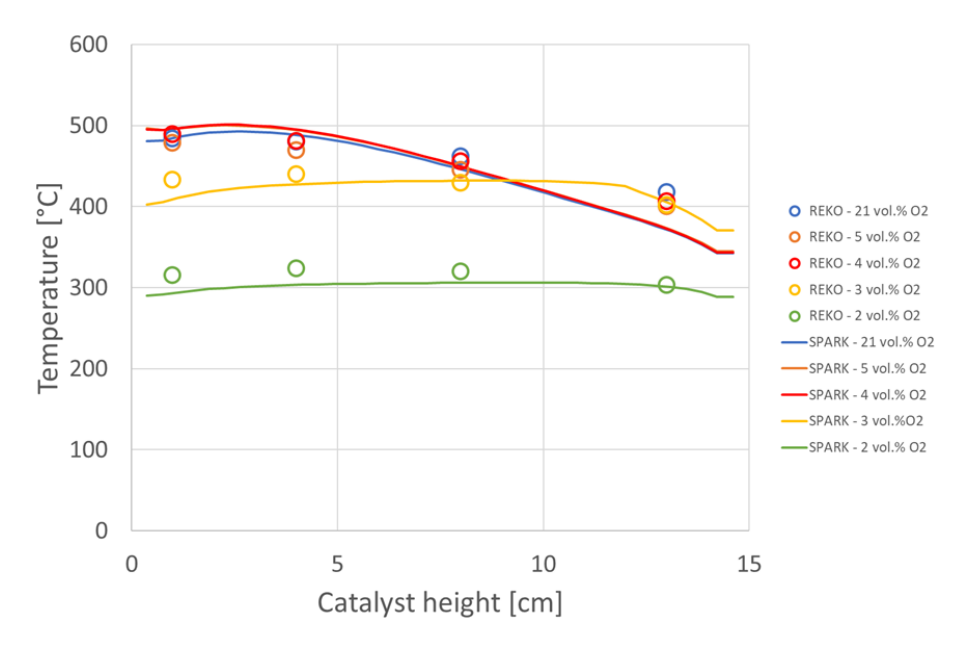


Figure 87. SPARK: Catalyst surface temperature along catalyst height for 3 vol.% H₂ and O₂ content varying from 21 to 2 vol.%: Comparison between REKO-3 results and SPARK simulations

The effect of steam on the catalyst temperature has also been analysed with the presence of carbon monoxide and no restriction of oxygen. For a mixture of 2 vol.% hydrogen, 100 % relative humidity and carbon monoxide varying from 0 to 4 vol.% at 0.5 m/s and 80 °C, the results are shown in Figure 88. The catalyst temperature obtained with SPARK are coherent with the temperatures measured at the bottom of the catalyst.

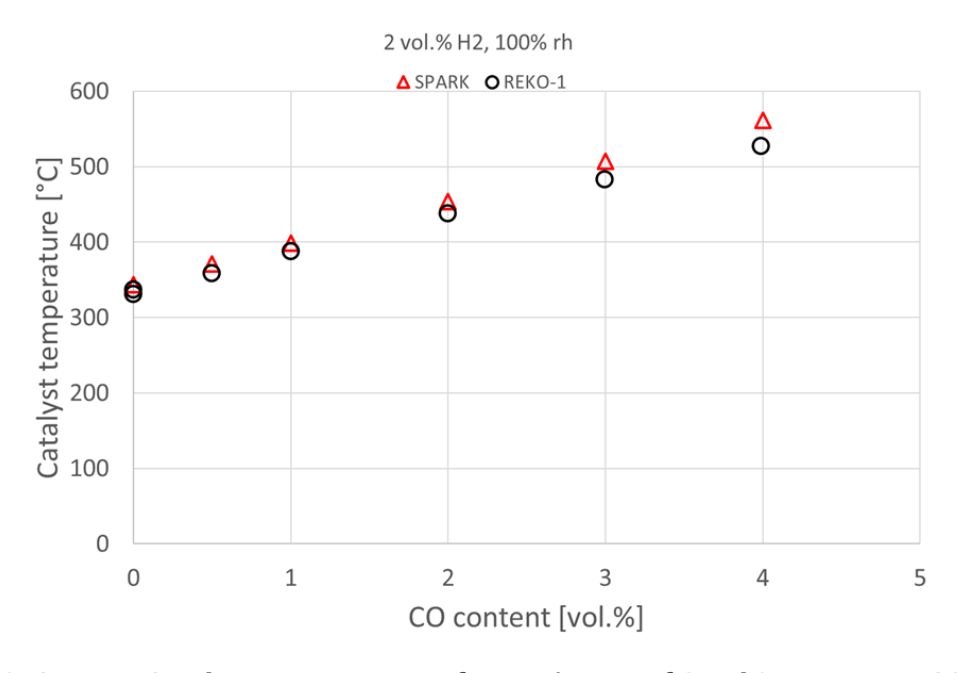


Figure 88. SPARK: Catalyst temperatures for a mixture of 2 vol.% H₂ versus CO content under dry and steam conditions

SPARK simulations of H₂/CO/air mixtures

First, simulations for H₂/CO/air mixtures are presented in order to show that SPARK is able to predict deactivation. Then, calculations performed to analyse the impact of different parameters on the catalyst deactivation are shown. Finally, the numerical simulations are compared to the experimental results.

The calculations were performed using REKO-3 geometry since it is more appropriate for the 2D SPARK simulations. However, they are compared with REKO-1 and REKO-3 experimental data since the difference in the catalyst deactivation observed in REKO-1 and REKO-3 (Figure 89) is not so significant. The difference between the two facilities can be explained by the fact that with REKO-1 facility there is a lot of heat losses due to its geometry so the same difference is expected for SPARK simulations.

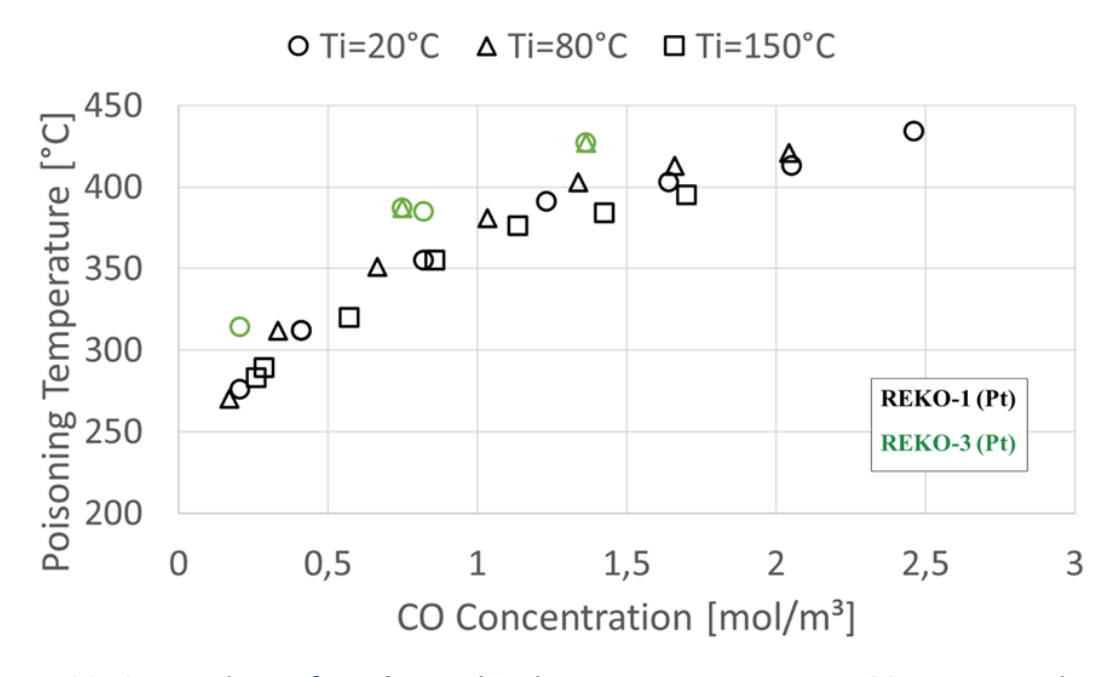


Figure 89. Comparison of catalyst poisoning temperature versus CO concentration for REKO-1 and REKO-3 (4 vol.% H₂)

Catalyst deactivation was identified in the REKO experiments by a significant drop of the catalyst temperature, indicating that the hydrogen is no longer being recombined as it is during normal operation. The same parameter has been used with the SPARK code. Figure 90 shows the temperature at the lower edge of the catalyst for different values of the oxygen fraction for a mixture of 4 vol.% H₂, 0.5 vol.% CO at 0.5 m/s with inlet gas temperature of 20 °C. The black circles represent the temperature measured and the red triangles represents the SPARK results. The oxygen is reduced until the catalyst is deactivated. The temperatures measured at REKO-3 are slightly higher than the ones calculated with SPARK. The catalyst deactivation is predicted by the SPARK code for an oxygen fraction below 2.8 vol.% where the catalyst temperature is 383 °C.

In the experiments, the catalyst deactivation was observed for lower values, when the oxygen fraction was around 2 vol.% O_2 and the catalyst temperature was 340 °C.

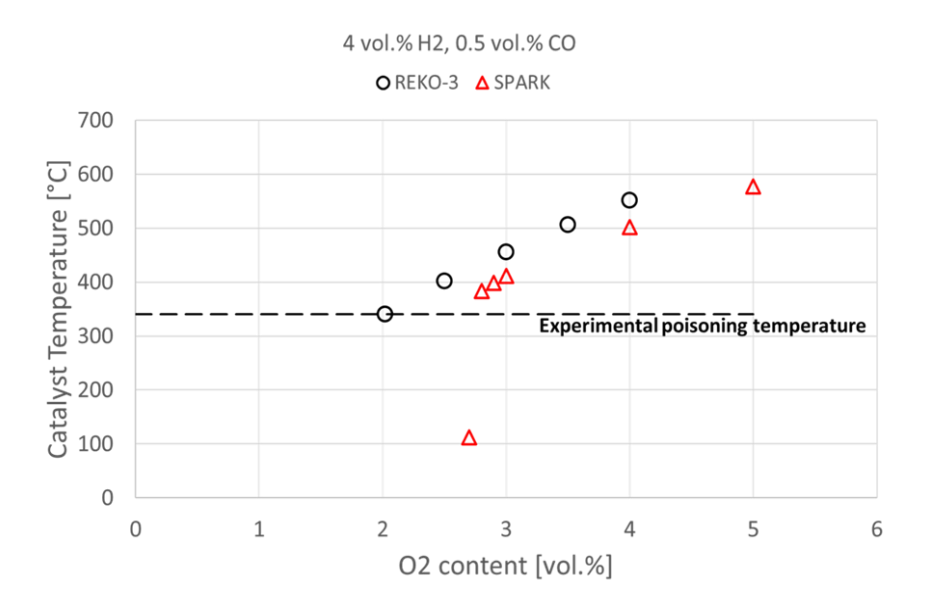


Figure 90. SPARK: Catalyst temperature for a mixture with 4 vol.% H₂, 0.5 vol.% CO and reduction of oxygen

Figure 91 shows the temperature at the bottom of the catalyst for a mixture of 4 vol.% H_2 , 2 vol.% CO at 0.5 m/s with inlet gas temperature of 80 °C. Once again, the SPARK code predicts deactivation at higher oxygen fraction and catalyst temperature. It was observed at 2.4 vol.% O_2 and a catalyst temperature of 390 °C while it is predicted at 2.6 vol.% O_2 and a catalyst temperature of 400 °C.

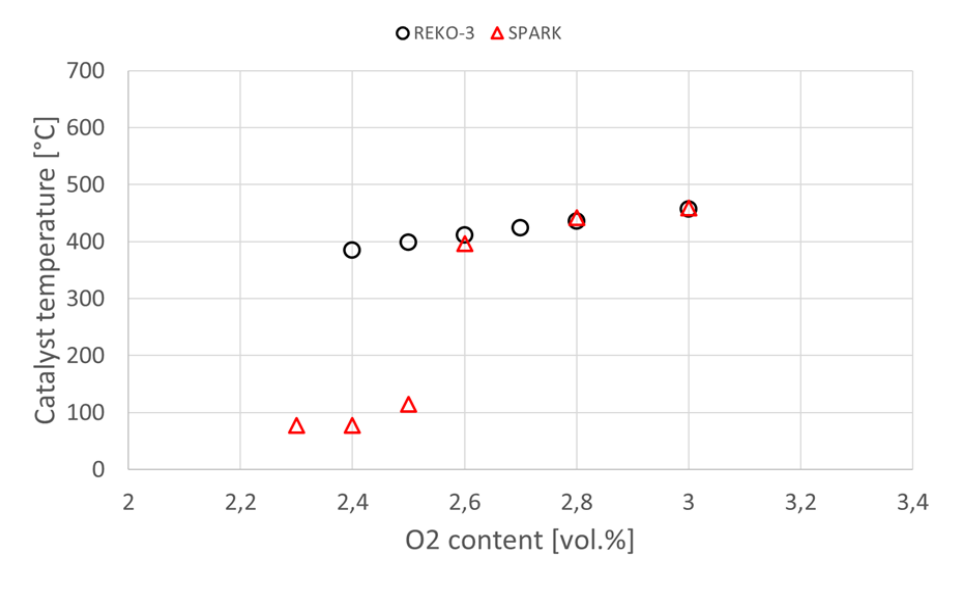


Figure 91. SPARK: Catalyst temperature for a mixture with 4 vol.% H₂, 2 vol.% CO, gas at 80°C and reduction of oxygen

The SPARK code allows a detailed analysis of the REKO-3 tests. Figure 92 shows the hydrogen fraction present in the gas phase in the channel between two catalyst sheets (dimensions as in the tests) for the previous mixture: 21 vol.% O_2 on the left and 3 vol.% on the right. The hydrogen starts being converted once it is in contact with the catalytic plate, confirming what was observed with the temperature field. It can be noted that the conversion is less efficient for a mixture with 3 vol.% of oxygen. The most part of hydrogen is recombined at the entry of the recombiner, at the bottom of the catalyst.

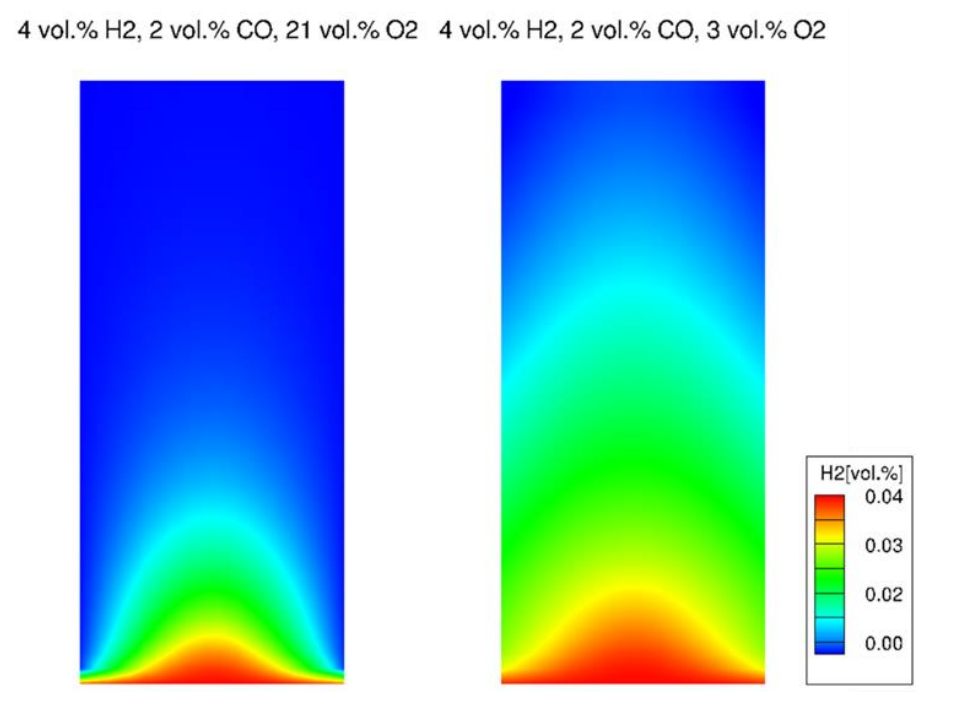


Figure 92. SPARK: Hydrogen distribution on the channel between catalysts, for 21 vol.% O_2 (left) and 3 vol.% O_2 (right)

The carbon monoxide present in the channel for the same gas mixture during normal operation are shown in Figure 93. The figure shows that not all carbon monoxide is converted, indicating that the conversion of hydrogen is privileged in these conditions. However, the carbon monoxide is still recombined and it does not block the catalytic surface.

Figure 94 represents the catalyst temperature during normal operation for the same mixtures previous presented in Figure 87: 21 vol.% O_2 on the left and 3 vol.% O_2 on the right. For both cases, it is possible to observe that the hydrogen starts being recombined at the lower edge of the catalyst. However, when the oxygen content is 21 vol.%, the temperature at the bottom of the catalyst is higher while for 3 vol.%, the temperature starts decreasing at this point. This behaviour shows that the effects of oxygen starvation is first observed at the lower edge of the catalyst, confirming what was observed in the experiments.

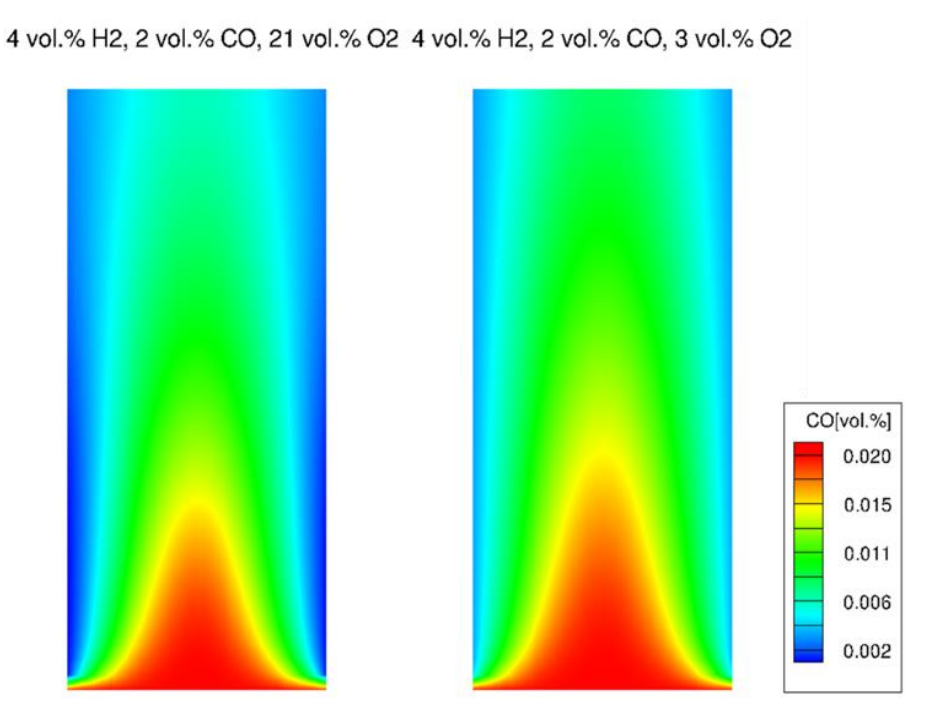


Figure 93. SPARK: Carbon monoxide distribution in the REKO-3 channel between two catalyst plates, for 21 vol.% O₂ (left) and 3 vol.% O₂ (right)

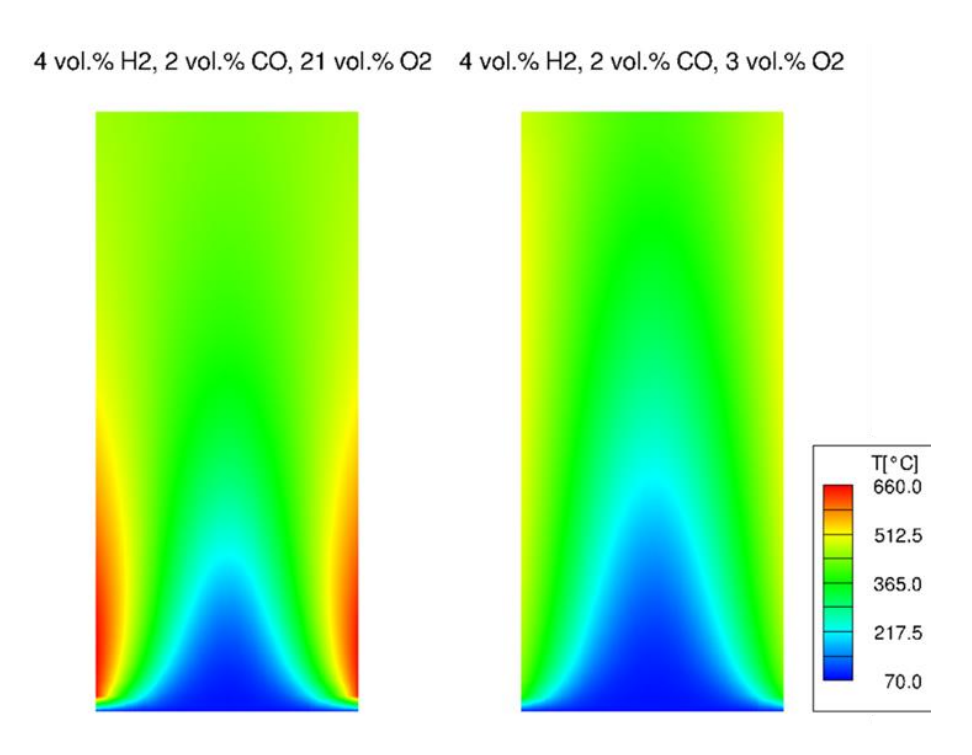


Figure 94. SPARK: Temperature fields for a mixture with 4 vol.% H_2 , 2 vol.% CO, gas at 80 °C and 21 vol.% O_2 (left) and 3 vol.% O_2 (right)

For the mixture considered (4 vol.% H₂, 2 vol.% CO), the catalyst deactivation is predicted around 2.6 vol.% O₂. Figure 95 shows the hydrogen distribution for three different fractions of oxygen during deactivation: on the left, 2.6 vol.% O₂ represents the beginning of poisoning, in the middle during the deactivation process and on the right 2.3 vol.% O₂, showing the catalyst already completely deactivated. On the left, for 2.6 vol.% O₂, the hydrogen fraction at the inlet of the channel keeps unchanged, indicating that the lower edge of the catalyst is no longer converting hydrogen. In the middle, for 2.5 vol.% of oxygen, the part of the catalyst that is not recombining the hydrogen increases, moving upwards on the catalyst. However, once the gas mixture reaches the part of the catalyst that is not deactivated, the hydrogen is recombined. On the right, for 2.3 vol.% O₂, the entire catalyst seems to be deactivated and almost no hydrogen is being converted. The same can be observed for the carbon monoxide fraction between plates in Figure 96.

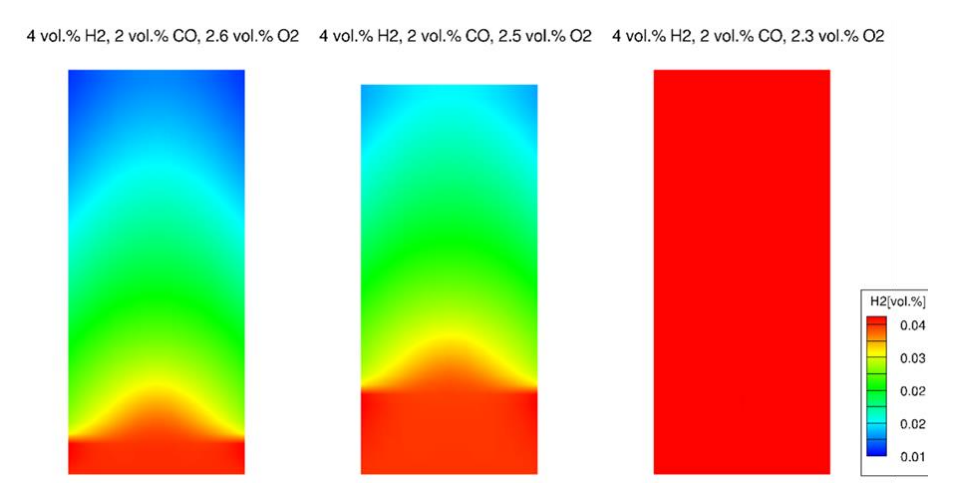


Figure 95. SPARK: Hydrogen distribution in the REKO-3 channel between two catalyst plates for 2.6 vol.% O₂ (left), 2.5 vol.% O₂ (middle) and 2.3 vol.% O₂ (right)

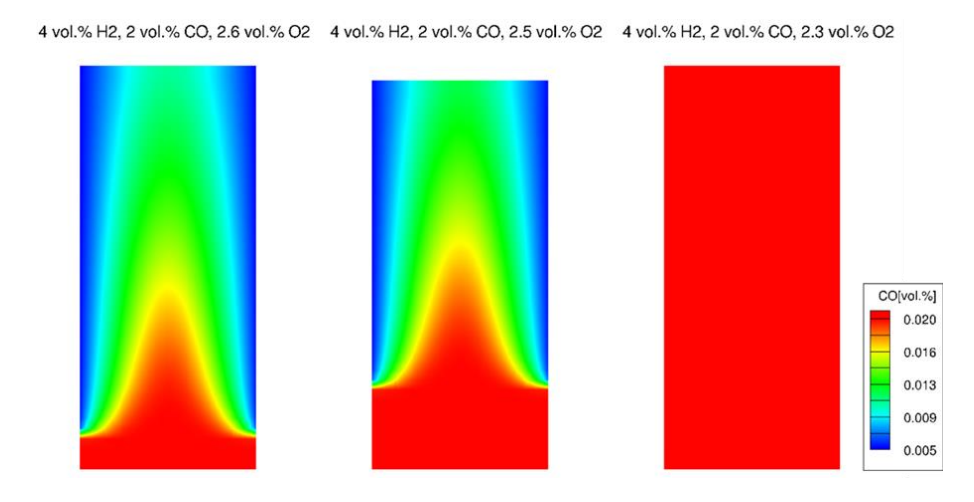


Figure 96. SPARK: Carbon monoxide distribution in the REKO-3 channel between two catalyst plates for 2.6 vol.% O₂ (left), 2.5 vol.% O₂ (middle) and 2.3 vol.% O₂ (right)

Figure 97 shows the temperature field between two catalyst sheets for three different oxygen fractions during deactivation. The temperature at the bottom of the catalyst starts to decrease when the fraction of oxygen is 2.6 vol.%, showing that there is no reaction occurring at that spot. When further decreasing the oxygen fraction to 2.5 vol.%, the temperature starts decreasing in the upper parts of the catalyst as well. At 2.3 vol.%, the entire catalyst temperature is around 78 °C, indicating complete deactivation.

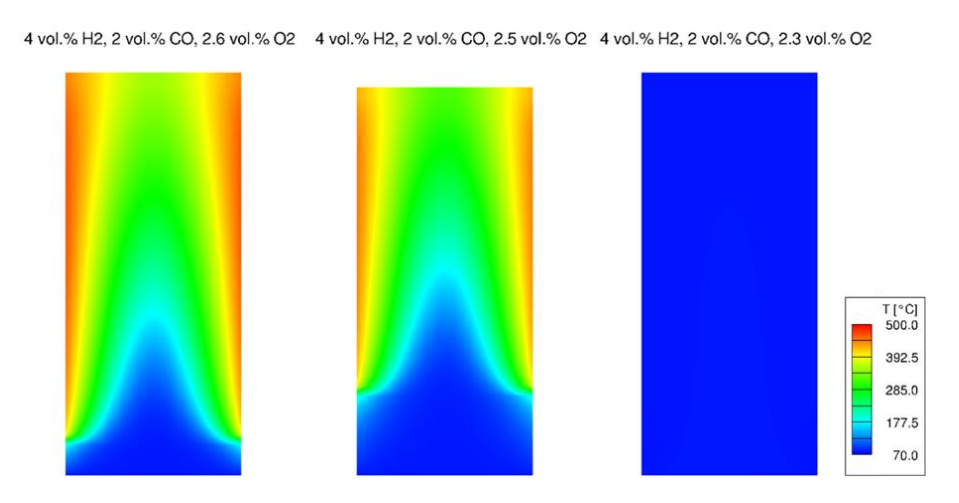


Figure 97. SPARK: Temperature fields for a mixture with 4 vol.% H₂, 2 vol.% CO, gas at 80°C during deactivation: 2.6 vol.% O₂ (left), 2.5 vol.% O₂ (middle) and 2.3 vol.% O₂ (right)

Figure 98 shows the fraction of carbon monoxide on the catalytic surface. At the beginning of catalyst deactivation (2.6 vol.% oxygen), on the left, the carbon monoxide blocks the lower edge of the catalytic surface. At 2.5 vol.% of oxygen, the surface blocked by carbon monoxide is extended by a few centimetres. At 2.3 vol.%, the entire surface of the catalyst is blocked by carbon monoxide, confirming the catalyst deactivation by this product.

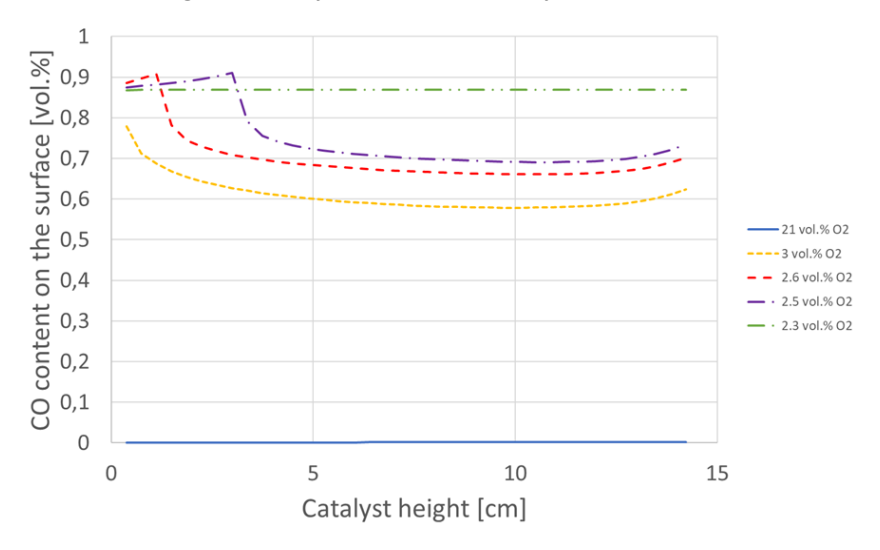


Figure 98. SPARK: Carbon monoxide distribution along the catalyst plate for a mixture with 4 vol.% H₂, 2 vol.% CO and oxygen varying from 21 to 2.3 vol.%

Characterization of catalyst deactivation for different parameters

A set of calculations has been performed to evaluate the poisoning temperature for different combinations of hydrogen, carbon monoxide, initial gas temperatures and flow velocities.

Impact of hydrogen content on the poisoning temperature

Figure 99 shows the poisoning temperature predicted by SPARK for different hydrogen and carbon monoxide fractions at 0.5 m/s, using a platinum catalyst. The blue symbols represent the poisoning for mixtures with 1 vol.% of hydrogen. The red triangles represent 2 vol.% hydrogen; purple circles indicate 3 vol.% H_2 and the black squares represent a hydrogen fraction of 4 vol.%.

The deactivation is predicted at similar temperature for the different hydrogen fractions. However, for 1 vol.% of hydrogen the poisoning temperature is lower. Also, the higher is the carbon monoxide fraction, the higher the poisoning temperature is.

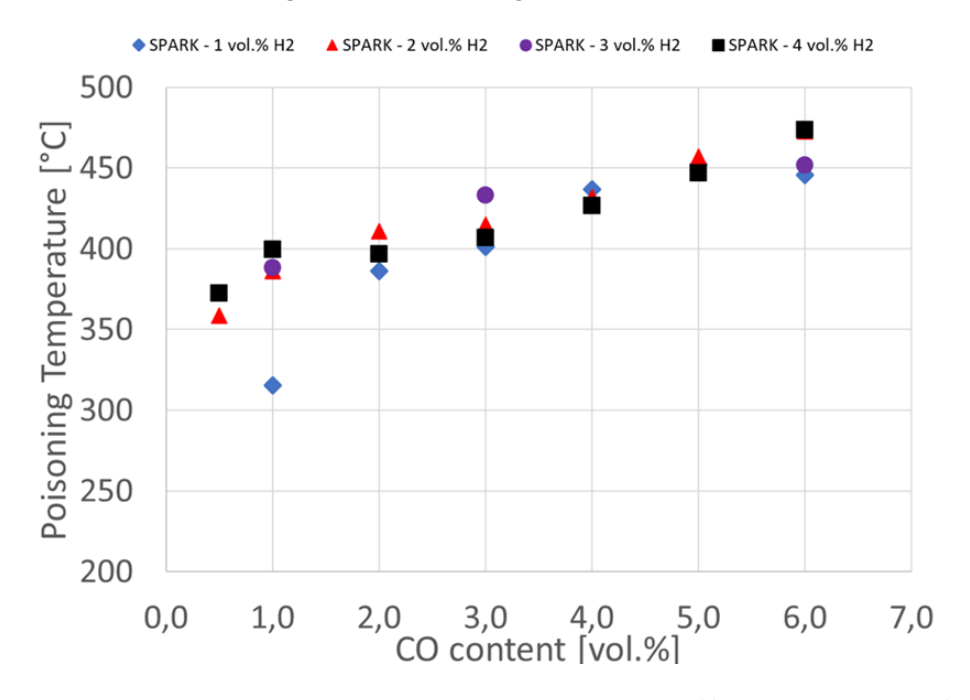


Figure 99. SPARK: Predicted poisoning temperature at different hydrogen fractions

Impact of inlet velocity on the poisoning temperature

Figure 100 represents the poisoning for a mixture with 2 vol.% hydrogen for two different flow velocities and for different carbon monoxide fraction. The open triangle represents the poisoning for mixtures at 0.5 m/s while the filled triangles represent 1 m/s. The values of the temperature when deactivation occurs are similar for both cases. The flow velocity seems to not have a significant impact on the poisoning.

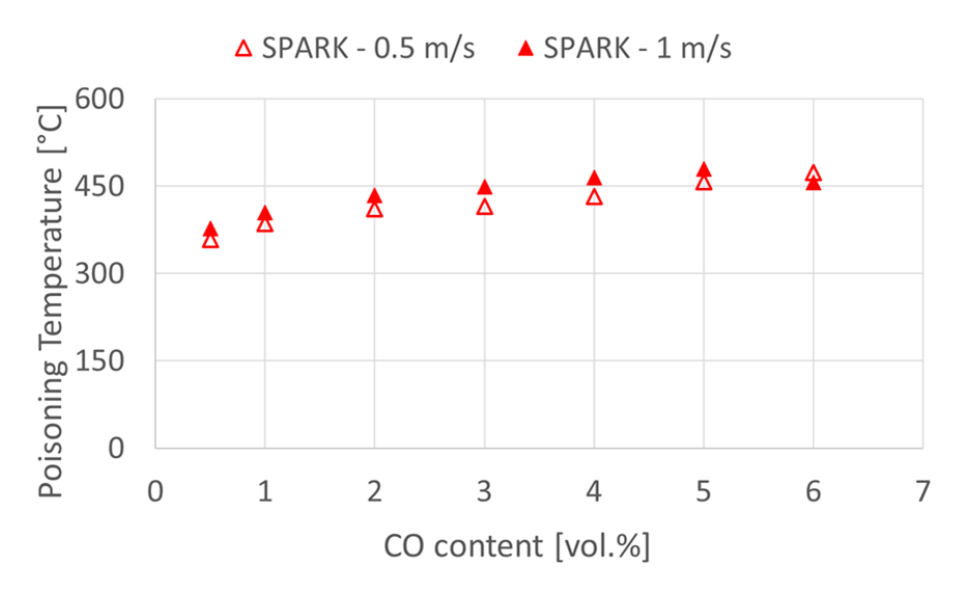


Figure 100. SPARK: Predicted poisoning temperature for two flow velocities (2 vol.% H₂)

Impact of inlet gas temperature on the poisoning temperature

Figure 101 shows the impact of the initial inlet gas temperature on the poisoning of a mixture of 4 vol.% hydrogen for different carbon monoxide concentrations using a platinum catalyst. In order to compare the different gas temperatures, the carbon monoxide concentration and not the carbon monoxide fraction is shown. The circle represents the case where the initial gas temperature was 20 °C, triangle for 80 °C and squares for 150 °C. For this type of catalyst, the inlet gas temperature seems to have no impact on the poisoning temperature.

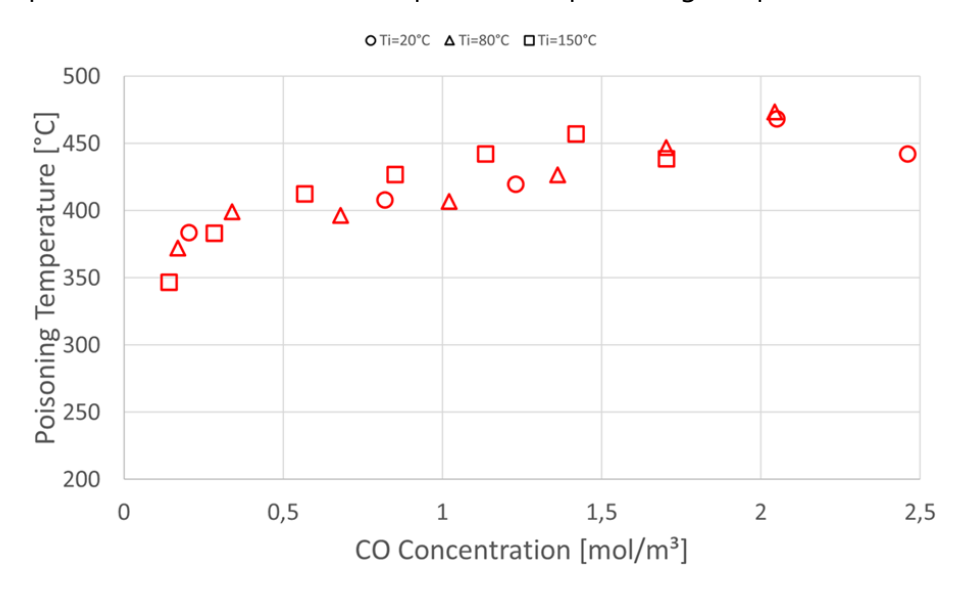


Figure 101. SPARK: Predicted poisoning temperature for three initial gas temperatures $(4 \text{ vol.}\% \text{ H}_2)$

Impact of steam content on the poisoning temperature

Figure 102 represents the effect of steam on the deactivation for a mixture of 4 vol.% hydrogen. The red triangles represent the case where there is no steam and the initial gas temperature is 80 °C while the purple triangles represent the case with steam at 100 % relative humidity at 80 °C. The deactivation occurs at a higher temperature when the catalyst is under steam conditions.

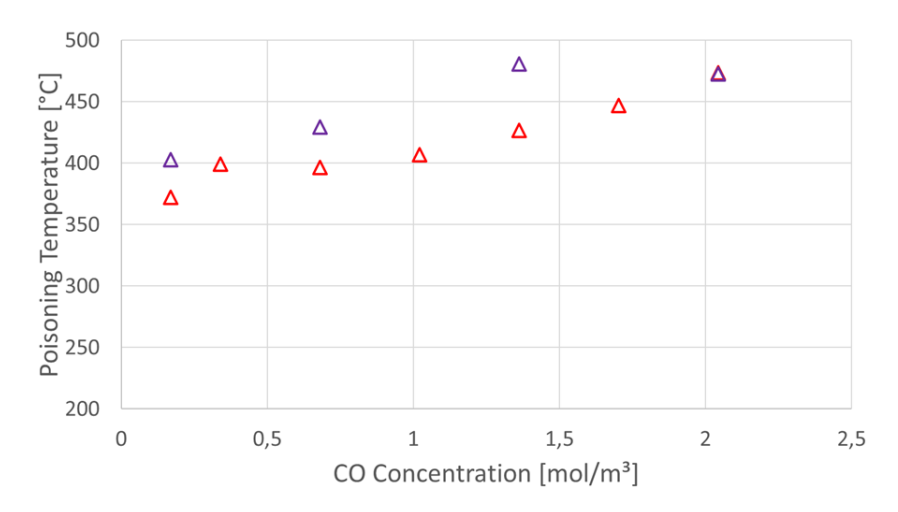


Figure 102. SPARK: Predicted poisoning temperature for dry test and test with steam $(4 \text{ vol.}\% \text{ H}_2)$

O₂ content when catalyst deactivation occurs

Figure 103 represents the oxygen fraction at beginning of catalyst deactivation for each hydrogen and carbon monoxide mixture. The oxygen fraction when catalyst deactivation occurs increases with H_2+CO content and decreases with inlet gas temperature.

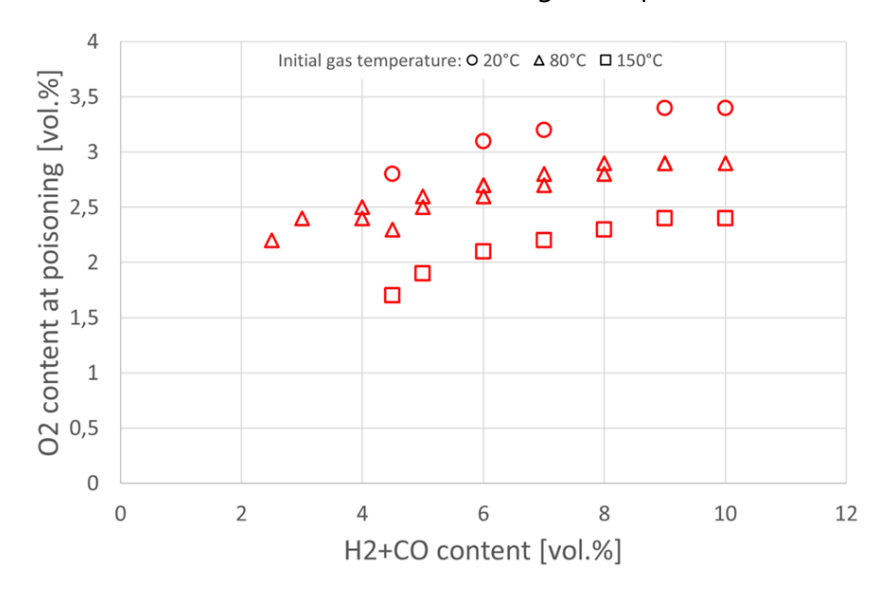


Figure 103. SPARK: Predicted oxygen content at poisoning versus the H₂+CO molar percent at different initial gas temperatures

Comparison with experimental data

Figure 104 represents the comparison between the data obtained from the experiments performed at REKO-1 and SPARK results using REKO-3 geometry since this geometry is more suited for the calculations and more representative of a real recombiner. The open symbols represent the experimental results and the filled symbols the numerical results. Even though SPARK predicts the poisoning at a higher temperature, it is possible to observe that the deactivation trend is similar to the one observed on a single catalyst sample. This difference in the temperature can be explained by the fact that, with REKO-1 facility, the heat losses are more important due to its geometry.

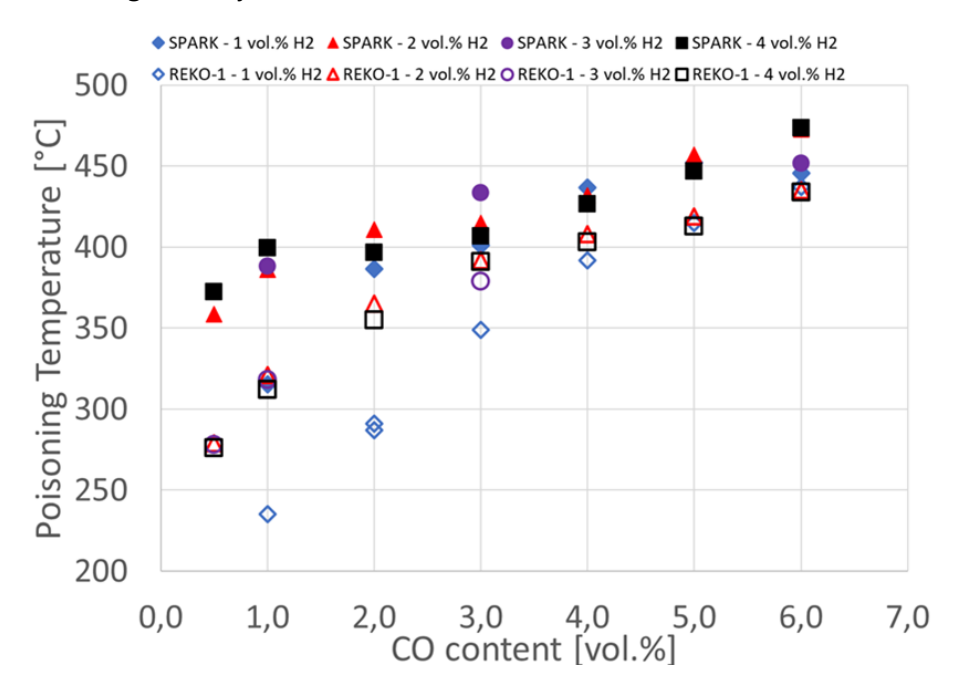


Figure 104. SPARK: Evolution of the poisoning temperature versus the CO molar percent at different H₂ content. Comparison between experiments (open symbols) and simulation (solid symbols)

The comparison of the experimental and numerical results for the effect of the flow velocity is shown in Figure 105. Once again, the experimental data is obtained from REKO-1 and the simulations using REKO-3 geometry, explaining the discrepancy in the temperature values. However, the catalyst presents the same behaviour.

Figure 106 indicates the poisoning temperature for a mixture of 4 vol.% hydrogen for each carbon monoxide concentration and different initial gas temperatures for platinum catalyst. The black symbols represent the results obtained from REKO-1, the orange symbols the results from REKO-3 and the red ones from the results calculated with SPARK. The poisoning temperature predicted by SPARK seems to be coherent with the ones measured at REKO-3. Even though the simulated temperature is higher than the ones measured at REKO-1, it can be noted that the

both curves have the same tendency, and the temperature difference can be explained by the heat losses due to REKO-1 geometry.

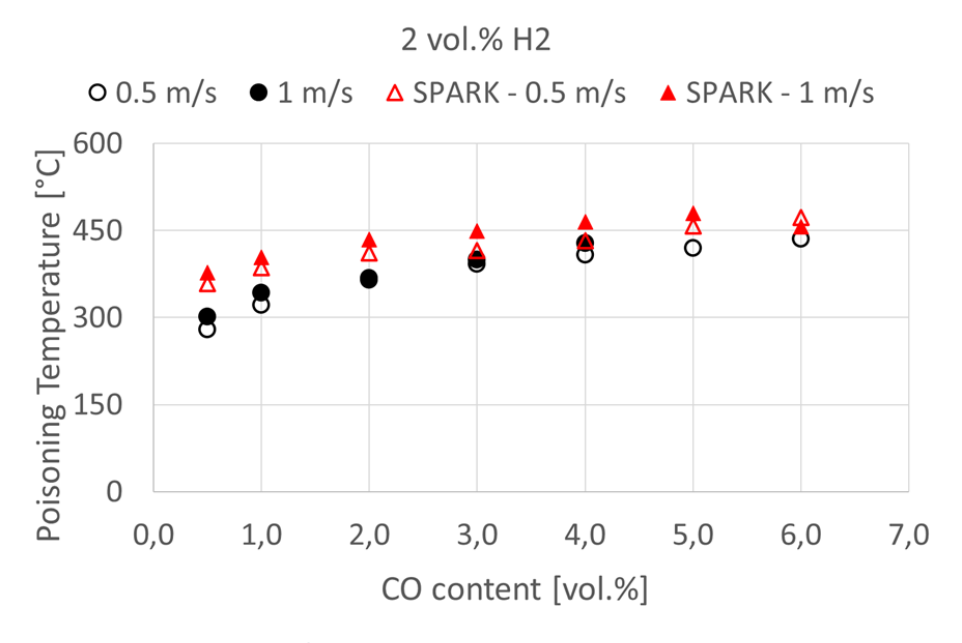


Figure 105. SPARK: Evolution of the poisoning temperature versus the CO molar fraction at different flow velocities: 0.5 m/s and 1 m/s. Comparison between experimental results and SPARK simulation

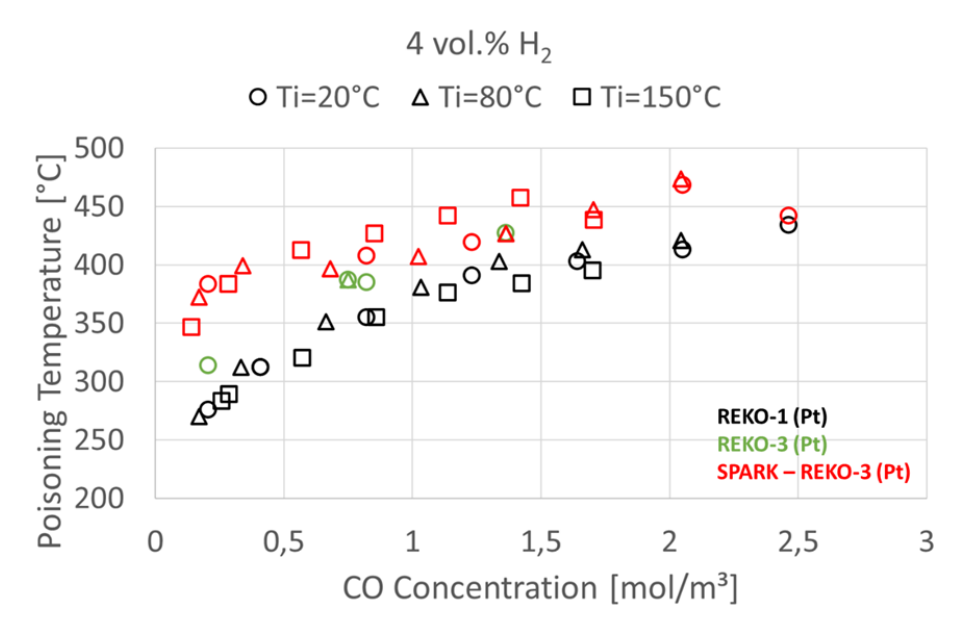


Figure 106. SPARK: Catalyst poisoning temperature at different carbon monoxide concentrations for three initial gas temperatures: 20 °C, 80 °C and 150 °C. Comparison with REKO-1 and REKO-3 data

4.2.3.3. Conclusion

Calculations have been performed for hydrogen-air mixtures in order to verify that the SPARK code is able to reproduce the experimental results. Simulations using REKO-1 geometry have been performed. The results using normal operation conditions are consistent with the experimental data. However, during oxygen starvation the results show that SPARK predicts the phenomena slightly earlier than observed in the experiments. Since the geometry of REKO-1 is a cylinder with a single catalyst sample, the 2D simulations performed at SPARK is not the most adapted.

The simulations using REKO-3 geometry have been performed as well using different hydrogen/air mixtures. The catalyst behaviour for conditions where there is oxygen reduction has also been simulated. The effect of steam on the catalyst temperature has also been analysed with the presence of carbon monoxide and no restriction of oxygen. The numerical results are consistent with the experimental results for all the cases, confirming that the SPARK code can predict the catalyst temperature for oxygen-rich conditions, oxygen starvation conditions and when in presence of steam.

In order to enhance the knowledge on the impact of carbon monoxide on the catalyst behaviour, experiments have been performed at the REKO facilities. In a first scoping test series, the deactivation conditions of a single catalyst sample have been investigated in the REKO-1 facility. For this purpose, platinum- and palladium-based catalyst samples have been exposed to mixtures of hydrogen, carbon monoxide, air, nitrogen and steam at different temperatures and flow velocities. The experiments revealed that the poisoning can be predicted by the carbon monoxide fraction, the oxygen fraction and the catalyst temperature. Furthermore, the palladium catalyst is deactivated at lower catalyst temperatures than the platinum catalyst. The results show that the catalyst temperature in which the platinum is poisoned is independent from the gas temperature, while for the palladium catalyst the gas temperature seems to influence the poisoning temperature. In a second step, the REKO-3 facility is used to study the effect of carbon monoxide on a section of a recombiner with four full scale catalyst sheets arranged vertically inside a rectangular channel. These experiments provide data for the further enhancement of numerical codes in the framework of the AMHYCO project and the SPARK code.

SPARK simulations for H2/CO/air mixtures were performed and the impact of different parameters was analysed. The comparison of the simulations with the numerical results reveals that SPARK code is able to reproduce catalyst deactivation by carbon monoxide, and notably to capture the transition from partial to complete deactivation. The code predicts higher poisoning temperature than the ones observed in the experiments.

Even though a new reaction mechanism for H_2/CO on palladium was presented, the calculations could not be finished, and more experimental data is necessary to validation. This will be addressed in future work.

4.2.4.REKO-DIREKT

REKO-DIREKT has been used to calculate the new THAI database.

Figure 107 shows the comparison of calculated hydrogen outlet concentrations with the values from the THAI database. The agreement is very good over the entire range.

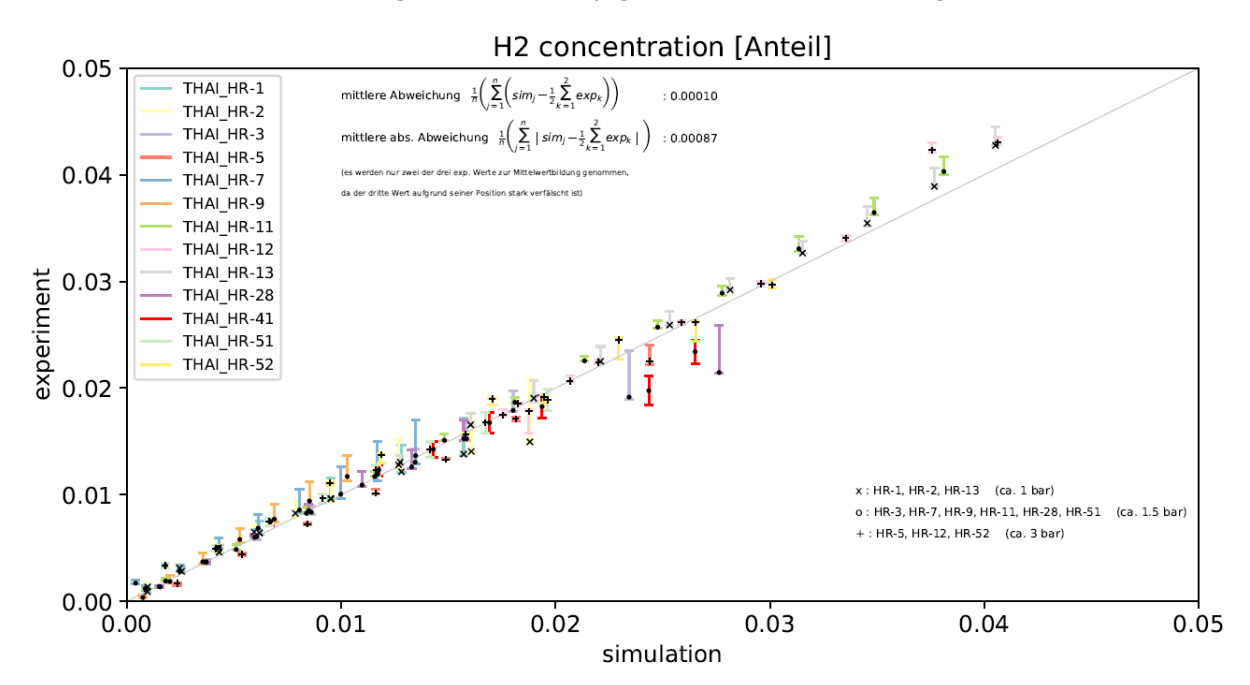


Figure 107. REKO-DIREKT: Calculated outlet hydrogen concentration compared with data from the THAI database

A specific feature of REKO-DIREKT is the calculation of the temperature profile along the catalyst sheets. A comparison of calculated and measured values is shown in Figure 108. Again, the agreement is very good, although the calculated temperature values are systematically too high.

Another code advancement is the introduction of two different poisoning criteria based on the findings from REKO-3 poisoning experiments (see section 3.2.6). For this purpose, the selection of platinum- or palladium-based catalyst in the user input has been implemented.

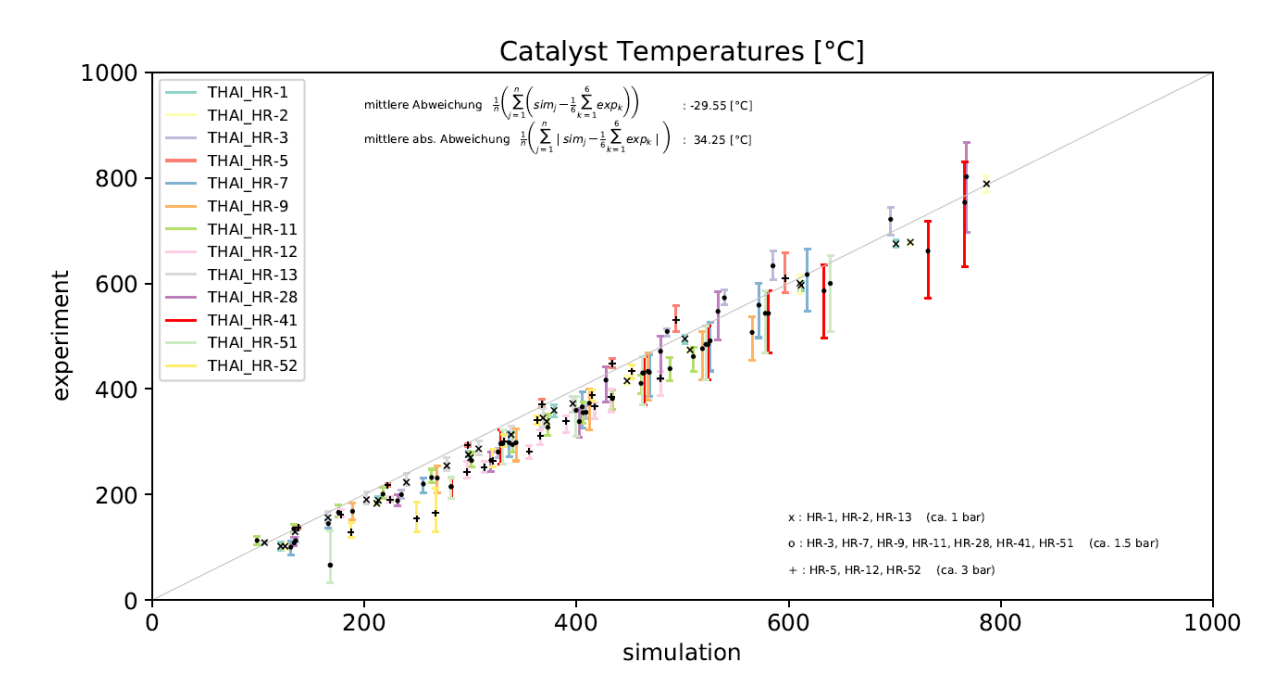


Figure 108. REKO-DIREKT: Calculated catalyst temperatures compared with data from the THAI database

5. Bibliography

Bachellerie E., Arnould F., Auglaire M., de Boeck B., Braillard O., Eckardt B., Ferroni F. & Moffett R. (2003). Generic approach for designing and implementing a passive autocatalytic recombiner PAR-system in nuclear power plant containments. *Nuclear Engineering and Design* 221(1-3) 151-165.

Bentaïb A. (2020). WP1: Critical review. AMHYCO Kick-off Meeting, virtual, October 26-27, 2020.

Böhm J. (2007). Modelling of Processes in Catalytic Recombiners, Forschungszentrum Jülich Energy Technologies Vol. 61, ISBN 978-3-89336-473-2.

Chakraborty A., Reinecke E.-A., Meynet N., Bentaib A., Chaumeix N. & Allelein H.-J. (2017). Investigation of ignition characteristics of passive autocatalytic recombiners. Proc. Int. Congress on Advances in Nuclear Power Plants (ICAPP 2017), Fukui and Kyoto, Japan, April 24-28, 2017.

Chakraborty A. (2020). Optimization of Passive Autocatalytic Recombiners (PARs) with respect to Gas-phase Ignition, PhD Thesis, RWTH Aachen University.

Chatelard P., Reinke N., Arndt S., Belon S., Cantrel L., Carenini L., Chevalier-Jabet K., Cousin F., Eckel J., Jacq F., Marchetto C., Mun C. & Piar L. (2014). ASTEC V2 severe accident integral code main features, current V2.0 modelling status, perspectives. *Nuclear Engineering and Design* 272 119-135.

Deutschmann O., Schmidt R., Behrendt F. & Warnatz J. (1996). Numerical modeling of catalytic ignition. *Symposium (International) on Combustion* 26(1) 1747-1754.

Domínguez-Bugarín A., Jiménez M. Á., Reinecke E.-A. & Jiménez G. (2022). PARUPM: A simulation code for passive auto-catalytic recombiners. *EPJ Nuclear Sci. Technol.* 8(32).

Domínguez-Bugarín A., Reinecke E.-A., Jiménez M. Á. & Jiménez G. (2023). Validation of the passive autocatalytic recombiner simulation code PARUPM using experimental data from REKO-3 and THAI program tests. Proc. European Nuclear Young Generation Forum ENYGF'23, May 8-12, 2023, Kraków, Poland.

Elenbaas W. (1942). Heat dissipation of parallel plates by free convection. *Physica* 9(1), 1-28.

EPRI (2018). GOTHIC 8.3 Thermal Hydraulic Analysis Package. User Manual. Palo Alto, CA.

Framatome (2019). Passive Autocatalytic Recombiner - Combustible Gas Control System, https://www.framatome.com/solutions-portfolio/docs/default-source/default-document-

library/product-sheets/a0642-p-ge-g-en-201908-par.pdf?sfvrsn=748c9be2_2 (accessed March 20, 2023).

Gupta S., Schmidt E., von Laufenberg B., Freitag M., Poss G., Funke F. & Weber G. (2015). THAI test facility for experimental research on hydrogen and fission product behaviour in light water reactor containments. *Nuclear Engineering and Design* 294 183-201.

Gupta S., Freitag M. & Poss G. (2016). THAI experimental programme for containment safety assessment under severe accident conditions. *Kerntechnik* 81(2) 138-141.

Herranz L. E. & Fontanet J. (2022). D2.2 – Identification and analysis of accidental sequences posing high H_2/CO combustion risk. AMHYCO Report WP2.

Herranz L. E. & Fontanet J. (2022). AMHYCO – WP2 link to WP3. PowerPoint presentation.

Jiménez M. Á. (2007). Recombinación del hidrógeno en dispositivos autocatalíticos pasivos y sus implicaciones en la seguridad de las centrales nucleares. PhD Thesis, Universidad Politécnica de Madrid.

Jiménez M. Á., Martín-Valdepeñas J. M., Martín-Fuertes F. & Fernández J.A. (2007). A detailed chemistry model for transient hydrogen and carbon monoxide catalytic recombination on parallel flat Pt surfaces implemented in an integral code, *Nuclear Engineering and Design* 237 460.

Klauck M., Reinecke E.-A., Kelm St., Meynet N., Bentaïb A. & Allelein H.-J. (2014). Passive autocatalytic recombiners operation in the presence of hydrogen and carbon monoxide: experimental study and model development. *Nuclear Engineering and Design* 266 137-147.

Klauck M., Reinecke E.-A. & Allelein H.-J. (2021). Effect of PAR deactivation by carbon monoxide in the late phase of a severe accident. *Annals of Nuclear Energy* 151 107887.

Liang Z., Sonnenkalb M., Bentaïb A. & Sangiorgi M. (2014). Status Report on Hydrogen Management and Related Computer Codes. NEA/CSNI/R(2014)8.

Liang Z., Gardner L. & Clouthier T. (2020). Experimental study of the effect of carbon monoxide on the performance of passive autocatalytic recombiners. *Nuclear Engineering and Design* 364 110702.

Meynet N., Bentaïb A. & Giovangigli V. (2014). Impact of oxygen starvation on operation and potential gas-phase ignition of passive auto-catalytic recombiners. *Combustion and Flame* 161 2192-2202.

Meynet N., (2015). SPARK - Logiciel de calcul pour les recombineurs catalytiques. IRSN report PSN-RES/SAG/2015-00036.

Mimouni S., Mechitoua N. & Ouraou M. (2011). CFD Recombiner Modelling and Validation on the H2-PAR and Kali-H2 Experiments, *Science and Technology of Nuclear Installations* 2011 574514.

Nobrega G. (2022). Etude de l'empoisonnement des recombineurs auto-catalytiques passifs. PhD Thesis, Université d'Orléans.

OECD-NEA (2023). https://www.oecd-nea.org/jcms/pl_58863/thai-experiments-on-mitigation-measures-and-source-term-issues-to-support-analysis-and-further-improvement-of-severe-accident-management-measures-themis-project (accessed March 20, 2023).

Payot F., Reinecke E.-A., Morfin F., Sabroux J.-C., Meynet N., Bentaïb A., March P. & Zeyen R. (2012). Understanding of the operation behaviour of a Passive Autocatalytic Recombiner (PAR) for hydrogen mitigation in realistic containment conditions during a severe light water nuclear reactor (LWR) accident. *Nuclear Engineering and Design* 248 178-196.

Petit M., Alsmeyer H. & Gustavsson V. (2001). In-vessel and ex-vessel hydrogen sources, part ii: GAMA perspective statement on ex-vessel hydrogen sources. NEA/CSNI/R(2001)15.

Reinecke E.-A., Tragsdorf I.M. & Gierling K. (2004). Studies on innovative hydrogen recombiners as safety devices in the containments of light water reactors. *Nuclear Engineering and Design* 230 49–59.

Reinecke E.-A., Kelm S., Simon B., Klauck M. & Allelein H.-J. (2014). Interpretation of the entire OECD/NEA-THAI HR test series including AREVA and AECL PARs using the code REKO-DIREKT. OECD/NEA THAI2 Final Seminar, Frankfurt/Main, Germany, November 18-19, 2014.

Reinecke E.-A., Kelm S., Steffen P.-M., Klauck M. & Allelein H.-J. (2016). Validation and application of the REKO-DIREKT code for the simulation of passive auto-catalytic recombiners (PARs) operational behavior. *Nuclear Technology* 196(2) 355-366.

Reinecke E.-A., Kelm S., Struth S., Schwarz U. & Tragsdorf I. M. (2007). Performance of catalytic recombiners for hydrogen mitigation in severe accidents under oxygen depletion conditions. Proc. 15th International Conference on Nuclear Engineering, Nagoya, Japan, April 22-26, 2007.

Reinecke E.-A., Bentaïb A., Chaumeix N., Chakraborty A., Heidelberg D., Kelm S., Maas L. & Steffen P.-M. (2018). Operating behavior of passive auto-catalytic recombiners under severe accident conditions. International Severe Accident Management Conference (ISAMC), Ottawa (Ontario), Canada, October 15-18, 2018.

Reinecke E.-A., Fontanet J., Herranz L.E., Liang Z., Maas L., Mazurok O., Park J.-S., Visser D.C., Hupp M. & Gupta S. (2022). PAR model development exercise in the framework of SAMHYCO-NET. *Nuclear Engineering and Design* 399 112035.

Reinecke E.-A. (2022). Preliminary proposal for a modification of the existing PAR correlation model to be used in WP4 simulations. AMHYCO Report WP3.

Warnatz J., Dibble R.W. & Mass U. (1996). Combustion: Physical and chemical fundamentals, modeling and simulation. Springer, New York.

Zheng X., Schultze M., Mantzaras J. & Bombach R. (2013). Effects of hydrogen addition on the catalytic oxidation of carbon monoxide over platinum at power generation relevant temperatures. *Proceedings of the Combustion Institute* 34(2) 3343-3350.